การศึกษาทางทฤษฎีของกระบวนการถ่ายโอนอิเล็กตรอนในดีอะมิโนแอซิดออกซิเดสกับสารยับยั้ง

นายอาทิตย์ เนื่องอุดม

วิทยานิพนธ์นี้เป็นส่วนหนึ่งของการศึกษาตามหลักสูตรปริญญาวิทยาศาสตรดุษฎีบัณฑิต

สาขาวิชาเคมี ภาควิชาเคมี

คณะวิทยาศาสตร์ จุฬาลงกรณ์มหาวิทยาลัย

ปีการศึกษา 2558

ลิขสิทธิ์ของจุฬาลงกรณ์มหาวิทยาลัย

THEORETICAL INVESTIGATION OF ELECTRON TRANSFER PROCESS IN D-AMINO ACID OXIDASE WITH ITS INHIBITORS

Mr. Arthit Nueangaudom

A Dissertation Submitted in Partial Fulfillment of the Requirements

for the Degree of Doctor of Philosophy Program in Chemistry

Department of Chemistry

Faculty of Science

Chulalongkorn University

Academic Year 2015

Thesis Title	THEORETICAL INVESTIGATION OF ELECTRON TRANSFER PROCESS IN D-AMINO ACID OXIDASE WITH ITS INHIBITORS
By	Mr. Arthit Nueangaudom
Field of Study	Chemistry
Thesis Advisor	Associate Professor Dr. Sirirat Kokpol
Thesis Co-Advisor	Assistant Professor Dr. Somsak Pianwanit

Accepted by the Faculty of Science, Chulalongkorn University in Partial Fulfillment of the Requirements for the Doctoral Degree

⋯⋯⋯⋯⋯⋯⋯⋯⋯⋯⋯⋯⋯Dean of the Faculty of Science

(Associate Professor Dr. Polkit Sangvanich)

THESIS COMMITTEE

⋯⋯⋯⋯⋯⋯⋯⋯⋯⋯⋯⋯⋯Chairman

(Associate Professor Dr. Vudhichai Parasuk)

⋯⋯⋯⋯⋯⋯⋯⋯⋯⋯⋯⋯⋯Thesis Advisor

(Associate Professor Dr. Sirirat Kokpol)

⋯⋯⋯⋯⋯⋯⋯⋯⋯⋯⋯⋯⋯Thesis Co-Advisor

(Assistant Professor Dr. Somsak Pianwanit)

⋯⋯⋯⋯⋯⋯⋯⋯⋯⋯⋯⋯⋯Examiner

(Associate Professor Dr. Pornthep Sompornpisut)

⋯⋯⋯⋯⋯⋯⋯⋯⋯⋯⋯⋯⋯Examiner

(Assistant Professor Dr. Warinthorn Chavasiri)

⋯⋯⋯⋯⋯⋯⋯⋯⋯⋯⋯⋯⋯External Examiner

(Assistant Professor Dr. Nadtanet Nanthaboot)

อาทิตย์ เนื่องอุดม : การศึกษาทางทฤษฎีของกระบวนการถ่ายโอนอิเล็กตรอนในดีอะมิโนแอซิดออกซิเดสกับสารยับยั้ง (THEORETICAL INVESTIGATION OF ELECTRON TRANSFER PROCESS IN D-AMINO ACID OXIDASE WITH ITS INHIBITORS) อ.ที่ปรึกษาวิทยานิพนธ์หลัก: รศ. ดร. ศิริรัตน์ ก๊กผล, อ.ที่ปรึกษาวิทยานิพนธ์ร่วม: ผศ. ดร. สมศักดิ์ เพียรวณิช, 192 หน้า.

ศึกษาอัตราการถ่ายโอนอิเล็กตรอนที่เหนี่ยวนำด้วยแสง (PET) ระหว่าง Iso และกรดอะมิโนที่อยู่ใกล้เคียงของดีอะมิโนแอซิดออกซิเดส (DAAO) ด้วยทฤษฎีอิเล็กตรอนทรานสเฟอร์ของกากิทานิ-มาทากะและโครงสร้างของ DAAO จากการจำลองพลวัตเชิงโมเลกุล (MD) อัตรา PET ของ DAAO ทำให้จุดประกายความสนใจในการค้นหาสารยับยั้งชนิดใหม่ของ DAAO ด้วยการยับยั้งกระบวนการอิเล็กตรอนทรานสเฟอร์ ส่วนแรกของวิทยานิพนธ์ ทำการศึกษาอันตรกิริยาและสมบัติเชิงพลวัตของ DAAO จากไตหมูทั้งหมด 4 ระบบ ได้แก่ DAAO มอนอเมอร์ DAAO ไดเมอร์ สารเชิงซ้อนระหว่าง DAAO กับเบนโซเอต (DAOB) มอนอเมอร์ และ DAOB ไดเมอร์ โดยทำการศึกษาด้วย MD ผลจาก MD ของ DAAO และ DAOB ทำให้เห็นโครงสร้างที่แตกต่างกันระหว่างมอนอเมอร์และไดเมอร์ และโครงสร้างที่ไม่เหมือนกันในโมเลกุลไดเมอร์ ผลลัพธ์จากการวิเคราะห์ PET ของ DAAO แสดงให้เห็นว่า อัตราการถ่ายโอนอิเล็กตรอนที่เร็วที่สุดสามอันดับคือ จาก Tyr224 Tyr228 และ Tyr314 ไปยัง Iso* ของ DAAO เบนโซเอตใน DAOB ในสภาวะที่เป็นสารยับยั้งแบบแข่งขัน เป็นตัวให้อิเล็กตรอนไปยัง Iso* ได้ดีที่สุดเมื่อเทียบกับกรดอะมิโนอื่น ๆ ซึ่งสอดคล้องกับข้อมูลการรบกวนฟลูออเรสเซนต์ที่ได้จากการทดลอง ส่วนที่สองของวิทยานิพนธ์ ทำการศึกษา DAAO จากมนุษย์ เพื่อหาสารยับยั้ง DAAO ที่มีศักยภาพสำหรับการรักษาโรคจิตเภทด้วยเทคนิคการคัดกรองเสมือนจริง โดยทำการคัดกรองสารประกอบสี่ล้านโมเลกุลที่อยู่ในฐานข้อมูลนามิกิด้วยรูปแบบโครงสร้างที่จำเป็นต่อการออกฤทธิ์และวิธีโมเลคิวลาร์ด็อกกิง ได้สารประกอบ 22 สาร ซึ่งจะทำการทดสอบฤทธิ์ทางชีวภาพต่อไป

ภาควิชา	เคมี	ลายมือชื่อนิสิต	....
สาขาวิชา	เคมี	ลายมือชื่อ อ.ที่ปรึกษาหลัก	....
ปีการศึกษา	2558	ลายมือชื่อ อ.ที่ปรึกษาร่วม	....

5273873123 : MAJOR CHEMISTRY

KEYWORDS: D-AMINO ACID OXIDASE / PHOTOINDUCED ELECTRON TRANSFER ANALYSIS / MOLECULAR DYNAMICS SIMULATION / VIRTUAL SCREENING / DAAO INHIBITORS

ARTHIT NUEANGAUDOM: THEORETICAL INVESTIGATION OF ELECTRON TRANSFER PROCESS IN D-AMINO ACID OXIDASE WITH ITS INHIBITORS. ADVISOR: ASSOC. PROF. DR. SIRIRAT KOKPOL, CO-ADVISOR: ASST. PROF. DR. SOMSAK PIANWANIT, 192 pp.

The photoinduced electron transfer (PET) rates between Iso and nearby amino acid residues of D-amino acid oxidase (DAAO) were studied using Kakitani-Mataka ET theory and DAAO conformations from molecular dynamics (MD) simulation. These PET rates of DAAO were inspired to a novel way for discovery new DAAO inhibitors by inhibiting ET process. The first part of this thesis,   the interaction and dynamics properties of DAAO from pig kidney for four systems i.e. DAAO monomer, DAAO dimer, DAAO complexed with benzoate (DAOB) monomer, and DAOB dimer were studied by MD simulations. DAAO and DAOB MD simulation results revealed the different conformations between monomer and dimer, as well as the non-equivalent conformations in dimer. The results of PET analysis of DAAO showed that the three fastest ET rates are from Tyr224, Tyr228, and Tyr314 to Iso* of DAAO. The benzoate in DAOB, as a competitive inhibitor, is the best electron donor to Iso* compare to other amino acids which is agreed with the experimental fluorescence lifetime quenching. The second part of this thesis, DAAO from human was studied to find potential DAAO inhibitors for schizophrenia treatment using virtual screening technique. Four million compounds on Namiki database were screened using pharmacophore model and molecular docking. The 22 hit compounds will be tested biological activity.

Department:	Chemistry	Student's Signature	....
Field of Study:	Chemistry	Advisor's Signature	....
Academic Year:	2015	Co-Advisor's Signature	....

ACKNOWLEDGEMENTS

CONTENTS

LIST OF TABLES

จุฬาลงกรณ์มหาวิทยาลัย
CHULALONGKORN UNIVERSITY

LIST OF FIGURES

LIST OF ABBREVIATION

Bz	=	Benzoate
DAAO	=	D-Amino acid oxidase
DAOB	=	D-Amino acid oxidase complexed with benzoate
DET	=	Dark electron transfer
EC	=	Electronic coupling
EPS	=	Dielectric constant
eqn	=	Equation
ES	=	Electrostatic
ESDA	=	Electrostatic energy between donor and acceptor
ET	=	Electron transfer
FAD	=	Flavin adenine dinucleotide
FISA	=	Hydrophilic components of the solvent-accessible surface area
FMN	=	Flavin mononucleotide
GTRAM	=	Exponential term
H-bond	=	Hydrogen bonding
hDAAO	=	Human D-amino acid oxidase
Iso	=	Isoalloxazine ring
Iso*	=	Excited isoalloxazine ring
KM	=	Kakitani-Mataga
MD	=	Molecular dynamics
MDS	=	Molecular dynamic simulations
MO	=	Molecular orbital
NetES	=	Electrostatic energy
NMDA	=	N-Methyl-D-aspartate
PE	=	Pre-exponential
PET	=	Photoinduced electron transfer
PISA	=	π (Carbon and attached hydrogen) components of the solvent-accessible surface area

pkDAAO	=	Pig kidney D-amino acid oxidase
QSAR	=	Quantitative structure-activity relationship
Rc	=	Center to center distance
Re	=	Edge to edge distance
RESP	=	Restrained electrostatic potential
RH	=	H-bond distance
RMSD	=	Root mean square deviation
RMSF	=	Root mean square fluctuation
SE5	=	4-(4-chlorophenethyl)-1H-pyrrole-2-carboxylic acid
SQ	=	Square root
Sub	=	Subunit
Trp	=	Tryptophan
Tyr	=	Tyrosine
VS	=	Virtual screening
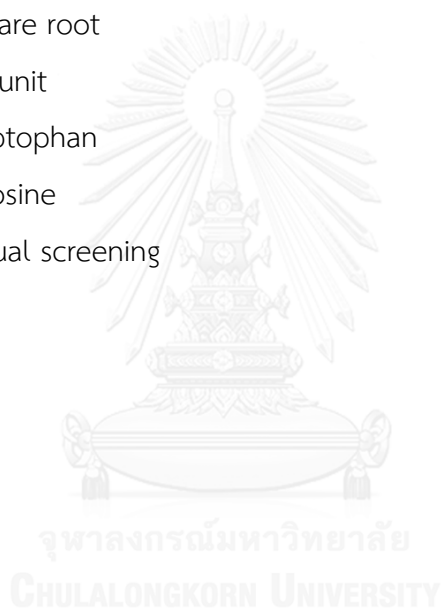
CHAPTER I

INTRODUCTION

1.1 RESEARCH RATIONALES AND THEORIES

1.1.1 D-Amino acid oxidase

D-Amino acids plays a more significant in living cells role in the regulation of many processes such as hormone secretion, aging, and neural signaling.[1] For instance, D-serine was reported to be effective in reducing negative symptoms of schizophrenia.[2] The decreased D-serine level was considered to relate to schizophrenia and cause of the neurobiological insufficiencies.[3] The main cause of the decreased D-serine in mammals is reduction of D-amino acid oxidase (DAAO, Enzyme Class 1.4.3.3). DAAO is a flavoenzyme containing flavin adenine dinucleotide (FAD) as a cofactor, the two dimensional structure of FAD is shown in Figure 1.1, exists in a varied species from microbes to mammals. Its function is to oxidize D-amino acids to yield the corresponding α–keto acids, ammonia and hydrogen peroxide as shown in Figure 1.2.

Therefore, the inhibitors of DAAO has been investigated to find the potential compounds that can inhibit DAAO activity as a means to maintain normal level of D-serine. Generally, a basis knowledge about mechanism of DAAO was related to electron transfer (ET) between D-amino acids and FAD, which is the important process for DAAO role. This ET process of DAAO and substrates was inspired to new way for discovery new DAAO inhibitors. We hope to use some ET parameters from ET analysis to be a criterion for virtual screening that was applied to discover new DAAO inhibitors.
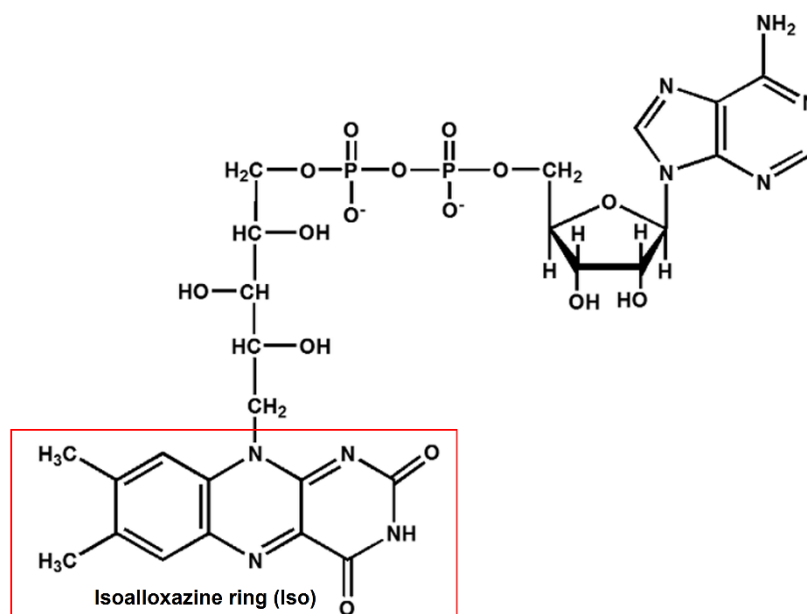
Figure 1.1 *The two-dimensional structure of FAD.*
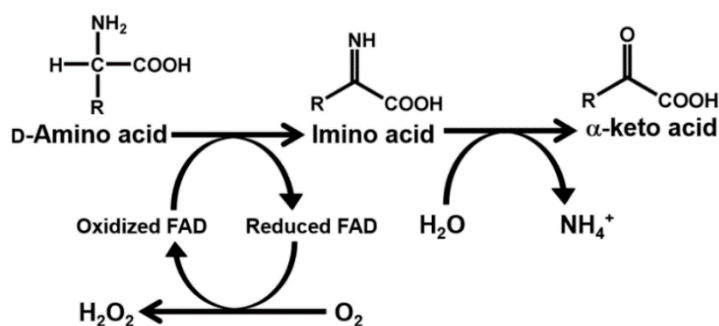
Figure 1.2 *Scheme of the oxidation-reduction reaction of DAAO catalyzed D-amino acid.*

Since fluorescence emissions of riboflavin (vitamin B_2) and FAD as flavins were discovered by Weber,[4] the fluorescence spectroscopy became a useful tool for studying flavoproteins. In many flavoproteins, the fluorescence of flavins is strongly quenched. This is ascribed to photoinduced electron transfer (ET) from tryptophan (Trp) and/or tyrosine (Tyr) to the excited isoalloxazine (Iso*).[5-7] Fluorescence dynamics of flavoproteins in the picoseconds domain have been studied by photon-

counting method.[8-10] Furthermore, the ultrafast fluorescence dynamics of some flavoproteins have been investigated in the femtoseconds-picoseconds time domain by fluorescence up-conversion method.[11-16]

However, the fluorescence lifetime of human (h) DAAO has not be done from the experimentally, also difficult to prepare and expensive. From these reasons, pig kidney (pk) DAAO is the best alternative choice because there are a lot of the fluorescence lifetime measurements.[15, 17, 18] Furthermore, pkDAAO in the crystal structure with complexed with benzoate, DAOB, (PDB code: 1VE9) [19] compared with the crystal structure of hDAAO complexed with also benzoate (PDB code: 2DU8) [20], in Figure 1.3, show the high sequence identity 84.7% and high sequence similarity 93.2% between two enzymes.
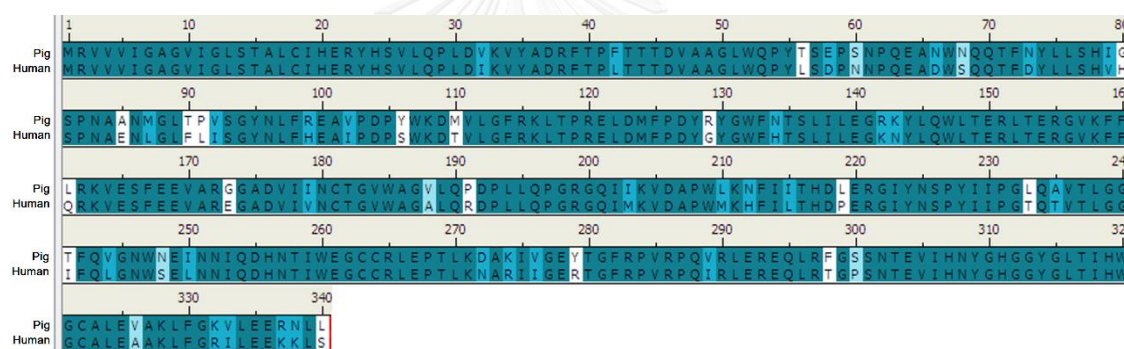
Figure 1.3 Sequence alignments of pig kidney DAAO and human.

Moreover, when the dimer structures of pkDAOB complex and hDAOB complex were compared by superimposition as shown in Figure 1.4 (A), the benzoates, as an inhibitor, of both structures formed similar three hydrogen bonds, i.e. with Tyr228 (one hydrogen bond) and Arg283 (two hydrogen bonds) in Figure 1.4 (B).
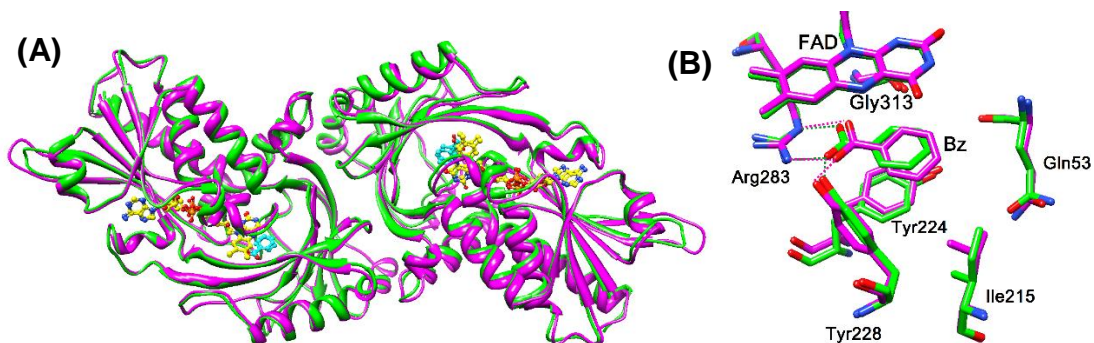
Figure 1.4 (A) *The superimposition of hDAAO (magenta) and pkDAAO (green) in dimer form,* **(B)** *Representation the hydrogen bonds between amino acid residues in active site and benzoate of both the enzymes. Dash lines denote hydrogen bonding.*

The activity of some DAAO inhibitors were tested in both hDAAO and pkDAAO by Berry et al. [21] Interestingly, most inhibitors showed similar activity in the two DAAOs (as Figure 1.5) i.e., good inhibitors for hDAAO also showed good activity for pkDAAO. Considering the similarity in the structures as well as the inhibition activities, pkDAAO is a good model of hDAAO in this study.
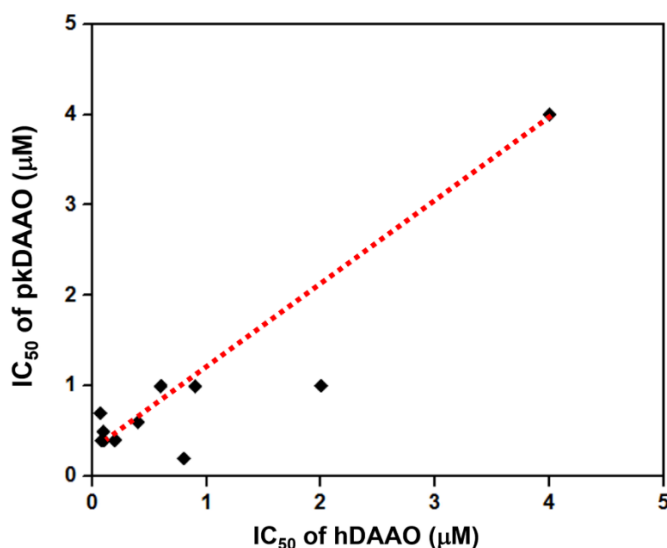
Figure 1.5 *The relationship of the inhibition activities of DAAO inhibitors for pkDAAO and hDAAO.*

1.1.1.1 Pig kidney DAAO (pkDAAO)

PkDAAO was first discovered by Hans Krebs.[22] The pkDAAO (Mw 40 kDa per monomer) in solution can exist in many forms e.g. monomer, dimer, and tetramer, at low concentrations [23-26] it is in a monomer–dimer equilibrium state and may be in a dimer–tetramer equilibrium at higher concentrations [27-29] as shown in Figure 1.6 (A), (B), and (C), respectively. Shiga et al. reported that the equilibrium constant of the association from monomer to dimer state displayed a discontinuous change at 18 $^\circ$C as the temperature was varied.[30] The temperature transition of DAAO has been thoroughly investigated by measuring the fluorescence lifetimes of FAD in a picoseconds time domain, by varying the temperature and protein concentration.[18] Although many works have investigated the temperature-transition in the experimentally, but no work has provided a structural basis for this temperature-transition. This led to the computational simulation of DAAO in order to understanding the structural basis for the temperature-transition, which has been discussed in Chapter II.

(A)

(B)

(C)
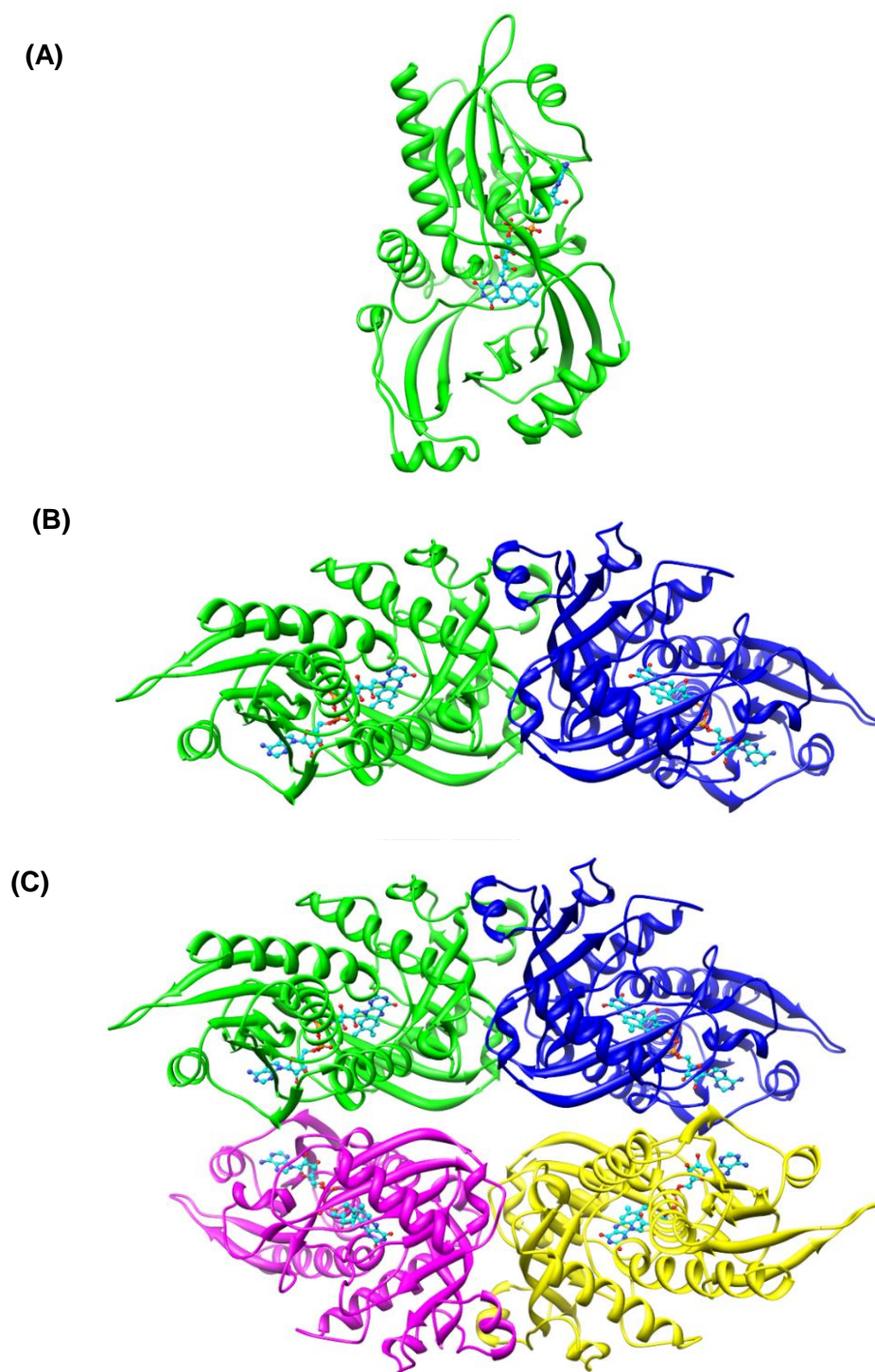
Figure 1.6 *The three-dimensional structures of pkDAAO (A) monomer, (B) dimer, and (C) two dimer (or tetramer) in crystal structures. FADs are indicated in ball and stick models of each subunit.*

Benzoate (Bz) is a competitive inhibitor which binds to DAAO and stabilizes the enzyme. The fluorescence lifetimes of pkDAAO in monomer form [18] and pkDAAO-benzoate complex (DAOB) in monomer form [15], have been reported to be 177 and 60 ps, respectively. For the fluorescence lifetimes of dimeric forms, DAAO was reported to be 44 ps [18] as well as DAOB displays two fluorescence lifetimes of 0.85 ps and 4.80 ps [15]. These data suggest that the structural conformations of DAAO and DAOB may affect the fluorescence lifetimes. However, the experimental results cannot demonstrate the structural differences of DAAO and DAOB.

In this work, the molecular dynamics (MD) simulations have been used to calculate the time dependent behavior of a molecular system that is conformation structures. The ET rates in flavoproteins have been analyzed by using fluorescence dynamics from experimental results and the atomic coordinates from MD simulations.[31-42] The calculations, results, and discussions were provided in Chapter II-V.

1.1.1.2 Human DAAO (hDAAO)

In human, hDAAO is mostly expressed in the kidney, liver, and brain and is responsible for the metabolism of D-amino acids. For instance, D-serine is an endogenous agonist at the N-Methyl- D-aspartate (NMDA) receptor glycine modulatory site. DAAO has gained substantial interest as a therapeutic target for disorders associated with NMDA receptor dysfunction such as schizophrenia.[3]

Schizophrenia affects more than 21 million people globally as reported by the World Health Organization (WHO).[43] Schizophrenia is a mental disorder, characterized by deep disruptions in thinking, acting, and seeing the world. Currently, therapies are insufficient and have side effect. Hence, the important attempts have been made to identify potent and selective DAAO inhibitors as novel therapeutic agents.

Several compounds have been reported to inhibit hDAAO, including benzoic acid **1**,[44] pyridine-2,3-diol **2**,[45] 4H-furo[3,2-b]pyrrole-5-carboxylic acid **3**,[46] 4H-thieno[3,2-b]pyrrole-5-carboxylic acid **4**,[46] 5-methylpyrazole-3-carboxylic acid (AS057278) **5**,[47] 1-hydroxy-1H-benzo[d]imidazole-2(3H)-one **6**,[21] 6-chlorobenzo

[d]isoxazole-3-ol (CBIO) **7**,[48] 3-hydroxychromen-2-one **8**,[49] 8-methylpyrido[2,3-b]pyrazine-2,3(1H,4H)-dione**9**,[50] 6-[2(3,5-difluorophynyl)ethyl]-4-hydroxypyridazin-3(2H)-one **10**,[45] as shown in Figure 1.7. Moreover, these structures have been modified to increase the inhibition activity of DAAO, at present the DAAO inhibitors cannot yet go through to drug for schizophrenia treatment.
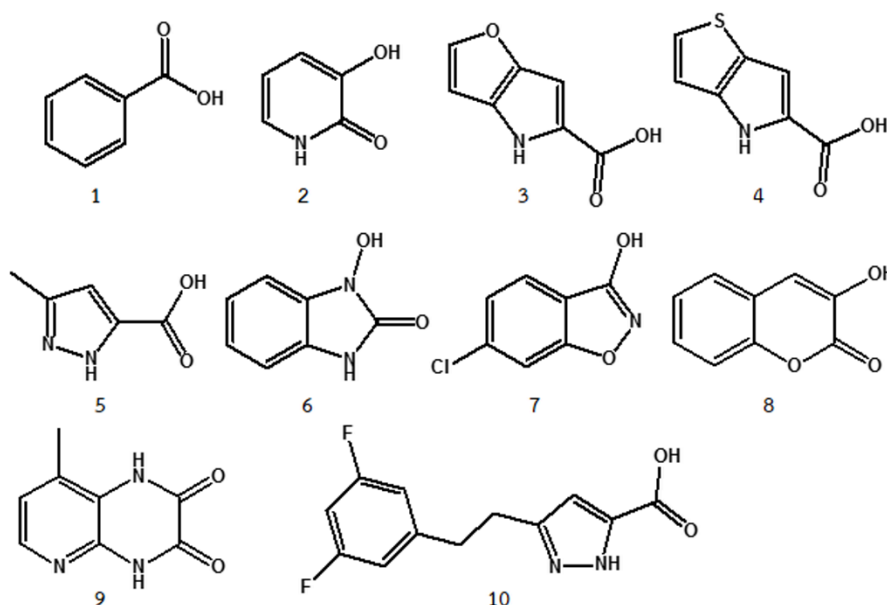
Figure 1.7 *The inhibitors of DAAO*

However, the preparatory and high throughput screening of numerous compounds for testing activity is time-consuming and costly in general.[48, 51, 52] Recent advances in computational chemistry have enabled to perform structure-based virtual screening of many compounds listed in chemical structure databases. Virtual screening is a cost-effective first screening method, and results from the screening can then be used as a guide for library construction before an actual screening is performed.[53-55]

In this study, we used the virtual screening technique including pharmacophore model and ligand-docking method to screen a large number of compounds in database with the hope to find some candidate compounds. This work shows that

some of these compounds will be possible lead compounds for the development of a clinically useful DAAO inhibitor.

1.1.2 Electron transfer theory

PET is one of the most abundant and fundamental phenomena in the field of chemistry, biology and physics. Many biological and chemical processes involve ET reactions such as photosynthesis, detoxification, respiration, and other biological processes, including bioelectronics and biosensor [1, 56-58]. Several theories on ET and PET have been reported. The first generally accepted theory was developed by Rudolph A. Marcus. This Marcus theory [59] can be applied to only adiabatic (strong coupling) system. However, in enzyme or protein, the ET process usually occur between donor and acceptor with a weak coupling. Therefore, improved versions of the Marcus theory have been formulated, e.g. the Marcus-Hush theory [60], and the Kakitani-Mataga (KM) theory [61]. The KM theory can apply for both strong coupling (adiabatic) and weak coupling (non-adiabatic) PET processes. In the present works KM theory was used because it can well reproduce experimental fluorescence lifetimes and fluorescence decays of flavoproteins.[31-42] The KM theory is express in the following equation.

$$k_{ET} = \frac{v_0}{1+\exp\left\{\beta(R-R_0)\right\}}\sqrt{\frac{k_B T}{4\pi\lambda_S}}\exp\left[-\frac{\left\{\Delta G^0 - e^2/\varepsilon_0 R + \lambda_S + ES\right\}^2}{4\lambda_S k_B T}\right] \qquad (1.1)$$

where v_0 is a frequency and β is a coefficient related to ET process. The ET process has been classified to be adiabatic when $R < R_0$, and non-adiabatic when $R > R_0$ where R is defined as the center-to-center distance and R_0 is the critical distance. The standard free energy change (ΔG^0) is expressed by $E_{IP(donor)}$ (ionization potential of electron donor) and $G^0_{ISO(acceptor)}$ (standard Gibbs energy related to electron affinity of the excited acceptor), as shown in eqn (1.2).

$$\Delta G^0 = E_{IP(donor)} - G^0_{ISO(acceptor)} \qquad (1.2)$$

In addition, since all the experimental values related to electron transfer in enzyme are measured from ensemble of conformations, molecular dynamics (MD) simulation technique is employed to include structural dynamics of DAAO in the ET calculations. The MD simulation also allows the investigation of important interaction between DAAO and its inhibitors at molecular level.

1.1.3 Virtual screening

In a search for new drug, especially for costly target, a virtual screening (VS) technique is usually and widely employed because it can quickly search chemical structures from large libraries to identify potential candidate (hits) inhibiting the target. As all the processes are done in computer, it can greatly reduce the budget. Several criteria, typically drug-like properties and molecular docking, can be used to screen out inappropriate compounds. In this work, relationship between chemical properties (e.g. electron transfer or structural dynamics) and inhibitory activity is explored in order to establish effective criteria for virtual screening of DAAO inhibitors. All the obtained information will be helpful for designing novel DAAO inhibitor as a target for treatment of schizophrenia.

1.2 RESEARCH OBJECTIVES

1.2.1 To investigate electron transfer process and the structural properties of pkDAAO and pkDAOB.

1.2.2 To explore novel inhibitors of hDAAO by virtual screening technique.

1.3 RESEARCH METHODOLOGY

In this thesis, focusing on only DAAO from pig kidney and human, which were divided in two parts. Namely, part 1 concerns an electron transfer analyses on pig kidney DAAO because there are many fluorescence results from the experiments. The detailed calculations, results and discussions are given in Chapters II-IV as research articles. In part 2, DAAO from human was studied by virtual screening technique to find

the novel inhibitors for schizophrenia treatment. The details for methodology, results and discussions are contained as a manuscript in Charter V. The Scheme for the overview of this dissertation is shown in Figure 1.8.

All articles, which were published, are part of this dissertation in partial fulfillment of requirements for the degree of Doctor of Philosophy in Chemistry at Chulalongkorn University.
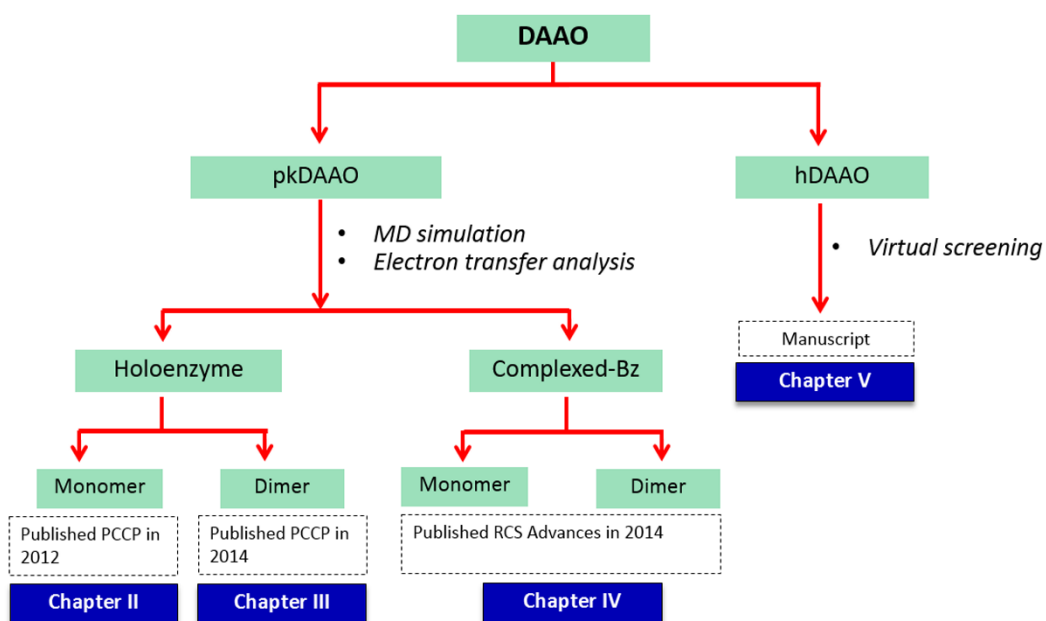
Figure 1.8 *Scheme for the overview of this dissertation.*

1.3.1 Photo-induced electron transfer analysis

The procedure related to the ET rate and physical quantities in the ET theory calculation is described below and demonstrated in Figure 1.9;

1.3.1.1 The time-dependent DAAO conformations of pkDAAO were obtained by using MD simulation method.

1.3.1.2 The ET rates contain several parameters as v_0^q, β^q and R_0^q for Tyr and Trp, G_{Iso}^0 and ε_0 were determined by the KM theory, given by eqn (1.1).

1.3.1.3 The assume initial values for the ET analysis were obtained from the previously related work [42].

1.3.1.4 The fluorescence lifetimes were calculated by taking the average over the MD simulation time.

1.3.1.5 The minimum chi-square was calculated in order to justify the best-fit between the calculated and observed fluorescence decay.

1.3.1.6 The new ET parameters were generated by the non-linear least square method. The calculation was being processed until less chi-square value than the previous calculation was obtained. Step 1.3.1.4 to 1.3.1.6 were repeated until the minimum value of the chi-square is obtained.

Determination the time-dependent atomic coordinates in a protein by MD simulation.

ET rate (ET parameters)

Set initial values of ET parameters

Calculate fluorescence decays with ET rate using the ET parameters

Calculate chi-square between the observed and calculated fluorescence lifetimes

Set new ET parameters so as to obtain smaller value of the chi-square, by a non-linear least-square method

Calculate ET rate, related physical quantities and fluorescence lifetimes with the best-fit ET parameters, when the minimum value of chi-square is obtained

Figure 1.9 *The overall processes for ET analysis.*

1.3.2 Virtual screening

Virtual screening (VS) is used in drug discovery to search and screen small molecules in order to discover novel candidate compounds, which may be develop to new drug in the future. It is sequential scheme in Figure 1.10, more details as below;

1.3.2.1 Generate 3D pharmacophore model from ligand template by SYBYL-X 2.0.

1.3.2.2 Use pharmacophore model to screen on the Namiki chemical compound database (4 million compounds).

1.3.2.3 Use the binding pocket surface constrains to reduce the number of compounds.

1.3.2.4 Classify the active and the inactive compounds by means of binary QSAR using correlation of the structural properties and the biological activity.
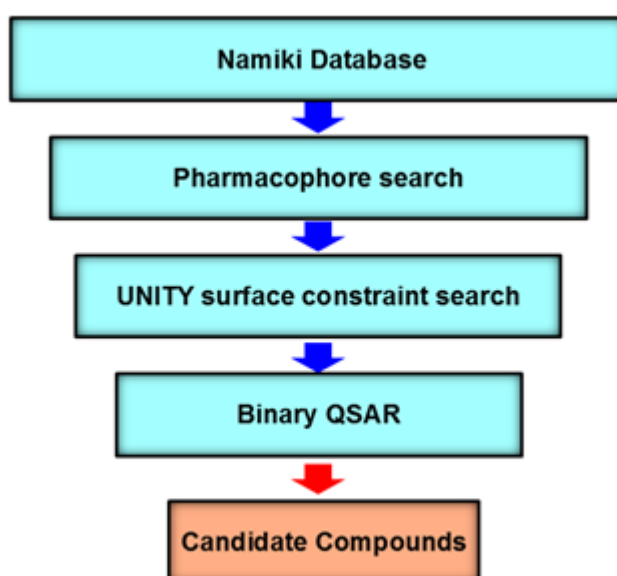
Figure 1.10 *The overall procedures of virtual screening.*

1.4 SCOPE OF THIS DISSERTATION

In this dissertation, the purpose is to investigate the ET rate in pkDAAO using MD simulation and the KM ET theory. Significant parameters affecting the ET rate are elucidated. Relationship between inhibitory activity and chemical properties, which are related to ET rate, structural dynamics, and DAAO-inhibitor interactions, are explored in order to establish effective criteria for virtual screening of DAAO inhibitors.

1.5 EXPECTED BENEFICIAL OUTCOMES

1.5.1 Fundamental information of structural and dynamics properties of pkDAAO and pkDAOB both monomer and dimer forms.

1.5.2 Discovery of the potent hDAAO inhibitors for schizophrenia treatment.

From this dissertation, in pkDAAO part, we anticipate that combining these results should provide the understanding in ET and the relationship of parameters which influential upon the ET rate for DAAO. For hDAAO part, it is hope that these results could be useful for obtaining high potent DAAO inhibitors. Furthermore, it may be utilized as a basic knowledge for novel drug discovery in the future.

CHAPTER II

STRUCTURAL BASIS FOR THE TEMPERATURE-INDUCED TRANSITION OF D-AMINO ACID OXIDASE FROM PIG KIDNEY REVEALED BY MOLECULAR DYNAMIC SIMULATION AND PHOTO-INDUCED ELECTRON TRANSFER

Structural Basis for the Temperature-Induced Transition of D-Amino Acid Oxidase from Pig Kidney Revealed By Molecular Dynamic Simulation and Photo-Induced Electron Transfer

Arthit Nueangaudom[a], Kiattisak Lugsanangarm[a], Somsak Pianwanit[a,b], Sirirat Kokpol[a,b], Nadtanet Nunthaboot[c] and Fumio Tanaka[a,d]

[a] Department of Chemistry, Faculty of Science, Chulalongkorn University, 254 Phayathai Road, Bangkok 10330, Thailand.

[b] Center of Excellence for Petroleum, Petrochemicals, and Advanced Materials, Chulalongkorn University, Bangkok 10330, Thailand.

[c] Department of Chemistry, Faculty of Science, Mahasarakham University, Thailand.

[d] Division of Laser Biochemistry, Institute for Laser Technology, Utsubo-Honmachi, 1-8-4, Nishiku, Osaka 550-0004, Japan.

2.1 ABSTRACT

The structural basis for the temperature-induced transition in the D-amino acid oxidase (DAAO) monomer from pig kidney was studied by means of molecular dynamic simulations (MDS). The center to center (Rc) distances between the isoalloxazine ring (Iso) and all aromatic amino acids (Trp and Tyr) were calculated at 10 °C and 30 °C. Rc was shortest in Tyr224 (0.82 and 0.88 nm at 10 and 30 °C, respectively), and then in Tyr228. Hydrogen bonding (H-bond) formed between the Iso N1 and Gly315 N (peptide), between the Iso N3H and Leu51 O (peptide) and between the Iso N5 and Ala49 N (peptide) at 10 °C, whilst no H-bond was formed at the Iso N1 and Iso N3H at 30 °C. The H-bond of Iso O4 with Leu51 N (peptide) at 10 °C switched to be with Ala49 N (peptide) at 30 °C. The reported fluorescence lifetimes (228 and 182 ps at 10 and 30 °C, respectively), of DAAO were analyzed with Kakitani and Mataga (KM) ET theory. The calculated fluorescence lifetimes displayed an excellent agreement with the observed lifetimes. The ET rate was fastest from Tyr224 to the excited Iso (Iso*) at 10 °C and from Tyr314 at 30 °C, despite that the Rc was shortest between Iso and Tyr224 at the both temperatures. This was explained by the electrostatic energy in the protein. The difference in the observed fluorescence lifetimes at 10 and 30 °C were ascribed to the difference in electron affinity of the Iso* at both temperatures, in which the free energies of the electron affinity of Iso* at 10 and 30 °C were -8.69 eV and -8.51 eV respectively. The other physical quantities related to ET did not differ appreciably at both temperatures. The electron affinities at both temperatures were calculated with a semi-empirical molecular orbital method (MO) of PM6. Mean calculated electron affinities over 100 snapshots with 0.1 ps intervals were -7.69 eV at 10 °C and -7.59 eV at 30 °C. The difference in the calculated electron affinities, -0.11 eV was close to the observed difference in the free energies, -0.18 eV. The present quantitative analysis predicts that the highest ET rate can occur from a donor with longer donor-acceptor distance, which was explained by differences in electrostatic energy.

2.2 INTRODUCTION

D-Amino acid oxidase (DAAO) is a peroxisomal enzyme, containing flavin adenine dinucleotide (FAD) as a cofactor, that exists in a wide range of species from yeasts to human.[62] Its function is to oxidize D-amino acids to the corresponding imino acids, producing ammonia and hydrogen peroxide. Recently, mammalian DAAO has been demonstrated to connect with the brain D-serine metabolism and to the regulation of the glutamatergic neurotransmission.[63, 64] DAAO from pig kidney is in a monomer (Mw 40 kDa) - dimer equilibrium state at relatively low concentrations,[23-26, 65] and may be in a dimer - tetramer equilibrium at higher concentrations.[27-29]

A temperature-induced conformational change (temperature-transition) of DAAO was first reported by Massey et al.,[66] who showed that the tryptophan fluorescence displayed a temperature transition at around 15 °C. The Arrhenius plot of the enzyme activity was non-linear and best expressed by two straight lines with different activation energies. Koster and Veeger [67] concluded from their study of the enzyme activity that there is a temperature-dependent equilibrium between the high and low temperature states, whilst Shiga and Shiga [30] reported that the equilibrium constant of association from the monomer to dimer state exhibited a discontinuous change at 18 °C as the temperature was varied. Despite these findings, however, a differential scanning micro-calorimetric study indicated no evidence for the expected specific heat change at the transition temperature.[68] The temperature transition of DAAO has been systematically investigated by measuring the fluorescence lifetimes of FAD in a picoseconds time domain, by changing the protein concentration and temperature.[18] Temperature-dependent quenching constants of FAD were expressed by the absolute rate theory. Both the activation enthalpy gap and the entropy gap of DAAO displayed different values in the lower and higher temperature ranges, but not in free FAD.

Crystal structures of various forms of DAAO have been determined. The three-dimensional structure of the pig kidney DAAO – benzoate complex was first determined by Mattevi et al. [69] and Mizutani et al. [19] The structures of reduced DAAO complexed with imino Trp and a covalent adduct of DAAO with methyl-2-oxo-

valeic acid were also determined by Todone et al.[70] The crystal structures of DAAO–*o*-amino benzoate and a purple intermediate of pig kidney DAAO were determined by Miura et al. [71] and Mizutani et al. [72], respectively. The three-dimensional structure of human DAAO was first determined by Kawazoe et al.[73] Molecular dynamic simulation (MDS) has been established as a useful tool to understand the dynamic behavior of protein structures. Tilocca et al. [74] theoretically studied the activation energy of D-alanine oxidation catalyzed by DAAO, by means of MDS. Recently, the dynamic structure of DAAO and the reactivity of molecular oxygen penetrated into its active site was studied by means of MDS by Saam et al.[75]

Since Weber discovered the fluorescent emission from flavins,[4] fluorescence spectroscopy has been a useful tool to study the conformational change of flavoproteins. In particular, time-resolved fluorescence spectroscopy has provided precise information on the dynamics of the molecular interactions between the excited isoalloxazine ring (Iso*) and the surrounding amino acids.[8, 10] The fluorescence lifetimes of DAAO and its benzoate complex have been determined in the picoseconds time domain.[17, 76, 77] In many "non-fluorescent" flavoproteins, a fluorescence with sub-picosecond lifetimes has been observed when the proteins were excited with ultra short pulse lasers.[12-16] The remarkable fluorescence quenching in these flavoproteins is ascribed to photoinduced electron transfer (ET) from the aromatic amino acids, as Trp and Tyr, to Iso*.[5-7] The short fluorescence lifetimes in DAAO compared to free FAD[16] are considered to be due to the ET from the aromatic amino acids to Iso*.

Since the seminal work on electron transfer theory by Marcus,[78-80] several researchers have further developed the Marcus ET theory.[81-86] The ET rates in flavoproteins [32, 33, 39-42, 87] have been analyzed with ultrafast fluorescence dynamics experimentally obtained and Kakitani and Mataga (KM) theory,[84-86] using the atomic coordinates obtained by MDS.[32, 33, 39-42, 87]

Although a number of workers have experimentally demonstrated the temperature-transition, as described above,[18, 30, 66-68] no work has provided a structural basis for this temperature-transition. In the present work we have

demonstrated the structural basis for the temperature-transition in the pig kidney DAAO monomer, by means of MDS and KM ET theory.

2.3 METHODS OF ANALYSES

2.3.1 MDS calculations

The starting structure of the pig kidney DAAO monomer was obtained from using the X-ray structure of the DAAO – benzoate complex dimer (PDB code 1VE9),[69] removing benzoate and one of the subunits. All calculations were carried out using the AMBER 10 suite of programs.[88] The parm99 force field [89] was used to describe the protein atoms whereas the general Amber force field [90] with the restrained electrostatic potential (RESP) [91] charges was used for the ligand and FAD. All missing hydrogen atoms of the protein were added using the LEap module of AMBER 10. The simulated systems were subsequently solvated with a cubic box of 3,230 TIP3P water molecules. The electroneutrality of the system was attained by adding four sodium counterions. The added water molecules were first minimized, while the protein and FAD coordinates were kept fixed. Then, the system was relaxed by performing two steps of energy minimization. In the first step, the protein-ligand complex structure was kept fixed by a 500 kcal/mol force constant, while the water molecules and counterions were allowed to adjust their positions by applying 2,000 steps of steepest descent followed by 3,000 steps of conjugate gradient of energy minimization. Subsequently, the second step of energy minimization was employed using the same protocols as just described except that the force constraint was not applied for all atoms in the system. Afterwards, a position-restrained MDS phase, meaning that positions of the protein and FAD were restrained with a weaker force constant of 100 kcal/mol, was performed through the first 100 ps. Both systems were heated from 0 K to 283 K or 0 K to 303 K (for the 10 and 30 $^\circ$C MDS, respectively) over 100 ps and were further equilibrated under periodic boundary conditions at 283 K and 303 K. The systems were set up under the isobaric-isothermal ensemble with a constant pressure of 1 atm and constant temperature of either 283 K or 303 K. Electrostatic interactions were corrected by the Particle Mesh Ewald method.[92] The SHAKE algorithm [93] was

employed to constrain all bonds involving hydrogen atoms. A cutoff distance of 1 nm was employed for non-bonded pair interactions. MDS based calculations were performed with a time steps of 2 fs and the coordinates of the MDS snapshots were collected every 0.01 ps. The stability of the system was checked by investigating the convergence of the energies, temperature, pressure and global root mean square deviation of the system. The equilibrium was found to be attained after 20 ns of the MDS calculation, by monitoring these quantities. Then the calculation was continued for up to a further 30 ns, and data from the last 10 ns were used for the analyses.

2.3.2 Residue-based root of mean square fluctuation (RMSF)

The residue-based RMSF of each amino acid, which indicates the structural flexibility for each amino acid residue, was obtained by superposition of the trajectory conformations and the reference conformation of the investigated amino acid over the equilibrium MDS snapshots using the *ptraj* module of the Amber program.[88] The RMSF is defined as $RMSF(i) = \sqrt{\left\langle \left(R_i - \langle R_i \rangle \right)^2 \right\rangle}$, where R_i is the position vector of atom *i* (in this work, C_A, N and O atom coordinates were evaluated). The chevron brackets represent the time average over the whole trajectory (10 ns).

2.3.3 ET theory

The original Marcus theory [78-80] has been modified in various ways.[81-86] In the present analysis, KM - ET theory [84-86] was used, because it is applicable for non-adiabatic ET process in addition to adiabatic ET process, and has been found to give satisfactory results for both static [11, 94, 95] and dynamic ET analyses.[32, 33, 39-42, 87] The ET rate described by the KM theory is expressed by eqn (2.1).

$$k_{ET}^{j}\left(T\right) = PE \exp\left[-\frac{\left\{ \Delta G_q^0 - e^2 / \varepsilon_0^q R_j + \lambda_S^{qj} + ES_j \right\}^2}{4\lambda_S^{qj} k_B T} \right] \tag{2.1}$$

The pre-exponential factor (*PE*) is given by eqn (2.2).

$$PE = \frac{v_0^q}{1+\exp\left\{\beta^q\left(R_j - R_0^q\right)\right\}}\sqrt{\frac{k_B T}{4\pi\lambda_S^{qj}}}$$ (2.2).

Here $k_{ET}^j(T)$ is the ET rate from a donor j to the Iso* at temperature T (°C), and q denotes Trp or Tyr. v_0^q is an adiabatic frequency, β^q is the ET process coefficient. R_j and R_0^q are the donor j–Iso distance and its critical distance for the ET process, respectively. R_j is expressed as a center-to-center (Rc) distance rather than as an edge-to-edge (Re) distance.[32, 33, 39-42, 87] The ET process is adiabatic when $R_j < R_0^q$, and non-adiabatic when $R_j > R_0^q$. T in the right hand sides of eqn (2.1) and (2.2) is temperature, but expressed in K. The terms k_B and e are the Boltzmann constant and electron charge, respectively. ES_j is the electrostatic (ES) energy of the donor j, which is described below.

The pig kidney DAAO monomer contains 10 Trp and 14 Tyr residues. In the present work the ET rates from all of these aromatic amino acids to Iso* were taken into account for the analysis.

λ_S^{qj} is the solvent reorganization energy [78-80] of the ET donor qj, and is expressed as eqn (2.3).

$$\lambda_S^{qj} = e^2\left(\frac{1}{2a_{Iso}} + \frac{1}{2a_q} - \frac{1}{R_j}\right)\left(\frac{1}{\varepsilon_\infty} - \frac{1}{\varepsilon_0^q}\right)$$ (2.3)

where a_{Iso} and a_q are the radii of Iso and Trp or Tyr, with these reactants being assumed to be spherical, and ε_∞ and ε_0^q are the optical and static dielectric constants, respectively. In this study, the optical dielectric constant used was 2.0. The radii of Iso (a_{Iso}), Trp (a_{Trp}) and Tyr (a_{Tyr}) were those previously determined [32, 33, 39-42, 87] to be 0.224, 0.196 and 0.173 nm, respectively.

The standard free energy change was expressed with the ionization potential of the ET donor, E_{IP}^q, as eqn (2.4).

$$\Delta G_q^0 = E_{IP}^q - G_{Iso}^0$$ (2.4)

where G_{Iso}^0 is the standard Gibbs energy related to the electron affinity of Iso*. The values of E_{IP}^q for Trp and Tyr were 7.2 eV and 8.0 eV, respectively.[96]

2.3.4 Electrostatic energy in DAAO

Protein systems contain many ionic groups, which may influence the ET rate. The pig kidney DAAO contains Iso as the ET acceptor, and 10 Trp residues and 14 Tyr residues as potential ET donors. The FAD cofactor in DAAO has two negative charges at the pyrophosphate, whilst DAAO itself contains 22 Glu, 13 Asp, 12 Lys and 21 Arg residues.

The *ES* energy between the Iso anion radical or donor cation *j* and all other ionic groups in the protein is expressed by eqn (2.5).

$$E(j) = \sum_{i=1}^{22} \frac{C_j C_{Glu}}{\varepsilon_0 R_j(Glu-i)} + \sum_{i=1}^{13} \frac{C_j C_{Asp}}{\varepsilon_0 R_j(Asp-i)}$$
$$+ \sum_{i=1}^{12} \frac{C_j C_{Lys}}{\varepsilon_0 R_j(Lys-i)} + \sum_{i=1}^{21} \frac{C_j C_{Arg}}{\varepsilon_0 R_j(Arg-i)} + \sum_{i=1}^{4} \frac{C_j C_P}{\varepsilon_0 R_j(P-i)} \tag{2.5}$$

where *j* = 0 for the Iso anion radical, 1 - 10 for the Trp cation radicals and 11 - 24 for the Tyr cation radicals. C_j is the charge of the aromatic ionic species *j*, that is -*e* for *j* = 0 and +*e* for *j* = 1 to 24. C_{Glu} (= - *e*), C_{Asp} (= - *e*), C_{Lys} (= + *e*), and C_{Arg} (= + *e*) are the charges of the Glu, Asp, Lys and Arg residues, respectively. FAD contains 2 phosphate atoms, each of which binds 2 oxygen atoms. It was assumed that the charge of each oxygen atom is C_P = -0.5*e*, though total charge of two phosphate atoms is -2*e*. We assumed that these groups are all in an ionic state in solution. The distances between the aromatic ionic species *j* and the *i*th Glu (*i* = 1 – 22) are denoted as $R_j(Glu-i)$, whilst the distances between the aromatic ionic species *j* and the *i*th Asp (*i* = 1 – 13) are denoted as $R_j(Asp-i)$, and so on for the each amino acid residue.

ES_j in eqn (2.1) was then expressed as follows in eqn (2.6).

$$ES_j = E(0) + E(j) \tag{2.6}$$

Here j is from 1 to 24, and represents the jth ET donor, as described above.

2.3.5 Determination of the ET parameters

The observed fluorescence lifetimes of the pig kidney DAAO monomer are reported to be τ_{obs}^{10} = 228 ps at 10 °C and τ_{obs}^{30} = 182 ps at 30 °C.[18] The calculated lifetimes at temperature T were given by eqn (2.7).

$$\tau_{calc}^{T} = 1 / \sum_{j=1}^{24} k_{ET}^{j}(T) \qquad (2.7)$$

The fluorescent lifetimes were expressed in ps. In the present work the physical quantities related to the electronic coupling (v_0^q, β^q and R_0^q) for Trp and Tyr were taken from those reported for the flavin mononucleotide binding proteins,[39] which were assumed to be independent of temperature within the temperature range (10-30 °C) of the present work. The unknown quantities were $\varepsilon_0(T)$ and $G_{Iso}^{0}(T)$ at the temperatures 10 °C and 30 °C. The other physical quantities were calculated from the atomic coordinates obtained by MDS at 10 °C and 30 °C.

$\varepsilon_0(10)$, $\varepsilon_0(30)$, $G_{Iso}^{0}(10)$ and $G_{Iso}^{0}(30)$ were determined so as to obtain the minimum value of χ^2, as given by eqn (2.8).

$$\chi^2 = \frac{1}{2}\left[\left(\tau_{obs}^{10} - \tau_{calc}^{10} \right)^2 + \left(\tau_{obs}^{30} - \tau_{calc}^{30} \right)^2 \right] \qquad (2.8)$$

2.3.6 Molecular orbital method

The heat of formations of Iso anion radical and Iso* were calculated by a semi-empirical molecular orbital (MO) method with a software package of the MOPAC2009. The key words, EF (geometrical optimization), PRECISE (accurate calculation), RM1 (semi-empirical Hamiltonians), XYZ (geometry expressed by (x, y, z) coordinates), GEO-OK (neglect check on abnormal access of atoms), EPS (dielectric constant for COSMO solvation energy). The details of these Keywords are found on the website:

http://openmopac.net. In addition to these key words, the key word UHF and CHARGE = -1 were used for Iso anion radical, and C.I. = 8 (configuration interaction with eight microstates), SINGLET and ROOT = 2 were used for Iso*. The values of EPS (ε_0) were obtained by ET analysis, described above.

2.4 RESULTS

2.4.1 Geometrical factors near Iso

Figure 2.1 shows snapshots of the local pig kidney DAAO structures near the Iso binding site and showing the potential ET donors to Iso* at 10 and 30 $^\circ$C, where clear structural differences between the structures at the two temperatures are apparent, especially around the Tyr314 and Tyr55 region.
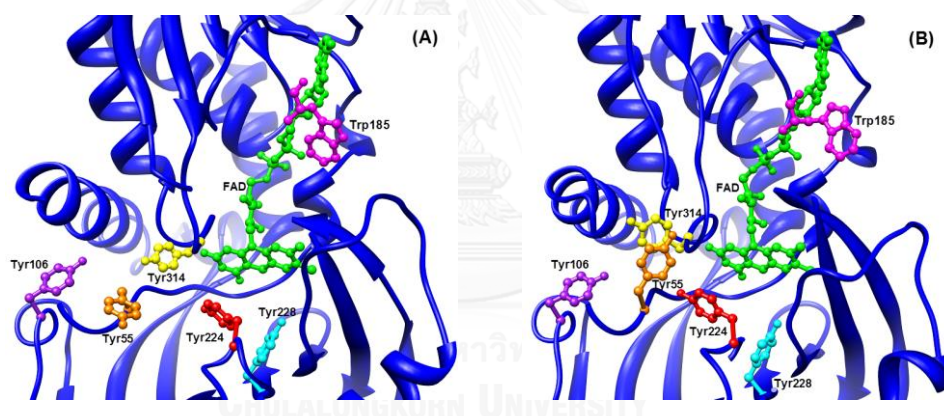
Figure 2.1 *Snapshots of the pig kidney DAAO monomer near the Iso binding site at (A) 10 $^\circ$C and (B) 30 $^\circ$C. The ball and stick models of FAD and six aromatic amino acid residues (Tyr55, Tyr106, Tyr224, Tyr228, Tyr314 and Trp185) are shown in green, orange, purple, red, cyan, yellow and magenta colors, respectively.*

Figure 2.2 shows the time evolution of the center-to-center distances (Rc) between the Iso and the five closest aromatic amino acids that are potential ET donors, with the dramatic change in the Rc value of Trp185/Tyr55 as the temperature changed from 10 to 30 $^\circ$C. The mean Rc values from over the 10 ns (0.1 ps time intervals) MDS time range is shown in Table 2.1. The aromatic amino acid with the shortest Rc donor-

acceptor distance was found to be Tyr224 at both temperatures (0.82 and 0.88 nm at 10 and 30 °C, respectively), followed by Tyr228 and then Tyr314. Tyr224, Tyr228 and Tyr314 are also the three closest residues to Iso in terms of the edge-to-edge distances (Re).
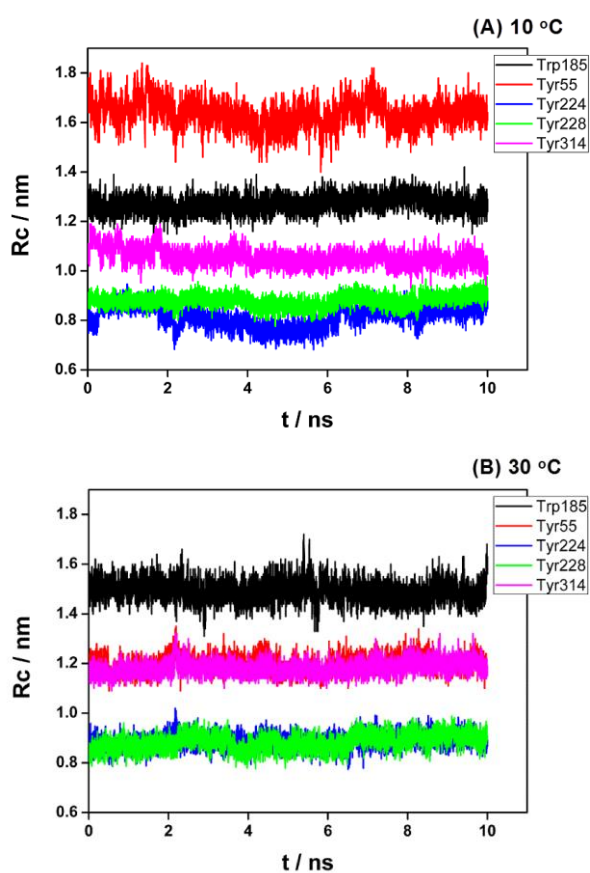
Figure 2.2 *Center to center (Rc) distance between the Iso and the indicated five nearby aromatic amino acid residues (potential ET donors) at (A) 10 °C and (B) 30 °C.*

Table 2.1 Mean values of Rc, Re and inter-planar angles between Iso and nearby aromatic amino acid residues.[a]

	Trp185		Tyr55		Tyr106		Tyr224		Tyr228		Tyr314	
	10 °C	30 °C	10 °C	30 °C	10 °C	30 °C	10 °C	30 °C	10 °C	30 °C	10 °C	30 °C
Rc (nm)	1.27	1.49	1.64	1.20	1.86	1.78	0.82	0.88	0.88	0.88	1.06	1.18
Re (nm)	0.61	0.84	1.09	0.70	1.10	1.09	0.43	0.59	0.42	0.44	0.45	0.54
Angle (°)	-20.70	-58.96	-63.85	-49.05	-9.95	36.39	-32.80	-18.60	52.55	68.68	26.80	-47.01

[a] The mean values were obtained over 100,000 snapshots. Rc and Re denote center-to-center distance and edge-to-edge distance.

Figure 2.3 shows a comparison of the time-evolution of the Rc distances between Iso and Tyr314 and Tyr224 for the two different temperatures (10 °C and 30 °C). In both amino acid residues the Rc values rapidly fluctuated around a central definitive value at 30 °C, whilst at 10 °C the Rc values varied greatly and with a rather long period, in addition to rapid fluctuation. The mean distance from Iso to Tyr224 and Tyr 314 was shorter at 10 °C by 0.02 and 0.09 nm, respectively, compared to that found at 30 °C (Table 2.1). The time-evolution of the inter-planar angles between Iso and the four nearest aromatic amino acids (Trp185, Tyr224, Tyr228 and Tyr314), revealed that the angles mostly fluctuated around ± 20 ° at a definite value (Figure S2.1 in Supplemental Information of Chapter II; note that Tyr 55 and Tyr106 were omitted from Figure S2.1 for clarity as they are too far away). However, the angle of Tyr314 varied far more with time and displayed a sudden change from -50 ° to -100 ° at around 1.2 ns at 10 °C. The time-dependent inter-planar angles of Tyr314 and Tyr224 with Iso were compared between 10 °C and 30 °C in Figure S2.2 (Supplemental Information of Chapter II), and the mean angles for all six nearest aromatic amino acids are also listed in Table 2.1. The angles showed temperature-dependent changes in all cases, but ranged from fairly small (14.2 ° to 16.1 °) in Tyr55, Tyr224 and Tyr228, to fairly large in Trp185 (39.3 °) and Try106 (46.3 °) and very large in Tyr314 (93.8 °).
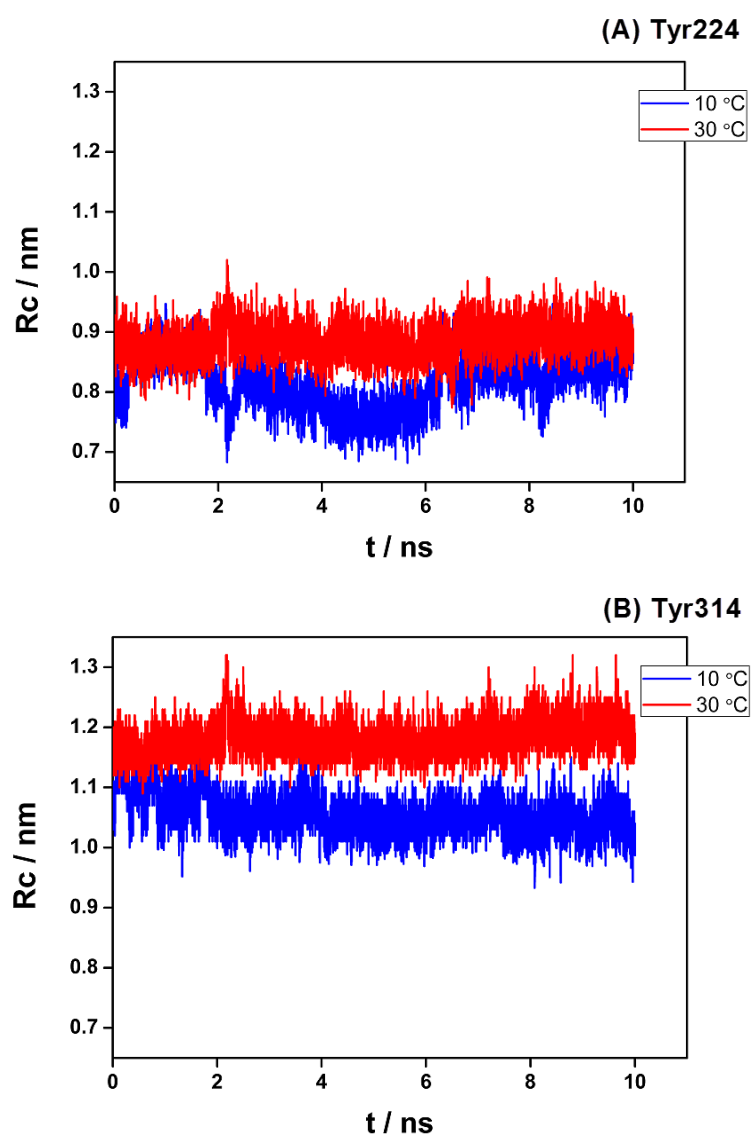
Figure 2.3 *Comparison of the Rc values of (A) Tyr314 and (B) Tyr224 residues at 10 °C and 30 °C. The data for Tyr314 and Tyr224 were selected for display since they show the two fastest ET rates amongst the 24 aromatic amino acids.*

2.4.2 RMSF

The RMSF of each residue in the pig kidney DAAO monomer is shown in Figure 2.4. The RMSF at 30 $^{\circ}$C was appreciably higher than that at 10 $^{\circ}$C for all residues, but the difference in the RMSF (ΔRMSF) between the two temperatures was highest at around Ser60, Asn61 and Pro62, then at around Pro191, Asp192 and Pro193 and finally at around Val244, Gly245 and Asn246. Other significant but lesser ΔRMSF peaks include around residues Pro105-Tyr106-Trp107-Lys108-Asp109, Val164-Glu165-Ser166-Phe167 and Pro284-Val285-Arg286. In these amino acid residues the protein structure should be quite different between the high (30 $^{\circ}$C) and low (10 $^{\circ}$C) temperatures.
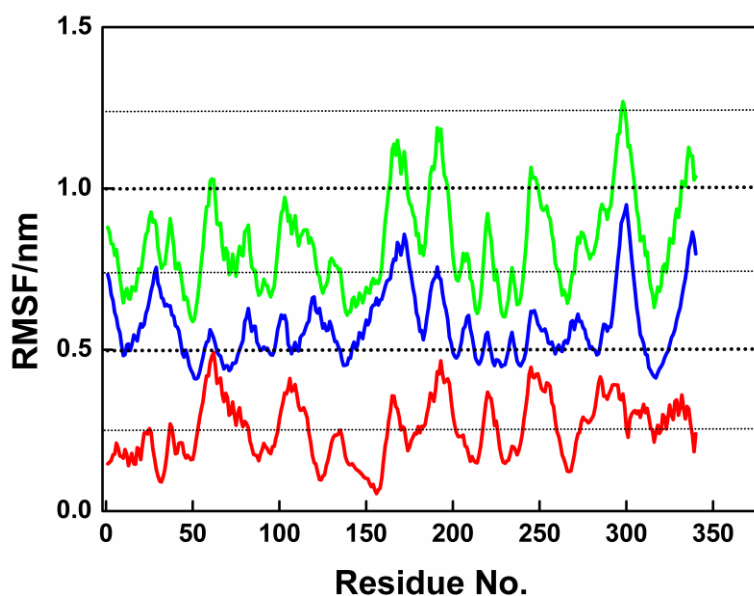
Figure 2.4 *Time-dependent changes in the RMSF. Blue line shows RMSF at 10 $^{\circ}$C, and green line at 30 $^{\circ}$C. Red line shows difference between those at both temperatures.*

Figure 2.5 shows the protein flexibilities at 10 and 30 $^{\circ}$C, defined as rigid, moderate and flexible when the RMSF was < 0.75, 0.75 to 1.0 and > 1.0 nm, respectively. Note that the protein domains are indicated in Figure 2.5B. Protein structures at loops 1- 2 and 4 - 5 were rigid, and at loops 3 and 6 - 7 were moderately flexible at 10 $^{\circ}$C, whilst the structures at loops 3 – 7 were flexible and loops 1 – 2 moderately flexible at 30 $^{\circ}$C. The proportion of protein domains with a flexible part were greatly reduced at 10 $^{\circ}$C compared to that at 30 $^{\circ}$C, whereas the proportion of rigid parts were far more common at 10 $^{\circ}$C than at 30 $^{\circ}$C.
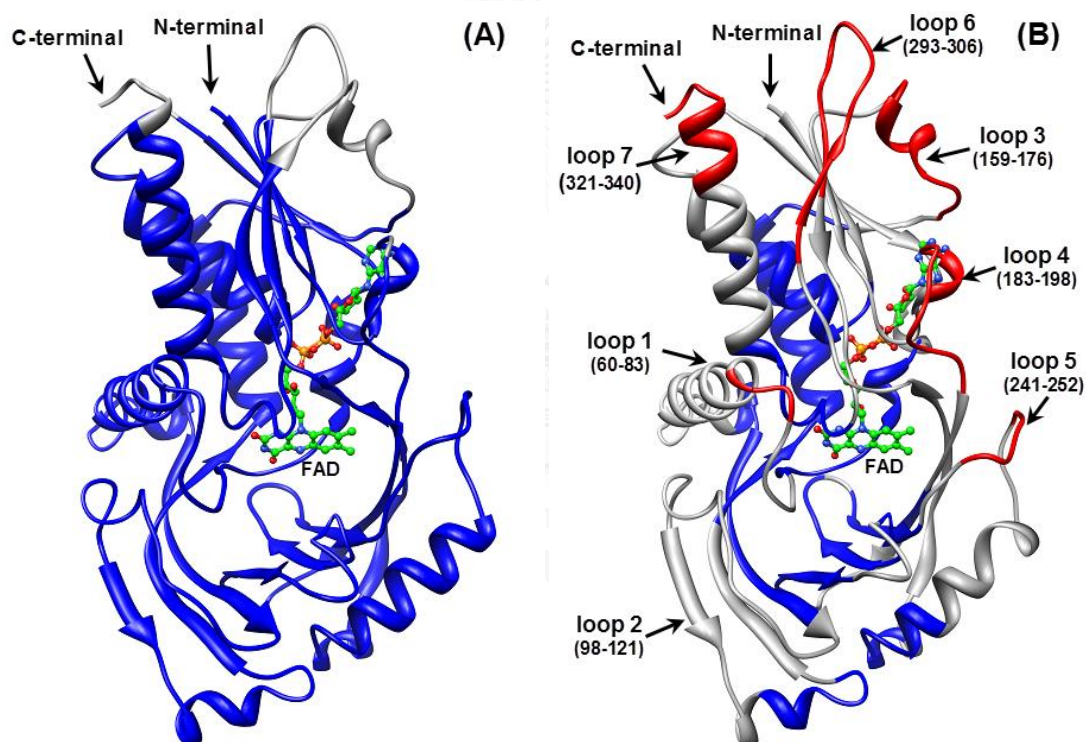
Figure 2.5 *Comparison of the protein flexibility between (A) 10 $^{\circ}$C and (B) 30 $^{\circ}$C. The flexibility is defined as rigid (RMSF < 0.75 nm: blue), moderate (0.75 nm < RMSF < 1.00 nm: gray) and flexible (RMSF > 1.00 nm: red). The structures were determined by taking an average over 10 ns.*

2.4.3 Hydrogen bonding (H-bond) dynamics

H-bond dynamics were compared in the pig kidney DAAO monomer at 10 °C and 30 °C. The time-evolution of the proton donor – acceptor Rc distance between the N atoms in Iso (see Chart 2.1 for atom notations of Iso) and the three nearby aromatic amino acids are shown in Figure 2.6, where the distances were noted to rapidly fluctuate with time, especially at 30 °C but also to show changes between the two temperatures (*e.g.* N3/Leu51 O).

The distances between the Iso O2 or Iso O4 and the respective three nearby amino acids are shown in Figures S2.3 and S2.4 (Supplemental Information of Chapter II), and reveal the aforementioned rapid fluctuations over time and also changes between temperatures. The distance distributions are summarized in Figure 2.7.
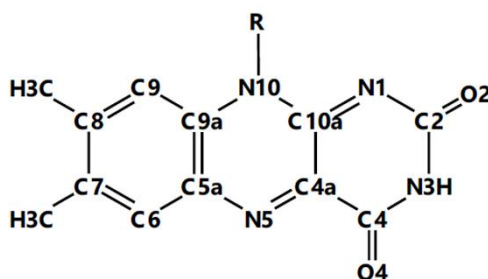
Chart 2.1 Chemical structure of Iso and its atom notations.
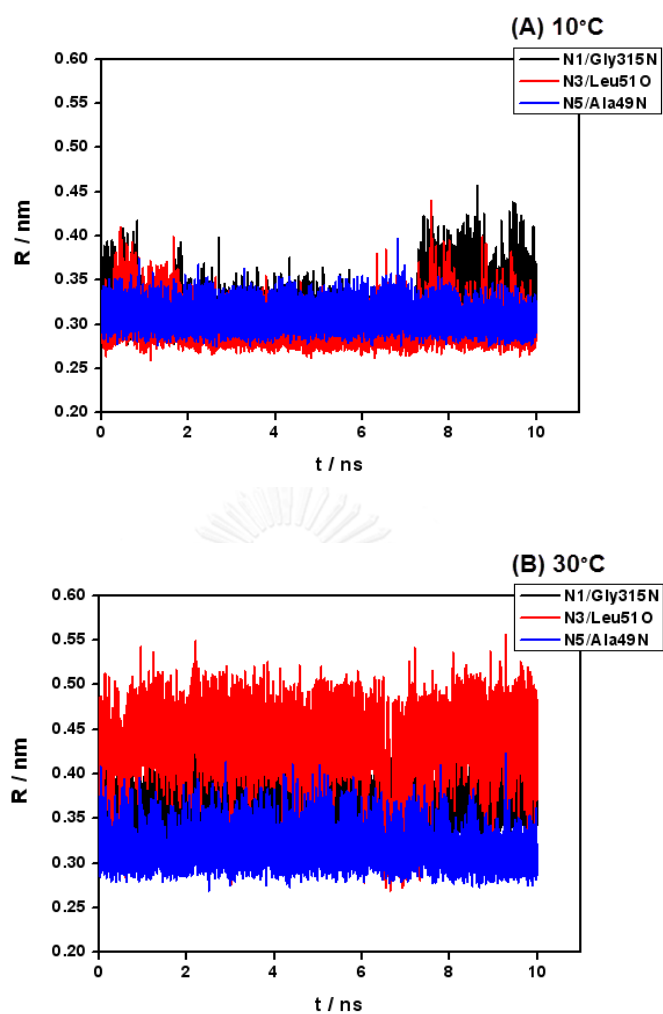
Figure 2.6 *H-bond dynamics between the three N atoms in Iso and the three nearby amino acids at (A) 10 °C and (B) 30 °C.*
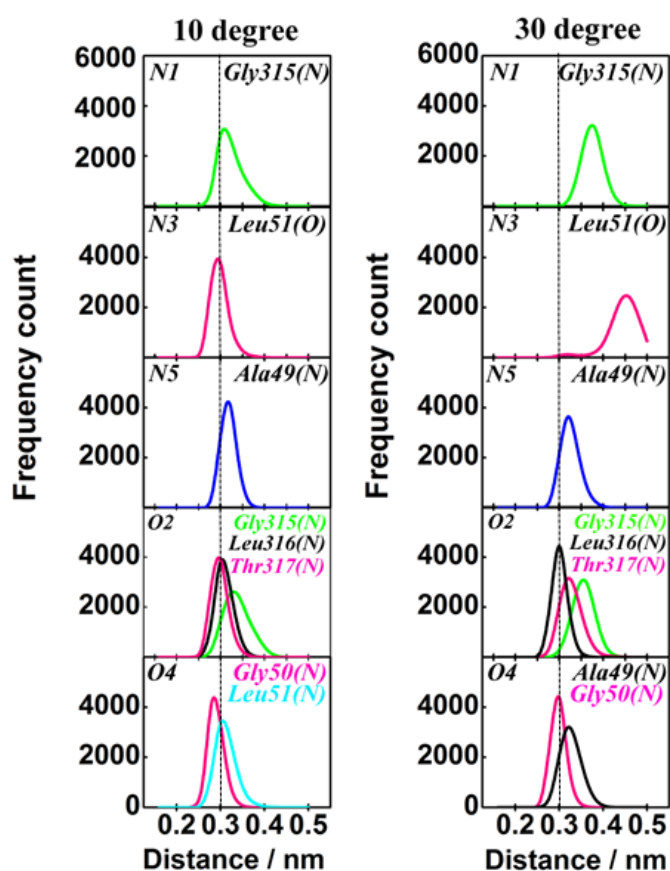
Figure 2.7 *Comparison of the H-bond-distance distributions in DAAO at 10 °C and 30 °C. Proton donor and acceptors in Iso are indicated at the upper left and those of the surrounding amino acids at the right upper section in each panel. Vertical lines at 0.3 nm are shown for ease of comparison between the distributions at both temperatures and represent the likely strong H-bond formation threshold.*

Iso N1 displayed an appreciable distribution within the acceptable H-bond distance (0.35 nm) with the Gly315 N (peptide) at 10 °C, whereas the distribution within 0.35 nm was negligible at 30 °C. This implies that Iso N1 forms an H-bond with Gly315 N (peptide) at 10 °C, but not at 30 °C. The distance distribution between Iso N3H and Leu51 O (peptide) was mostly within 0.35 nm at 10 °C, but at 30 °C two maxima were observed, being a H-bond minority at 0.32 nm and a no H-bond vast majority at around 0.45 nm. Thus, the strong H-bond formation between the Iso N3H and Leu51 O at 10 °C is instead weak or largely absent at 30 °C. In the same analytical manner, Iso

N5 formed an H-bond with Ala49 N (peptide) at both temperatures. Potential proton donors for Iso O2 were the Gly315 N (peptide), Leu316 N (peptide) and Thr317 N (peptide). The distances between Iso O2 and Leu316 N and between Iso O2 and Thr317 N both displayed sharp distributions at around 0.3 nm at 10 °C, whilst the H-bond at Iso O2 formed only with Leu316 N at 30 °C. Here, the distribution of Gly315 N displayed a broad maximum at around 0.35 nm at both temperatures. The potential proton donors for Iso O4 were the Gly50 N (peptide) and Leu51 N (peptide) at 10 °C, but Ala49 N (peptide) and Gly50 N (peptide) at 30 °C. This suggests that the H-bond pairs at Iso O4 were modified when the temperature increased. In summary of the above information, Figure S2.5 (Supplemental Information of Chapter II) illustrates the H-bond pairs between Iso and the surrounding amino acids at 10 °C and 30 °C. In addition, the mean H-bond distances are listed in Table 2.2. The distances obtained by MDS at 10 °C were comparable with those obtained from the crystal structure, but quite different from those obtained by MDS at 30 °C.
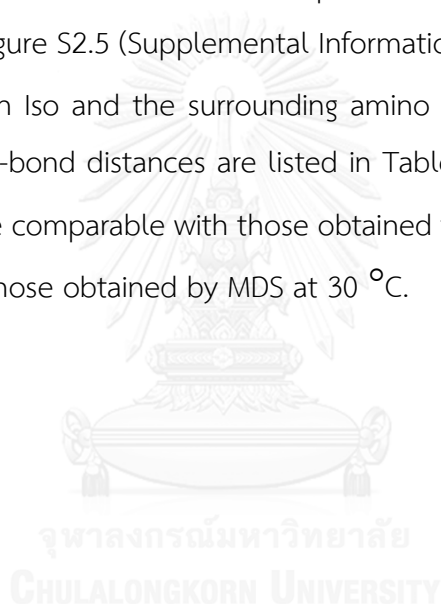
Table 2.2 Comparison of the mean H-bond distances between the Iso atoms and the respective nearby amino acid residues.[a]

H-bond pair	Crystal [a]	MD simulations	
		10 °C	30 °C
N1-Gly315(N)	0.35	0.32	--
N3-Leu51(O)	0.28	0.30	--
N5-Ala49(N)	0.30	0.31	0.32
O2-Gly315(N)	0.35	0.34	0.35
O2-Leu316(N)	0.31	0.31	0.29
O2-Thr317(N)	0.30	0.30	0.32
O4-Ala49(N)	--	--	0.32
O4-Leu51(N)	0.31	0.31	--
O4-Gly50(N)	0.32	0.29	0.29

[a] The H-bond distances shown for the crystal structure were obtained from the previously reported crystal structure (PDB code: 1VE9 [69]).

2.4.4 Physical quantities related to ET

The observed fluorescent lifetimes at 10 °C and 30 °C were 228 ps and 182 ps respectively, as reported previously.[18] The agreement between the observed and calculated lifetimes were exact (Table 2.3), when ε_0^{10} (static dielectric constant at 10 °C) = 5.88, ε_0^{30} = 5.89 at 30 °C, $G_{Iso}^0(10)$ at 10 °C = 8.69 eV and $G_{Iso}^0(30)$ at 30 °C = 8.51 eV. The dielectric constants did not differ at 10 °C and 30 °C. G_{Iso}^0 represents the standard free energy of electron affinity of Iso* and was 0.18 eV higher at 10 °C than at 30 °C, a difference that may be ascribed to the difference in the H-bond pairs between the two temperatures.

Table 2.3 ET parameters determined. [a]

| Temperature (°C) | ε_0 | G^0_{Iso} (eV) | τ (ps) | | χ^2 |
			Obs.	Calc.	
10	5.88	8.69	228	228	4.71×10^{-18}
30	5.89	8.51	182	182	2.79×10^{-13}

[a] ET parameters contained in the pre-exponential term of KM-ET theory were v_0^{Trp} = 1016 (ps^{-1}), from v_0^{Tyr} = 197 (ps^{-1}), β^{Trp} = 21.0 (nm^{-1}), β^{Tyr} = 6.25 (nm^{-1}), R_0^{Trp} = 0.663 (nm) and R_0^{Tyr} = 0.499 (nm). These were taken from those of FMN binding proteins.[11, 39] The observed lifetimes were taken from the previously reported work.[18]

Figure 2.8 shows the time-evolution of the ET rates from the five fastest donors, revealing the changes with time, especially at 10 °C, and the changes with temperature (e.g. Tyr55). For clarity, the mean values of the fastest seven ET rates over the MDS time range at 10 °C are listed in Table 2.4, and at 30 °C in Table 2.5. The ET rate was fastest from Tyr224 at 10 °C and from Tyr314 at 30 °C. The fastest ET rate was greater at 30 °C than at 10 °C. This is in accord with that the observed lifetime was shorter at 30 °C than at 10 °C. The ranked order (fastest to slowest) at 10 °C appeared to be Tyr224, Tyr314, Tyr228, Trp185 and Tyr275. The order at 30 °C was Tyr314, Tyr224, Tyr55, Tyr228 and Tyr106. The order was quite different between the both temperatures.
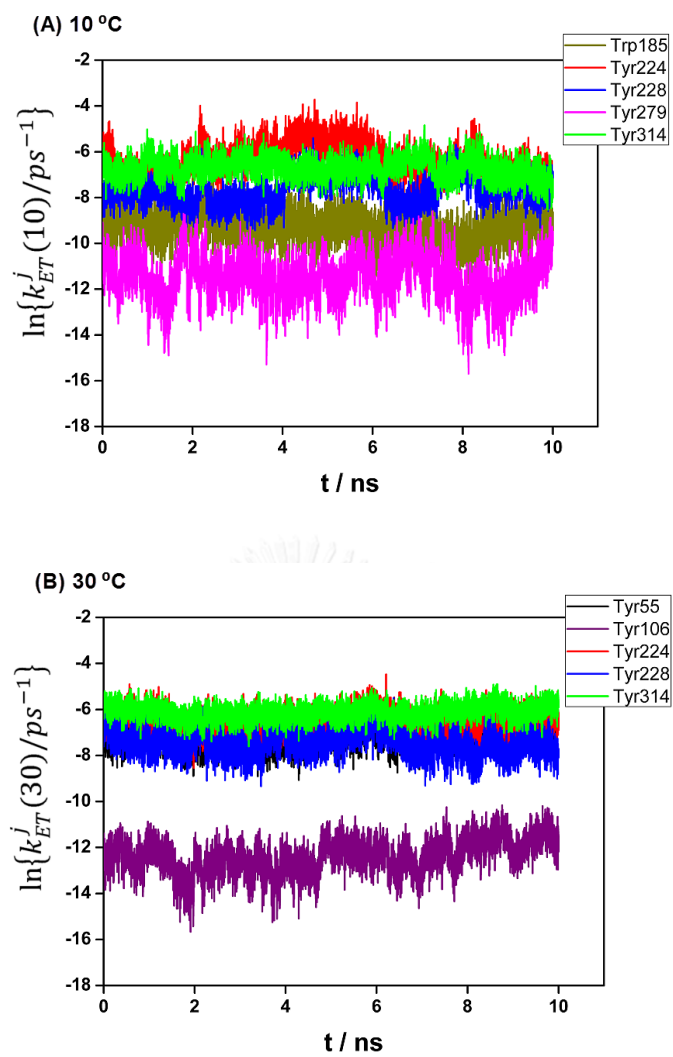
Figure 2.8 *The ET rate from the five indicated fastest aromatic amino acids at (A) 10 °C and (B) 30 °C.*

Table 2.4 Physical quantities related to the ET parameters of the indicated (fastest seven donor) aromatic amino acids at 10 °C [a]

Donor	$k_{ET}^j(10)$ (ps^{-1})	$\ln\{k_{ET}^j(10)/PE\}$	λ_s^{qj} (eV)	ES_j (eV)	$-e^2/\varepsilon_0^q R_j$ (eV)	ΔG_q^0 (eV)	$-\Delta G_T^0$ (eV)
Tyr224	2.27 × 10-3	-12.955	1.848	0.193	-0.311	-0.692	0.801
Tyr314	1.38 × 10-3	-11.936	1.981	-0.074	-0.232	-0.692	0.999
Tyr228	5.92 × 10-4	-13.888	1.891	0.217	-0.279	-0.692	0.755
Trp185	1.16 × 10-4	-6.905	1.897	-0.250	-0.193	-1.492	1.936
Tyr279	1.53 × 10-5	-15.539	2.052	0.145	-0.196	-0.692	0.743
Tyr55	3.63 × 10-6	-14.352	2.141	-0.061	-0.150	-0.692	0.903
Tyr106	3.60 × 10-6	-13.020	2.176	-0.224	-0.132	-0.692	1.049

[a] Meanings of the physical quantities are described in the text below eqn (2.1).

Table 2.5 Physical quantities related to the ET parameters of the indicated (fastest seven donors) aromatic amino acids at 30 °C [a]

Donor	$k_{ET}^j(30)$ (ps^{-1})	$\ln\{k_{ET}^{ji}(30)/PE\}$	λ_S^{qi} (eV)	ES_j (eV)	$-e^2/\varepsilon_0^q R_j$ (eV)	ΔG_q^0 (eV)	$-\Delta G_I^0$ (eV)
Tyr314	2.34 × 10-3	-10.567	2.033	-0.436	-0.207	-0.507	1.150
Tyr224	1.67 × 10-3	-12.702	1.898	-0.035	-0.276	-0.507	0.819
Tyr55	7.93 × 10-4	-11.603	2.038	-0.325	-0.204	-0.507	1.037
Tyr228	6.78 × 10-4	-13.657	1.896	0.051	-0.277	-0.507	0.733
Tyr106	5.39 × 10-6	-13.134	2.169	-0.343	-0.137	-0.507	0.987
Tyr309	4.72 × 10-6	-13.278	2.165	-0.324	-0.139	-0.507	0.970
Tyr279	1.74 × 10-6	-17.463	2.071	0.132	-0.187	-0.507	0.562

[a] Meanings of the physical quantities are described in the text below eqn (2.1).

Time-dependent changes of the net ES energy (ES_j) are shown in Figure 2.9, with considerable rapid variation and longer time oscillations at both temperatures, and from this the mean values of the net ES energies are listed in Tables 2.4 and 2.5 for those at 10 and 30 $^\circ$C, respectively. The net ES energy at 10 $^\circ$C was positive and highest in Tyr228 and lowest in Trp185, whilst at 30 $^\circ$C it was positive and highest in Tyr279 and lowest in Tyr314. The mean net ES energies of Tyr224 and Tyr314, which had the fastest ET rate at 10 $^\circ$C and at 30 $^\circ$C, respectively, were 0.193 and -0.436 eV at 10 and 30 $^\circ$C, respectively.
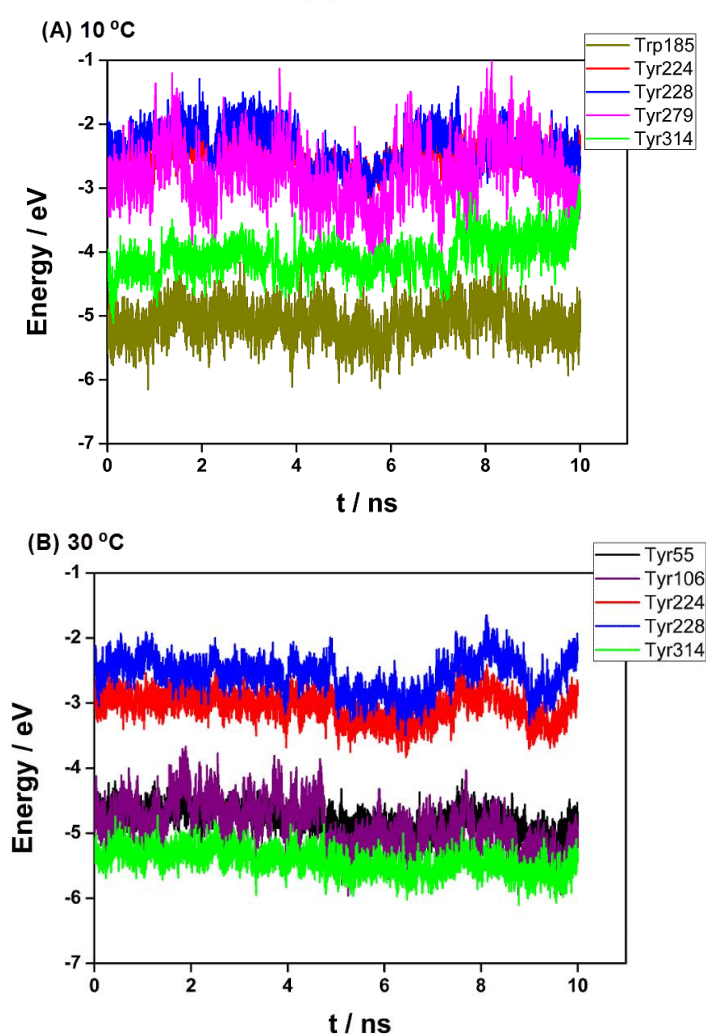
Figure 2.9 *Time-dependent changes in the net ES energy of the five indicated Tyr residues (ET donors) at (A) 10 $^\circ$C and (B) 30 $^\circ$C.*

2.4.5 Energy gap law

The total standard free energy gap of donor j is obtained by eqn (2.9).

$$-\Delta G_T^0\left(j\right) = -\left(ES_j - e^2 / \varepsilon_0 R_j + \Delta G_q^0\right)$$

(2.9)

The mean values $-\Delta G_T^0\left(j\right)$ over the MDS time range of 10 ns (0.1 ps time intervals) were obtained for all 24 potential donor amino acid residues, and those for the seven fastest ET rates are listed in Tables 2.4 and 2.5 for 10 and 30 $^\circ$C, respectively. The normal energy gap law is obtained by plotting $\ln k_{ET}^j\left(T\right)$ against $-\Delta G_T^0\left(j\right)$, and this is shown at both temperatures in Figure 2.10A. The values of $\ln k_{ET}^j\left(T\right)$ were discontinuous along $-\Delta G_T^0\left(j\right)$. Trp and Tyr displayed different functions of $-\Delta G_T^0\left(j\right)$ at both temperatures. The phenomenon has never been reported to occur in other flavoproteins.[32, 39] The reason for it may be that the *PE* in eqn (2.1) is dependent on $-\Delta G_T^0\left(j\right)$. However, *PE* does not depend on $-\Delta G_T^0\left(j\right)$ explicitly, but it may depend on it implicitly through R_j. We define here a reduced energy gap law in eqn (2.10).

$$\ln\left[k_{ET}^j\left(T\right)/PE\right] \propto \left\{\Delta G_T^0\left(j\right) + \lambda_S^{qj}\right\}^2$$

(2.10)

The analysis derived from the use of this reduced energy gap law is shown in Figure 2.10B, where excellent parabolic functions were obtained at both temperatures. In the reduced energy gap law, however, at the maximum value of $k_{ET}^j\left(10\right)/PE$, the ET rate was not always as fast as the normal energy gap law. Thus, the value of $-\Delta G_T^0$ for Tyr224 at 10 $^\circ$C was 0.80 eV and one for Tyr314 at 30 $^\circ$C, 1.15 eV, which had the greatest ET rate, whilst the values of $-\Delta G_T^0$ at a maximum ET rate / *PE* were both 1.9 eV.
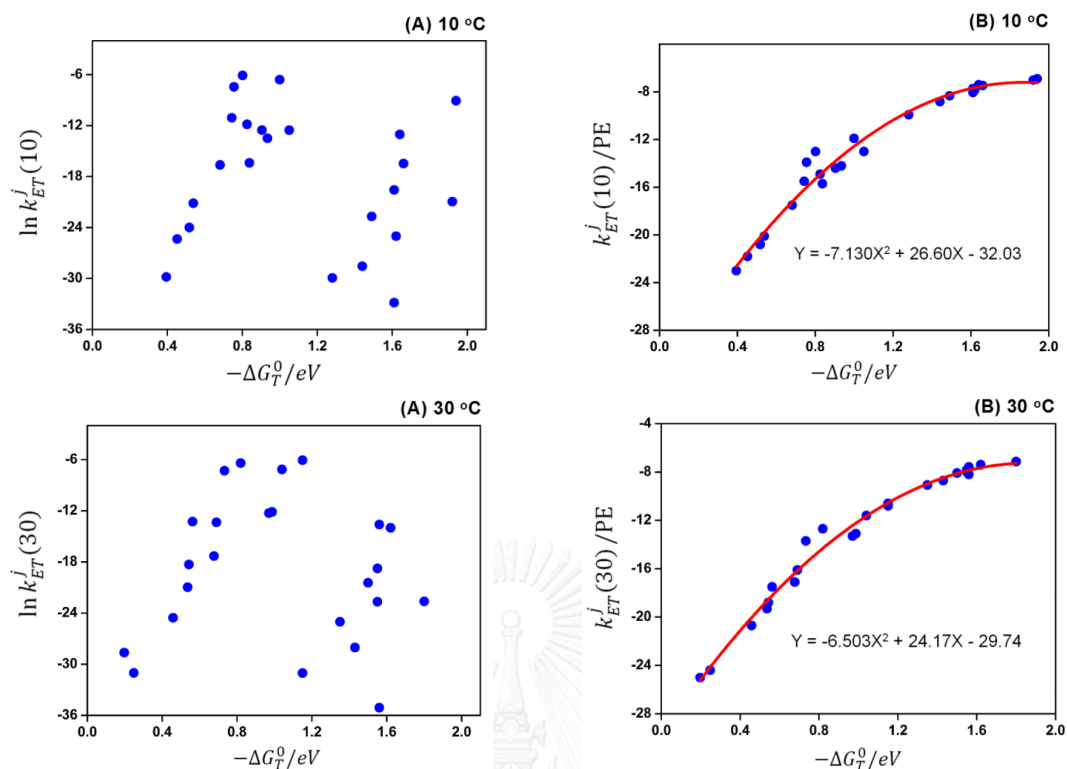
Figure 2.10 *Energy gap law in DAAO. (A) Normal energy gap law at 10 °C and 30 °C, as represented by eqn (2.9) in the text and (B) the reduced energy gap law, as expressed by eqn (2.10) in text. Inserts in (B) indicate the best-fit parabola functions of* $\ln\left[k^j_{ET}(T)/PE\right]$ *(Y) against* $-\Delta G^0_T(j)$ *(X).*

2.4.6 Temperature transition of the lifetimes

The calculated fluorescence lifetimes were obtained as the inverse of the total ET rates, as in eqn (2.7). The lifetimes at 10 °C were calculated with ε_0 and G^0_{Iso} at 10 °C (see Table 2.3), as a function of T. Likewise, the lifetimes at 30 °C were obtained with ε_0 and G^0_{Iso} at 30 °C. The temperature-dependence of the fluorescence lifetimes at both temperatures is shown in Figure 2.11, where the two curves should be a continuous function of T. The plausible transition is indicated by a green curve (transition temperature, T_c = 20 °C). Experimentally T_c was reported to be 14–20 °C. [18, 30, 66-68]
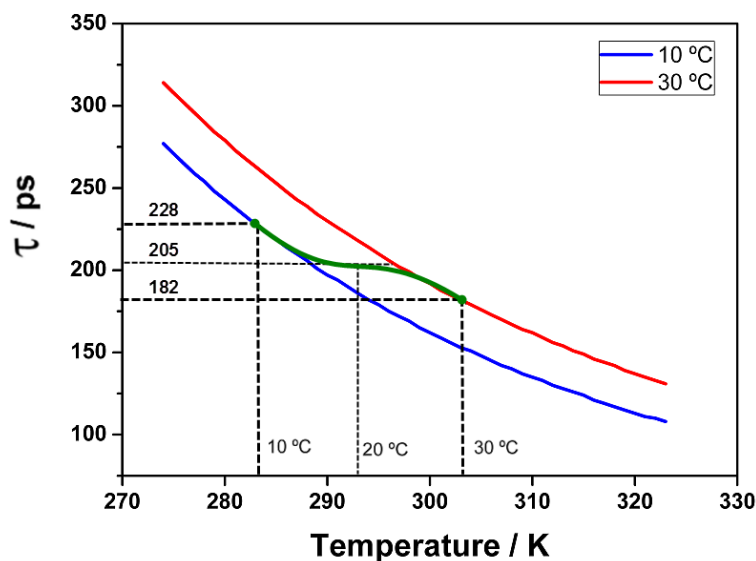
Figure 2.11 *Temperature transition of lifetimes in DAAO. Green solid curve indicates possible temperature-dependence of the lifetime as temperature was elevated from 10 °C to 30 °C. The temperature at middle-point of this curve may transition temperature (20 °C).*

2.4.7 Quantum chemical basis for the standard Gibbs energy related to the electron affinity of Iso*

Electron affinities of Iso* were calculated with the semi-empirical MO. Standard free energy of electron affinity of Iso* was approximately expressed by eqn (2.11).[97]

$$-G_{Iso}^{0}(T) = H_{f}^{anion}(T) - H_{f}^{*}(T) \qquad (2.11)$$

Here $H_{f}^{anion}(T)$ and $H_{f}^{*}(T)$ are heat of formations of Iso anion radical and Iso* in the H-bond cluster at T. The H-bond clusters at both temperatures were obtained as described above. Figure 2.12 illustrates one of energetically minimized structure of Iso with H-bond cluster at respective temperature. MO calculations were performed starting 100 MDS snapshots with 100 ps time intervals at the both temperatures. Time-evolutions of heat of formation of Iso anion radical, Iso*, $-G_{Iso}^{0}(T)$ and difference of $-G_{Iso}^{0}(T)$ between the both temperatures are illustrated in Figure 2.13. These values

fluctuated around mean values. The mean values over 100 snapshots were -22.1 eV at 10 $^{\circ}$C and -22.0 eV at 30 $^{\circ}$C in $H_f^{anion}(T)$, -14.4 eV at both temperatures in $H_f^*(T)$, and -7.69 eV at in 10 $^{\circ}$C, and -7.59 eV at 30 $^{\circ}$C in $-G_{Iso}^0(T)$. Experimental values of $-G_{Iso}^0(T)$ obtained in the present work were -8.69 eV at 10 $^{\circ}$C and -8.51 eV at 30 $^{\circ}$C. Negative sign in the experimental values was taken from eqn (2.4). The calculated values of $-G_{Iso}^0(T)$ were 1.0 eV higher at 10 $^{\circ}$C and 1.9 eV higher at 30 $^{\circ}$C than those of the experimental values. However, the difference, $-G_{Iso}^0(10)+G_{Iso}^0(30)$, was -0.11 eV in the calculated value, while it was -0.18 eV in the experimental value, which were quite close to the calculated value.
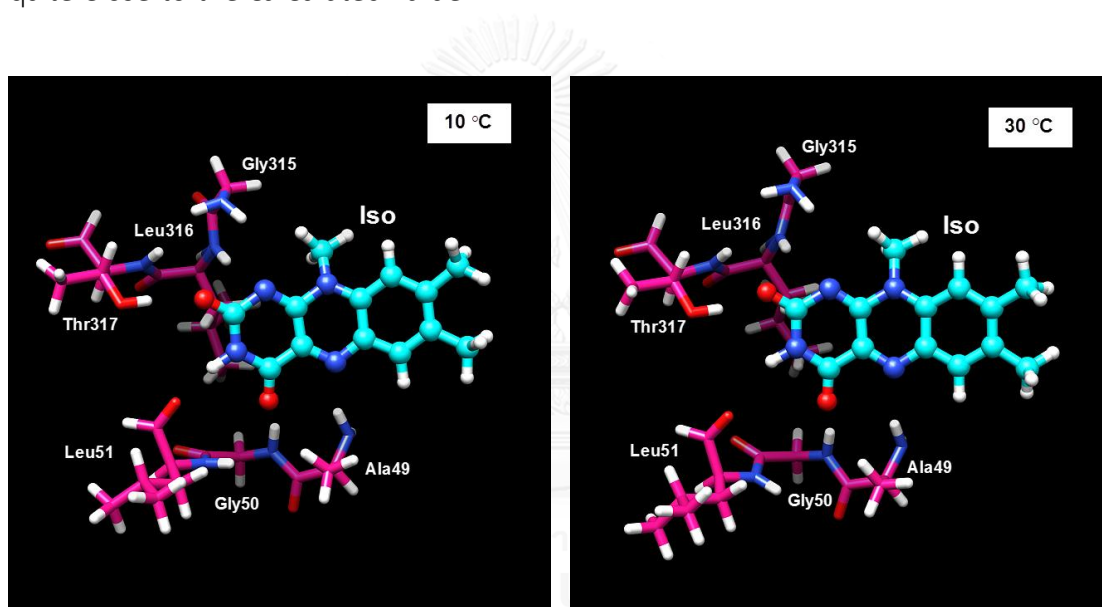
Figure 2.12 *Iso and surrounding H-bond clusters at 10 $^{\circ}$C and 30 $^{\circ}$C. MO calculations were performed for 100 snapshots with 100 ps time intervals at each temperature. Atomic coordinates of these structures were taken from one of MO output files at each temperature.*
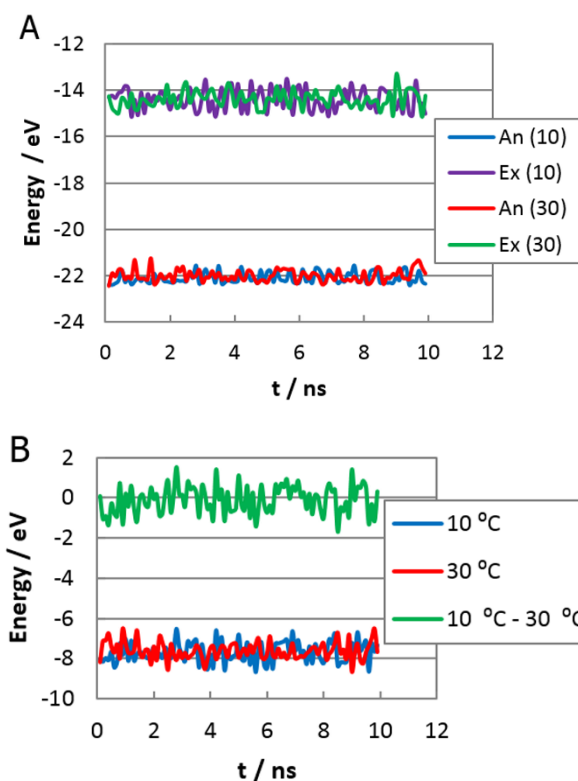
Figure 2.13 *Heat of formation of Iso anion and Iso*, and* $-G_{Iso}^0(T)$. *Panel A shows hear of formation of Iso anion and Iso* at 10 and 30 °C, Panel B* $-G_{Iso}^0(T)$ *and difference of* $-G_{Iso}^0(T)$ *between 10 and 30 °C. An and Ex in insert A denote Iso anion and Iso*. 10 °C, 30 °C and 10 °C – 30 °C in insert B indicate* $-G_{Iso}^0(T)$ *at 10 °C,* $-G_{Iso}^0(T)$ *at 30 °C, and difference in* $-G_{Iso}^0(T)$ *between the both temperatures.*

2.5 DISCUSSION

In the present work the structural basis for the temperature-transition has been demonstrated from various aspects. The donor-acceptor distance (center-to-center distance Rc) of Tyr224, which showed the fastest ET rate at 10 °C, were different being 0.82 and 0.88 nm at 10 and 30 °C, respectively, and one of Tyr314, which showed the fastest ET rate at 30 °C, 1.06 and 1.18 nm. Rc of Tyr55 was displayed greatest difference, 1.64 nm at 10 °C and 1.2 nm at 30 °C. The inter-planar angle between Iso and Tyr314 was displayed marked difference from 27 ° at 10 °C to -47 ° at 30 °C. In

addition the RMSF (residue-based root of mean square fluctuation) at 10 $^\circ$C was considerably lower than that at 30 $^\circ$C, especially around Ser60-Pro62, Pro191-Pro193 and Val244-Asn246. The likely H-bond pairs between Iso and the surrounding amino acids displayed notable differences between 10 $^\circ$C and 30 $^\circ$C. Iso N1 formed a likely H-bond with Gly315 N (peptide) at 10 $^\circ$C, but not at 30 $^\circ$C. Iso N3H formed a likely H-bond with Leu51 O (peptide) at 10 $^\circ$C, but not at 30 $^\circ$C. In addition the H-bond pair of Iso O4 and Leu51 N (peptide) at 10 $^\circ$C switched to Ala49 N (peptide) at 30 $^\circ$C.

The temperature transition of DAAO was also found in the ET rate, where the ET rate displayed a different temperature-dependence at the two temperatures. This may be ascribed to the difference in the G_{Iso}^0 values (free energy related to electron affinity of Iso*) at both temperatures, being 8.69 and 8.51 eV at 10 and 30 $^\circ$C, respectively. The difference in the G_{Iso}^0 may in turn be explained by the different H-bond patterns at the two temperatures.

The values of $-G_{Iso}^0$ in the systems of Iso* under H-bond clusters at the both temperatures were calculated with MO method. Coincidences between the calculated $-G_{Iso}^0$ and one obtained by ET analysis were quite good at both temperatures. Mean heat of formation of Iso anion radical were -22.1 eV at 10 $^\circ$C and -22.0 eV at 30 $^\circ$C in the H-bond clusters, while -6.29 eV at 10 $^\circ$C and -6.07 eV at 30 $^\circ$C in isolated Iso anion radical. Mean heat of formation of Iso* over 100 snapshots in the H-bond cluster was -14.4 eV at the both temperatures, while one of isolated Iso* 0.66 eV. These results suggest that H-bond cluster plays important role on these energies.

The normal energy gap law did not appear to hold in DAAO, with the ET rates of Tyr displaying different $-\Delta G_T^0$ dependencies from that of Trp, which has never been observed before in other flavoproteins.[32, 39] Instead, we proposed a reduced energy gap law, where the ET rates were divided by *PE* as shown in eqn (2.10). The difference in $-\Delta G_T^0$ at maximum ET rate / *PE* may be related to the different G_{Iso}^0 values at both temperatures.

It is of interest that the ET rate is not always fastest from a donor with the shortest R_j (center to center distance between Iso and the donor *j*). Thus, whilst the R_j was shortest in Tyr224, at 0.82 and 0.88 nm at 10 and 30 $^\circ$C, respectively

(Table 2.1), the ET rate from Tyr224 was slower than Tyr314 at the higher temperature (Tables 2.4 and 2.5). The reason why the ET rate from Tyr314 was faster than that from Tyr224 at 30 $^{\circ}$C, despite the shorter R_j in Tyr224 by 0.3 nm at 30 $^{\circ}$C, may be explained in the following way. The shorter R_j directly influences the ET rate through the solvent reorganization energy, λ_S^{qj}, the ES energy between the donor cation and acceptor anion, $-e^2/\varepsilon_0^q R_j$, and $\exp\left\{\beta^q\left(R_j - R_0^q\right)\right\}$ in the electronic coupling term of PE in eqn (2.2). The term $\exp\left\{\beta^q\left(R_j - R_0^q\right)\right\}$ contributes to reduce the ET rate, since R_j is always longer than R_0^{Tyr} (0.499 nm). Sums of λ_S^{qj} and $-e^2/\varepsilon_0^q R_j$ in Tyr224 and Tyr314 at 30 $^{\circ}$C were 1.62 eV and 1.83 eV, respectively. The differences in these sums between Tyr224 and Tyr314 were thus 0.21 eV at 30 $^{\circ}$C, which are compared to the differences in ES energies, ES_j, between Tyr224 and Tyr314, 0.40 eV at 30 $^{\circ}$C. Thus, variation in ES_j which represents ES energy between the photoproducts and ionic groups in the protein, and do not depend explicitly on R_j, was greater than those in the sums of the donor-acceptor distance-dependent quantities, λ_S^{qj} and $-e^2/\varepsilon_0^q R_j$. This may be the reason why the ET rate from Tyr314 was faster than that from Tyr224 at 30 $^{\circ}$C, despite the shorter R_j in Tyr224 by 0.3 nm at 30 $^{\circ}$C. It was previously believed that the donor-acceptor distance is the most influential factor upon the ET rate in proteins. The present work revealed that ET can occur from a donor without having the shortest donor-acceptor Rc (or Re) distance, when more than one donor exists near an acceptor. The importance of the ES energy has also been experimentally and theoretically demonstrated in FMN binding proteins.[11, 39]

Beratan et al. [98-100] have developed a pathway model for electron transfer rate in proteins, based on the Fermi golden rule, in which protein structures mediate tunneling, a) through bonds, b) through space, c) through H bonds. The following points are different between our flavoprotein systems and the electron transfer systems of Beratan's group, 1) in our systems ET takes place in the time-domain of femtoseconds-picoseconds, while Beratan's group deal with dark electron transfer (DET) in the time domain much longer than ET, 2) the donor-acceptor distance is not always most influential factor for ET rate in flavoproteins, while the donor-acceptor distance is always most important factor in their systems, 3) ES energy between the photo-

products and ionic groups inside the proteins much influences the ET rates,[11, 39] while it was not taken into account in their works, 4) ET in flavoproteins including D-amino acid oxidase should be through space, because no direct covalent bonds or H-bonds exists between Iso and Trp or Tyr, while the DET is most effective trough bonds. These differences may be ascribed to the difference in the phenomena of ET and DET.

CHAPTER III

NON-EQUIVALENT CONFORMATIONS OF D-AMINO ACID OXIDASE DIMER FROM PORCINE KIDNEY BETWEEN THE TWO SUBUNITS. MOLECULAR DYNAMIC SIMULATION AND PHOTOINDUCED ELECTRON TRANSFER

Non-Equivalent Conformations of D-Amino Acid Oxidase Dimer from Porcine Kidney between the Two Subunits. Molecular Dynamic Simulation and Photoinduced Electron Transfer

Arthit Nueangaudom[a], Kiattisak Lugsanangarm[a], Somsak Pianwanit[a], Sirirat Kokpol[a], Nadtanet Nunthaboot[b] and Fumio Tanaka[a,c]

[a] Department of Chemistry, Faculty of Science, Chulalongkorn University, 254 Phayathai Road, Bangkok 10330, Thailand.

[b] Department of Chemistry, Faculty of Science, Mahasarakham University, Thailand.

[c] Division of Laser Biochemistry, Institute for Laser Technology, Utsubo-Honmachi, 1-8-4, Nishiku, Osaka 550-0004, Japan.

3.1 ABSTRACT

The structural difference between two subunits of D-amino acid oxidase dimer from porcine kidney was studied by molecular dynamics simulation (MDS) and rate of photoinduced electron transfer (ET) from aromatic amino acids as tyrosines (Tyr) and tryptophanes (Trp) to the excited isoalloxazine (Iso*). The donor–acceptor distances (Rc) between isoalloxazine (Iso) and the donors were shortest in Tyr224 (0.74 nm) in Sub A at 10 $^{\circ}$C (Sub A10), in Tyr224 (0.79 nm) in Sub B at 10 $^{\circ}$C (Sub B10), in Tyr228 (0.85 nm) in Sub A at 30 $^{\circ}$C (Sub A30), and in Tyr224 (0.72 nm) in Sub B at 30 $^{\circ}$C (Sub B30). The Rcs were mostly shorter in the dimer than those in the monomer. Hydrogen bonding (H-bond) pairs between Iso and surrounding amino acids varied with the subunit and temperature. O2 of the Iso ring formed an H-bond exclusively with Thr317OG1 (side chain) in both Sub A10 and Sub A30, while it formed with Gly315N (peptide), Leu316N and Thr317N in Sub B10 and Sub B30. N3H of Iso formed an H-bond with Leu51O (peptide) in Sub A10 and Sub A30, but not in Sub B10 and Sub B30. Electron affinity of Iso* was appreciably lower in Sub A10 compared to Sub B10, while it was opposite at 30 $^{\circ}$C. ET rate to Iso* was fastest from Tyr224 in Sub A10, while it was fastest from Tyr314 in Sub B10. The ET rate was fastest from Tyr314 in Sub A30, while it was fastest from Tyr224 in Sub B30. The greater ET rates in the dimer as compared to those in the monomer were elucidated with shorter Rc in the dimer as compared to the monomer. The static dielectric constants inside the subunits and the static dielectric constant between Iso and Tyr224 or Tyr228 were not different appreciably. A few water molecules and sometimes an amino acid were located between Iso and Tyr224, which may be the reason why the dielectric constant of the entire subunits did not differ from that between Iso and Tyr224.

3.2 INTRODUCTION

D-Amino acid oxidase (DAAO) is a peroxisomal enzyme containing flavin adenine dinucleotide (FAD) as a cofactor which exists in a wide range of species from yeasts to humans. Its function is to oxidize D-amino acids to the corresponding imino acids, producing ammonia and hydrogen peroxide. A number of review articles have been reported on DAAO from porcine kidney [101, 102] from yeast to human,[62] and from human.[103, 104] Recently, mammalian DAAO has been demonstrated to connect with the brain D-serine metabolism and to the regulation of the glutamatergic neurotransmission.[63, 64] Various novel inhibitors to human DAAO have been found using the in silico screening technique.[49]

DAAO from porcine kidney is in a monomer (Mw 39 kDa) – dimer equilibrium state at relatively low concentrations,[23-26] and may be in a dimer–tetramer equilibrium at higher concentrations.[27-29] The crystal structures of DAAO from porcine kidney were determined by Miura et al. [19] and Mattevi et al. [69]. A temperature-induced conformational change of the DAAO has been reported by many workers.[17, 18, 30, 66, 67, 77] The fluorescence lifetime of the dimer is ca. 40 ps while that of the monomer is 160 ps, which suggests that the structure near to Iso in the dimer is quite different from the monomer.[17, 18, 77]

The fluorescence of flavins in many flavoproteins is strongly quenched, which is ascribed to photoinduced electron transfer (ET) from tryptophanes (Trp) and/or tyrosines (Tyr) to the excited isoalloxazine (Iso*).[5-7] Ultrafast fluorescence dynamics of some flavoproteins in the time domain of femtoseconds–picoseconds have been studied by a fluorescence up-conversion technique.[11-13, 15, 16] The ultrafast fluorescence dynamics of some flavoproteins have been analyzed with the protein structures obtained by molecular dynamics simulation (MDS) and an electron transfer theory.[32, 35, 39, 42]

The structural basis for temperature-induced transition of DAAO monomer from porcine kidney has been analyzed with this method. The conformational change was characterized from the ET rates from Tyr224, Tyr228 and Tyr314 to the Iso*.[105] The ultrafast fluorescence dynamics of DAAO–benzoate complex has also been analyzed

with MDS snapshots and Kakitani and Mataga (KM) theory.[106] In the present work we have demonstrated by means of the MDS structures and ET analysis that the structure of DAAO dimer is quite different between the two subunits, and provide the structural basis of the conformational difference between dimer and monomer.

3.3 METHOD OF ANALYSIS

3.3.1 MDS calculations

All MDS were performed using the Amber10 suite program.[88] The starting structure from the X-ray structure of the DAAO–benzoate complex dimer (PDB code 1VE9) [19] was removing two benzoate molecules from each subunit. The protein was added hydrogen atoms for all missing hydrogen atoms using LEaP module of Amber10.[88] Subsequently, the protein complex was solvated with a cubic box of 7395 TIP3P water molecules and eight sodium counterions added for the electroneutrality of the system. The parm99 force field [89] was used to generate the protein topology and the restrained electrostatic potential (RESP) [91] charges was used for the FAD. The simulated system was minimized with 2000 steps of the steepest descent followed by 3000 steps of conjugate gradient of energy minimization. Afterwards, both systems were heated from 0 to 283 K or from 0 to 303 K (for the 10 and 30 $^{\circ}$C MDS, respectively) over 100 ps and were further equilibrated under periodic boundary conditions at 283 and 303 K. The systems were set up under the isobaric–isothermal ensemble with a constant pressure of 1 atm and constant temperature of either 283 or 303 K. The electrostatic interactions were corrected by the Particle Mesh Ewald method.[92] The SHAKE algorithm [93] was employed to constrain all bonds involving hydrogen atoms. MDS based calculations were performed with time steps of 2 fs and a cutoff distance of 1 nm was employed for non-bonded pair interactions. The stability of the system was checked by investigating the convergence of the energies, temperature, pressure and global root mean square deviation of the system. The equilibrium was found to be attained after 20 ns of the MDS calculation, by monitoring these quantities. Then the calculation was continued for up to further 30 ns, and data from the last 5 ns were used for the analyses.

3.3.2 ET theory

The original Marcus theory [78, 79] has been modified in various ways.[61, 80, 107, 108] In the present analysis, KM theory [107] was used, because it is applicable for non-adiabatic ET process in addition to adiabatic ET process, and has been found to give satisfactory results for both static [11, 94, 95] and dynamic ET analyses.[32, 35, 39, 42, 105, 106] The ET rate described by the KM model is expressed by eqn (3.1).

$$
k_{ET}^{jk}(T) = \frac{v_0^q}{1+\exp\left\{\beta^q(R_{jk}-R_0^q)\right\}} \sqrt{\frac{k_B T}{4\pi\lambda_{jk}^q}}
$$
$$
\times \exp\left[-\frac{\left\{\Delta G_k^0(T) - e^2/\varepsilon_0^{pk}R_{jk} + \lambda_{jk}^q + E_{Net}^k(j)\right\}^2}{4\lambda_{jk}^q k_B T}\right] \tag{3.1}
$$

Here $k_{ET}^{jk}(T)$ is the ET rate from a donor j to the Iso* in subunit k (k = Sub A or Sub B) at temperature T ($^\circ$C), and q denotes Trp or Tyr. v_0^q is an adiabatic frequency, β^q is the ET process coefficient. R_{jk} and R_0^q are the donor j–Iso distance in subunit k and its critical distance for the ET process, respectively. Rjk is expressed as a center-to-center distance (Rc) rather than as an edge-to-edge (Re) distance.[32, 35, 39, 42, 105, 106] The ET process is adiabatic when $R_{jk} < R_0^q$, and non-adiabatic when $R_{jk} > R_0^q$. T in the right hand sides of eqn (3.1) is temperature expressed in K unit. The term, $-e^2/\varepsilon_0^{pk}R_{jk}$, in eqn (3.1) is electrostatic (ES) energy between Iso anion and a donor cation. The static dielectric constant (ε_0^{pk}) is discussed below eqn (3.2). The terms k_B and e are the Boltzmann constant and electron charge, respectively. $E_{Net}^k(j)$ is the Net ES energy of the donor j in subunit k, which is described later. The porcine kidney DAAO monomer contains 10 Trp and 14 Tyr residues. In the present work the ET rates from all of these aromatic amino acids to Iso* were taken into account for the analysis.

λ_{jk}^q is the solvent reorganization energy [78, 79] of the ET donor qj, and is expressed as eqn (3.2).

$$\lambda_{jk}^q = e^2 \left(\frac{1}{2a_{Iso}} + \frac{1}{2a_q} - \frac{1}{R_{jk}} \right) \left(\frac{1}{\varepsilon_\infty} - \frac{1}{\varepsilon_0^{pk}} \right) \tag{3.2}$$

where a_{Iso} and a_q are the radii of Iso and Trp or Tyr, with these reactants being assumed to be spherical, and ε_∞ is optical dielectric constant, and ε_0^{pk} static dielectric constant of subunit k. It was assumed that for Tyr224 and Tyr228 ε_0^{pA} (Sub A) = ε_0^{pB} (Sub B) = ε_0^{DA}, where ε_0^{pA} is static dielectric constant between the donor and Iso, because these donor–acceptor distances were always much shorter than 1 nm, and for the other donors ε_0^{pA} (Sub A) = ε_0^{pB} (Sub B) = ε_0^B. The optical dielectric constant used was 2.0. The radii of Iso (a_{Iso}), Trp (a_{Trp}) and Tyr (a_{Tyr}) were those previously determined [32, 35, 39, 42] to be 0.224, 0.196 and 0.173 nm, respectively.

The standard free energy change was expressed with the ionization potential of the ET donor, E_{IP}^q, as eqn (3.3).

$$\Delta G_k^0(T) = E_{IP}^q - G_k^0(T) \tag{3.3}$$

where $G_k^0(T)$ is the standard Gibbs energy related to the electron affinity of Iso* in subunit k at temperature T. The values of E_{IP}^q for Trp and Tyr were 7.2 and 8.0 eV, respectively.[96]

3.3.3 Electrostatic energy in DAAO dimer

Protein systems contain many ionic groups, which may influence the ET rate. The porcine kidney DAAO contains Iso as the ET acceptor, and 10 Trp residues and 14 Tyr residues per subunit as potential ET donors. The FAD cofactor in DAAO has two negative charges at the pyrophosphate, whilst DAAO itself contains 22 Glu, 13 Asp, 12 Lys and 21 Arg residues per subunit. Therefore total numbers of ionic groups are double of those in one subunit. The ES energy between the Iso anion or donor cation j and all other ionic groups in subunit k (Sub A or Sub B) is expressed by eqn (3.4).

$$E_k(j) = \sum_{i=1}^{44} \frac{C_j C_{\text{Glu}}}{\varepsilon_0^{\text{pk}} R_j(\text{Glu}-i)} + \sum_{i=1}^{26} \frac{C_j C_{\text{Asp}}}{\varepsilon_0^{\text{pk}} R_j(\text{Asp}-i)}$$
$$+ \sum_{i=1}^{24} \frac{C_j C_{\text{Lys}}}{\varepsilon_0^{\text{pk}} R_j(\text{Lys}-i)} + \sum_{i=1}^{42} \frac{C_j C_{\text{Arg}}}{\varepsilon_0^{\text{pk}} R_j(\text{Arg}-i)} + \sum_{i=1}^{8} \frac{C_j C_{\text{P}}}{\varepsilon_0^{\text{pk}} R_j(\text{P}-i)} \tag{3.4}$$

Here j = 0 for the Iso anion in subunit k, 1–10 for the Trp cations in Sub A and 11–20 for Trp in Sub B, 21–34 for the Tyr cations in Sub A, and 35–48 for Tyr cations in Sub B. C_j is the charge of the aromatic ionic species j, that is, -e for j = 0 and +e for j = 1 to 48. C_{Glu} $(=-e)$, C_{Asp} $(=-e)$, C_{Lys} $(=+e)$, and C_{Arg} $(=+e)$ are the charges of the Glu, Asp, Lys and Arg residues, respectively. FAD contains 2 phosphate atoms, each of which binds 2 oxygen atoms. It was assumed that the charge of each oxygen atom is $C_{\text{P}} =$ -0.5e, though total charge of four oxygen atoms is -2e. We also assumed that these groups are all in an ionic state in solution. The distances between the aromatic ionic species j and the ith Glu (i = 1–44) are denoted as $R_j(\text{Glu}-i)$, whilst the distances between the aromatic ionic species j and the ith Asp (i = 1–26) are denoted as $R_j(\text{Asp}-i)$, and so on for the each amino acid residue.

$E_{\text{Net}}^k(j)$ in eqn (3.1) was then expressed as eqn (3.5).

$$E_{\text{Net}}^k(j) = E_k(0) + E_k(j) \tag{3.5}$$

Here j is from 1 to 48, and represents the jth ET donor, as described above.

3.3.4 Determination of the ET parameters

The observed fluorescence lifetimes of the porcine kidney DAAO monomer are reported to be τ_{obs}^{10} = 44.2 ps at 10 $^\circ$C and τ_{obs}^{30} = 37.7 ps at 30 $^\circ$C.[18] The calculated lifetimes of subunit k at temperature (T) were given by eqn (3.6).

$$\tau_{\text{Calc}}^{\text{Tk}} = \frac{1}{\sum_{j=1}^{48} k_{\text{ET}}^{jk}(T)} \tag{3.6}$$

The fluorescent lifetimes were expressed in unit of ps. In the present work the physical quantities related to the electronic coupling term (ν_0^{q}, β^{q} and R_0^{q}) for Trp and Tyr were taken from those reported for the flavin mononucleotide binding proteins,[39] which were assumed to be independent of temperature within the temperature range (10–30 $^{\circ}$C) as in previous works.[105, 106] On the contrary, the free energy, $G_{k}^{0}(T)$, related to the electron affinity of Iso* was assumed to be both temperature- and subunit-dependent, because $G_{k}^{0}(T)$ is modified with the hydrogen bonding (H-bond) structure.[105, 106] The unknown ET parameters were $G_{A}^{0}(10)$, $G_{B}^{0}(10)$, $G_{A}^{0}(30)$ and $G_{B}^{0}(30)$ in eqn (3.3), and ε_0^{A}, ε_0^{B} and ε_0^{DA} which were assumed to be independent of temperature.[105, 106] These ET parameters were determined so as to obtain the minimum value of χ^2, as given by eqn (3.7).

$$\chi^2 = \frac{\left(\tau_{\text{Calc}}^{10A} - \tau_{\text{Obs}}^{10}\right)^2}{\tau_{\text{Calc}}^{10A}} + \frac{\left(\tau_{\text{Calc}}^{10B} - \tau_{\text{Obs}}^{10}\right)^2}{\tau_{\text{Calc}}^{10B}} + \frac{\left(\tau_{\text{Calc}}^{30A} - \tau_{\text{Obs}}^{30}\right)^2}{\tau_{\text{Calc}}^{30A}} + \frac{\left(\tau_{\text{Calc}}^{30B} - \tau_{\text{Obs}}^{30}\right)^2}{\tau_{\text{Calc}}^{30B}}$$ (3.7)

3.4 RESULTS

3.4.1 Local structure near Iso binding site in DAAO dimer obtained by MDS

Figure 3.1 shows MDS snapshots near FAD binding sites in DAAO dimer at 10 and 30 $^{\circ}$C. In the Figure the structures of Sub A and Sub B are illustrated separately. Aromatic amino acids of potential ET donor are also shown in addition to FAD. Tyr224, Tyr228, Tyr55, Tyr314 and Tyr279 are five closest donors to Iso in Sub A at 10 $^{\circ}$C (Sub A10; Figure 3.1A). In Sub B10 the aromatic amino acids of five closest to Iso were the same with those in Sub A (Figure 3.1B). In Sub A30 Tyr228, Tyr224, Tyr314, Tyr279 and Tyr55 were five closest donors to Iso (Figure 3.1C). In Sub B30 Tyr224, Tyr228, Tyr314, Tyr55 and Trp185 were closest to Iso (Figure 3.1D). Figure 3.2 shows time evolutions of Rc between these aromatic amino acids and Iso. Figure 3.3 shows the Rc-distributions. The distributions may be clearer to understand differences in the Rc and extent of the distance fluctuation. Rc of Tyr185 displayed double maxima in both Sub A10 at around 1.35 nm with a major distribution and 1.5 nm with a minor

distribution. Rc in Sub B10 also displayed double maxima with minor distribution at around 1.5 nm and with major distribution at around 1.7 nm. The Rc of Tyr185 in monomer at 10 °C did not show such double maxima, a single peak at around 1.3 nm, which was similar to the major peak in Sub A at 10 °C. The distributions of Trp185 in dimer displayed single peaks in both Sub A and Sub B at 30 °C. The distribution of Rc in Tyr55 displayed double maxima in Sub A30, but single peak in Sub B30. The Rc at the main peak was much longer than those in Sub B30, and also in both Sub A10 and Sub B10. These results in Rc suggest that the protein conformation is quite different between Sub A and Sub B, and is appreciably modified by temperature.

Table 3.1 lists mean values of Rc over 5000 snapshots with 1 ps time intervals. In Sub A10 the Rc values were 0.74 nm in Tyr224, 0.82 nm in Tyr228, 1.07 nm in Tyr55, and 1.11 nm in Tyr314. In Sub B10 the Rc values were 0.79 nm in Tyr224, 0.83 nm in Tyr228, 0.99 nm in Tyr55, and 1.05 nm in Tyr314. Comparing between Sub A10 and Sub B10, the Rc values of Tyr55 and Tyr314 are a little shorter by 0.06–0.08 nm in Sub B. In Sub A30 the Rc values were 0.85 nm in Tyr228, 0.90 nm in Tyr224 and 1.06 nm in Tyr314. In Sub B30 the Rc values were 0.72 nm in Tyr224, 0.81 nm in Tyr228, 1.06 nm in Tyr55 and Tyr314. Comparing between Sub A30 and Sub B30, the Rc value of Tyr55 in Sub B were remarkably shorter by 0.41 nm than that in Sub A.
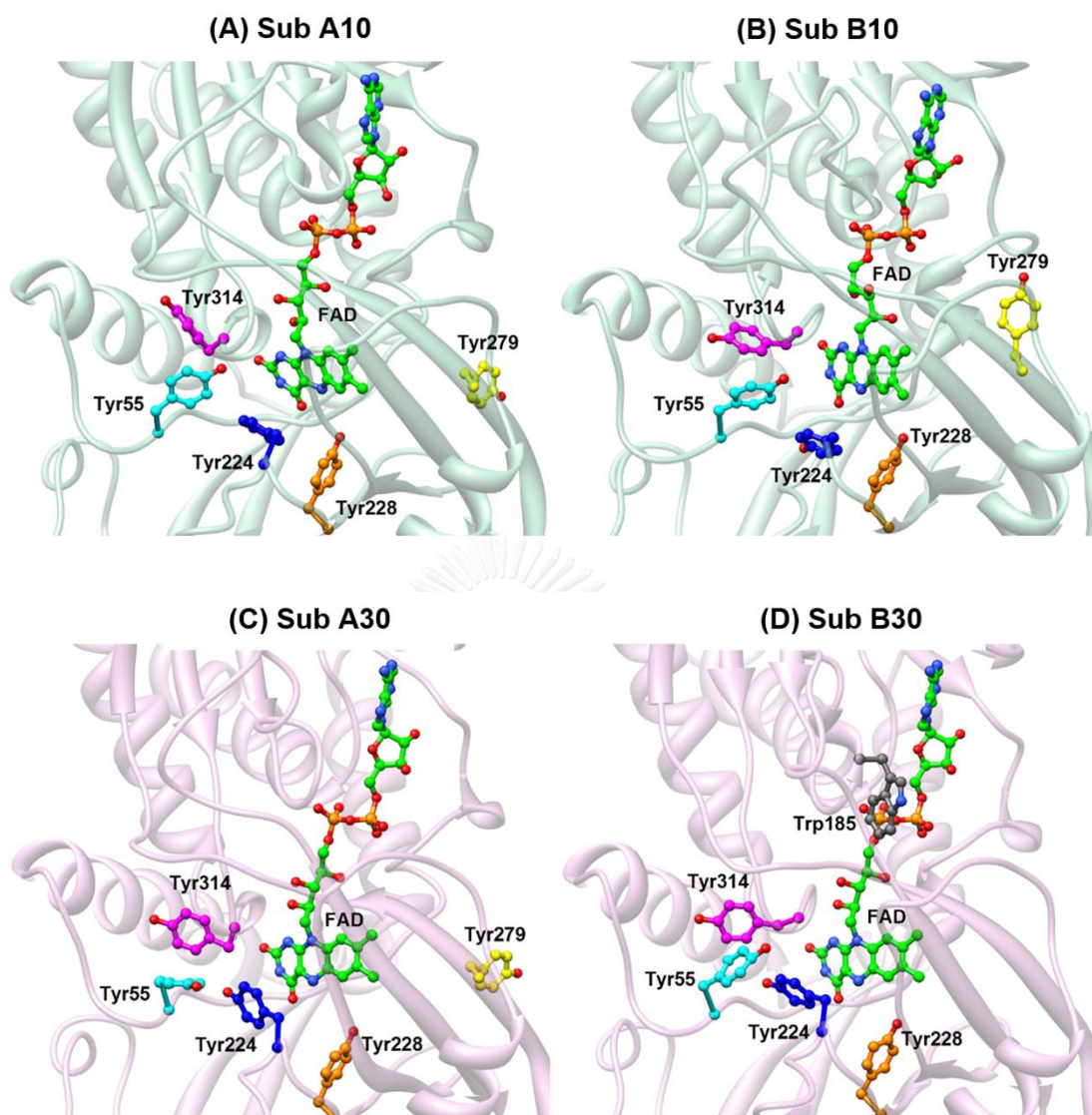
Figure 3.1 *Local structure of FAD binding site in DAAO obtained by MDS. The five fastest ET donors are illustrated with stick model, together with FAD. Sub A10 and Sub B10 denote subunits of A and B at 10 ℃, and Sub A30 and Sub B30 denote subunits of A and B at 30 ℃. MDS calculations were performed independently both at 10 ℃ and 30 ℃.*

Figure 3.2 *Time evolution of the donor–acceptor distance. ET donors are aromatic amino acids indicated in the insets, and acceptor is Iso*. The distances are expressed with the center-to-center distance (Rc). Sub A10 and Sub B10 denote subunits of A and B at 10 °C, and Sub A30 and Sub B30 denote subunits of A and B at 30 °C. MDS calculations were performed independently both at 10 and 30 °C.*
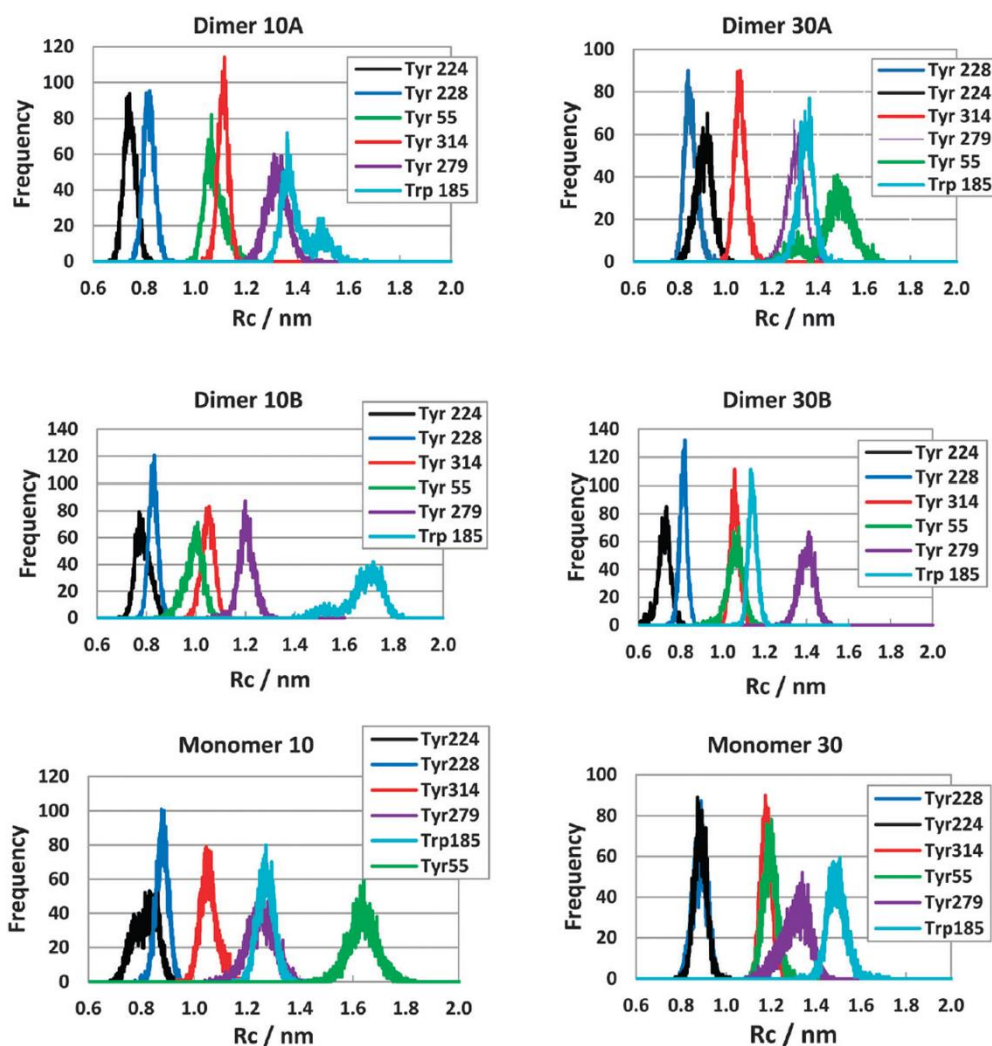
Figure 3.3 The distribution of the donor–acceptor distance. The distances are expressed with center-to-center distance (Rc). 10A and 10B denote Sub A and Sub B at 10 ℃, and 30A and 30B, Sub A and Sub B at 30 ℃. Sub A and Sub B denote subunits A and B. Time evolutions of the distances are shown in Figure 3.2. MDS were performed at 10 ℃ and 30 ℃. The distributions for monomers are also illustrated for comparison.[105]

Table 3.1 ET donor-acceptor distance. [a]

DAAO	T (°C)	Subunit	Donor[b] (Rc / nm)				
Dimer	10	A	Tyr224 (0.74)	Tyr228 (0.82)	Tyr55 (1.07)	Tyr314 (1.11)	Tyr279 (1.32)
	10	B	Tyr224 (0.79)	Tyr228 (0.83)	Tyr55 (0.99)	Tyr314 (1.05)	Tyr279 (1.20)
	30	A	Tyr228 (0.85)	Tyr224 (0.90)	Tyr314 (1.06)	Tyr279 (1.30)	Tyr55 (1.47)
	30	B	Tyr224 (0.72)	Tyr228 (0.81)	Tyr314 (1.06)	Tyr55 (1.06)	Trp185 (1.14)
Monomer[c]	10		Tyr224 (0.82)	Tyr228 (0.88)	Tyr314 (1.06)	Trp185 (1.27)	Tyr55 (1.64)
	30		Tyr224 (0.88)	Tyr228 (0.88)	Tyr314 (1.18)	Tyr55 (1.20)	Trp185 (1.49)
Benzoate complex monomer[d]	20		Tyr228 (0.81)	Tyr224 (0.97)	Tyr279 (1.24)	Tyr74 (1.80)	Benzoate (0.61)

[a] Mean center-to-center distances (Rc) are listed over 5000 snapshots. [b] Five shortest distances between Iso and the aromatic amino acids or benzoate are listed in order from shorter to longer distances. [c] Data taken from [105]. [d] Data taken from [106].

The donor–acceptor distances in the dimer were compared to those in the monomer.[105] Table 3.1 also lists the mean Rc values of the monomer. Most marked change was Tyr55 as revealed in the distance distributions. The Rc values ofTyr55 in the dimer were 1.07nm in Sub A10 and 0.99 nm in Sub B10, and 1.47 nm in Sub A30 and 1.06 nm in Sub B30, while Rc values in the monomer are 1.64 nm at 10 $^{\circ}$C and 1.20 nm at 30 $^{\circ}$C. These donor–acceptor distances mostly became shorter in dimer compared to those in monomer.

3.4.2 Inter-subunit structure

The dynamics of distances between Iso in Sub A and Iso in Sub B are shown in Figure S3.1 (Supplemental Information of Chapter III). The centre-to-centre distances (Rc) were shorter at 30 $^{\circ}$C than at 10 $^{\circ}$C. The distance distributions are shown in the right column. The dynamics and distributions of Iso–Iso inter-planar angles are shown in the bottom panels. The mean distances over 5000 snapshots were 4.15 nm at 10 $^{\circ}$C and 4.09 nm at 30 $^{\circ}$C. The mean angles were 781 at 10 $^{\circ}$C and 851 at 30 $^{\circ}$C.

3.4.3 Root of mean square fluctuations

The root of mean square fluctuation (RMSF) is considered to be a good index for structural fluctuation of an individual amino acid, which was obtained by Amber10.[88] Figure 3.4 shows RMSF of Sub A and Sub B at both 10 $^{\circ}$C and 30 $^{\circ}$C. RMSF was highest around residue No. 300 in all four systems, Arg297-Phe298-Gly299-Ser300-Ser301-Asn302-Thr303. The highest amino acids were Ser300 in Sub A10, Gly299 in Sub B10, Ser300 in Sub A30 and Gly299 in Sub B30. Next highest regions were around the residue No. 170. The peak amino acids in this region were Arg172 in Sub A10 and in Sub B10, and Gly173 in Sub A30 and Arg172 in Sub B30. The third highest RMSF were near C-terminals, Asn338 in Sub A10, Arg337 in Sub B10, Arg337 in Sub A30, and Glu336 in Sub B30. The values of RMSF were always higher at 10 $^{\circ}$C than at 30 $^{\circ}$C, despite that thermal fluctuation of the protein should increase with temperature. Mean RMSF

over all residues were highest in Sub B10 (0.403), followed by Sub A10 (0.401), Sub A30 (0.294) and Sub B30 (0.285).
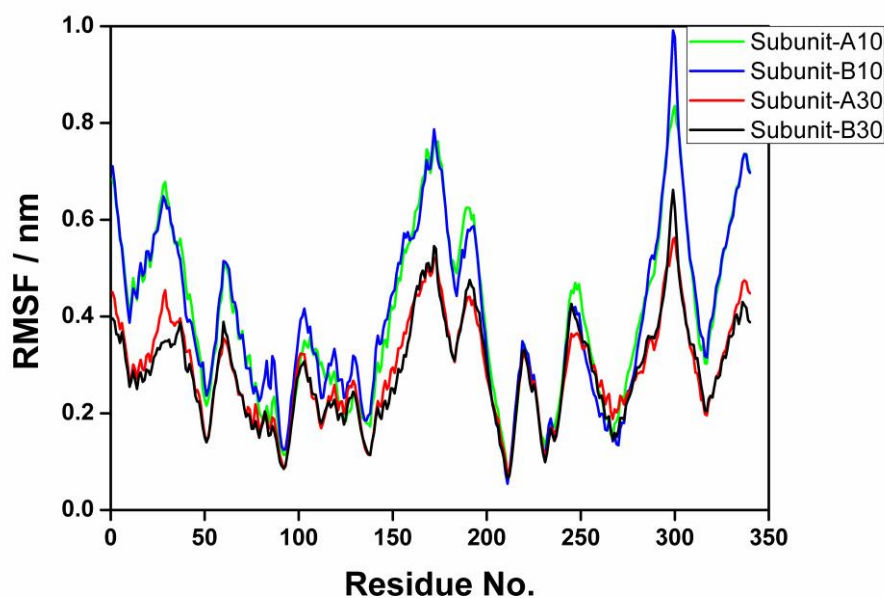
Figure 3.4 RMSF of DAAO dimer. RMSF of Sub A at 10 $^{\circ}$C is illustrated with green line, Sub B at 10 $^{\circ}$C with blue line, Sub A at 30 $^{\circ}$C with red line, Sub B at 30 $^{\circ}$C with a black line. Maximum RMSFs were obtained at Ser300 in Sub A10, Gly299 in Sub B10, Ser300 in Sub A30 and Gly299 in Sub B30. Next highest regions were around the residue No. 170. The peak amino acids in this region were Arg172 in Sub A10 and in Sub B10, and Gly173 in Sub A30 and Arg172 in Sub B30.

3.4.4 H-bond structure between Iso and surrounding amino acids

Figure 3.5 shows the H-bond structure. Table 3.2 lists the mean H-bond distances (RH) over 5000 snapshots within 0.3 nm. The atom notations of the Iso ring are shown in Chart 3.1. In both Sub A10 and Sub B10 IsoN3H forms H-bond with Leu51O (peptide) with RH values of both 0.29 nm, but not at all in both Sub B10 and Sub B30. IsoN5 form H-bond with Ala49N (peptide) only in Sub A10 (RH 0.29 nm). IsoO2 forms H-bonds with peptide nitrogen of Gly315N (RH 0.29 nm), Leu316N (RH 0.28 nm) and Thr317 (RH 0.29 nm) in both Sub B10 and Sub B30, but not H-bonds in Sub A at both

temperatures. IsoO2 in Sub A forms single H-bond with side-chain OH of Thr317 in both Sub A10 and Sub A30 (RH 0.28 nm), but not in Sub B. IsoO4 forms H-bonds with peptide nitrogen atoms of Gly50 and Leu51 only in Sub A10, but not in Sub B at both temperatures. These findings suggest that Sub A and Sub B are not equivalent at Iso binding sites.
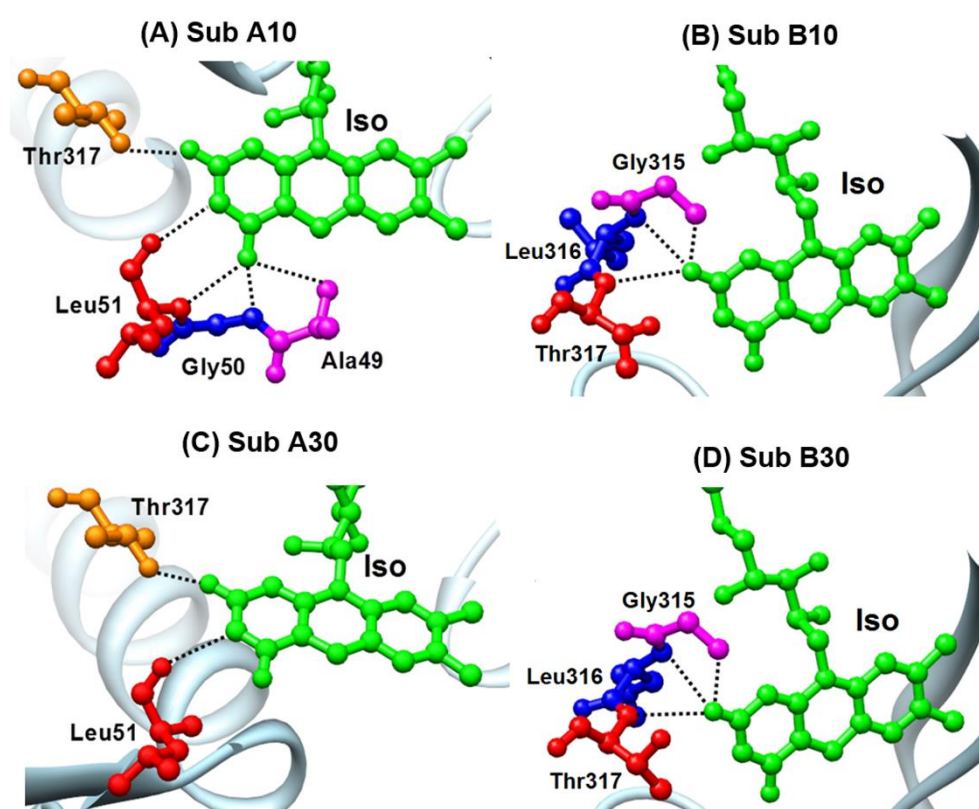
Figure 3.5 H-bond structure between the Iso ring and the nearby amino acids. Sub A10 and Sub B10 denote subunits of A and B at 10 °C, and Sub A30 and Sub B30 denote subunits of A and B at 30 °C. The H-bond distances are listed in Table 3.2.

Table 3.2 Comparison of H-bond distances in DAAO-dimer.

Iso ring[b]	Amino acid	Distance (nm)[a]					
		Subunit A		Subunit B		Monomer[c]	
		10 °C	30 °C	10 °C	30 °C	10 °C	30 °C
N3H	Leu51 O	0.29	0.29	-	-	-	-
N5	Ala49 N	0.29	-	-	-	-	-
O2	Gly315 N	-	-	0.29	0.29	-	-
	Leu316 N	-	-	0.28	0.28	-	0.29
	Thr317 N	-	-	0.29	0.29	-	-
	Thr317 OG1	0.28	0.28	-	-	-	-
O4	Gly50 N	0.29	-	-	-	029	0.29
	Leu51 N	0.29	-	-	-	-	-

[a] Criteria for H-bond distance was taken as within 0.3 nm.

[b] Atomic notations in Iso are as indicated in Chart 3.1.
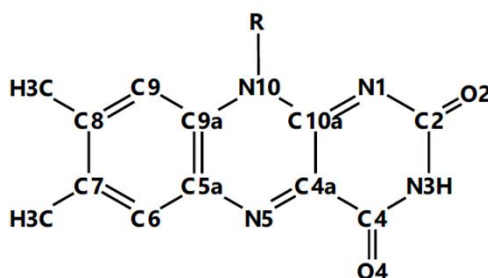
Chart 3.1 *Chemical structure and atom notations of Iso*

3.4.5 ET parameters

ET parameters obtained by the method described above are listed in Table 3.3. The static dielectric constants inside the protein were $\varepsilon_0^A = \varepsilon_0^B = 5.8$, which were obtained assuming to be independent of temperature.[105] The dielectric constant for Tyr224 and Tyr228 between the donors and acceptor (ε_0^{DA}) was also 5.8, which did not change from those inside Sub A and Sub B (ε_0^k, k = A and B). The reason for it is discussed later. Free energies related to electron affinity of Iso* $\{G_k^0(T)\}$ were 8.2 eV in Sub A10 and 8.5 eV in Sub B10, and 8.7 eV in Sub A30 and 8.5 eV in Sub B30. The calculated lifetimes completely coincided with the observed lifetimes.[18]

Table 3.3 Best-fit ET parameter. [a]

T (°C)	Subunit	ε_0^{pk} [b]	$G_k^0(T)$ [c] (eV)	$\Delta G_k^0(T)$ [d] (eV)		τ (ps)		Chi-sq. [g]
				Trp	Tyr	Obs [e]	Cal [f]	
10	Sub A	5.79	8.16	-1.41	-0.607			3.22×10^{-28}
	Sub B	5.82	8.54	-1.34	-0.536	44.2	44.2	7.47×10^{-28}
	Monomer [h]	5.88	8.69	-1.49	-0.690	228	228	-
30	Sub A	5.79	8.73	-1.53	-0.736			1.10×10^{-25}
	Sub B	5.82	8.48	-1.28	-0.481	37.7	37.7	2.16×10^{-28}
	Monomer [h]	5.89	8.51	-1.31	-0.480	182	182	-

[a] The reported values of ET parameters were used for the electronic coupling term [39] (V_0^{Trp} = 1016 ps^{-1}, V_0^{Tyr} = 197 ps^{-1}, β^{Trp} = 21.0 nm^{-1}, β^{Tyr} = 6.25 nm^{-1}, R_0^{Trp} = 0.663 nm, R_0^{Tyr} = 0.499 nm). The optical dielectric constant used was 2 as in the previous works.[32, 35, 39, 42, 105, 106] [b] Static dielectric constants inside Sub A (ε_0^A) and inside Sub B (ε_0^B), which were assumed to be temperature-independent.[105, 106] [c] Temperature dependent standard free energy gap, given by eqn (3.3) in text. [d] Temperature-dependent electron affinity of Iso*. [e] Reported fluorescence lifetimes.[18] [f] The lifetimes of Sub A and Sub B could not be differentiated within the experimental resolutions.[18] [g] Chi-square between the observed and calculated lifetimes given by eqn (3.7) in text. Total Chi-square was 2.8 x 10^{-26}. [h] ET parameters for monomer were taken from the reported work for comparison.[105]

3.4.6 ET rates from aromatic amino acids to Iso*

Time evolutions of logarithmic ET rates are shown in Figure 3.6. In Sub A10 the rate was fastest from Tyr224. The rate from Trp185 displayed sudden transitions at around 1 ns and 2.5 ns, which may be related to the double maxima in Rc distribution. In Sub B10 the rate was fastest from Tyr314. The fastest donors were Tyr228 in Sub A30 and Tyr314 in Sub B30. Mean ET rates over MD simulation snapshots (5000 with 1 ps intervals) are listed in Table 3.4. In Sub A10 the rates from Tyr224, Tyr314 and Tyr228 were 1.3×10^{-2}, 7.6×10^{-3}, and 1.2×10^{-3} ps^{-1}, respectively, followed by Tyr55 and Trp185. The order of Rc in Sub A10 were Tyr224, Tyr228, Tyr55, Tyr314 and Tyr279, which were considerably different from the order in ET rates. In Sub B10, the ET rates were 1.4×10^{-2} from Tyr314, 6.0×10^{-3} from Tyr224 and 1.5×10^{-3} ps^{-1} from Tyr55, followed by Tyr228 and Tyr279. The order of Rc in Sub B10 were the same with Sub A10. Rc of Tyr314 in Sub B10 was the fourth shortest, but the ET rate was fastest. In Sub A30 five fastest donors were Tyr314 (1.6×10^{-2} ps^{-1}), Tyr228 (5.9×10^{-3} ps^{-1}), Tyr224 (3.5×10^{-3} ps^{-1}), Tyr55 and Trp52 in this order, while the order of Rc in Sub30A was Tyr228, Tyr224, Tyr314, Tyr279 and Tyr55. In Sub B30 they were Tyr224 (1.7×10^{-2} ps^{-1}), Tyr314 (6.5×10^{-3} ps^{-1}), Trp185 (1.4×10^{-3} ps^{-1}), Tyr55 and Tyr228, while the order of Rc in Sub30B was Tyr224, Tyr228, Tyr314, Tyr55 and Trp185.

Figure 3.7 illustrates distribution of logarithmic ET rates from aromatic amino acids to Iso*. The distribution pattern was quite different between Sub A and Sub B, and also between 10 °C and 30 °C. Half width of the distribution indicates extent of fluctuation in the logarithmic rate. Most of the donors displayed marked fluctuations. The logarithmic rates from Tyr314 were relatively sharp in all cases. The distribution of Trp185 in Sub A10 displayed double maxima which should be ascribed to double maxima in Rc (see Figure 3.3). ET rate from Tyr228 was the second fastest in Sub 30A, but quite slow in Sub B30. The rate from Trp185 was the third fastest in Sub B30, but much slow in the other systems.
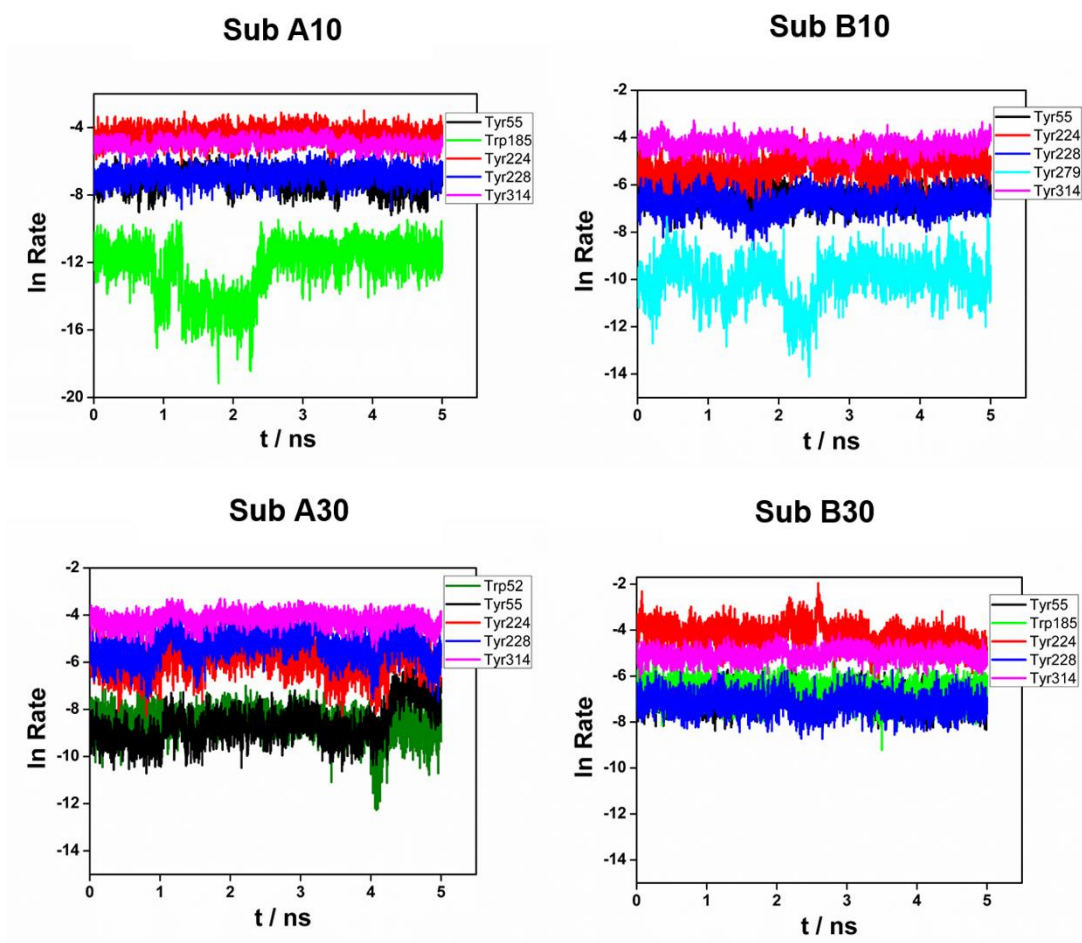
Figure 3.6 *Time evolution of ET rate from aromatic amino acids to Iso*. Insets show the five donors with fast ET rates. Mean ET rates over 5000 snapshots with 1 ps intervals are listed in Table 3.3.*

Table 3.4 Physical quantity related to ET rate. [a]

Dimer Subunit (T)	Donor	$k_{ET}^{jk}(T)$ [b] (ps^{-1})	$E_{Net}^k(j)$ [c] (eV)	λ_{jk}^q [d] (eV)	$-e^2/\varepsilon_0^{pk} R_{jk}$ [e] (eV)	Rc ratio [f]	Monomer [g]	Donor	$k_{ET}^{jk}(T)$ [b] (ps^{-1})	$E_{Net}^k(j)$ [c] (eV)
A (10)	Tyr224	1.29×10^{-2}	0.044	1.79	-0.331	0.82	10	Tyr224	2.27×10^{-3}	0.192
	Tyr314	7.57×10^{-3}	-0.406	1.99	-0.224	1.06		Tyr314	1.38×10^{-3}	-0.073
	Tyr228	1.20×10^{-3}	0.146	1.85	-0.300	0.88		Tyr228	5.94×10^{-4}	0.215
	Tyr55	9.08×10^{-4}	-0.119	1.97	-0.232	0.66		Trp185	1.15×10^{-4}	-0.249
	Trp185	9.71×10^{-6}	-0.104	1.92	-0.178	1.10		Tyr279	1.57×10^{-5}	0.144
B (10)	Tyr314	1.38×10^{-2}	-0.479	1.97	-0.236	0.99				
	Tyr224	5.96×10^{-3}	-0.021	1.83	-0.312	0.95				
	Tyr55	1.54×10^{-3}	-0.161	1.94	-0.250	0.60				
	Tyr228	1.25×10^{-3}	0.056	1.86	-0.297	0.94				
	Tyr279	6.08×10^{-5}	-0.076	2.03	-0.206	0.96				
A (30)	Tyr314	1.63×10^{-2}	-0.293	1.97	-0.231	0.90	30	Tyr314	2.35×10^{-3}	-0.434
	Tyr228	5.86×10^{-3}	0.130	1.87	-0.290	0.96		Tyr224	1.65×10^{-3}	-0.035
	Tyr224	3.39×10^{-3}	0.108	1.90	-0.272	1.02		Tyr55	8.00×10^{-4}	-0.324
	Tyr55	2.43×10^{-4}	-0.207	2.09	-0.168	1.23		Tyr228	6.85×10^{-4}	0.051
	Trp52	2.15×10^{-4}	-0.593	1.92	-0.178	0.96		Tyr106	5.47×10^{-6}	-0.342

B (30)						
	Tyr224	1.68×10^{-2}	-0.038	1.77	-0.340	0.82
	Tyr314	6.51×10^{-3}	-0.422	1.97	-0.234	0.90
	Trp185	1.43×10^{-3}	-0.465	1.85	-0.216	0.77
	Tyr55	9.70×10^{-4}	-0.210	1.97	-0.234	0.89
	Tyr228	8.30×10^{-4}	0.097	1.85	-0.302	0.92

[a] Mean values are listed over 5000 snapshots. ET parameters to obtain these quantities are given in Table 3.3. [b] ET rate is given by eqn (3.1). [c] Net ES energy is given by eqn (3.5). The Net ES energies were obtained in the entire protein. [d] Solvent reorganization energy is given by eqn (3.2). [e] Electrostatic energy between Iso anion and a donor cation. [f] Ratio, Rc in dimer / Rc in monomer. [g] Recalculated with the data given in [105, 106].
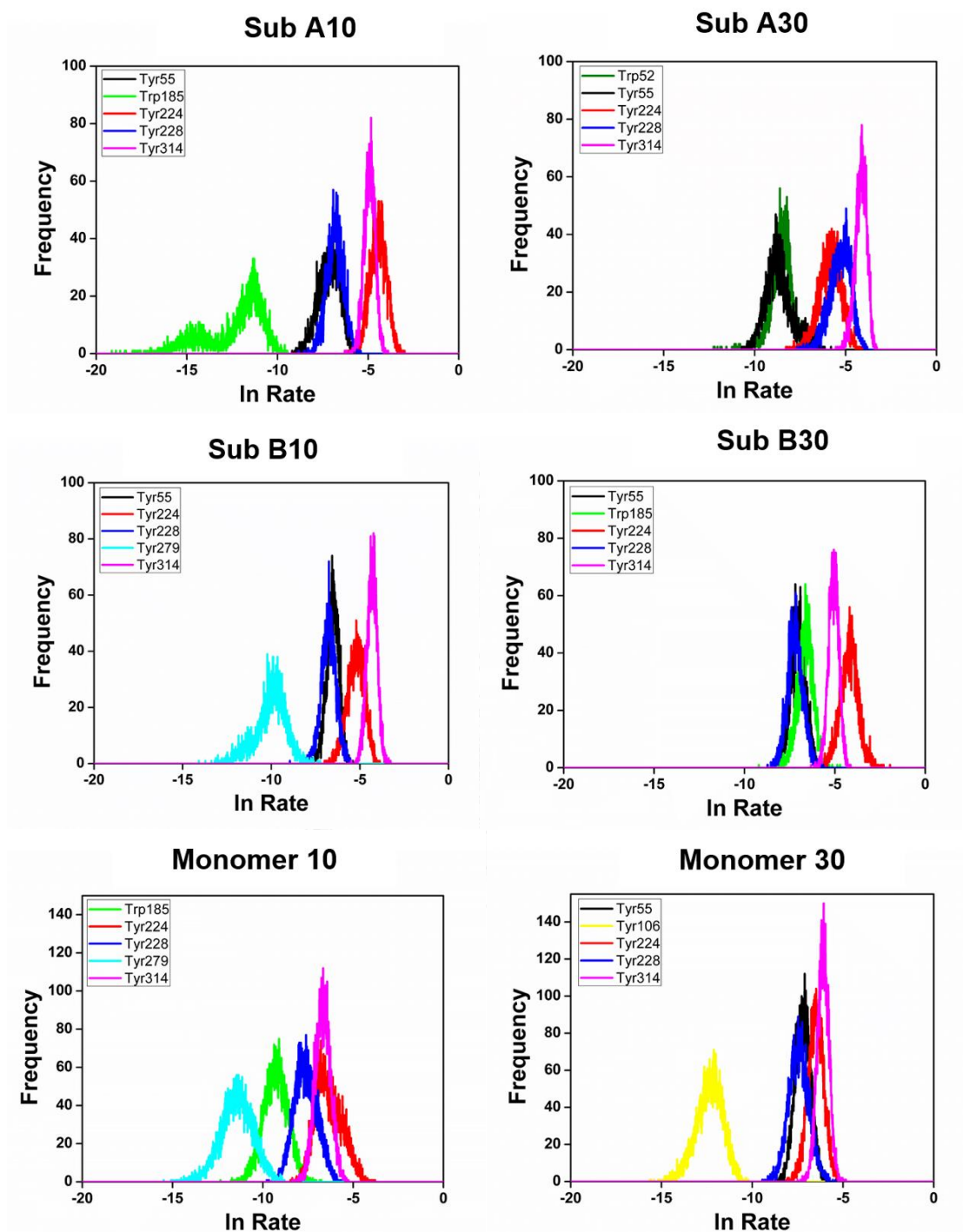
Figure 3.7 *Distribution of logarithmic ET rate from aromatic amino acids to Iso*. Sub A10 and Sub B10 denote Sub A and Sub at 10 ℃ in the dimer, and Sub A30 and Sub B30, Sub A and Sub B at 30 ℃. Insets show amino acids with top fastest ET rates. The distributions for DAAO monomers at 10 ℃ (Monomer10) and 30 ℃ (Monomer 30) are*

also shown for comparison. Kind of the amino acids are different among the six groups including monomer.

The effects of subunit structures on the ET rates are shown in Figure S3.2 (Supplemental Information of Chapter III). In independent model of Figure S3.2 (Supplemental Information of Chapter III) the ET rates were obtained separately in Sub A and in Sub. In the entire model the ET rates were obtained for the entire dimer. The distributions of the Net ES energies obtained with the entire model were quite different from those with the independent model.

3.4.7 Physical quantity related to ET rate

Figure 3.8 shows dynamics of Net ES energy obtained by eqn (3.5). The fluctuation of the energy in Tyr224 and Tyr228 were relatively small. The energy of Trp185 in Sub A10 displayed marked fluctuation. The Net ES energy, $E_{\text{Net}}^{\text{k}}(j)$, of Tyr314 were always low (-0.3 to -0.5 eV), despite the ET rate were fastest or second fastest among the donors. The reason for it is discussed later. Figure 3.9 shows distribution of Net ES energy. As stated above, Net ES energies of Tyr314 were always negative and very low. The Net ES energies of Tyr228 were always positive and highest among the donors with top five ET rates.
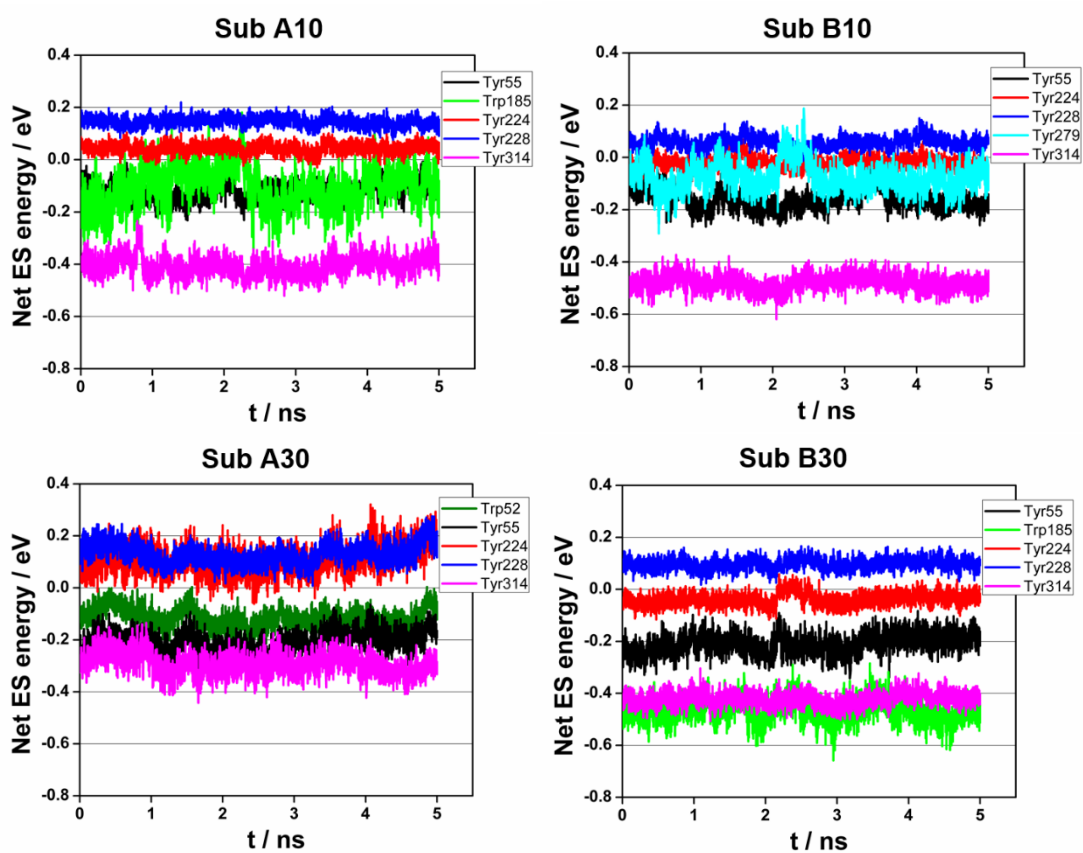
Figure 3.8 *Dynamics of Net ES energy in DAAO dimer. Sub A10 and Sub B10 denote Sub A and Sub B at 10 ℃, and Sub A30 and Sub B30, Sub A and Sub B at 30 ℃. Insets show donors with top fastest ET rates.*
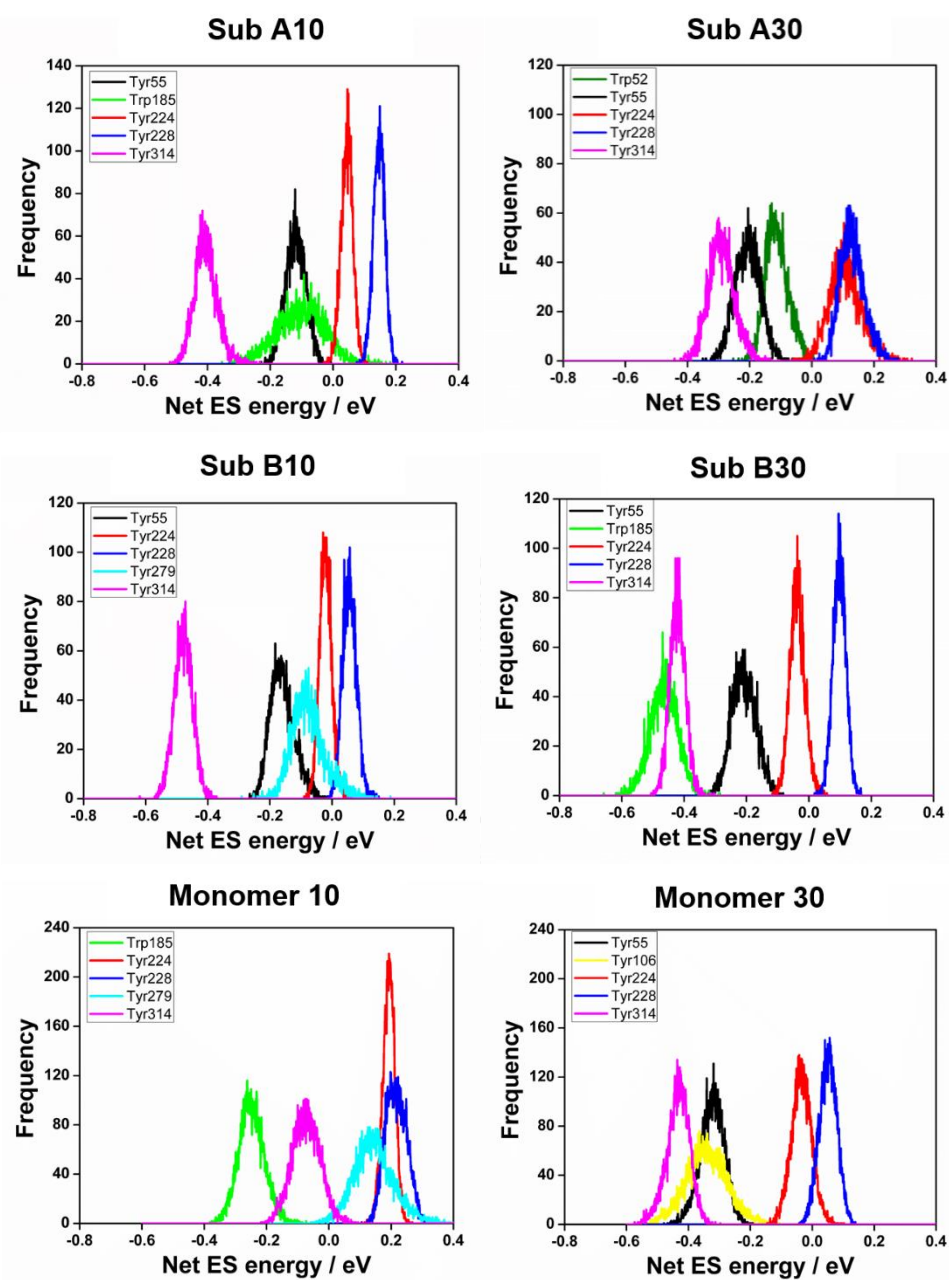
Figure 3.9 *Distributions of Net ES energy. The Net ES energies were obtained with the entire model in which contributions of the energies from both subunits are included. Insets show donors with top fastest ET rates.*

Physical quantities other than ET rate are listed in Table 3.4 including the Net ES energy. Solvent reorganization energy obtained by eqn (3.2), λ_{jk}^{q}, did not display much variation among the donors, 1.7–2.1 eV. ES energy between Iso anion and a donor cation, $-e^2 / \varepsilon_0^{pk} R_{jk}$, varied from -0.17 eV in Tyr55 of Sub A30 to -0.34 eV in Tyr224 of Sub B30.

The effects of subunit structures on the Net ES energies are shown in Figure S3.3 (Supplemental Information of Chapter III). In the independent model of Figure S3.3 (Supplemental Information of Chapter III) Net ES energies were obtained separately in Sub A and in Sub B. In the entire model the Net ES energies were obtained for the entire dimer. The distributions of the Net ES energies obtained with the entire model were quite different from those with the independent model. This suggests that appreciable Net ES energies from Sub B contribute to those in Sub A.

3.4.8 Dutton law

According to Moser et al.,[80] logarithmic ET rate linearly decreases with the donor–acceptor distance, which is called Dutton law. In the present work Tyrs are major donors to Iso*. Dutton law for Tyrs was examined in all Sub A10, Sub B10, Sub A30 and Sub B30. Figure 3.10 shows dependence of the logarithmic ET rates for all Tyrs on Rc. In all systems the logarithmic ET rates were well approximated with linear function, which reveals that Dutton law is valid in DAAO dimer. The slopes of the straight lines were -11.5 in Sub A10, -11.4 in Sub B10, -9.6 in Sub A30 and -11 5 in Sub B30. Dutton law for DAAO monomer was also examined at 10 °C and 30 °C for comparison (see bottom of Figure 3.10). The logarithmic rates of the monomer were also well described with linear functions of Rc. The slopes were -10.6 at 10 °C and -11.6 at 30 °C. Dutton law for all Trps is shown Figure S3.4 (Supplemental Information of Chapter III). The logarithmic ET rates of Trps also decreased linearly with Rc. The slopes of the linear functions were 20–23, which were quite different from those of Tyrs. The magnitude of the slope was least in Sub A30 as that of Tyrs (see Figure 3.10).
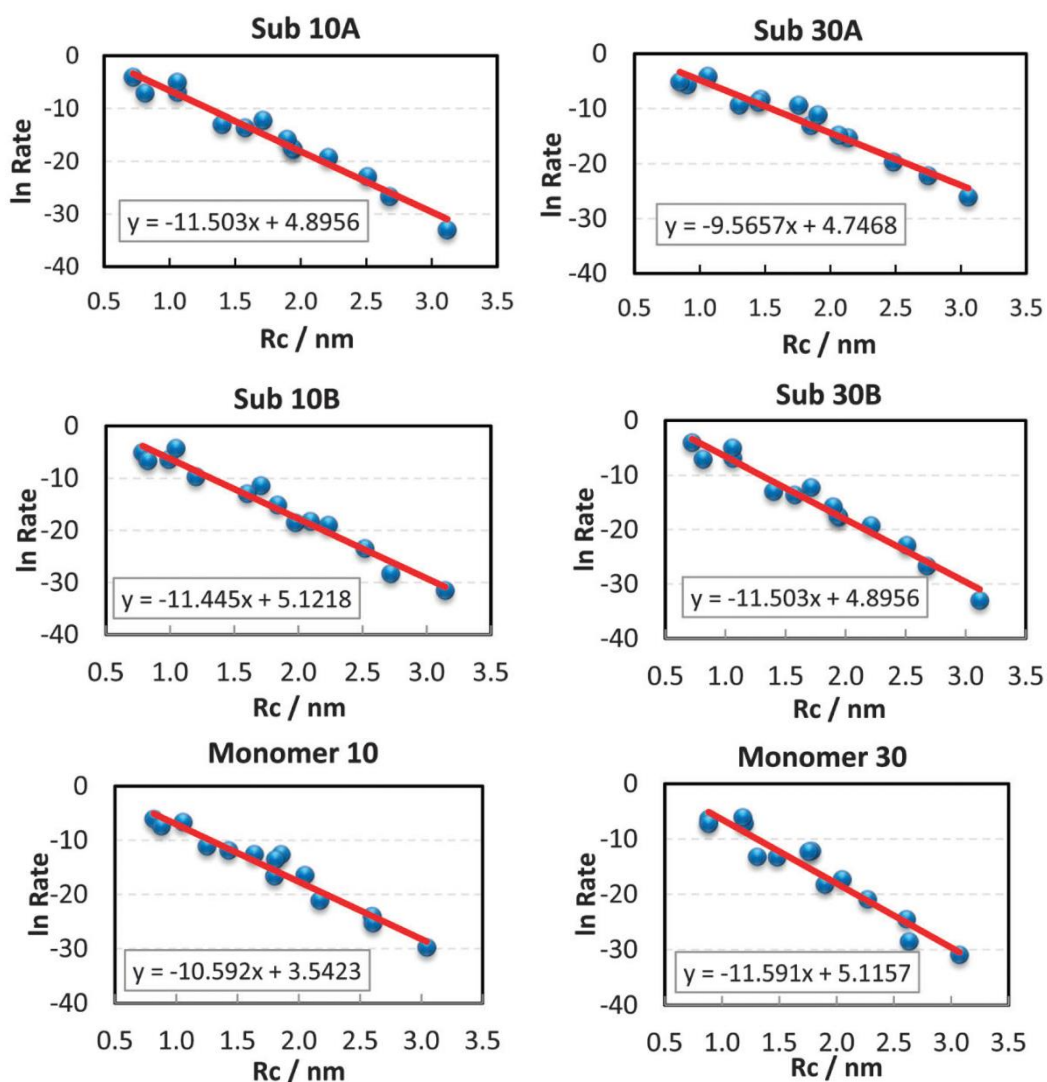
Figure 3.10 *Dutton law for Tyrs as ET donor in DAAO. All Tyrs were taken into account. Insets indicate approximate linear functions. Dutton law for the monomer is also shown for comparison. Absolute value of slope was least in Sub 30A in the dimer.*

3.7.9 Energy gap law

Dependence of logarithmic ET rates on total standard free energy gap $\left\{\Delta G_{\text{Total}}^{0}(T)\right\}$ is called energy gap law. $\Delta G_{\text{Total}}^{0}(T)$ is obtained by eqn (3.8).

$$\Delta G_{\text{Total}}^{0}(T) = -\left\{\Delta G_{\text{k}}^{0}(T) - e^2 / \varepsilon_0^{\text{pk}} R_{\text{jk}} + E_{\text{Net}}^{\text{k}}(j)\right\} \qquad (3.8)$$

The quantities of the right hand side for major donors (Tyrs) are given in Table 3.4. Figure S3.5 (Supplemental Information of Chapter III) shows the energy gap law of Tyrs as the donors in DAAO dimer. The energy gap law of Tyrs in DAAO monomer was also shown for comparison. The logarithmic rates were well approximated with parabolic functions in all systems. The insets in Figure S3.5 (Supplemental Information of Chapter III) represent approximate parabolic functions, $Y = aX^2 + bX + c$, where Y is $\ln k_{\text{ET}}^{\text{jk}}(T)$ and $\mathbf{X}$ is $\Delta G_{\text{Total}}^{0}(T)$. Figure S3.5 (Supplemental Information of Chapter III) reveals that ET from Tyr to Iso* in any cases takes place in normal region. Maximum rates in the dimer were expected at 1.2 eV of $\Delta G_{\text{Total}}^{0}(T)$ in Sub A10, at 1.6 eV in Sub B10, at 1.2 eV in Sub A30 and 1.8 eV in Sub B30. The maximum rates in the monomer were expected at 0.90 eV at 10 °C and at 0.77 eV at 30 °C, which were much smaller than those in the dimer.

3.5 DISCUSSION

Sub A and Sub B displayed quite different structures in solution. Accordingly different physical quantities related to ET were obtained in the following points; (1) Rcs of Tyr55, Tyr314 and Tyr279 quite shorter in Sub B10 than those in Sub 10A, while Rc of Trp185 was much longer in Sub B10 (see Table 3.1 and Figure 3.3), (2) IsoO2 formed H-bond exclusively with Thr317OG1 (side chain) in both Sub A10 and Sub A30, while it formed with Gly315N (peptide), Leu316N and Thr317N in Sub B10 and Sub B30, (3) IsoO4 formed H-bond with Gly50N and Leu51N in Sub A10, while it did not form H-bonds with any amino acids in Sub B10, (4) electron affinity of Iso* {$\Delta G_{\text{k}}^{0}(T)$ in eqn (3.3)} was appreciably lower in Sub A10 compared to Sub B10 (see Table 3.3), while static dielectric constant inside the subunits did not differ between Sub A and

Sub B, (5) ET rate to Iso* was fastest from Tyr224 in Sub A10, while it was fastest from Tyr314 in Sub B10.

The temperature transition in DAAO is also found in the dimer in fluorescence lifetimes,[18] though it is not so pronounced as in the monomer. The structures and the physical quantities were temperature-dependent in the following points; (1) Rc (0.74 nm) of Tyr224 which was shortest in Sub A10, became much longer (0.90 nm) in Sub A30, instead, Rc of Tyr224 in Sub B10 became a little shorter (0.72 nm) in Sub B30, (2) the values of $\Delta G_k^0(T)$ in Sub A10 and 8.5 eV in Sub B10, changed to 8.7 and 8.5 eV in Sub A30 and Sub B30, respectively, whereas the dielectric constant inside the protein did not depend on temperature, (3) ET rate from Tyr224 in Sub A10 reduced by 30% in Sub A30, while that of Tyr314 (second fastest in Sub A10) increased by twice in Sub A30, (4) ET rate from Tyr314 in Sub B10 which was fastest, reduced by 50% in Sub B30, while that of Tyr224 in Sub B10 increased by 3 times in Sub B30.

The fluorescence of DAAO dimer always decays with single lifetime upon changing both the protein concentration and temperature within experimental time resolution,[18] despite that the dimer is expected to display two-lifetime components from Sub A and Sub B if we consider the differences in the structures and physical quantities stated above. The fluorescence decays with total rate summed over the rates from all donors (see eqn (3.6)). The total rate did not differ appreciably between the two subunits. The fluorescence lifetimes of the monomer are around 160 ps, while it is ca. 40 ps in the dimer.[18] It is important to elucidate why the dimer has shorter lifetime than the monomer. In both DAAO dimer and monomer, Net ES energy $\{E_{Net}^k(j)\}$ were mostly negligible compared to solvent reorganization energy (λ_{jk}^q; see Table 3.4), which implies that the shorter lifetimes of Iso* in dimer cannot be elucidated solely in terms of the Net ES energies. On the other hand Rc between Iso and the donors were quite shorter in dimer than those in monomer. Rc ratio in Table 3.4 shows the ratio, Rc (dimer)/Rc (monomer). Mostly values of the ratio were smaller than 1, which means that Rc values of major donors in dimer are shorter than those in monomer. Dutton law in DAAO reveals that the logarithmic ET rates linearly decrease with Rc. This should be main reason why the lifetimes of dimer are shorter than those of monomer.[18]

The static dielectric constant, ε_0^{DA}, between Iso and donors (Tyr224 and Tyr228) did not change from those inside the entire subunits, ε_0^{A} and ε_0^{B}. This is in contrast with those of FMN binding proteins,[39] flavodoxin from *Helocobactor pylori* [34] and DAAO–benzoate complex,[106] where the values of ε_0^{DA} were less than 3. In these protein systems Rcs between Iso and the donors are very short, and so that no amino acid or water molecule can come into the region between Iso and the donors. In contrast with it Rc between Iso and Tyr224 or Tyr228 (shortest among the donors) in DAAO were quite long and so water molecules and other amino acids can be located in this region. Figure 3.11 shows radial distribution functions, G(*r*), of water molecules near Iso, which were obtained with MDS snapshots. The distribution displayed sharp peaks at around 0.3 nm (first layer from hetero atoms in Iso), which shows that the presence of water molecules was quite steady. Similar situation is found in the monomer.[106] Figure 3.12 shows presence of water molecules between Iso and Tyr224 obtained by a snapshot of MDS. In any systems more than one water molecules locate between Iso and Tyr224. These structures may be time-dependent. In some snapshots two or more water molecules came into the region, and also nearby amino acid. These results provide molecular basis for high ε_0^{DA} in DAAO dimer as in the monomer.[105, 106]
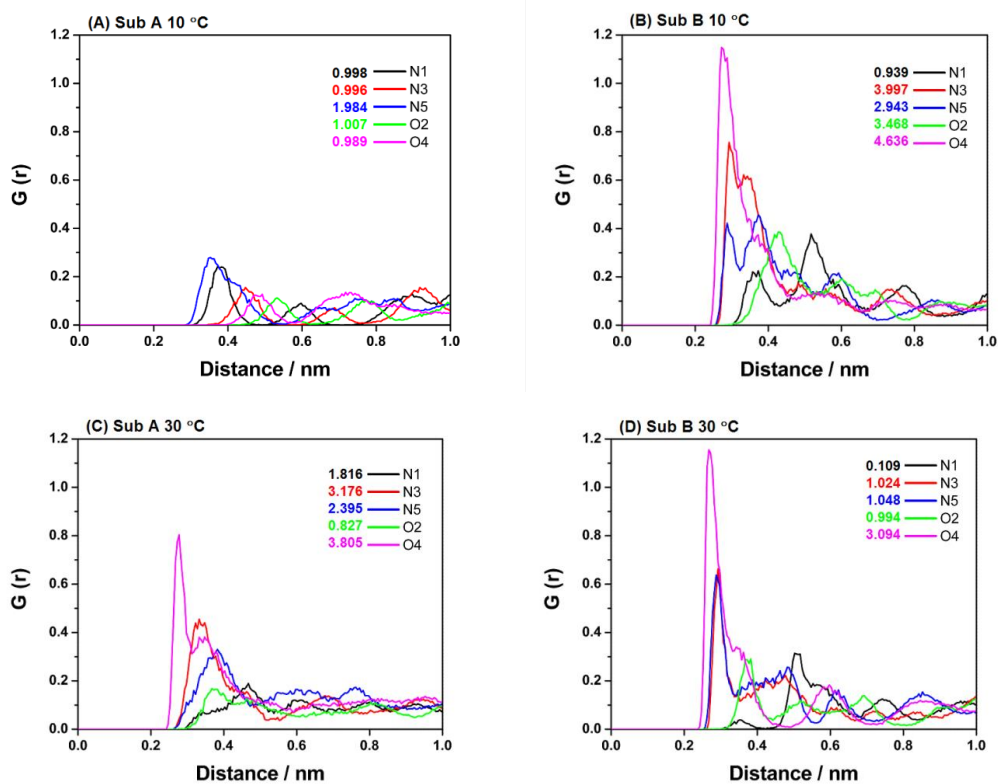
Figure 3.11 *Radial distribution function derived number of water molecules near hetero atoms in Iso ring in DAAO dimer. The radial distribution functions (RDF) were obtained by ptraj module of Amber10 program.[88] Insets indicate number of mean water molecules at the distances from the hetero atoms in Iso.*
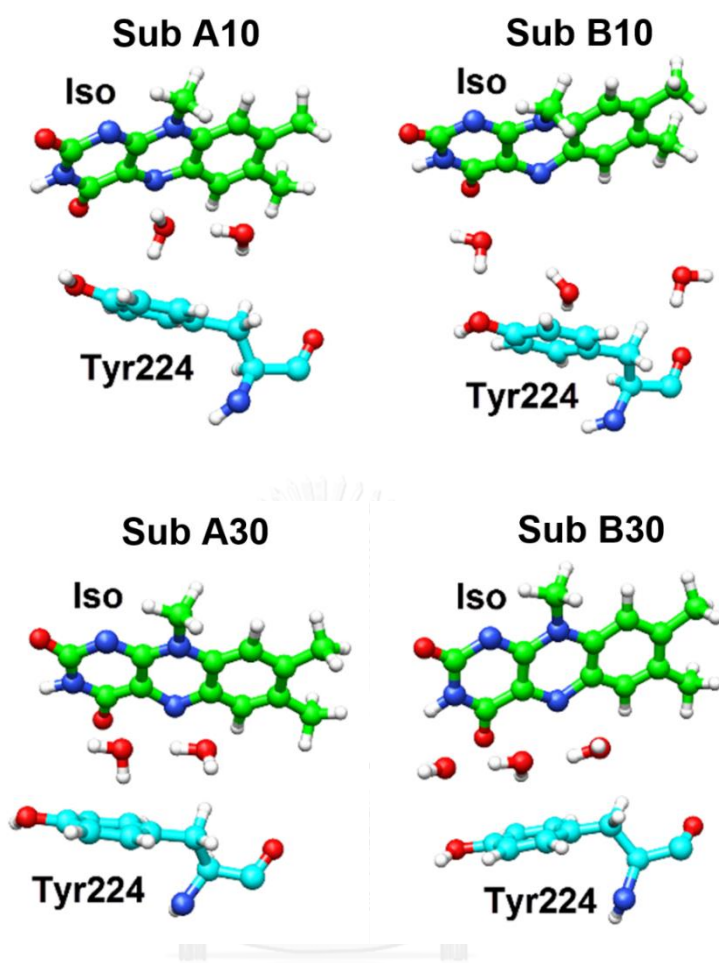
Figure 3.12 *Presence of water molecules between Iso and Tyr224. The structure was obtained from a snapshot in the respective category. Some times more than one water molecules and even an amino acid can come into the region between Iso and Tyr224.*

CHAPTER IV

THEORETICAL ANALYSES OF THE FLUORESCENCE LIFETIMES OF THE D-AMINO ACID OXIDASE–BENZOATE COMPLEX DIMER FROM PORCINE KIDNEY: MOLECULAR DYNAMICS SIMULATION AND PHOTOINDUCED ELECTRON TRANSFER

Arthit Nueangaudom[a], Kiattisak Lugsanangarm[a], Somsak Pianwanit[a], Sirirat Kokpol[a], Nadtanet Nunthaboot[b], Fumio Tanaka[ac], Seiji Taniguchi[c] and Haik Chosrowjan[c]

[a] Department of Chemistry, Faculty of Science, Chulalongkorn University, 254 Phayathai Road, Bangkok 10330, Thailand.

[b] Department of Chemistry, Faculty of Science, Mahasarakham University, Thailand.

[c] Division of Laser Biochemistry, Institute for Laser Technology, Utsubo-Honmachi, 1-8-4, Nishiku, Osaka 550-0004, Japan.

4.1 ABSTRACT

The mechanism of photoinduced electron transfer (ET) from benzoate (Bz) and aromatic amino acids to the excited isoalloxazine (Iso*) in the D-amino acid oxidase– benzoate complex (DAOB) dimer from porcine kidney was studied using molecular dynamics simulation (MDS) and an electron transfer theory, and compared with that in the DAOB monomer. The DAOB dimer displayed two fluorescent lifetime components of 0.85 ps and 4.8 ps, as reported. The ET parameters contained in the Kakitani and Mataga (KM) model were determined so as to reproduce these lifetimes with MDS atomic coordinates. The Bz– isoalloxazine (Iso) distances were 0.66 nm in subunit A (Sub A), 0.68 nm in subunit B (Sub B) and 0.61 nm in the monomer. The fluorescent lifetimes of 4.8 ps and 0.85 ps were found to originate from Sub A and Sub B, respectively. In Sub A, Tyr228 was the fastest ET donor followed by Bz and Tyr55, while Bz was followed by Tyr228 and Tyr314 in Sub B. The ET rate from Bz was fastest in Sub B, followed by that in Sub A and the DAOB monomer. The static dielectric constants obtained near Iso were 2.4–2.6 in the DAOB dimer and monomer and 5.8–5.9 in holo D-amino oxidase (DAAO). The different dielectric constants could account for the experimental fluorescence peak observed for DAOB (524 nm) and DAAO (530 nm). Logarithmic ET rates decreased linearly with the donor–acceptor distance expressed by both center to center distance (Rc) and edge to edge distance (Re) in Sub A and Sub B of DAOB dimer and monomer, which reveals that the conventional Dutton rule holds in the ET processes in DAOB. The logarithmic ET rates were decomposed into the electronic coupling (EC), square root (SQ) and exponential (GTRAM) terms. It was found that both the EC term and the GTRAM term also decreased linearly with Rc. The sum of the slopes in the EC and GTRAM vs. Rc plots coincided with the slopes in the logarithmic ET rate vs. Rc functions, suggesting that the GTRAM term makes a significant contribution to the linear relations between logarithmic ET rate and Rc.

4.2 INTRODUCTION

D-Amino acid oxidase (DAAO) from porcine kidney contains flavin adenine dinucleotide (FAD) as a cofactor,[101, 102] and exists in a wide range of species from yeasts to human.[62, 103, 104] Its function is to oxidize D-amino acids to the corresponding imino acids, producing ammonia and hydrogen peroxide. Recently, mammalian DAAO has been demonstrated to be involved in D-serine metabolism in the brain and to regulate glutamatergic neurotransmission.[63, 64] Various novel inhibitors to human DAAO have been found by means of in silico screening.[49]

DAAO from porcine kidney exists in a monomer (M_w 39 kDa)-dimer equilibrium state at relatively low concentrations,[23-26] and may be in a dimer-tetramer equilibrium at higher concentrations.[27-29] The crystal structures of the DAAO-benzoate (Bz) complex (DAOB) dimer have been determined.[19, 69] Each subunit of the DAOB dimer contains Iso as the ET acceptor, and one Bz, 10 Trp and 14 Tyr residues as potential ET donors.

The fluorescence of flavins in many flavoproteins is strongly quenched, which is ascribed to photoinduced electron transfer (ET) from tryptophans (Trp) and/or tyrosines (Tyr) to the excited isoalloxazine (Iso*).[5-7] Fluorescence dynamics of flavoproteins have been worked in the picoseconds domain by Visser et al,[8, 10] by means of photon-counting method. Ultrafast fluorescence dynamics of some flavoproteins in the time domain of femtoseconds to picoseconds have been studied by means of fluorescence up-conversion,[11-13, 15, 16] and theoretically by molecular dynamics simulation (MDS) and an electron transfer theory [32, 34, 35, 39, 42] using the available protein structures.[19, 69]

The structural basis for the temperature-induced transition of the DAAO monomer has been analyzed by MDS with the Kakitani and Mataga (KM) equation based ET theory.[105] The conformational change was characterized with the ET rates from Tyr224, Tyr228 and Tyr314 to the Iso*. The fluorescence lifetimes of flavin in DAAO and DAOB monomer have been reported to be 160 and 60 ps, respectively, with the decreased lifetime upon the binding of Bz to DAAO being ascribed to the fast ET from Bz to Iso*.[17, 106] The fluorescence dynamics of the DAOB dimer has been

reported by means of the up-conversion,[15] whilst it was recently reported that the DAAO dimer displays non-equivalent conformations between the two subunits.[109] In the present work we have demonstrated by means of MDS structures and KM-theory based ET analysis that not only the structure of the DAOB dimer is quite different from the DAOB monomer, but also the conformations of subunit A (Sub A) and Sub B of the DAOB dimer are non-equivalent.

4.3 METHODS OF ANALYSES

4.3.1 MDS calculation

The starting structure of DAOB was obtained from the X-ray structure in the protein data bank (PDB code: 1VE9).[19] The MDS and all calculations were performed using the AMBER 10 suite of programs.[88] The parm99 force field [89] was used to describe the protein atoms the general Amber force field with the restrained electrostatic potential [88] charges was used for the FAD and Bz, and all missing hydrogen atoms of the protein were added using the LEaP module.[91] The simulated systems were subsequently solvated with a cubic box of 27,390 TIP3P water molecules, and the electroneutrality of the system was attained by adding 10 sodium counter-ions. The systems were set up under the isobaric-isothermal ensemble with a constant pressure (1 atm) and temperature (293 K). Electrostatic interactions were corrected by the Particle Mesh Ewald method.[92] The SHAKE algorithm [93] was used to constrain all bonds involving hydrogen atoms. All MDS based calculations were performed with a time steps of 2 fs and a non-bond-interaction cut off radius of 10 Å. The coordinates of the MDS snapshots were collected every 0.1 ps. Equilibrium, attained after 20 ns of the MDS calculation, was ascertained by monitoring the global root mean square deviation (RMSD). The calculation was then continued for up to a further 30 ns, and the last 5 ns data were used for the analyses.

4.3.2 ET rates from Trp and Tyr

The original Marcus theory [78, 79] has been modified in various ways.[61, 80, 107, 108, 110] In the present analysis, KM theory [108] was used, because it is

applicable for both non-adiabatic ET processes and adiabatic ET processes, and has been found to give satisfactory results for both static,[11, 105, 106, 109] and dynamic ET analyses.[32, 34, 35, 39, 42] When the donor is Trp or Tyr, the ET rate described by the KM theory is expressed by eqn (4.1).

$$k_{ET}^{j} = \frac{\nu_0^q}{1 + \exp\left\{\beta^q (R_j - R_0^q)\right\}} \sqrt{\frac{k_B T}{4\pi\lambda_S^{qj}}} \exp\left[-\frac{\left\{\Delta G_q^0 - e^2 / \varepsilon_0^p R_j + \lambda_S^{qj} + ES_j(k)\right\}^2}{4\lambda_S^{qj} k_B T} \right] \quad (4.1)$$

Here k_{ET}^{j} is the ET rate from a donor j (j = 1–10 for Trp, j = 11–24 for Tyr) to the photoexcited Iso*, and q denotes Trp or Tyr. ν_0^q is an adiabatic frequency, β^q is the ET process coefficient. R_j and R_0^q is the donor j –Iso distance and its critical distance for the ET process, respectively. R_j is expressed as a center-to-center (Rc) distance rather than as an edge-to-edge (Re) distance.[11, 13, 32, 35, 39, 42, 107, 108] The ET process is adiabatic when $R_j < R_0^q$, and non-adiabatic when $R_j > R_0^q$. The terms k_B and e are the Boltzmann constant and electron charge, respectively. T is the temperature (K), and here was fixed at 293 K (20 $^\circ$C). The term $-e^2 / \varepsilon_0^p R_j$ in eqn (4.1) is the electrostatic energy (ES) between the Iso anion and a donor cation (ESDA). The static dielectric constant ε_0^p is described below. ES_j is a net the ES energy (NetES) between the donor j cation and other ionic groups, which is also described below. Each subunit of the DAOB dimer contains one Bz, 10 Trp and 14 Tyr residues as potential donors. The ET rates from all of these donors to Iso* were taken into account for the analysis.

λ_S^{qj} is the solvent reorganization energy [78, 79] of the ET donor q and j, and is expressed as eqn (4.2);

$$\lambda_S^{qj} = e^2 \left(\frac{1}{2a_{Iso}} + \frac{1}{2a_q} - \frac{1}{R_j} \right) \left(\frac{1}{\varepsilon_\infty} - \frac{1}{\varepsilon_0^p} \right), \tag{4.2}$$

where a_{Iso} and a_q are the radii of isoalloxazine (Iso) and one of Trp or Tyr, with these reactants being assumed to be spherical, and ε_∞ and ε_0^p are the optical and static dielectric constants in the domain among Iso and donors, respectively. In this study, the optical dielectric constant was set as 2.0. In eqns (4.1) and (4.2) it was assumed that $\varepsilon_0^p = \varepsilon_0^{DA}$ for Bz, Tyr55 and Tyr228 in Sub A, and $\varepsilon_0^p = \varepsilon_0^{DA}$ for Bz and Tyr228 in Sub B, where the mean Rc values were shorter than 1 nm (see Table 4.1), and $\varepsilon_0^p = \varepsilon_0$ for both Sub A and Sub B in the other donors.[109] The previously determined values for the radii of Iso (a_{Iso}), Trp (a_{Trp}) and Tyr (a_{Tyr}) of 0.224, 0.196 and 0.173 nm, respectively,[32, 34, 35, 39, 42, 105] were used.

Table 4.1 Mean donor-acceptor Rc value in the DAOB subunits and monomer.[a]

Donor	Sub A	Sub B	Monomer
Bz	0.66	0.68	0.61
Tyr55	0.95	1.05	1.31
Tyr144	1.32	1.38	1.43
Trp185	1.10	1.31	1.39
Tyr224	1.32	1.04	0.97
Tyr228	0.96	0.99	0.81
Tyr279	1.36	1.45	1.24
Tyr314	1.06	1.02	1.07

[a] The centre-to-centre distances (Rc) between the Iso acceptor and each donor of Sub A and Sub B in the dimer and in the monomer are shown as the mean values (nm) obtained from 5000 snapshots with 1 ps time intervals. Temperature was 20 °C. Bz denotes benzoate; Sub denotes subunit.

The standard free energy change was expressed with the ionization potential of the ET donor (E_{IP}^q) as eqn (4.3);

$$\Delta G_q^0 = E_{IP}^q - G_{Isop}^0 \,, \tag{4.3}$$

where G_{Isop}^0 is standard free energy related to the electron affinity of Iso*. $G_{Isop}^0 = G_{IsoA}^0$ for Sub A, and $G_{Isop}^0 = G_{IsoB}^0$ for Sub B. The values of E_{IP}^q for Trp and Tyr were 7.2 eV and 8.0 eV, respectively.[96]

4.3.3 ET rate from Bz

When the donor is Bz, the ET rate may be expressed by eqn (4.4);

$$k_{ET}^{Bz} = \frac{\nu_0^{Bz}}{1 + \exp\left\{\beta^{Bz}(R_{Bz} - R_0^{Bz})\right\}} \sqrt{\frac{k_B T}{4\pi \lambda_S^{Bz}}} \exp\left[-\frac{\left\{\Delta G_{Bz}^0 + E_{Iso}^{Bz} + \lambda_S^{Bz} + ES_{Bz}\right\}^2}{4\lambda_S^{Bz} k_B T}\right], \tag{4.4}$$

where ν_0^{Bz}, β^{Bz} and R_0^{Bz} are the adiabatic frequency, ET process coefficient and critical ET distance of Bz, respectively. In this case the solvent reorganization energy is represented as eqn (4.5);

$$\lambda_S^{Bz} = e^2 \left(\frac{1}{2a_{Iso}} + \frac{1}{2a_{Bz}} - \frac{1}{R_{Bz}}\right)\left(\frac{1}{\varepsilon_\infty} - \frac{1}{\varepsilon_0^p}\right), \tag{4.5}$$

where a_{Bz} was 0.108 nm.[106] R_{Bz} is the Rc distance between Iso and Bz. The ES energies between the photoproducts and ionic groups (ES_{Bz}), and between the Iso anion and a neutral radical of Bz (E_{Iso}^{Bz}) are described below. The standard free energy gap (ΔG_{Bz}^0) is given by eqn (4.6);

$$\Delta G_{Bz}^0 = E_{IP}^{Bz} - G_{Isop}^0 \,, \tag{4.6}$$

where E_{IP}^{Bz} denotes the ionization potential of Bz, which was previously determined to be 7.25 eV.[106]

4.3.4 Electrostatic energy in the DAOB dimer

Protein systems contain many charged/polar moieties which may influence the ET rate. Ionic groups in each subunit of DAOB are the negatively charged pyrophosphate (-2) in FAD, Bz (-1), 22 Glu (-1) and 13 Asp (-1), plus the positively charged 12 Lys (+1) and 21 Arg (+1) residues, resulting in a net charge of -5. In the dimer, the total number of point charges are double that of the monomer and was counterbalanced in the MDS by 10 sodium ions.

When the donor is Trp or Tyr, the ES energy between the donor cation $j \geq 1$ and all other ionic groups in the protein is expressed by eqn (4.7);

$$E(j) = \sum_{i=1}^{44} \frac{C_j C_{Glu}}{\varepsilon_0 R_j (Glu-i)} + \sum_{i=1}^{26} \frac{C_j C_{Asp}}{\varepsilon_0 R_j (Asp-i)}$$
$$+ \sum_{i=1}^{24} \frac{C_j C_{Lys}}{\varepsilon_0 R_j (Lys-i)} + \sum_{i=1}^{42} \frac{C_j C_{Arg}}{\varepsilon_0 R_j (Arg-i)} + \sum_{i=1}^{8} \frac{C_j C_P}{\varepsilon_0 R_j (P-i)}, \qquad (4.7)$$

where j = 1–10 for the Trp cations and 11–24 for the Tyr cations. C_j is the charge of the aromatic ionic species j, that is $+e$ for j = 1–24. C_{Glu} ($=-e$), C_{Asp} ($=-e$), C_{Lys} ($= +e$), and C_{Arg} ($= +e$) are the charges of the Glu, Asp, Lys and Arg residues, respectively. FAD contains two phosphorus atoms, each of which is bonded to two oxygen atoms with charges. It was assumed that the charge of each oxygen atom (C_P) is -0.5e, and then the total charge at the four phosphate atoms is -2e. We also assumed that these groups are all in an ionic state in solution. The pK$_a$ values of the charged amino acids (Glu, Asp, Lys, Arg and His) in water are 4.3, 3.9, 10.5, 12.5 and 6.0, respectively. Although these pK$_a$ values may be slightly modified in proteins, they are still likely to be fully ionized in the 17 mM pyrophosphate buffer (pH 8.3) that all the measurements were performed.[15] The positions of Glu and Asp were expressed by the coordinates of the center of the two O atoms of the side chain, Lys by the coordinates of N atom of the side chain and Arg by the coordinates of the center between two edge N atoms

of the side chain. The distances between the aromatic ionic species j and the ith Glu (i = 1–44) are denoted as $R_j(Glu-i)$, whilst the distances between the aromatic ionic species j and the ith Asp (i = 1–26) are denoted as $R_j(Asp-i)$, and so on for each ionic group. These distances were evaluated as the average distances over all atoms in the aromatic donors.

The ES energy between the Iso anion and the ionic groups was obtained by eqn (4.8);

$$E_{Iso} = \sum_{i=1}^{44} \frac{C_{Iso}C_{Glu}}{\varepsilon_0 R_{Iso}(Glu-i)} + \sum_{i=1}^{26} \frac{C_{Iso}C_{Asp}}{\varepsilon_0 R_{Iso}(Asp-i)}$$
$$+ \sum_{i=1}^{24} \frac{C_{Iso}C_{Lys}}{\varepsilon_0 R_{Iso}(Lys-i)} + \sum_{i=1}^{42} \frac{C_{Iso}C_{Arg}}{\varepsilon_0 R_{Iso}(Arg-i)} + \sum_{i=1}^{8} \frac{C_{Iso}C_{P}}{\varepsilon_0 R_{Iso}(P-i)}, \quad (4.8)$$

where C_{Iso} = $-e$. The distances between Iso and the ith Glu (i = 1–44) are denoted as $R_{Iso}(Glu-i)$, whilst the distances between Iso and the ith Asp (i = 1–26) are denoted as $R_{Iso}(Asp-i)$ and so on for all the aromatic amino acids.

ES_j in eqn (4.1) was expressed as eqn (4.9);

$$ES_j = E_{Iso} + E(j), \quad (4.9)$$

where j is from 1–24, and represents the jth ET donor, as described above.

When the donor is Bz, the ES energies have to be considered separately from Trp and Tyr, since the photoproduct of Bz is neutral, which is in contrast to that for Trp and Tyr which are cations. In the point charge approximate utilized above, the ES energies between the neutral radical of Bz produced by ET and all other ionic species totals to zero. Accordingly, these ES energies were calculated using the charge densities of atoms in neutral Bz by eqn (4.10);

$$E_{Bz} = \frac{1}{N_{Bz}} \sum_{l=1}^{N_{Bz}} \left[\sum_{i=1}^{44} \frac{D_{Bz}^l C_{Glu}}{\varepsilon_0 R_{Iso}(Glu-i)} + \sum_{i=1}^{26} \frac{D_{Bz}^l C_{Asp}}{\varepsilon_0 R_{Iso}(Asp-i)} \right.$$
$$\left. + \sum_{i=1}^{24} \frac{D_{Bz}^l C_{Lys}}{\varepsilon_0 R_{Iso}(Lys-i)} + \sum_{i=1}^{42} \frac{D_{Bz}^l C_{Arg}}{\varepsilon_0 R_{Iso}(Arg-i)} + \sum_{i=1}^{8} \frac{D_{Bz}^l C_P}{\varepsilon_0 R_{Iso}(P-i)} \right], \quad (4.10)$$

where D_{Bz}^l denotes the charge density of the neutral radical of Bz at atom l and N_{Bz} is the number of atoms in Bz and is equal to 14. $\sum_{l=1}^{N_{Bz}} D_{Bz}^l = 0$ holds. The ES energies between the Iso anion and the neutral Bz were also calculated from their respective charge densities using eqn (4.11),

$$E_{Iso}^{Bz} = \frac{e^2}{N_{Iso} N_{Bz}} \sum_{i=1}^{N_{Iso}} \sum_{j=1}^{N_{Bz}} \frac{D_{Iso}^i D_{Bz}^j}{\varepsilon_0^p R_i^j}. \quad (4.11)$$

The charge density of atom i in the Iso anion is denoted as D_{Iso}^i. $\sum_{i=1}^{N_{Iso}} D_{Iso}^i = -1$ holds. N_{Iso} is number of atoms of lumiflavin and is equal to 31. D_{Bz}^l and D_{Iso}^i were used as obtained and reported previously.[106] The NetES energy for Bz is given by eqn (4.12),

$$ES_{Bz} = E_{Bz} + E_{Iso}^{Bz}. \quad (4.12)$$

4.3.5 Determination of the ET parameters

The fluorescence spectrum of the DAOB dimer showed an emission peak at 524 nm (Figure S4.1, Supplemental Information of Chapter IV). The fluorescence decays of the DAOB dimer with two-exponential decay functions have been reported previously by Mataga et al.[15] and the decay functions at the emission wavelength (λ) are expressed by eqn (4.13);

$$F(\lambda t) = \alpha_1(\lambda) \exp\{-t/\tau_1(\lambda)\} + \alpha_2(\lambda) \exp\{-t/\tau_2(\lambda)\}, \quad (4.13)$$

where $\tau_1(\lambda)$ and $\tau_2(\lambda)$ are the emission wavelength-dependent fluorescence lifetimes of components 1 and 2, respectively, $\alpha_1(\lambda)$ and $\alpha_2(\lambda)$ are their emission

wavelength-dependent fractions and $\alpha_1(\lambda) + \alpha_2(\lambda) = 1$. The decay parameters are listed in Table S4.1 (Supplemental Information of Chapter IV).

Some of the ET parameters contained in eqns (4.1)–(4.11) have been reported previously,[32, 34, 35, 39, 42, 105, 106, 109] whilst the parameters used in the present work are listed in Table 4.2. First we tried to reproduce the experimental lifetimes with the previously obtained ET parameters, but the agreements between the calculated and observed lifetimes were not satisfactory (not shown). Accordingly, in the present ET analysis G_{IsoA}^0, G_{IsoB}^0, R_0^{Bz}, ε_0^{DA}, and ε_0^{DB} were chosen as adjustable parameters to obtain a best-fit between the observed and calculated lifetimes. G_{IsoA}^0 and G_{IsoB}^0 are the free energies related to electron affinities of Iso* in Sub A and Sub B, respectively, while ε_0^{DA} and ε_0^{DB} are the static dielectric constants between Iso and the donors (Bz, Tyr55 and Tyr228) in Sub A and between Iso and the donors (Bz and Tyr228) in Sub B, respectively (see below eqn (4.2)). R_0^{Bz} is the critical ET distance for Bz in eqn (4.4). The other ET parameters are common to both subunits. The unknown ET parameters were determined by two methods, where the minimum chi-squared values (χ_1^2 or χ_2^2) were derived from eqns (4.14) and (4.15) in methods 1 and 2, respectively:

$$\chi_1^2 = \frac{\left(\tau_{obs}^1 - \tau_{calc}^A\right)^2}{\tau_{calc}^A} + \frac{\left(\tau_{obs}^2 - \tau_{calc}^B\right)^2}{\tau_{calc}^B} ,$$
(4.14)

$$\chi_2^2 = \frac{\left(\tau_{obs}^1 - \tau_{calc}^B\right)^2}{\tau_{calc}^B} + \frac{\left(\tau_{obs}^2 - \tau_{calc}^A\right)^2}{\tau_{calc}^A} .$$
(4.15)

The observed lifetimes, τ_{obs}^1 (0.848 ps) and τ_{obs}^2 (4.77 ps), are the mean lifetimes of $\tau_1(\lambda)$ and $\tau_2(\lambda)$ in eqn (4.13), respectively, over 10 emission wavelengths (λ). In method 1 (χ_1^2) it was assumed that the fluorescent component with τ_{obs}^1 and τ_{obs}^2 were from Sub A and Sub B, respectively, whilst in method 2 (χ_2^2) it was assumed that the fluorescent component with τ_{obs}^1 and τ_{obs}^2 were from Sub B and Sub A, respectively. The obtained values of χ_1^2 and χ_2^2 were then compared to determine the likely ET mechanism in the DAOB dimer.

4.3.6 Molecular orbital study of charge densities of Iso and hydrogen bonding amino acids.

The charge densities were obtained by a semi-empirical MO method with the software package of MOPAC2009. The keywords, EF (geometrical optimization), PRECISE (accurate calculation), PM6 (semi-empirical Hamiltonians), XYZ (geometry expressed by (x, y, z) coordinates), GEO-OK (neglect check on abnormal access of atoms), EPS (dielectric constant for COSMO solvation energy) were used. The details of these keywords are found on the website: http://openmopac.net. In addition to these keywords, the keyword EXCITED was used for Iso*. The values of EPS were 2.6 both for Sub A and Sub B, because ε_0^{DA} and ε_0^{DB} were close to 2.6 (see Table 4.3). Sub A formed hydrogen bondings (H-bond) with Ala49, Leu51 and Thr317 in Sub A, and with Ala49 and Leu51 in Sub B. The charge densities of Iso and Iso* were calculated with and without H-bond clusters.

Table 4.2 ET parameters used for the ET analysis.

ν_0^{Trp} a (ps^{-1})	ν_0^{Tyr} a (ps^{-1})	β^{Trp} a (nm^{-1})	β^{Tyr} a (nm^{-1})	R_0^{Trp} a (nm)	R_0^{Tyr} a (nm)	ε_0 b	τ_1 c (ps)	τ_2 c (ps)	ν_0^{Bz} d (ps^{-1})	β^{Bz} d (nm^{-1})	E_{IP}^{Bz} d (eV)
1016	197	21	6.25	0.663	0.499	5.78	0.848	4.77	2001	15.0	7.25

a Data taken from Nunthaboot et al.[39]

b Data taken from Table S4.2 (Supplemental Information of Chapter IV).

c Mean shorter (τ_1) and longer (τ_2) lifetimes over ten decays with different emission wavelengths. Data taken from Mataga et al.[15] and listed in Table S4.1 (Supplemental Information of Chapter IV).

d Data taken from Nueangaudom et al.[105]

Table 4.3 Best-fit ET parameter.[a]

Method[b]	Model[c]	$G^{0\ d}_{IsoA}$ (eV)	$G^{0\ e}_{IsoB}$ (eV)	$\varepsilon^{DA\ f}_0$	$\varepsilon^{DB\ g}_0$	$R^{Bz\ h}_0$ (nm)	$\chi^{2\ i}_A$	$\chi^{2\ j}_B$	$\chi^{2\ k}_T$
1	τ^1_{obs} (τ^A_{calc}) τ^2_{obs} (τ^B_{calc})	8.34	8.48	2.65	2.56	0.417	1.79×10^{-19}	1.96×10^{-30}	8.76×10^{-20}
2	τ^1_{obs} (τ^B_{calc}) τ^2_{obs} (τ^A_{calc})	8.42	8.43	2.53	2.64	0.462	2.72×10^{-21}	2.23×10^{-30}	1.36×10^{-21}

[a] The calculated decays for Sub A and Sub B by Method 2 (Figure 4.5) use the ET parameters here. Other ET parameters used are listed in Table 4.2.

[b] Total chi-squared values for Methods 1 and 2 are given by eqns (4.14) and (4.15), respectively.

[c] The calculated fluorescence lifetimes for Sub A and Sub B are indicated as τ^A_{calc} and τ^B_{calc}, respectively. In Method 1 τ^A_{calc} was fit with τ^1_{obs}, and τ^B_{calc} with τ^2_{obs}. In Method 2, τ^A_{calc} was fit with τ^2_{obs} and τ^B_{calc} with τ^1_{obs}. The calculated lifetimes, τ^A_{calc} and τ^B_{calc} were 0.848 ps and 4.77 ps, respectively, which completely agreed with those of the observed lifetimes.

[d,e] Standard free energy related to electron affinity of Iso* in [d] Sub A and [e] Sub B.

[f,g] Static dielectric constant around Iso, Bz, Tyr55 and Tyr228 in f Sub A, and around Iso, Bz and Tyr228 in g Sub B.

[h] Critical ET distance of Bz as a donor.

[i,j] Chi-squared value for j Sub A and k Sub B. [k] Total chi-squared value for Method 1 (χ^2_1) and for Method 2 (χ^2_2).

4.4 Results

4.4.1 Comparisons between MDS snapshot and crystal structure and between the two subunits in the DAOB dimer

Figure 4.1 shows the MDS snapshot of the two subunits of the DAOB dimer superimposed on the crystal structure. In Figure 4.1A, the crystal structure of Sub A was superimposed on that of Sub B and in Figure 4.1B MDS snapshot of Sub A was superimposed on that of Sub B. In crystal the local structures of Sub A and Sub B [19] are almost equivalent. However, in the MDS snapshots the both structures displayed considerable difference between Sub A and Sub B, especially in the aromatic amino acids of Tyr224, Tyr55 and Tyr314 among the chromophores were quite different between Sub A and Sub B. The structures were compared between the crystal and MDS for Sub A in Figure 4.1C, and for Sub B in Figure 4.1D. It is obvious that the crystal and MDS structures are quite different both in Sub A and Sub B, not only near Iso binding site, but also in the entire protein (Figure 4.1E). This may be ascribed to the presence of freely mobile water molecules near the protein in MDS snapshots.
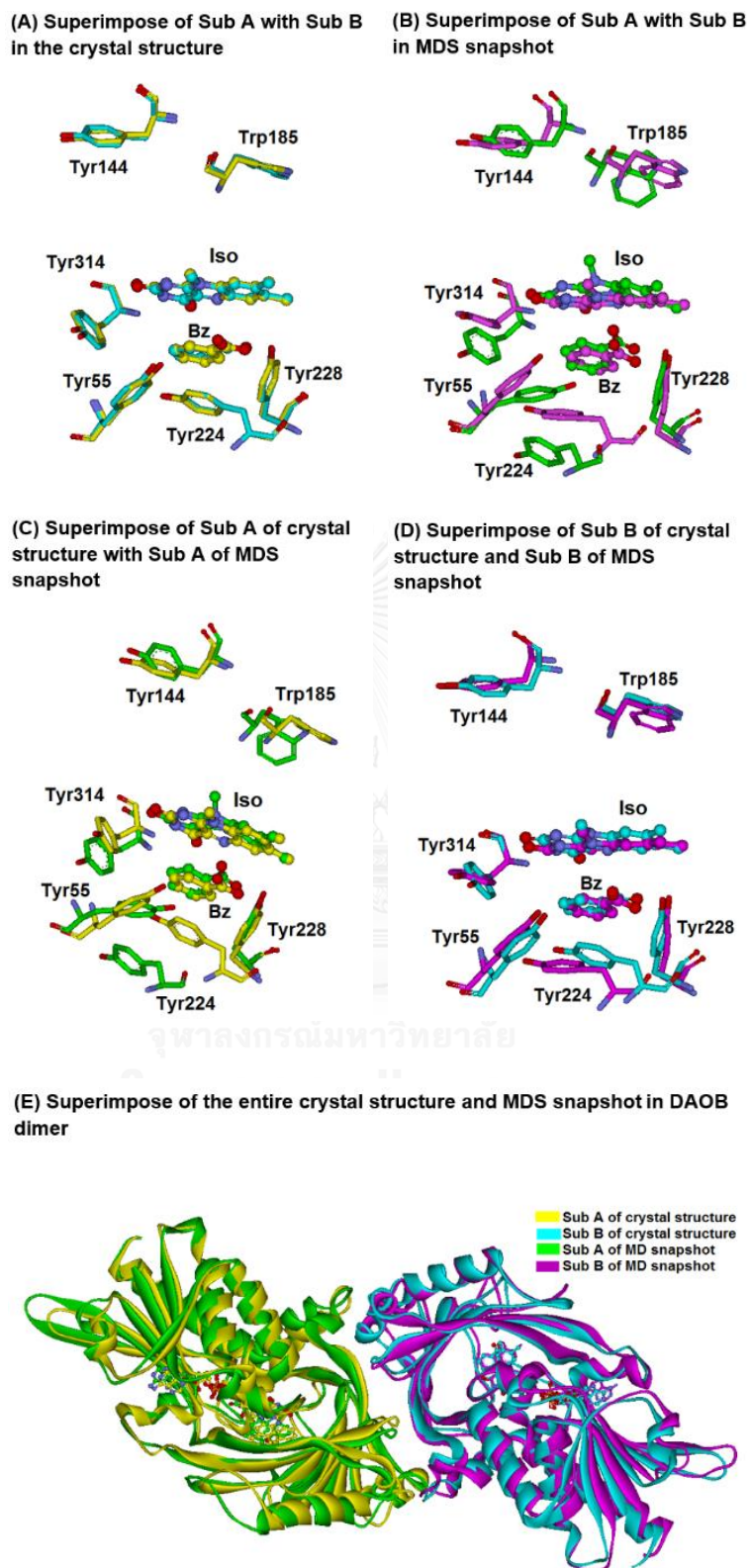
Figure 4.1 *Comparison of the protein structures between Sub A and Sub B in DAOB dimer. The structures were shown in yellow for Sub A and in cyan for Sub B in the*

crystal structures, and in green for Sub A and in magenta for Sub B in the MD snapshots. The crystal structure was taken from Mizutani et al.[19] The MDS calculation was performed at 20 °C. All figures superimposed using Discovery Studio program, alignment by 100% steric and align to consensus of protein.

Time-evolutions of the Rc between the potential donors and Iso are shown in Figure S4.2 (Supplemental Information of Chapter IV), whilst the Rc distributions of potential ET donors including Bz are shown in Figure 4.2, where large differences were evident in the Rc distributions of Tyr55 and Trp185 between Sub A and Sub B, whilst Tyr144 and Tyr224 were present only in Sub A or Sub B, respectively. The mean Rc values between Iso and these donors, derived from 5000 snapshots with 1 ps time intervals, are listed in Table 4.1. The Rc distance for Bz was shortest among the monomer and the dimer subunits, and slightly shorter in Sub A than Sub B. The Rc values were higher by 0.05 and 0.07 nm respectively in Sub A and Sub B compared to that in the monomer. Within the dimer subunits, the Rc for Trp185 was shorter in Sub A (1.10 nm) than in Sub B (1.31 nm), while it was 1.39 nm in the monomer. The Rc values of Tyr55 were slightly (1.1-fold) smaller in Sub A (0.95 nm) than Sub B (1.05 nm), but much larger in the monomer (1.31 nm) with only that in Sub A being < 1 nm. The Rc values of Tyr228 were similar in Sub A and Sub B (0.96 and 0.99 nm), but markedly smaller in the monomer (0.81 nm) and with all three being shorter than 1 nm. The Rc value for Tyr224 in sub B (1.04 nm) was closer to that of the monomer (0.97 nm) but was much larger in Sub A (1.32 nm). In contrast, the Rc values for Tyr314 were similar in all three systems. Thus, the protein conformations near Iso were quite different between Sub A and Sub B in the dimer, and in the monomer.
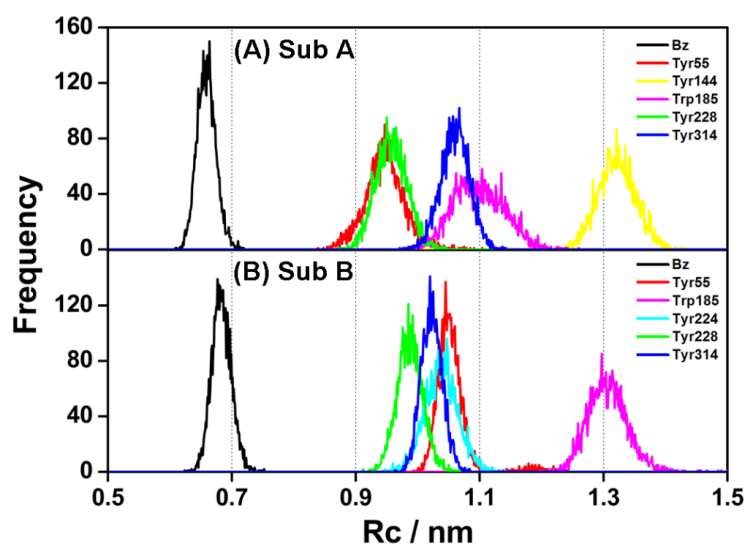
Figure 4.2 *Distribution of the Rc values in the DAOB dimer subunits. The distributions of Rc in Bz and five aromatic amino acids with the shortest Rc distances are shown for (A) Sub A and (B) Sub B. The distributions were obtained from 5000 MDS snapshots with 1 ps time intervals.*

4.4.2 Root of mean square deviation and root of mean square fluctuation

Root of mean square deviation (RMSD) and root of mean square fluctuation (RMSF) were obtained using the AMBER10 software. Time-evolutions of RMSD of the entire protein (Sub A and Sub B), FAD and Bz are shown in Figure S4.3 (Supplemental Information of Chapter IV). The RMSDs of all components attained equilibrium between 25–30 ns of MDS calculations. The RMSF is considered to be a useful index for protein fluctuation, and the RMSF for the amino acid residues is shown in Figure S4.4 (Supplemental Information of Chapter IV) along with those from the literature for the DAOB monomer,[106] holoDAAO monomer,[105] and Sub A and Sub B of the holoDAAO dimer [109] for comparison. The mean RMSF values over all the amino acids were small in Sub A and Sub B of the DAOB dimer (0.191 and 0.171, respectively), but much larger in the DAOB monomer (0.522), and in Sub A and Sub B of the holoDAAO dimer (0.347 and 0.344), respectively, and largest in the holoDAAO monomer (0.701).

The lowest mean RMSF values were hence found in the DAOB dimer and the highest in the holoDAAO monomer, whilst the mean RMSF value of the DAOB monomer was higher than those of the holoDAAO dimer. It is well known that Bz binding to holoDAAO from porcine kidney greatly stabilizes the protein, and indeed this trait is used in the purification of holoDAAO.[26] It is also recognized that the holoDAAO monomer is the most unstable of the protein species. Thus, the mean RMSD may be related to protein stability in general.

4.4.3 Best-fit ET parameters

In holoDAAO dimer the static dielectric constant (ε_0^{DA}) was introduced between Iso and the donors only when the mean Rc is shorter than 1 nm.[109] This model was also used in the present work (see below eqn (4.2)). However, in DAOB monomer ε_0^{DA} was introduced for all donors.[105] To compare the ET parameters in the DAOB dimer with those in the DAOB monomer, first the fluorescence lifetime of the DAOB monomer [17] (60 ps) was analyzed with the same model as the present work, introducing ε_0^{DA} only for the donors with the mean Rc shorter than 1 nm. The ET parameters of the monomer obtained with this model are listed in Table S4.2 (Supplemental Information of Chapter IV). The values of ν_0^{Bz}, β^{Bz} and E_{IP}^{Bz} (ionization potential of the Bz anion) were the same as those previously reported.[106] The obtained value of ε_0 was 5.78, which was similar to that previously reported, but the values of R_0^{Bz} (0.384 nm) and ε_0^{DA} (2.45) were a little larger (0.116 and 2.22 respectively).[106] The calculated lifetime of the DAOB monomer completely coincided with one of the observed lifetimes (that at 60 ps).[17]

The unknown ET parameters for the DAOB dimer were G_{IsoA}^0, G_{IsoB}^0, ε_0^{DA}, ε_0^{DB}, ε_0 and R_0^{Bz}. These best-fit parameters, obtained with methods 1 and 2 (see Determination of the ET parameters section), are listed in Table 4.4. The total chi-squared values were 64-fold larger with method 1 than with method 2, and so method 2 seems to be a better method. The best-fit parameters (from method 2) were G_{IsoA}^0 = 8.42 eV, G_{IsoB}^0 = 8.43 eV, ε_0^{DA} = 2.53, ε_0^{DB} = 2.64 and R_0^{Bz} = 0.462 nm.

Table 4.4 Physical quantities related to the ET in DAOB.[a]

Protein	Donor	k_{ET}^w (ps^{-1})	$\ln k_{ET}^w$ [b] (ps^{-1})	Rc[c] (nm)	λ_S^{wj} [d] (eV)	$ES_j(k)$ [e] (eV)	ESDA[f] (eV)
Sub A	Tyr228	1.17×10^{-1}	-2.15	0.957	0.619	0.0750	-0.594
	Bz	7.50×10^{-2}	-2.59	0.659	0.811	-0.0852	-0.0198
	Tyr55	1.14×10^{-2}	-4.48	0.946	0.617	-0.103	-0.601
	Trp185	4.65×10^{-3}	-5.37	1.10	1.83	-0.434	-0.226
	Tyr314	1.58×10^{-3}	-6.45	1.06	1.97	-0.323	-0.234
	Trp52	1.68×10^{-5}	-11.0	1.33	1.90	-0.113	-0.187
Sub B	Bz	8.92×10^{-1}	-0.114	0.683	0.939	-0.0944	-0.0217
	Tyr228	2.80×10^{-1}	-1.27	0.987	0.715	0.0698	-0.553
	Tyr314	6.56×10^{-3}	-5.03	1.02	1.95	-0.442	-0.243
	Tyr55	2.64×10^{-4}	-8.24	1.05	1.97	-0.159	-0.236
	Tyr224	5.38×10^{-5}	-9.83	1.04	1.96	-0.0099	-0.239
	Trp185	3.72×10^{-5}	-10.2	1.31	1.89	-0.183	-0.190
Monomer	Bz	9.92×10^{-3}	-4.61	0.611	0.687	0.898	0.140
	Tyr228	4.23×10^{-3}	-5.46	0.812	0.512	0.172	-0.725
	Tyr224	1.93×10^{-3}	-6.25	0.970	0.538	0.0221	-0.607
	Tyr314	5.05×10^{-4}	-7.59	1.07	1.97	-0.130	-0.232
	Tyr55	6.59×10^{-5}	-9.63	1.31	2.05	-0.171	-0.191
	Trp185	1.37×10^{-5}	-11.2	1.36	1.90	-0.0953	-0.184

[a] Mean values over 5000 snapshots are listed for the DAOB dimer obtained with the ET parameters listed in Table 4.4, whilst for the monomer the ET parameters listed in Table S4.2 (Supplemental Information of Chapter IV) were used. [b] Logarithmic ET rate of eqn (4.1). [c] Centre-to-centre distance (Rc) between Iso and the ET donors. [d] Solvent reorganization energy, derived from eqn (4.2). [e] NetES energies for Tyr and Trp derived from eqn (4.9), and for Bz from eqn (4.12). [f] ES energy between Iso anion and an aromatic amino acid cation or Bz neutral radical.

4.4.4 ET rates in DAOB dimer

The ET rates from all Tyr and Trp residues in addition to Bz were obtained with the ET parameters described above. Figure S4.5 (Supplemental Information of Chapter IV) shows the time-evolutions of the logarithmic ET rates of the six fastest donors, including Bz. Figure 4.3 shows the distributions of the logarithmic ET rates, with the distributions in the DAOB monomer, obtained with the ET parameters listed in Table S4.2 (Supplemental Information of Chapter IV) also shown for comparison. The distributions of logarithmic ET rate in Tyr314 of Sub A displayed a double maxima, and Trp185 displayed a broad shoulder. The distributions for each donor were markedly different between the two subunits and in the monomer. Table 4.5 lists the mean ET rates over 5000 snapshots with 1 ps time intervals, together with the physical quantities related to ET. In Sub A the fastest rate was from Tyr228, then followed by Bz, Tyr55, Trp185, Tyr314 and Trp52. However, in Sub B the fastest donor was Bz (11.8-fold faster than in Sub A, and 7.62-fold faster than Tyr228 in Sub A), and then followed by Tyr228, Tyr314, Tyr55, Tyr224 and Trp185. In the monomer, the fastest donor was also Bz and then followed by Tyr228, Tyr224, Tyr314, Tyr55 and Trp185, but the mean ET rates in each case were more than 10-fold slower than in the dimer subunits.
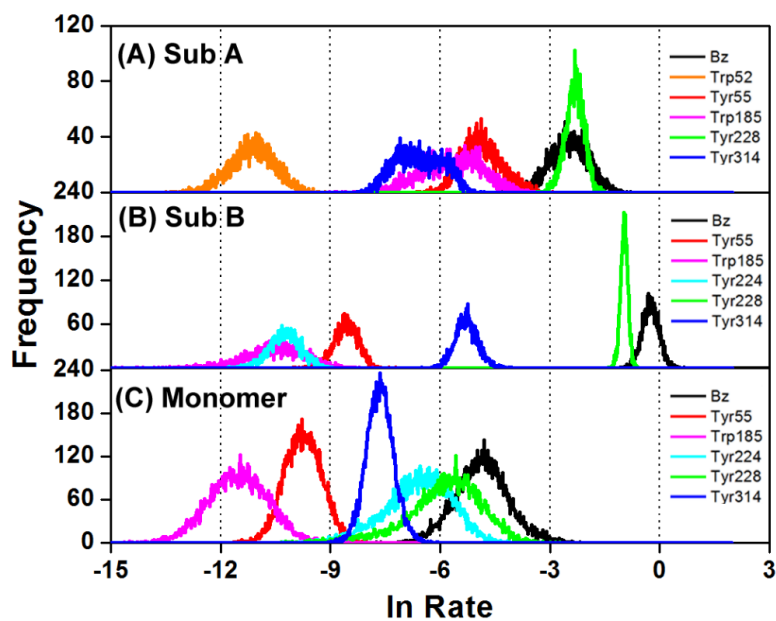
Figure 4.3 *Distribution of the logarithmic ET rates in the DAOB subunits for the six fastest ET donors. The observed fluorescence lifetime τ_{obs}^{1} (0.848 ps) was from Sub B and τ_{obs}^{2} (4.77 ps) from Sub A.*

Table 4.5 Individual terms of the ET rates in the DAOB Sub A and Sub B of the dimer, and with those for the monomer.[a]

Protein	Donor	$\ln EC^w$ [b]	$\ln SQ^w$ [c]	$GTRAM^w$ [d]	GT^w [e] (eV)	ln Rate[f]
Sub A	Tyr228	2.37	-2.87	-1.67	-0.322	-2.15
	Bz	4.62	-3.00	-2.68	-0.466	-2.59
	Tyr55	2.45	-2.86	-4.18	-0.509	-4.48
	Trp185	-1.88	-3.41	-0.0663	-0.0573	-5.37
	Tyr314	1.76	-3.44	-4.96	0.991	-6.45
	Trp52	-6.84	-3.43	-0.748	0.378	-11.0
Sub B	Bz	4.28	-3.07	-1.32	-0.353	-0.11
	Tyr228	2.19	-2.94	-0.531	-0.194	-1.27
	Tyr314	1.98	-3.44	-3.61	0.843	-5.03
	Tyr55	1.80	-3.44	-6.63	1.15	-8.24
	Tyr224	1.89	-3.44	-8.36	1.29	-9.83
	Trp185	-6.37	-3.42	-0.480	0.295	-10.2
Monomer	Bz	4.20	-2.92	-6.12	0.651	-4.61
	Tyr228	3.20	-2.77	-6.32	-0.569	-5.46
	Tyr224	2.30	-2.80	-6.10	-0.574	-6.25
	Tyr314	1.68	-3.44	-5.89	1.08	-7.59
	Tyr55	0.25	-3.46	-6.53	1.16	-9.63
	Trp185	-7.36	-3.43	-0.482	0.297	-11.2

[a] ET rates given by eqns (4.1) and (4.4) were decomposed into the EC^w, SQ^w and $GTRAM$ terms. The quantities were expressed as means over 5000 snapshots with 1 ps time intervals. [b] $\ln EC^w$ is the logarithmic electronic coupling term (ps^{-1}), derived from eqn (4.16). [c] Explicit form of $\ln SQ^w$, derived from eqn (4.17). [d] Explicit form of $GTRAM$, derived from eqn (4.19). [e] GT is total free energy gap, derived from eqn (4.18). [f] Logarithmic rate, derived from eqn (4.20).

4.4.5 NetES energy

The time-evolutions of NetES energies between the photoproducts and ionic groups in the DAOB dimer are shown in Figure S4.6 (Supplemental Information of Chapter IV) with the distributions of the NetES energies shown in Figure 4.4 along with those in the monomer for comparison. The NetES energies in the dimer ranged from -0.5 eV to 0.2 eV, while those in monomer ranged from -0.3–1.0 eV. The mean NetES energies are listed in Table 4.4. Tyr228 had the fastest ET rate and the highest NetES energy in Sub A, but in Sub B whilst Bz had the fastest ET rate, its NetES energy was 1.7 fold lesser than that for Tyr228. Thus, the NetES energy was highest in Tyr228 in both Sub A and Sub B. The lowest NetES energy was found in Trp185 in Sub A (followed by Tyr314) and in Tyr314 in Sub B (followed by Trp185), whilst the NetES energies of Bz were similar in both subunits. Note that the NetES energies of Tyr314 in Sub A displayed a double maximum at around -0.3 eV and -0.4 eV.
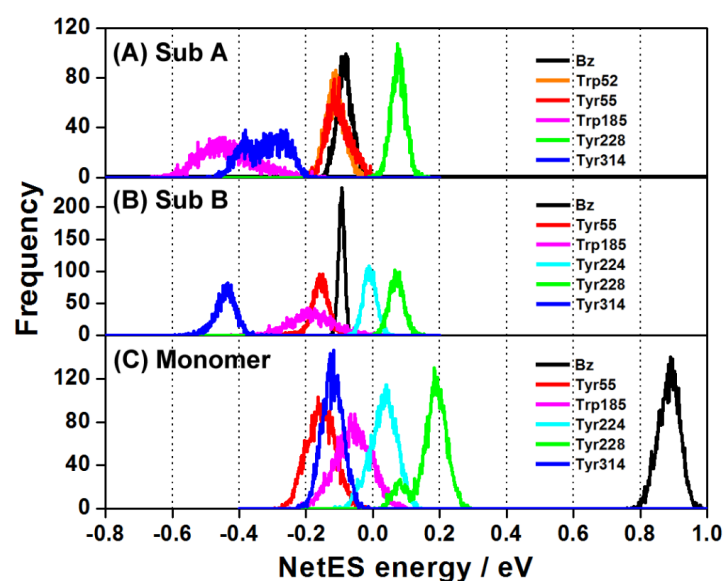
Figure 4.4 *Distribution of the NetES energy in the DAOB subunits for the six fastest ET donors, with that in the monomer for comparison. NetES energies are given by eqn (4.9) for Tyr and Trp, and by eqn (4.12) for Bz. Upper, middle and lower panels show the NetES energy of the DAOB Sub A, Sub B and the monomer, respectively.*

The NetES energy of Bz in the monomer was much higher (11-fold) than those in either subunits of the dimer, and the same trend was noted for all of the other five donors (Table 4.4). This revealed that in the dimer the NetES energies in each subunit were influenced by those in the other subunit.[17] The mean values of NetES energies in the aromatic amino acids of the monomer were also higher than in the dimer subunits.

4.4.6 The other physical quantities related to ET

The time-evolution of the ESDA between the Iso anion and donor cation (aromatic amino acids) or neutral radical (Bz) are shown in Figure S4.7 (Supplemental Information of Chapter IV) and the ESDA distributions and mean values are shown in Figure 4.5 and Table 4.4, respectively. The ESDA of the Bz neutral radical in the dimer fluctuated around zero (slightly negative) with appreciable portions of the ESDA distributions being negative in both Sub A and Sub B. The mean Bz ESDA values were the lowest in Sub B and the highest in the monomer. The distribution pattern of Tyr55 was quite different between Sub A and Sub B. In Sub A the distribution peak was highly negative (mean -0.601 eV; see Table 4.4), while in Sub B it was similar with those of Tyr224 and Tyr314 (mean -0.236 eV), and with one in the monomer (mean -0.191 eV). The mean ESDA values for Tyr228 were somewhat similar in Sub A and Sub B, but were significantly lower in the monomer.
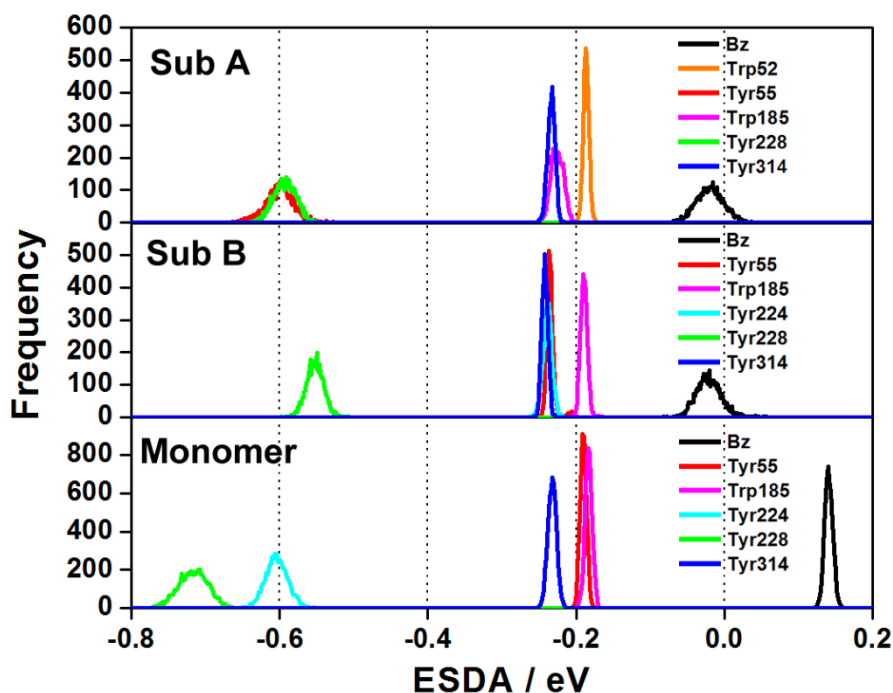
Figure 4.5 *Distribution of the ESDA between the photo-products in the DAOB subunits, with that in the monomer for comparison. The ESDA, the electrostatic energy (eV) between the photo-products, is expressed as $-e^2/\varepsilon_0^p R_j$ in eqn (4.1), using the static dielectric constants ε_{DA}^A for Sub A and ε_{DA}^B for Sub B. The acceptor was the Iso anion, and the donors were Trp cations or Tyr cations for aromatic amino acid donors. For Bz, the ESDA was obtained from eqn (4.11).*

The solvent reorganization energies (λ_S^{wj}) (Table 4.4) for Bz and Tyr228 were highest in Sub B (slightly more than in Sub A at 1.16- and 1.03-fold, respectively) but much lower in the monomer at 1.18- to 1.37-fold and 1.2- to 1.4-fold, respectively, whilst that for Tyr314 was essentially equally high in all three forms (Sub A, Sub B and the monomer).

4.4.7 Polarity around Iso

The polarity around Iso may be related to number of water molecules near it. The radial distribution functions of water molecules ($G(r)$) near the heteroatoms of Iso, which is considered to represent water molecules steadily located near the

heteroatoms of Iso, is shown in Figure S4.8 (Supplemental Information of Chapter IV). The $G(r)$ functions of Sub A and Sub B in the DAOB dimer are shown in red and blue respectively, whilst that for the monomer is shown in black and is taken from previous work [106] for comparison. In Sub B an average of 1.1 water molecules were located near O2 and N3 (see Chart 4.1 for atom notations), one molecule near O4, and approximately two molecules were located near N5. However, in Sub A no water molecule existed near these heteroatoms in Iso as in the monomer.
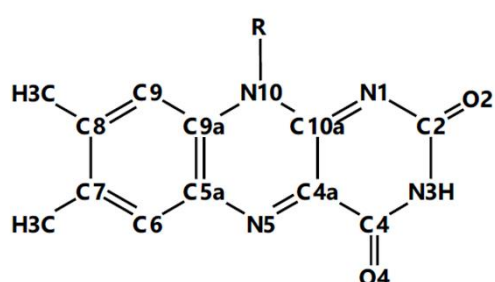
Chart 4.1 *Isoalloxazine ring (Iso) showing the atom notations.*

These results, and the $G(r)$ functions in Figure S4.8 (Supplemental Information of Chapter IV) suggest that the polarity near Iso was higher in Sub B than in Sub A. This is in accordance with the results of the dielectric constants ε_0^{DA} and ε_0^{DB} (2.53 and 2.64 respectively, Table 4.3) in the DAOB dimer, which suggests polarity near Iso, Bz, Tyr55 and Tyr228 in Sub A is a little lower than that near Iso, Bz and Tyr228 in Sub B (see descriptions on ε_0^{DA} and ε_0^{DB} below eqn (4.2)). In the monomer the value of ε_0^{DA} near Iso, Bz, Tyr224 and Tyr228 was 2.45 (Table S4.2, Supplemental Information of Chapter IV) and no water molecule was also found near heteroatoms of Iso. It should be noted that molecules other than water may also influence the polarity, such as any ionic groups near Iso.

Figure S4.9 in Supplemental Information of Chapter IV shows water molecules existing 0.7 nm from IsoN5. In Sub A Iso, Bz, Tyr55 and Tyr228 are shown, and in Sub B Iso, Bz and Tyr228 in a snapshot. The static dielectric constant in these domains are ε_0^{DA} for Sub A and ε_0^{DB} for Sub B. In Sub A there exist three water molecules, but no water molecule near Iso within 0.5 nm, as predicted by G(r) function in Figure S4.8

(Supplemental Information of Chapter IV). In Sub B some water molecules exist near Iso within 0.5 nm. These results are in accordance with the interpretation about the polarity near Iso described above.

Emission peak of fluorescence spectrum of a flavoprotein may be related to the static dielectric constant near Iso (ε_0^{DA} for Sub A and ε_0^{DB} for Sub B). Fluorescence spectrum of DAOB dimer is shown in Figure S4.1 (Supplemental Information of Chapter IV). The emission peak was 524 nm, while the peak of holoDAAO dimer is around 530 nm.[38] The static dielectric constants near Iso were 2.4–2.7 in DAOB dimer and monomer, while it is 5.8–5.9 in holoDAAO dimer and monomer.[105, 109] These results are in accordance with those of the static dielectric constant near Iso obtained by the present ET analyses. Similar result with respect to the relationship between the static dielectric constant near the donor and Iso, and emission peak of Iso was obtained in flavodoxins.[34] However, it should be noted that the fluorescence spectrum of Iso depends on two factors, polarity around Iso, (Stokes Shift) and hydrogen bond (H-bond) structure between Iso* and nearby amino acids. Iso contains five hydrogen bonding acceptors and one donor (see Chart 4.1). The energy shift of Iso upon H-bond formations has been studied by a MO method for the ground state of Iso.[111] It is well known that H-bond or proton transfer phenomena are different between the ground and excited states in general. Accordingly, the modifications of the transition energies of Iso by H-bond formations should be examined for Iso* by MO method.

4.4.8 Difference in the charge densities Iso and Iso* between sub A and sub B with and without H-bonds

Charge densities of atoms in free Iso and Iso with H-bond cluster were shown in Table S4.3 (Supplemental Information of Chapter IV). Numbering of atoms in Iso and H-bonded amino acids are shown in Figure S4.11 (Supplemental Information of Chapter IV). The charge densities were not much different between Sub A and Sub B. The charge densities with the differences greater than 0.01 are indicated in green in Table S4.3 (Supplemental Information of Chapter IV). In the ground state of Iso the atom O7 (O4 in the Chart 4.1), H19 and H21 displayed the differences greater than 0.01 between

Sub A and Sub B. In the excited state many more atoms displayed the greater differences. Atom N1 (N1 in Chart 4.1) displayed quite large difference by 0.03 between Sub A and Sub B. The differences were 0.25 in C8 (C4a in Chart 4.1), 0.24 in C11 (C6 in Chart 4.1), 0.28 in H29 (H connected to N10 in Chart 4.1), and 0.34 in H31 (H connected to N10 in Chart 4.1). H-bond cluster considerably modified the charge densities of Iso in the excited state, for example, by 0.027 in C10 (C5a in Chart 4.1) of Sub A, by 0.041 in C11 (C6 in Chart 4.1) of Sub A and by 0.017 in C11 of Sub B, by 0.05 in N27 (N10 in Chart 4.1) of Sub A. These differences in the charge densities between Sub A and Sub B in the excited state may be related to the difference in the ET rates between Sub A and Sub B. Figure S4.12 (Supplemental Information of Chapter IV) shows molecular orbitals of HOMO and LUMO of Iso in the ground and excited states without H-bond clusters. The LUMO and HOMO displayed considerable difference between the ground and excited states.

4.4.9 Relationship between logarithmic ET rate and Rc

The dependence of the logarithmic ET rate on the donor–acceptor distance (edge to edge distance, Re) is called as Dutton ruler.[80] The relationship between logarithmic ET rates and the donor–acceptor distances is shown in the DAOB dimer and the monomer in Figure 4.6, where Rc was used as the donor–acceptor distance. The relationship should be examined separately with each kind of ET donor, otherwise linear relations of the logarithmic ET rates with Rc cannot be expected. It has been noted that the Rc rather than the Re is responsible for the relationship between logarithmic ET rate and Rc in flavoproteins [94, 95] in contrast to photosynthetic systems where Re was used as the donor–acceptor distance.[80] In all three DAOB systems excellent linear relations were obtained, including in the monomer. The slopes for Trp were similar in the two dimer subunits (-22.1 and -22.2 in Sub A and Sub B, respectively), and a little higher in the monomer (-24.7), and likewise for Tyr they were -13.0, -13.2 and -14.6 in Sub A, Sub B and the monomer, respectively. Thus, the slopes for both Trp and Tyr were quite similar between Sub A and Sub B, but a little higher in the monomer than those in the dimer. The relationship between

logarithmic ET rate and the donor–acceptor distances was also examined with Re as shown in Figure 4.7. The ln rate vs. Re relationship also displayed linear functions. The slopes of the approximate functions of Trp were -19.1 in Sub A, -19.8 in Sub B and -19.7 in monomer, while those of Tyr were -14.2 in Sub A, -14.4 in Sub B, and -15.0 in monomer. These values were quite different from those with Rc as the donor–acceptor distance, which suggests that Rc and Re are proportional.

The Re values should be dependent on inter-planar angles between Iso and donors. Figure S4.10 (Supplemental Information of Chapter IV) shows the relationship between Iso and main donors, Tyr228 and Bz. In this figure the logarithmic ET rates did not display any clear relations with the inter-planar angles. This should be ascribed that any theories including KM rate do not explicitly include the angular-dependence between the donor and acceptor as Förster-type energy transfer rate.
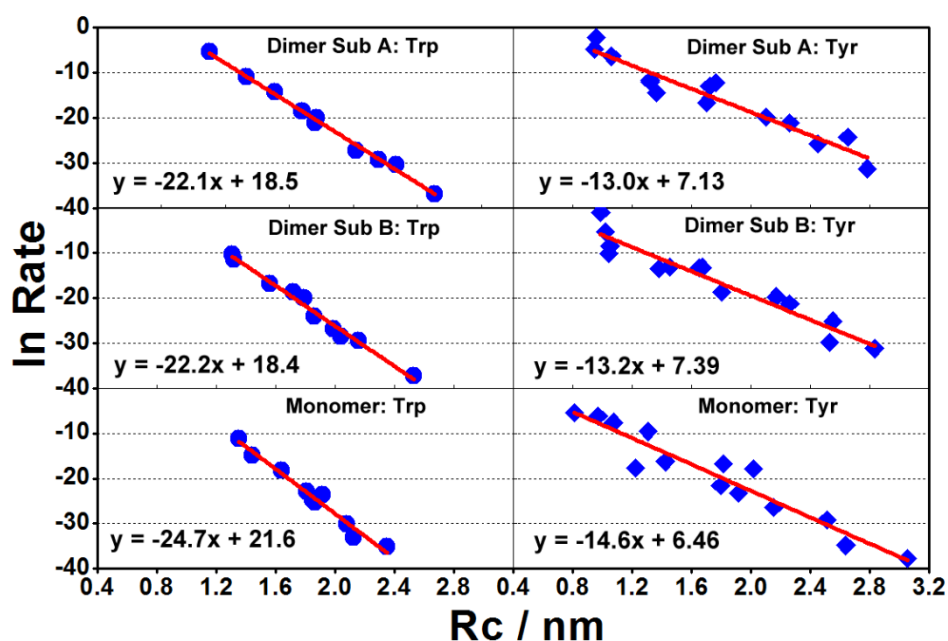
Figure 4. 6 *Relationship between logarithmic ET rates and Rc for the Trp and Tyr residues in the DAOB dimer and the DAOB monomer for comparison. Inserts show approximate linear functions of y ($\ln k_{ET}^{j}$) with x (Rc). The ET rates are expressed in unit of ps^{-1}.*

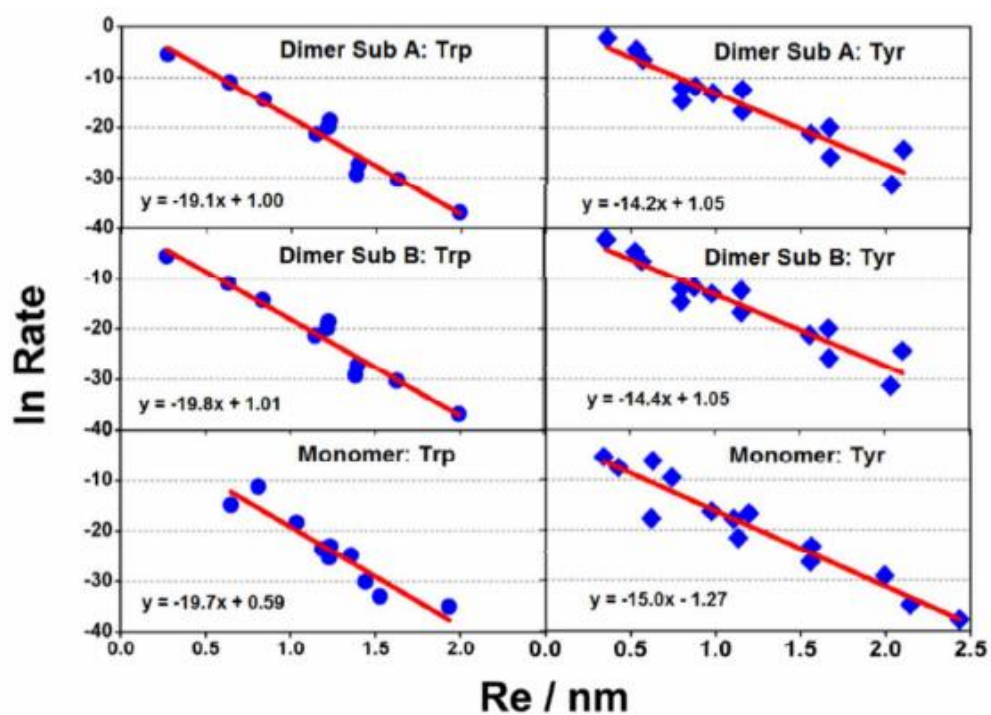*Figure 4.7* Relationship between logarithmic ET rates and Re in DAOB. The logarithmic
ET rates are taken from Figure 4.6. Re represents edge to edge distance.

4.4.10 Numerical elucidation of differences in the fluorescence lifetimes between two subunits in the DAOB dimer and between the dimer and monomer

The observed fluorescent lifetimes of DAOB were 4.77 ps in Sub A and 0.848 ps in Sub B in the dimer. It is then of interest to elucidate the difference in the lifetimes (ET rates) between the two subunits in the DAOB dimer. The logarithmic ET rate expressed by eqn (4.1) or (4.4) may be rewritten as eqn (4.16)–(4.19):

$$\ln EC^w = \ln\left[\frac{v_0^w}{1+\exp\left\{\beta^w(R_j - R_0^w)\right\}}\right], \tag{4.16}$$

$$\ln SQ^w = \ln\left\{\sqrt{\frac{k_B T}{4\pi\lambda_S^{wj}}}\right\}, \tag{4.17}$$

$$GT^w = \Delta G_w^0 - e^2 / \varepsilon_0^p R_j + \lambda_S^{wj} + ES_j(k), \tag{4.18}$$

$$GTRAM^w = -\frac{\left\{GT^{wj}\right\}^2}{4\lambda_S^{wj} k_B T}, \tag{4.19}$$

The logarithmic ET rate can then be obtained from eqn (4.20),

$$\ln k_{ET}^w = \ln EC^w + \ln SQ^w + GTRAM^w, \tag{4.20}$$

In these equations, q is Trp, Tyr or Bz, while $\ln k_{ET}^w$ is the logarithm of the ET rate given by eqn (4.1) for Trp and Tyr, and by eqn (4.4) for Bz. The meanings of each term in these equations are described below eqn (4.1) and (4.4), where EC^w the electronic coupling term, and GT^w is the total free energy gap and appeared in exponential functions of the rates. These values for several donors are listed in Table 4.5.

The contributions of the Bz and Tyr228 ET rates to the total rates (inverse of the fluorescence lifetime) were ca. 90% in all the systems. Given that the values of $\ln k_{ET}^{w}$ in Bz were -2.59 in Sub A and -0.114 in Sub B, this raises the question as to why the rate of Bz was some 22.7-fold slower in Sub A than in Sub B. The values of $\ln EC^{w}$ for Bz were slightly higher in Sub A than in Sub B. The values of $\ln SQ^{w}$ were similar between Sub A and Sub B, but the absolute value of $GTRAM^{w}$ for Bz was 2.1-fold higher in Sub A than in Sub B. The $\ln k_{ET}^{w}$ (Table 4.5) was obtained as sum of these values, according to eqn (4.20), and these were found to agree well with the $\ln k_{ET}^{w}$ values (Table 4.5). That the value of $\ln k_{ET}^{w}$ was smaller in Sub A (slower ET rate) than in Sub B was hence ascribed to the two-fold larger absolute value of $GTRAM^{w}$ in Sub A than in Sub B. $GTRAM^{w}$ is mainly determined by GT^{w} eqn (4.16), because there was very little variation in SQ between the subunits. The values of ΔG_{w}^{0} (given by eqn (4.6)) were similar in the two subunits, whilst the ESDA ($-e^{2}/\varepsilon_{0}^{p} R_{j}$), solvent reorganization energy (λ_{s}^{wj} from eqn (4.5)) and ES_{Bz} (from eqn (4.12)) were all quite similar (1.01- to 1.16-fold difference) in the two subunits (Table 4.4). The values of GT^{w} for Bz, obtained by the sum of each term according to eqn (4.18), were 1.32 fold higher in Sub A than in Sub. This is the reason why the absolute value of $GTRAM^{w}$ from eqn (4.19) was larger in Sub A than in Sub B, and so that the lifetime of Sub A is much longer than Sub B (ET rate of Sub A is much slower than Sub B, and note that $GTRAM^{w}$ is always negative, see eqn (4.19) and (4.20)). The reason why the absolute value of GT^{w} was greater in Sub A than in Sub B is due to the smaller value of λ_{s}^{wj} in Sub A than in Sub B, which in turn was due to the shorter Rc in Sub A than in Sub B and to the smaller dielectric constant of ε_{0}^{DA} than of ε_{0}^{DB}, as revealed by eqn (4.5).

It is also of interest why the fluorescent lifetime of the monomer is much longer than in the DAOB dimer, that is 12.6- and 70.8-fold longer than that for Sub A and Sub B, respectively.[17] The ET rate from Bz was the fastest among the donors in the monomer. The values of $\ln EC^{w}$ and $GTRAM^{w}$ for Bz in the monomer were 1.1- and 2.3- fold lower than in Sub A and 1.02- and 4.64-fold lower than in Sub B, respectively, although $\ln SQ^{w}$ was only 1.03- and 1.05-fold higher than in Sub A and Sub B,

respectively. Thus, the $GTRAM^w$ in the monomer was markedly smaller than those in Sub A and Sub B and this is likely to be the principal reason why the value of $\ln k_{ET}^w$ in the monomer was much smaller, and so the fluorescence lifetime was much longer, than those in the dimer subunits. $GTRAM^w$ is mainly dependent on GT^w (eqn (4.19)), which is itself derived from the summation of the ΔG_w^0, ESDA, λ_S^{wj} and ES_{Bz} values (eqn (4.18)). The values of ΔG_w^0, ESDA and λ_S^{wj} in Bz were not dramatically different (1.1- to 1.55-fold difference) between the monomer and the dimer subunits (Table 4.5). However, the NetES energy (ES_{Bz}) was markedly higher in the monomer than in the dimer subunits. Thus, the main reason why the fluorescent lifetime is much longer (slower ET rate) in the monomer than those in the dimer is due to greater NetES energy (ES_{Bz}) in the monomer compared to in the dimer. This was ascribed to the inter-subunit interactions in terms of the Rc and dielectric constant, as stated above.

The ET rate from Tyr228 to Iso* was 2.4-fold slower in Sub A than in Sub B, but some 660-fold faster than that in the monomer. That the ET rates from Tyr228 were much faster in the dimer subunits than in the monomer, despite that the donor–acceptor Rc distances of the dimer were ∼1.2-fold longer than that in the monomer, is because the absolute values of $GTRAM^w$ in the dimer were much smaller than that in the monomer. The greater absolute $GTRAM^w$ value in the monomer was mainly ascribed to the low λ_S^{qj} with a shorter Rc and a low ε_0^{DA} (Table S4.2, Supplemental Information of Chapter IV).

4.5 DISCUSSION

During 1980–2000 a number of workers have reported on ET and dark electron transfer in small molecules and in proteins.[98, 112-116] In these works, however, it was difficult to determine theoretically and experimentally individual ET parameters contained in the ET rates. Our approach to analyze ET rate quantitatively is that (1) fluorescence decays or lifetimes of flavoproteins are obtained from experimental results, (2) atomic coordinates of a flavoprotein are determined by MDS methods, (3) ET rates are evaluated with an analytical theory like KM rate or sometimes Marcus rate, (4) the several unknown ET parameters are determined by a non-linear least

squares method according to Marquardt algorithm. By using the above described strategy, we have reported on ET mechanisms on several flavoproteins.[32, 34, 35, 39, 42, 105, 106, 109]

Experimentally, the DAOB dimer displays two fluorescent species with lifetimes of 0.85 ps and 4.8 ps, which have been identified as being derived from Sub B and Sub A, respectively. The structural basis for the heterogeneity has been studied by means of MDS and ET analysis. The contributions of the ET rates from Bz and Tyr228 to the total rates were ∼90% in all systems, including in the monomer. The Rc distances of the main donors in Sub A and Sub B respectively, were 0.66 and 0.68 for Bz, compared to 0.96 and 0.99 nm for Tyr228, which did not correlate with the differences in the ET rates. This is in contrast to that for the DAAO holodimer,[109] where the difference in the fluorescence lifetime between the monomer and dimer was attributed to the difference in Rc. The ET rates of Bz were significantly different between Sub A and Sub B, being the second fastest in Sub A and the fastest in Sub B.

Decomposing the ET rate into the electronic coupling (EC^w), square root (SQ^w) and exponential ($GTRAM^w$) terms revealed that the main reason for the faster ET rate of Bz in Sub B was the two-fold larger absolute $GTRAM^w$ value in Sub A than in Sub B. This in turn was ascribed to the greater λ_S^{wj} in Sub B than in Sub A, because the Rc was longer and the dielectric constant was smaller in Sub B than in Sub A. That the fluorescence lifetime was 12.6- and 70.8-fold shorter (much faster ET rate) in the dimer than in the monomer was explained by the 2.3- and 4.64-fold larger $GTRAM^w$ values in the dimer compared to the monomer, which in turn was due to the much higher NetES energy (ES_{Bz}) in the monomer compared to the dimer.

Original Marcus theory [78, 79] was derived assuming that the donor and acceptor are spherical (also KM rate). It is not unreasonable to use Rc as the donor–acceptor distance for the ET analyses. If the molecules are spherical, Rc and Re should be identical. Firstly the relationship between logarithmic ET rate and the donor–acceptor distances has been experimentally obtained with Re in photosynthetic systems.[80] In these systems ET rates were slower (longer than 0.63 ps in the lifetimes), and so the distances were longer, comparing to in flavoproteins. When the

distance is quite long, and so the ET rate is relatively slow, the effects of the difference between Rc and Re on the theoretical ET rates or the logarithmic rates *vs.* the donor–acceptor distance relationship may not be significant. When the donor–acceptor distances become shorter, and so ET rates are faster than *ca.* 0.5 ps in lifetimes, the behavior of logarithmic ET rates vs. the donor–acceptor distances are quite different. The logarithmic ET rates deviates from a linear function of Rc which was obtained at relatively longer distances.[94, 95]

The relationship between logarithmic ET rate and Rc in DAOB was analyzed with the EC^w, SQ^w and $GTRAM^w$ terms. If it can be explained by the EC^w term alone (or principally) then the slopes should equate to or be close to $-\beta^w$ (w ; Trp, Tyr and Bz; see Table 4.2). However, there were considerable discrepancies between the slope of ln rate *vs.* Rc function and $-\beta^w$ in Tyr. The logarithmic ET rate could be decomposed into its constitutive three terms (eqn (4.20)), where the dependence of the logarithmic ET rate on Rc could be expressed as a sum of those for EC^w and $GTRAM^w$, since the variation in $\ln SQ^w$ between Sub A, Sub B and the monomer was essentially negligible compared to the two other terms. Figure 4.8 shows relationship between $GTRAM^w$ and Rc in Tyr. The slopes were -6.98 in Sub A, -7.31 in Sub B and -8.44 in monomer. Sums of these slopes and $-\beta^{Tyr}$ were -13.2 in Sub A, -13.6 in Sub B and -14.7 in monomer, which are compared to the slopes in Figure 4.6, -13.0 in Sub A, -13.2 in Sub B and -14.6 in monomer. The slope calculated based on logarithmic ET rate *vs.* Rc function was practically identical to the sum of the slope in Figure 4.8 and $-\beta^{Tyr}$ in each system. This implies that the slope in the $GTRAM^w$ *vs.* Rc relationship considerably contributes to the slope in the relationship between logarithmic ET rate and Rc. Further it is concluded that a linear relationship between the logarithmic ET rates and Rc is obtained only when $GTRAM^w$ linearly depends on Rc.
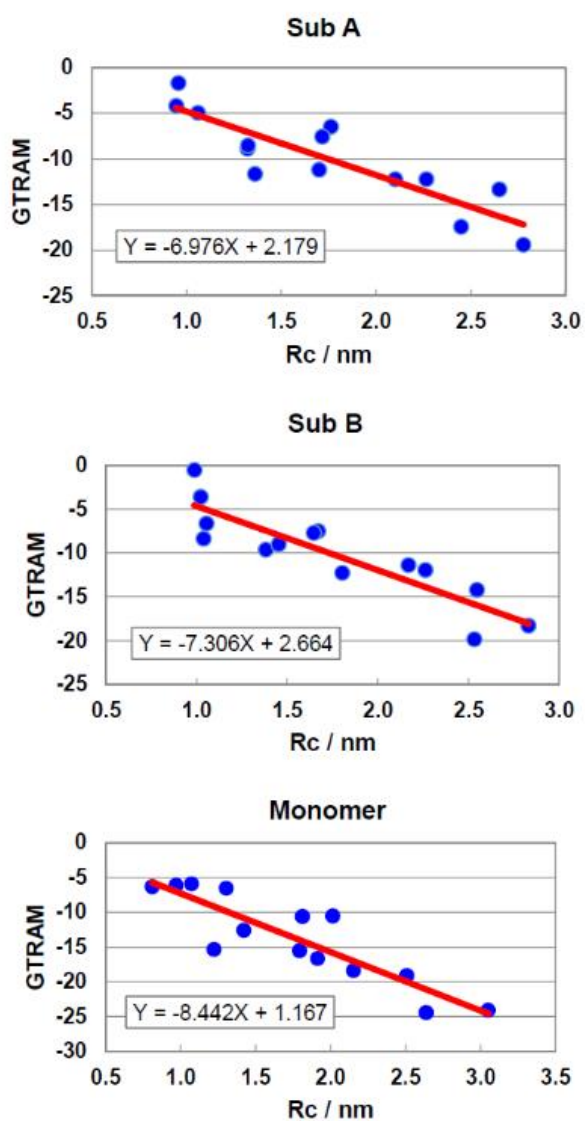
Figure 4.8 *Relationship between GTRAM ^{w} and Rc of Tyr in Sub A and Sub B in the DAOB dimer and the DAOB monomer. GTRAM ^{w} is defined by eqn (4.19). Inserts show approximate linear functions of Y (GTRAM ^{w}) with X (Rc).*

It has been reported that the relationship between logarithmic ET rate and Rc in flavin mononucleotide (FMN) binding proteins displays a bell-shaped (not linear) function in the ET processes from Trp to Iso* when the ET rates are ultrafast (10–15 ps^{-1}).[66] This work emphasized that the $GTRAM^w$ term plays the main role determining the bell-shaped behaviour. However, a bell-shape was not observed in the ET from Tyr to Iso* in the flavodoxin from *Helocobactor pylori*,[34] even though the ET rate was ultrafast at 6–23 ps^{-1}. Thus, the bell-shape behaviour can only be observed when GT^w linearly depends on Rc, and so $GTRAM^w$ becomes a parabolic function of Rc. In DAOB, the rates (0.01–0.9 ps^{-1}) were much slower than those in the FMN binding proteins and the flavodoxins, and in addition the $GTRAM^w$ was a linear function of Rc, not parabolic.

4.6 CONCLUSION

Experimental fluorescence dynamics of DAOB dimer displays two lifetime components, 0.85 ps and 4.8 ps. It was identified that the fluorescence with the shorter lifetime is from Sub B and one with the longer lifetime from Sub A. The difference in the lifetimes was mainly ascribed to differences in the ET rates from Bz to Iso* in the two subunits. This is because the absolute value of GT^w for ET from Bz in Sub A is greater than that in Sub B.

Relationship between logarithmic ET rate and Rc displayed linear functions both for Tyrs and for Trps as ET donors. Sum of the slopes of the $GTRAM^w$ *vs.* Rc functions and of $\ln EC^w$ *vs.* Rc functions were almost identical with the slopes of $\ln k_{ET}^w$ *vs.* Rc functions, which reveals that the $GTRAM^w$ term considerably contributes to the slope of the $\ln k_{ET}^w$ *vs.* Rc function.

CHAPTER V

VIRTUAL SCREENING OF NOVEL D-AMINO ACID OXIDASE INHIBITORS

Virtual Screening of Novel D-Amino Acid Oxidase Inhibitors

Arthit Nueangaudom[a], Kiattisak Lugsanangarm[a], Somsak Pianwanit[a], Sirirat Kokpol[a], Fumio Tanaka[a], Noriyuki Yamaotsu[b], and Shuichi Hirono[b]

[a] Department of Chemistry, Faculty of Science, Chulalongkorn University, 254 Phayathai Road, Bangkok 10330, Thailand.
[b] Laboratory of Physical Chemistry for Drug Design, Graduate School of Pharmaceutical Sciences, Kitasato University, Tokyo 108-8641, Japan.

5.1 ABSTRACT

D-Serine, one of the amino acid is a coagonist of the N-Methyl- D-aspartate (NMDA) receptor. Malfunction of the NMDA receptor neurotransmission has been implicated in the various mental disorder such as schizophrenia. D-Amino acid oxidase (DAAO) inhibitor is expected to inhibit DAAO activity for increasing D-serine level to activate NMDA receptor, which is a treatment of schizophrenia. In this work, we searched a new potent DAAO inhibitor from a large number of compounds on Namiki chemical compound database. The last screening result, we obtained 33 candidate compounds from pharmacophore model and surface constraint screening. These compounds were classified to active and inactive compounds using binary QSAR lead to 22 hit compounds, and then their biological activities can be further tested.

5.2 INTRODUCTION

D-Amino acid oxidase (DAAO, Enzyme class 1.4.3.3) is a flavoenzyme that catalyzes D-amino acids and produces the corresponding α-keto acids, hydrogen peroxide, and ammonia.[117, 118] It was discovered by Hans Krebs [119], which exists in a wide range of species from microbes to mammals. In human, DAAO is mostly expressed in the kidney, liver, and brain and is responsible for the metabolism of D-amino acids. For instance, instant, D-serine is an endogenous agonist at the *N*-Methyl-D-aspartate (NMDA) receptor glycine modulatory site. DAAO has gained substantial interest as a therapeutic target for disorders associated with NMDA receptor hypofunction such as schizophrenia.[3]

Schizophrenia affects more than 21 million people globally which is reported by the World Health Organization (WHO). [120] Schizophrenia is a mental disorder, characterized by deep disruptions in thinking, acting, and seeing the world. Currently, therapies are insufficient and side effect. Hence, the important attempts have been made to identify potent and selective DAAO inhibitors as novel therapeutic agents.

Several compounds have been reported to inhibit DAAO in Figure 5.1, including benzoic acid **1**,[44] 5-methylpyrazole-3-carboxylic acid (AS057278) **2**,[47] 6-chlorobenzo[d]isoxazole-3-ol (CBIO) **3**,[48] 4H-thieno[3,2-b]pyrrole-5-carboxylic acid **4**,

and 4H-furo[3,2-b]pyrrole-5-carboxylic acid **5**,[46] 5-chloro-6-fluoro-3-hydroxy-1,8-naphthyridin-2(1H)-one **6**, [121] 4,6-difuloro-1-hydroxy-1H-benzo[d]imidazol-2(3H)-one **7**,[21] and pyridine-2,3-diol **8** [45]. Moreover, their structures have been modified to increase the inhibition activity of DAAO, the DAAO inhibitors cannot yet go through to drug for schizophrenia treatment.
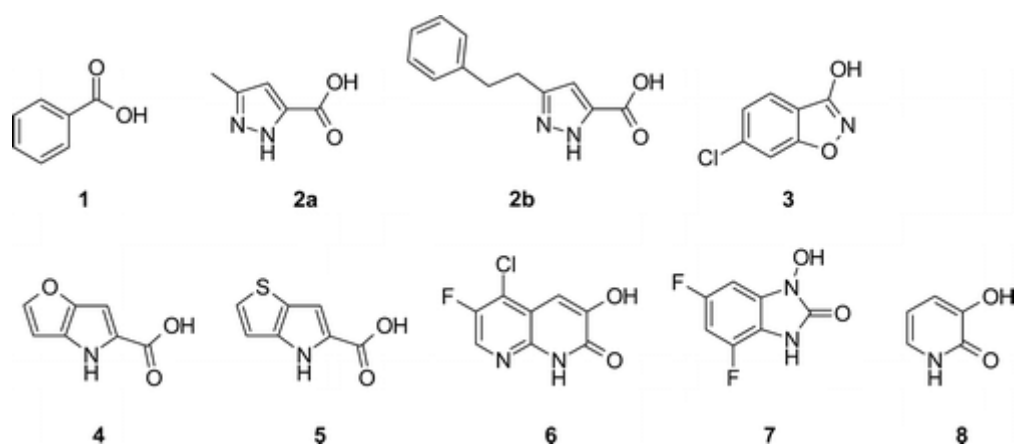
Figure 5.1 The inhibitors of DAAO.

However, the preparatory and high throughput screening of numerous compounds for testing activity is time-consuming and costly in general.[48, 51, 52] Recent advances in computational chemistry have enabled to perform structure-based virtual screening of many compounds listed in chemical structure databases. Virtual screening is a cost-effective first screening method, and results from the screening can then be used as a guide for library construction before an actual screening is performed.[53-55]

In this study, we used the virtual screening technique concluding pharmacophore model and ligand-docking method to screen a large number of compounds in database and several compounds were estimated as candidates. This work shows that some of these compounds will be possible lead compounds for the development of a clinically useful DAO inhibitor.

5.3 METHODS

5.3.1 Preparation of protein structure

The crystal structure of human DAAO complexed with 4-(4-chlorophenethyl)-1H-pyrrole-2-carboxylic acid (PDB code: 3ZNO) [122] was prepared for docking calculation and pharmacophore searching using the Protein Preparation Wizard software (Schrödinger Suite 2012).[123] The OPLS-AA force field was used for adding hydrogen atoms, optimizing the protonation state of His residues, and correcting the orientations of hydroxyl groups.[124]

5.3.2 Virtual screening

The multiple steps in virtual screening procedure were used in this study as Figure 5.2.
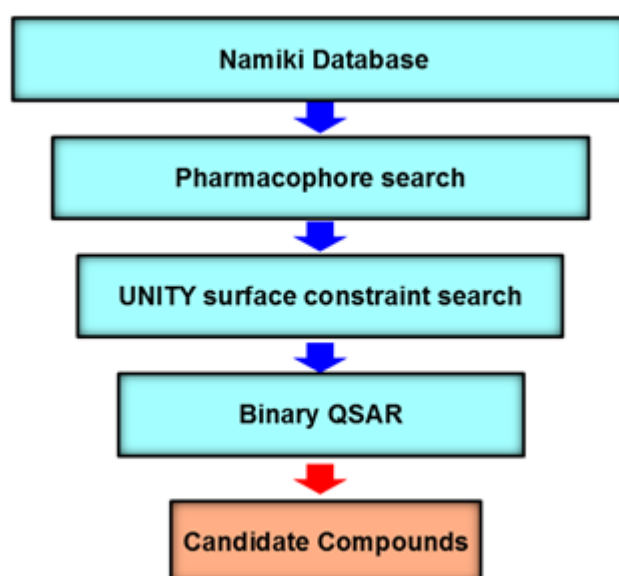
Figure 5.2 *The overall procedures of virtual screening.*

The 4-(4-chlorophenethyl)-1H-pyrrole-2-carboxylic acid which complexed with human DAAO in x-ray crystal structure PDB code: 3ZNO [122] was used as template for generating three-dimensional pharmacophore model. The 3D pharmacophore model

was generated using SYBYL-X 2.0 software. The screen used the Unity 3D search module which screened on Namiki chemical compound database (commercially available 4 million compounds), provided by Namiki Shoji Co. Ltd. By applying this first screening, we obtained 517,773 compounds as "first hit compounds". The second screening, the protein surface was defined the binding pocket for screening first hit compounds by MOLCAD surface in the UNITY surface constrains. We found 33 compounds which were called "second hit compounds".

For the last screening step, binary QSAR was used a criterion for the candidate compound selections as described below. The known activity 21 compounds as training set (Table 5.1) were taken from Hondo et. al. [45], which has been evaluated as novel DAAO inhibitors for the second binding site. The three dimensional structures of these compounds were built and optimized by using Gaussian09 software. Docking calculations of the obtained 3D ligands into the binding site of DAAO were performed using Glide software (Schrödinger Suite 2012) in standard precision mode, which docking grids were generated around the active site including Leu215, Tyr224, Tyr228, Arg283, and Gly313. The best docking pose with the lowest Glide score was taken of each compound to evaluate the pharmaceutically relevant properties by using QikProp software (Schrödinger Suite 2012). The binary QSAR analysis procedure used in this study. Binary QSAR estimates from a training set which separates the active is $IC_{50} < 4$ nM and the inactive is $IC_{50} \geq 4$ nM.

5.4 RESULTS

5.4.1 Pharmacophore search

The template for generating pharmacophore model used 4-(4-chlorophenethyl)-1H-pyrrole-2-carboxylic acid (SE5) from the crystal structure of human DAAO (PDB code: 3ZNO) as shown in Figure 5.3 (A). This inhibitor has been laid in binding site of DAAO whereas some part of molecule extended to the secondary binding site in Figure 5.3 (B). In this work, we want to discover the new inhibitors which can bind into both the first and the second binding sites.
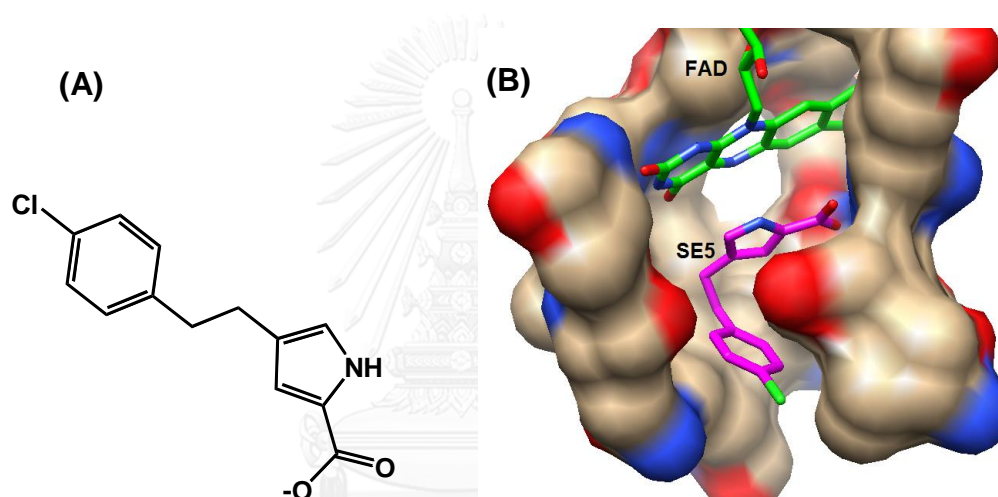
Figure 5.3 (A) *Two dimensional structure of 4-(4-chlorophenethyl)-1H-pyrrole-2-carboxylic acid (SE5) as template for pharmacophore model of DAAO inhibitors.* *(B)* *The binding mode of SE5 was taken from x-ray crystal structure (PDB code: 3ZNO).*

The pharmacophore model was generated using 4-(4-chlorophenethyl)-1H-pyrrole-2-carboxylic acid from the crystal structure of human DAAO (PDB code: 3ZNO) as shown in Figure 5.4. This pharmacophore model was defined to five significant features including two atom acceptor features (AA), one aromatic feature (AR), and two hydrophobic features (HY).
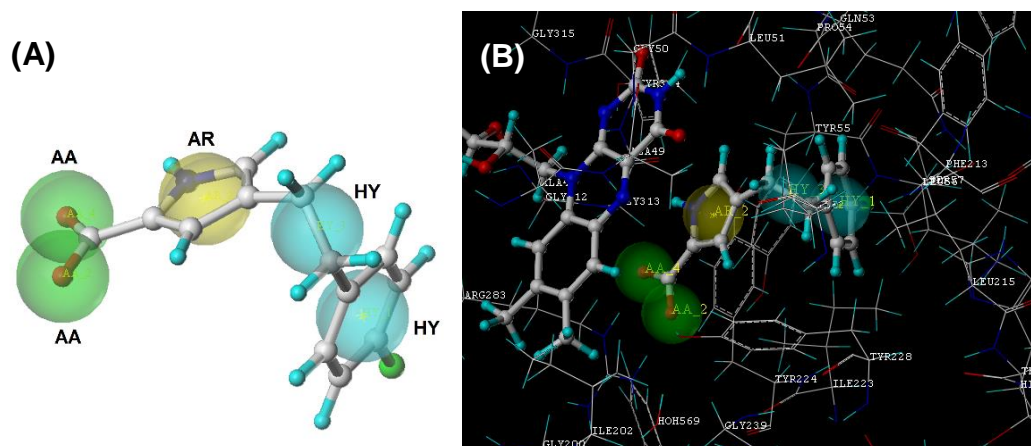
Figure 5. 4 (A) *Pharmacophore model of DAAO inhibitors generated by SYBYL-X 2.0. AA, AR, and HY denote atom acceptor site, aromatic feature, and hydrophobic feature, respectively. **(B)** Show over all of the template inhibitor, pharmacophore model, and DAAO structures.*

The virtual screening in this step, we used the UNITY 3D/flexible searching which are applied with the Lipinski's rule of five [125] to filter structures. The drug-like properties according to Lipinski's rule five can also be applied in order to reduce the number of compounds. The Lipinski's rule states that compounds used as orally active drugs in humans should no more than one violate of the following criteria: a molecular weight less than 500 daltons, no more than five hydrogen bond donors, less than ten hydrogen bond acceptors, and log P (an octanol-water partition coefficient) less than five.

The 517,773 compounds were obtained by the first screening from 4 million compounds on Namiki database which was screened by the pharmacophore model in Figure 5.4 (A) using SYBYL-X 2.0 program. We obtained 517,773 compounds from pharmacophore search.
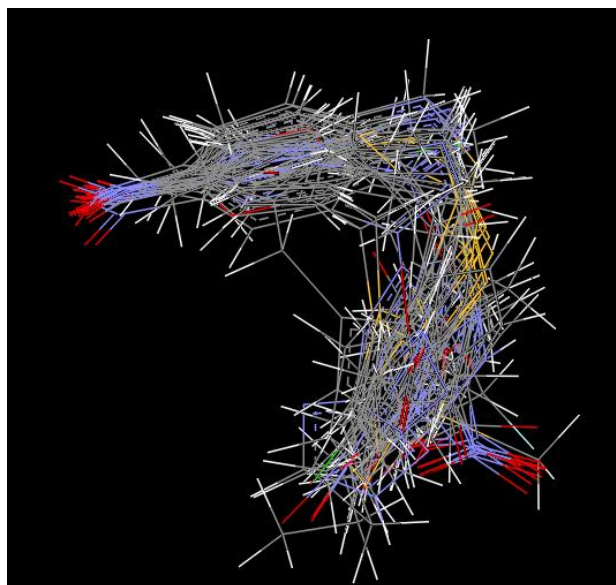
5.4.2 Surface constraint search

The surface constraint was used to be a criterion for screening to find molecules in database which were suitable and fit with protein pocket (active site). Figure 5.4 shown the surface constraint of DAAO (PDB code: 3ZNO) was generated using MOLCAD module in SYBYL-X 2.0 program for screening the first hit compounds.
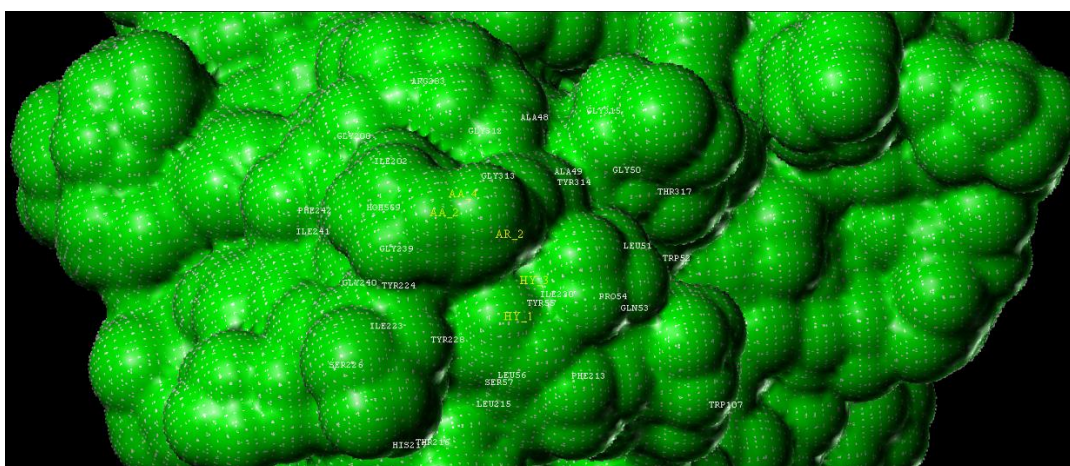
Figure 5. 5 *The surface constraint was generated by UNITY surface constraint.*

The obtained 517,773 compounds from pharmacophore model searching were screened by surface constraint. The result shown that the first hit compounds were reduced to 33 compounds which we called the second hit compounds as shown in Figure 5.5.

Figure 5.6 *The 33 second hit compounds were obtained from surface constraint searching.*
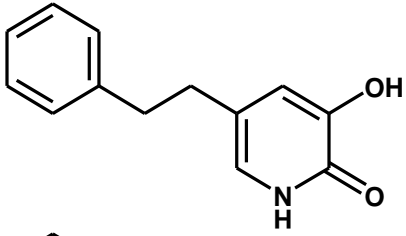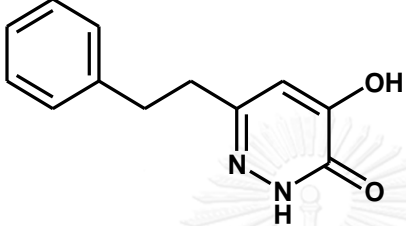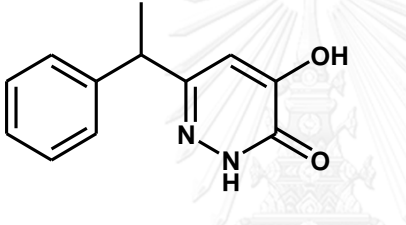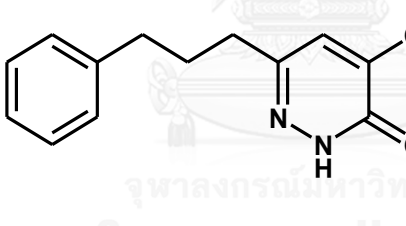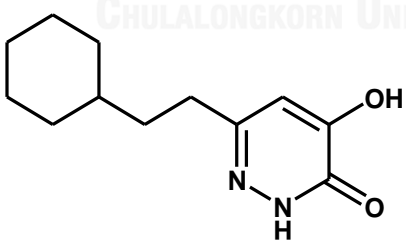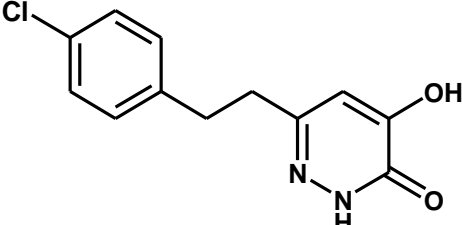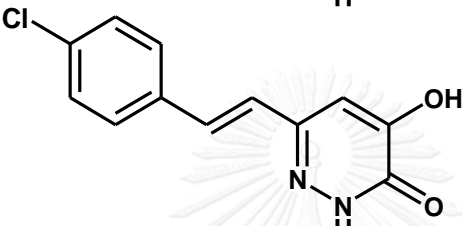
5.4.3 Binary QSAR
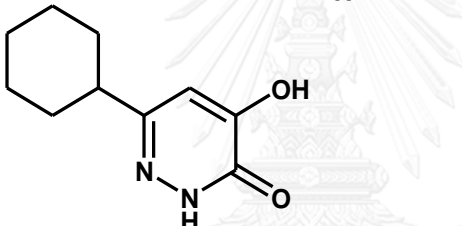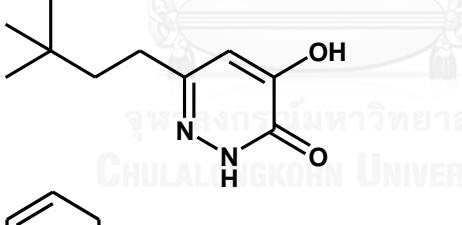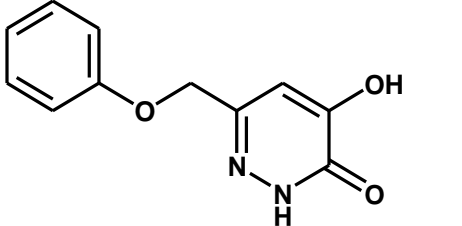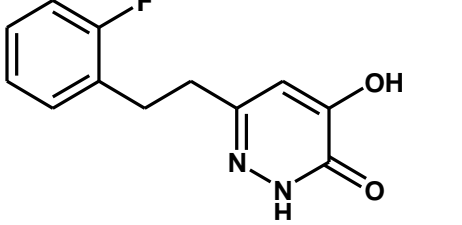
- Generate binary QSAR model

Binary quantitative structure-activity relationship (QSAR) is a kind of QSAR which approach for the analysis of high throughput screening data by structural properties of molecules relating with a binary expression of biological activity as active = 1 and inactive = 0. The binary QSAR is suitable for virtual screening and has been used in several screening researches.[126-130] In this study, the binary QSAR analysis estimates from a training set which classify the compounds with $IC_{50} < 4$ nM is the active compounds and $IC_{50} \geq 4$ nM is the inactive compounds. Base on this criterion, the 21 compounds in Table 5.1, the 11 known compounds were classified to be active and the 10 known compounds were inactive compounds. Then results from docking and properties calculations of these compounds were used to generate an equation for activity score calculation.
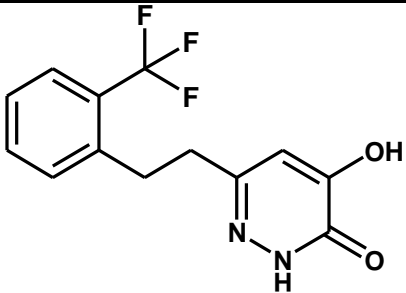
Table 5.1 The 21 compounds of the training set were classified to be active and inactive for binary QSAR.

Compound	Structure	IC_{50} (nM)	Classify
1		3.9	active
2		3.8	active
3		4.9	inactive
4		13	inactive
5		4.7	inactive
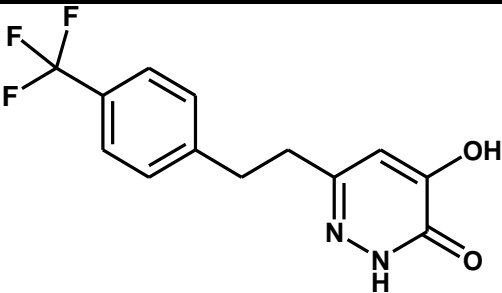
Table 5.1 The 21 compounds of the training set were classified to be active and inactive for binary QSAR. (Continue)

Compound	Structure	IC_{50} (nM)	Classify
6		2.7	active
7		120	inactive
8		300	inactive
9		670	inactive
10		2.2	active
11		2.0	active

Table 5.1 The 21 compounds of the training set were classified to be active and inactive for binary QSAR. (Continue)

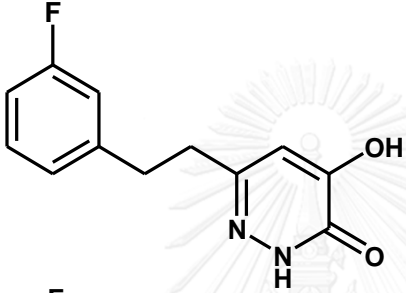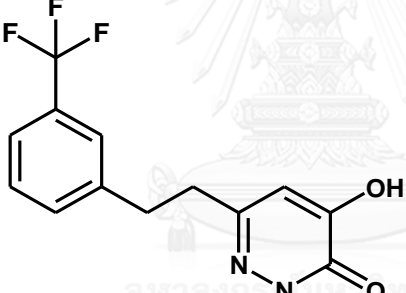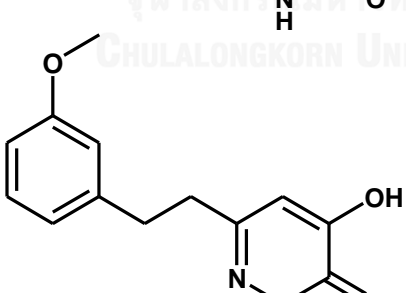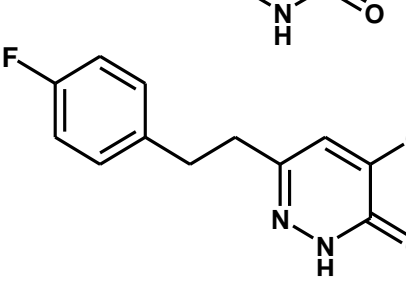| Compound	Structure	IC_{50} (nM)	Classify
12		8.4	inactive
13		1.4	active
14		2.4	active
15		2.1	active
16		3.1	active

Table 5.1 The 21 compounds of the training set were classified to be active and inactive for binary QSAR. (Continue)

Compound	Structure	IC_{50} (nM)	Classify
17		12	inactive
18		2.9	active
19		1.5	active
20		63	inactive
21		13	inactive

The 21 known activity compounds as training set were docking and properties calculations. The results of them were shown in Table S5.1 (Supplemental Information of Chapter V). We found the relationship between structural properties and biological activity by means binary QSAR. An equation for calculating score activity was generated as shown in eqn (5.1).

$$\text{Activity Score} = -1.02315 \times (\text{docking score}) + 0.02286 \times (\text{FISA})$$
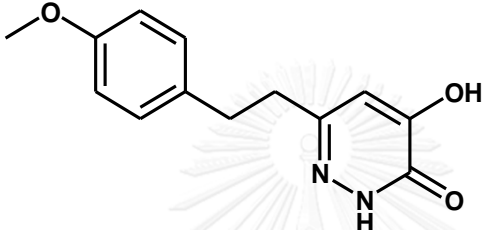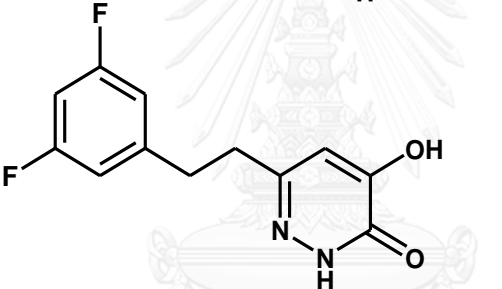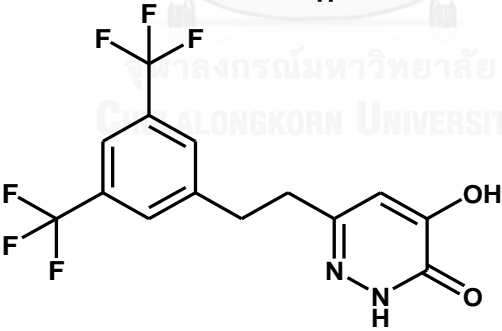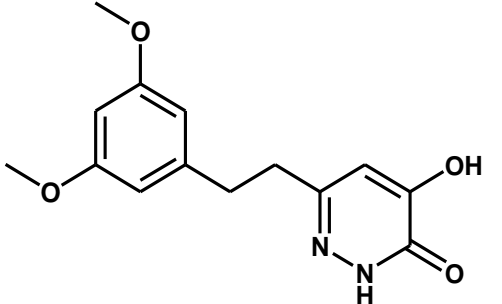$$+ 0.02189 \times (\text{PISA}) - 15.9131, \tag{5.1}$$

where docking score is calculated by Glide program (Schrödinger Suite 2012). FISA and PISA are the hydrophilic and π (carbon and attached hydrogen) components of the solvent-accessible surface area, respectively, are calculated by QikProp program (Schrödinger Suite 2012). The compound is defined as active if "Activity Score" is greater than 0 and as inactive if "Activity Score" is equal to or less than 0. The equation provides an accuracy of calculation 95.71 % which was internal validated by the training set of 21 compounds.

- Activity score calculations

In this study, the binary QSAR model used docking scores, FISA, and PISA to calculate activity scores of the 33 hit compounds. Therefore, the 33 hit compounds were docking calculated by using Glide software (Schrödinger Suite 2012). The best docking poses of the 33 hit compounds were shown in Figure 5.6 and the best docking scores of each compound were shown in Table 5.2.
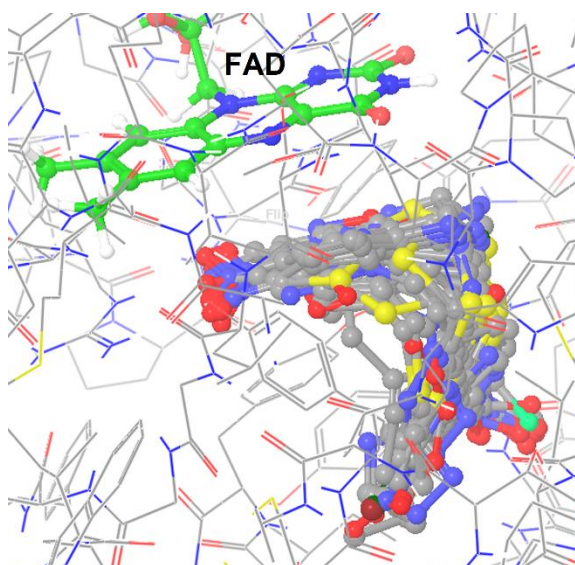
Figure 5.7 *Representation the best docking poses of the 33 second hit compounds were calculated by molecular docking using Glide program.*

In addition, the 33 hit compounds were calculated structural properties (FISA and PISA) for activity score calculations by using QikProp software (Schrödinger Suite 2012), which the results were shown in Table 5.2. The docking score, FISA, and PISA were taken to calculate by eqn (5.1) which the results of score activity calculations as Table 5.2.

Table 5. 2 Docking scores, hydrophilic component (FISA), and π-carbon and attached hydrogen component (PISA) of the solvent-accessible surface area of the 33 hit compounds.
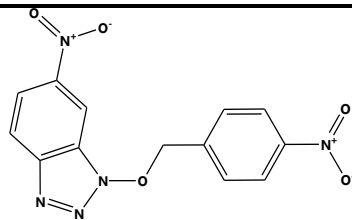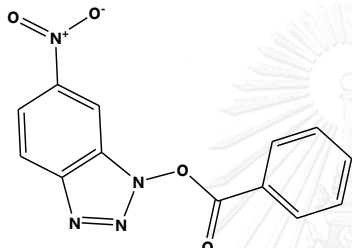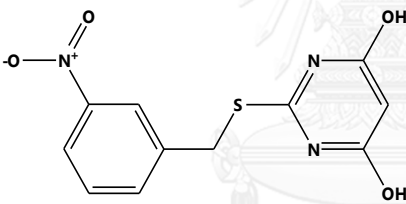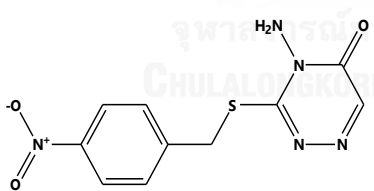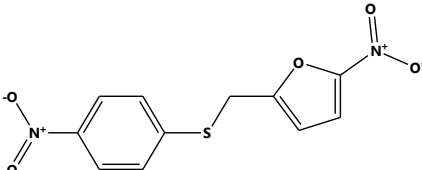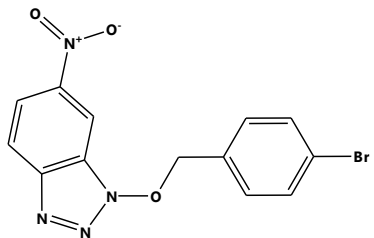
Comp	Structure	Docking score	FISA	PISA	Activity Score
1		-8.779	269.043	252.839	4.754
2		-7.760	202.256	316.703	3.583
3		-8.513	253.091	198.897	2.937
4		-8.367	254.467	195.811	2.751
5		-8.965	204.493	199.097	2.292
6		-8.195	171.803	263.668	2.171

Table 5.2 (Continue)
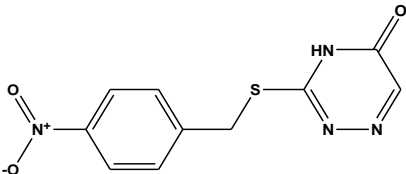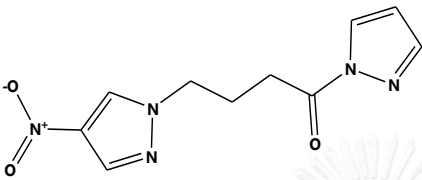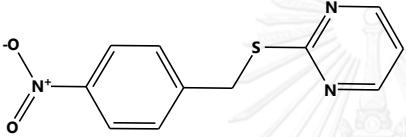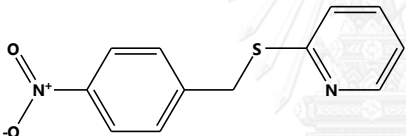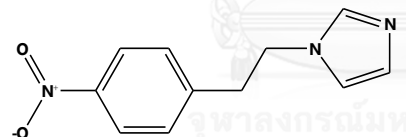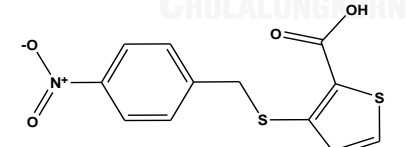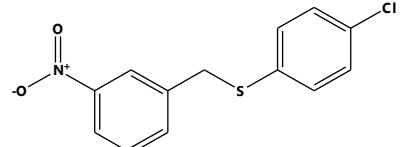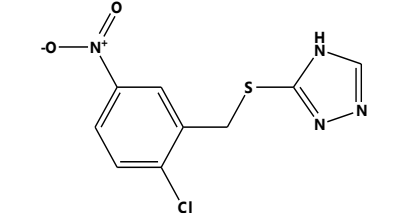
Comp	Structure	Docking score	FISA	PISA	Activity Score
7		-8.167	219.654	207.822	2.014
8		-8.413	196.009	215.559	1.894
9		-8.190	127.946	293.229	1.810
10		-8.556	116.324	273.945	1.496
11		-8.262	130.917	268.745	1.416
12		-9.306	165.023	183.306	1.393
13		-8.302	97.215	293.229	1.220
14		-8.813	184.202	172.88	1.099

Table 5.2 (Continue)
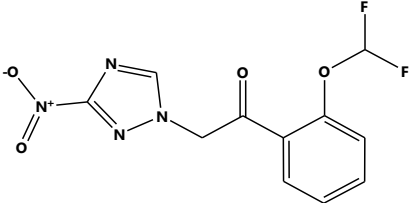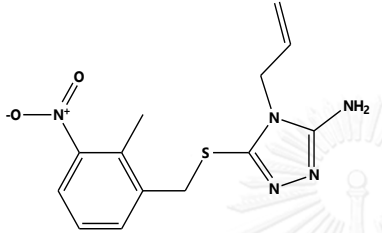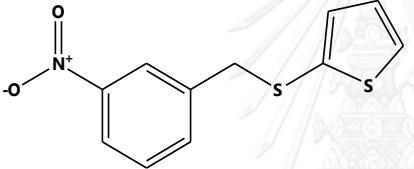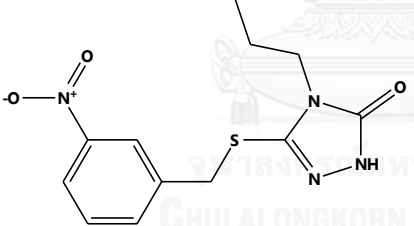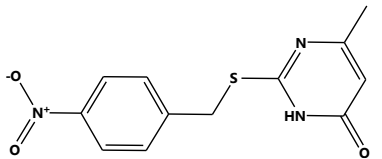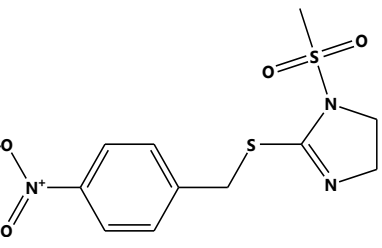
Comp	Structure	Docking score	FISA	PISA	Activity Score
15		-8.389	179.854	196.217	1.078
16		-8.219	191.088	181.436	0.836
17		-8.572	97.240	260.428	0.782
18		-8.288	207.643	147.093	0.534
19		-7.806	185.094	190.05	0.465
20		-8.574	189.954	146.572	0.410

Table 5.2 (Continue)
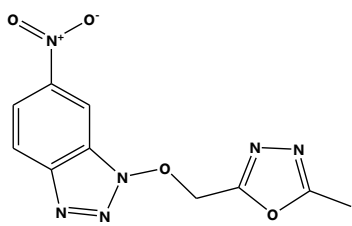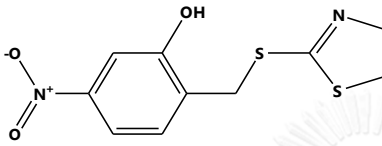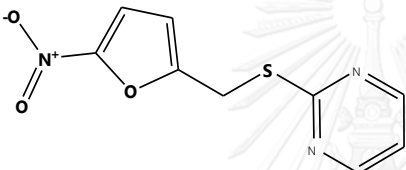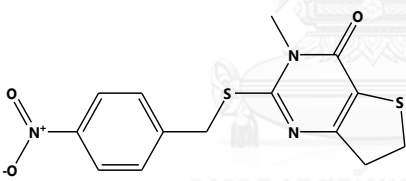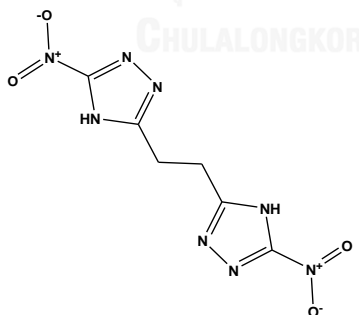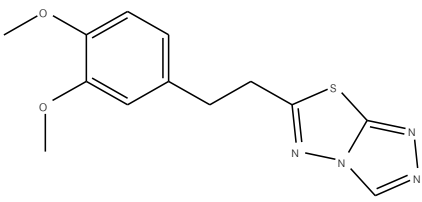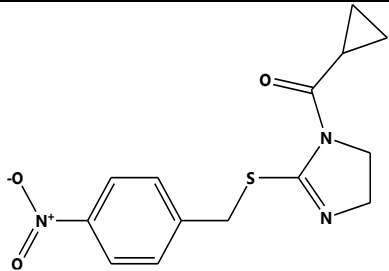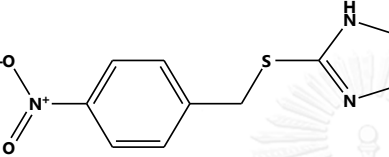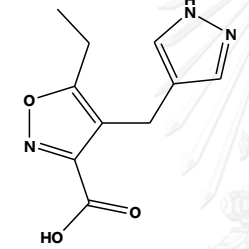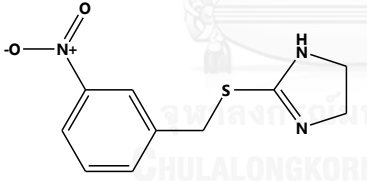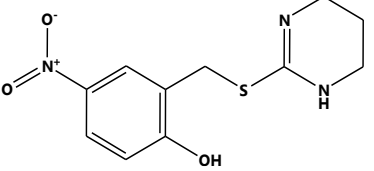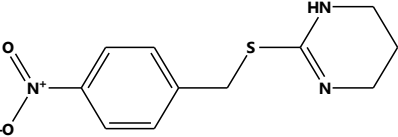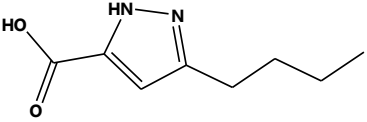
Comp	Structure	Docking score	FISA	PISA	Activity Score
21		-7.703	238.933	133.882	0.361
22		-9.433	163.315	120.886	0.118
23		-7.875	137.354	214.271	-0.026
24		-8.497	150.888	160.466	-0.258
25		-6.633	356.532	29.523	-0.330
26		-9.281	94.361	171.871	-0.498

Table 5.2 (Continue)

Comp	Structure	Docking score	FISA	PISA	Activity Score
27		-8.634	142.511	148.678	-0.567
28		-7.867	139.309	150.474	-1.386
29		-8.043	207.687	69.141	-1.422
30		-7.725	139.284	150.319	-1.534
31		-7.551	168.711	119.964	-1.705
32		-7.888	125.114	149.643	-1.707
33		-8.126	171.307	31.655	-2.989

The results from molecular docking shown the important binding modes of DAAO and its inhibitors. Here, we selected compound **12** and 4-(4-chlorophenethyl)-1H-pyrrole-2-carboxylic acid (SE5) as template for pharmacophore model to discuss about the interactions between amino acid residues in active site and them. The binding positions of SE5 is similar to the binding positions of Compound **12** as shown in Figure 5.7 (A). There are four hydrogen bonds between SE5 and DAAO such as two hydrogen bonds with Arg283, one hydrogen bond with Tyr228, and one hydrogen bond with Gly313 in Figure 5.7 (B). However, hydrogen bond of Compound **12** was included four hydrogen bonds: two hydrogen bonds with Arg283, one hydrogen bond with Tyr228, and one hydrogen bond with Gln53, which is more interactions in the secondary binding site than SE5. This result, we hope the new hit compounds can be the efficient inhibitors for DAAO inhibition.
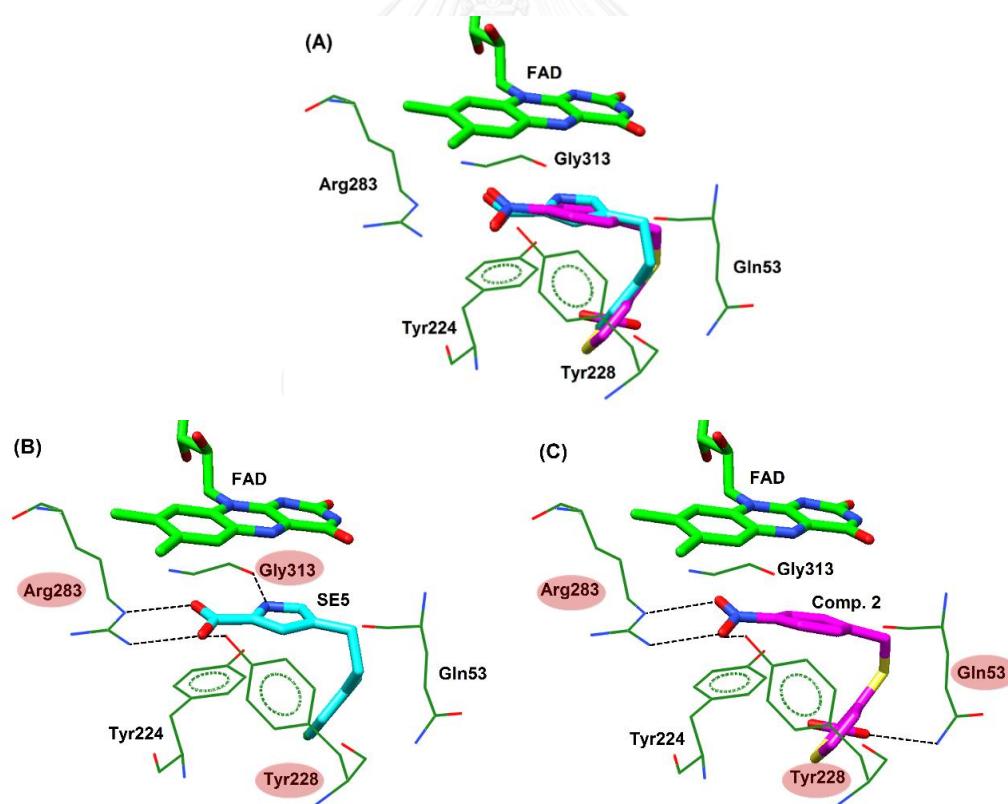
Figure 5.8 *Representation (A) the docking poses of the SE5 and Compound* **12**, *(B) the hydrogen bonding of SE5, and (C) the hydrogen bonding of Compound* **12** *with DAAO.*

5.5 DISCUSSION

There are many DAAO inhibitors are suggested [21, 44-48, 121] but most of these inhibitors are small molecules which have interaction at the first binding site (active site between Iso ring and Tyr224). Recently, the second binding site was studied by Hondo et. al. [45] by synthesize the molecules for the second binding site of DAAO. In this work, we used a second binding site DAAO inhibitor (SE5) as model to find novel DAAO inhibitors. The pharmacophore model, molecular docking, and binary QSAR were successfully used to find the 22 novel DAAO inhibitors. The 22 candidate compounds are interesting compounds, and expected to be the efficient inhibition. Most of DAAO inhibitors are discovered carboxyl compounds ($-CO_2^-$), whereas most of the novel 22 candidate compounds are nitro compounds ($-NO_2^-$). Docking poses of all candidate compounds remained keeping the important interactions (H-bond) with Tyr228 and Agr283. The aromatic moieties of these hit compounds were aligned in sandwiched parallel between Iso ring and Tyr224, these aromatic π–stacking interactions also contributed to binding modes of inhibitors.

Moreover, these candidate compounds laid in both the first and the second binding sites which can be increased the interactions more than the former DAAO inhibitors that interact only with the first binding site. These candidate compounds will be taken to run assay for testing activities.

CHAPTER VI

CONCLUSIONS

In this research, several computational chemistry techniques were applied to study D-amino acid oxidase from pig kidney and human in two main areas. Therefore, the conclusion for each part is given below.

6.1 PHOTOINDUCED ELECTRON TRANSFER ANALYSIS

Experimentally, the photoinduced electron transfer (PET) rate in DAAO dimer form is faster than monomer form. Moreover, DAAO complexed with benzoate (DAOB), the PET rate in DAOB is faster than DAAO. However, the experiments were reported only the fluorescence lifetimes which cannot demonstrate more details what happen in these systems. Therefore, we try out to use the theoretical study to explain these PET phenomena. In this thesis, we have been studied dynamics properties, we used MD simulations and PET analysis to study in four systems, i.e. DAAO monomer (Chapter II), DAAO dimer (Chapter III), DAOB monomer - dimer (Chapter IV). We can conclude that

1). DAAO and DAOB are simulated the dynamics structures in solution by MD simulation, while their structural changes are determined by the fluorescence lifetime measurements from the rate of ET from the excited Iso and the aromatic amino acids. Therefore, we used the MD simulation structures and the experimental fluorescence lifetimes to provide more information on the structure changes of DAAO and DAOB by ET analysis.

2). There are many factors for the structure changes of DAAO in monomer and dimer forms, are that (i) the number of hydrogen bonds between Iso and amino acids in DAAO dimer higher than in DAAO monomer, which presented the stable structure in DAAO dimer more than DAAO monomer, (ii) the Rc distances between Iso and Typ/Tyr in DAAO dimer are shorter than in DAAO monomer, which may causes the fluorescence lifetime in DAAO dimer shorter than DAAO monomer corresponding with the experimental results, (iii) the net electrostatic energy values of most donors are

different in both DAAO monomer (-0.434 to 0.192 eV) and dimer (-0.593 to 0.146 eV) because of the long range electrostatic energy. From these results, the interaction between Iso and DAAO dimer is stronger than DAAO monomer, which suggest that DAAO dimer form is stable than monomer form.

3). The temperature transition of DAAO monomer in the observed fluorescence lifetimes between 10 and 30 °C was discussed in Chapter II, which was attributed to the differences in the net electrostatic energy and the standard free energy gap of both temperatures. The different hydrogen bonds between Iso and the nearby amino acid residues were ascribed to the difference in the standard free energy gap at two temperatures.

4). In DAAO dimer, the two subunits are not equivalent in solution from MD simulation results. Although, DAAO dimer from X-ray crystal structure as a starting form is holodimer. Therefore, the Rc of ET donor-acceptor and the hydrogen bonding between Iso and amino acid residues in Sub A are quite different from Sub B. These results may cause to the non-equivalent ET rates and other related physical quantities of both subunits (in Chapter III).

5). The observed fluorescence lifetime of DAOB dimer is shorter than DAOB monomer. From MD simulation results, The Rc between Iso and benzoate in DAOB dimer (0.66 nm in Sub A and 0.68 nm in Sub B) is longer than DAOB monomer (0.61 nm), and the number of hydrogen bonds between Iso and amino acid residues in monomer (eight H-bonds) more than in dimer of each subunit (seven H-bonds in Sub A and five H-bonds in Sub B). These results suggest that the PET process not only is the effect from Rc but also affects form the other factors, which no one can clear in all factors.

6). The observed fluorescence lifetimes of DAOB dimer are 4.8 and 0.85 ps. The two fluorescence lifetime compositions maybe result from the non-equivalent structures for the two subunits, which were represented by MD simulation results (in Chapter IV). The Rc of Iso and the ET donors are quite different in two subunits, particularly, Tyr55 and Trp185. The H-bonds between Tyr228 and Bz, and between Thr317 and Iso in Sub A were not formed in Sub B. From ET analysis, we expected the

fluorescence lifetimes in Sub B was faster than Sub A. Moreover, the net electrostatic energy values between two subunits are not similar which was discussed in Chapter IV.

7). The experimental fluorescence lifetimes in DAOB are shorter than DAAO because DAOB were changed the structures near Iso with benzoate, which are ascribed to the fastest ET by benzoate. The conformations of DAAO and DAOB were visibly different when compared by the Rc values between Iso and aromatic amino acids. As the Rc of Tyr224 in DAAO (0.82 nm in Sub A and 0.76 nm in Sub B) are shorter than DAOB (1.32 nm in Sub A and 1.04 nm in Sub B). The RMSF of the overall amino acids represented the monomer form is higher fluctuation than dimer forms in both DAAO and DAOB. The DAAO monomer is the most unstable and the DAOB dimer is the most stable.

8). The polarity near Iso in DAAO is higher than DAOB, which presented by the static dielectric constants between Iso and ET donors in DAAO (5.7 – 5.9) are larger than DAOB (2.54 – 2.64). We observed a higher number of water molecules near Iso in DAAO by RDF analysis.

These results of this part could provide the important interactions of DAAO, Iso, and an inhibitor (benzoate). Moreover, the interactions of Iso binding, benzoate binding, and the atomic level of their dynamics behavior are provided. Nevertheless, there are some unclearly questions need to be answered in the future works. Here, we do not enough the experimental results for PET analysis to find some parameters which maybe relate between ET and inhibition of inhibitors. Therefore, we used the general criteria for virtual screening part to find the novel inhibitors.

6.2 VIRTUAL SCREENING

We used pharmacophore and docking techniques which combined with drug-like property to screen new DAAO inhibitor. The commercially available four million compounds from Namiki database were screened by many our criteria, i.e. Lipinski's rule of five, pharmacophore model, binding site surface, docking scores, binary QSAR. We obtained 22 hit compounds as novel hit compounds for DAAO inhibitors. The

aromatic moieties of these hit compounds were aligned in sandwiched parallel between Iso ring and Tyr224, so aromatic π–stacking interactions also contributed to binding modes of inhibitors. In addition, almost all hit compounds are nitro compounds (nitro group) which interacted with side chain of Arg283 and Tyr228 which other works are carboxyl group compounds. These hit compounds not only have interactions at first binding site, they also interacted with secondary binding site. More interactions of them were expected to increase their inhibitions. We hope the 22 novel candidate compounds can be the potential inhibitors of DAAO and should be assayed for activity tests.

6.3 SUGGESTION FOR FUTURE WORK

1). QM/MM/MD will be used to study ET analysis because this method can give more accurate charges than conventional MD simulation.

2). More DAAO-inhibitors systems will be used to measure fluorescence lifetime for ET calculation in order to construct the relationship between ET parameters and biological activity.

3). The 33 hit compounds obtained from virtual screening will be tested for biological activity.

SUPPLEMENTAL INFORMATION

SUPPLEMENTAL INFORMATION OF CHAPTER II

Structural Basis for the Temperature-Induced Transition of D-Amino Acid Oxidase
from Pig Kidney Revealed By Molecular Dynamic Simulation and
Photo-Induced Electron Transfer
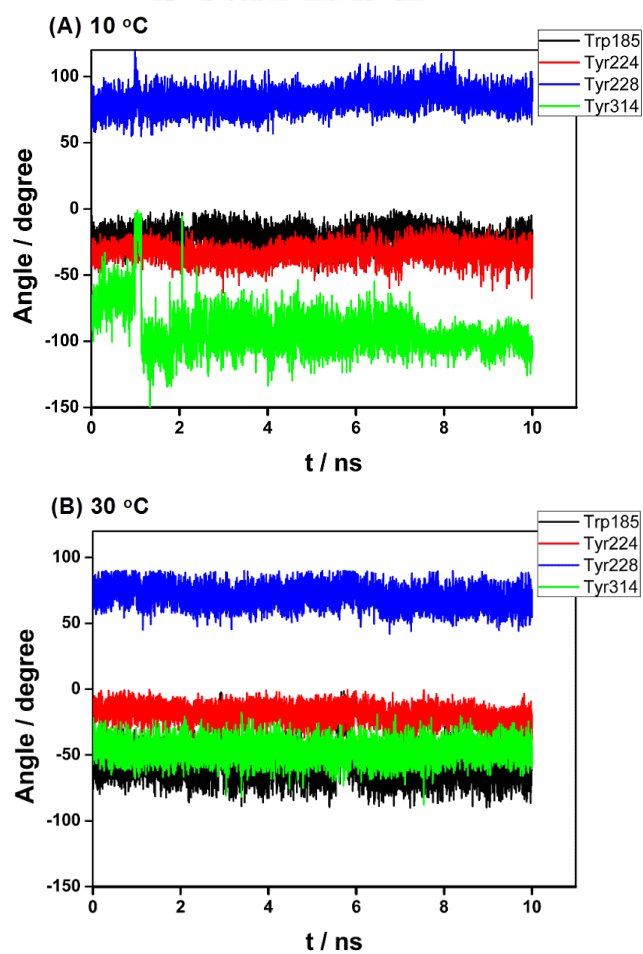
Figure S2.1 *Inter-planar angles between Iso and the indicated four nearby aromatic amino acids.*
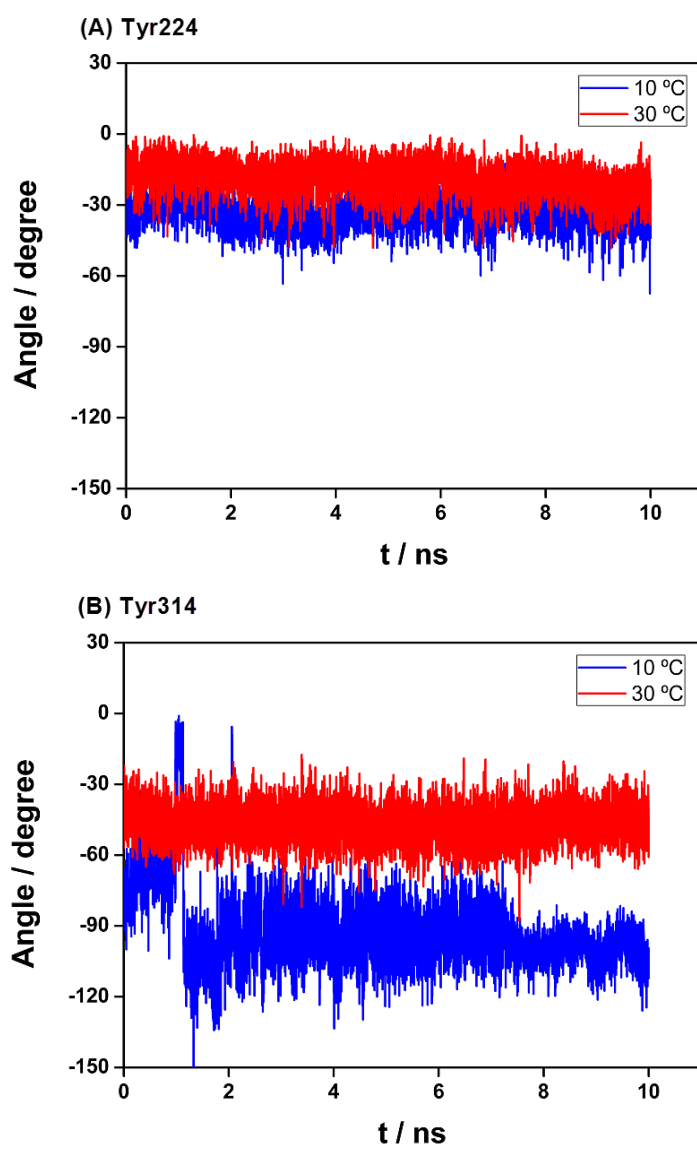
Figure S2.2 *Comparison of the inter-planar angles between Iso and (A) Tyr314 and (B) Tyr224 at 10 ℃ and 30 ℃.*
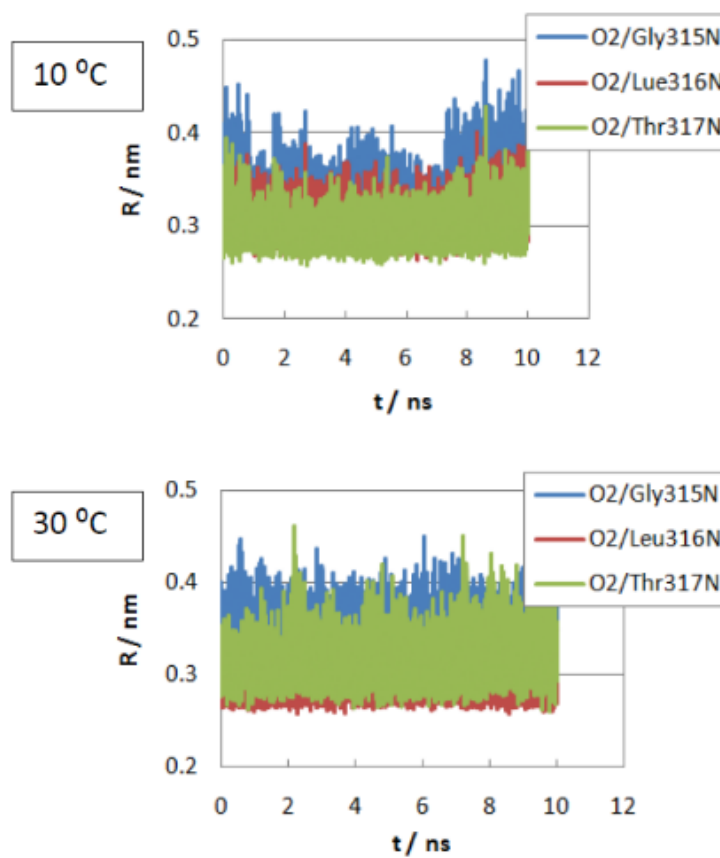
Figure S2.3 *H-bond dynamics between the Iso O2 atom and the three indicated nearby amino acids at (A) 10 ℃ and (B) 30 ℃.*
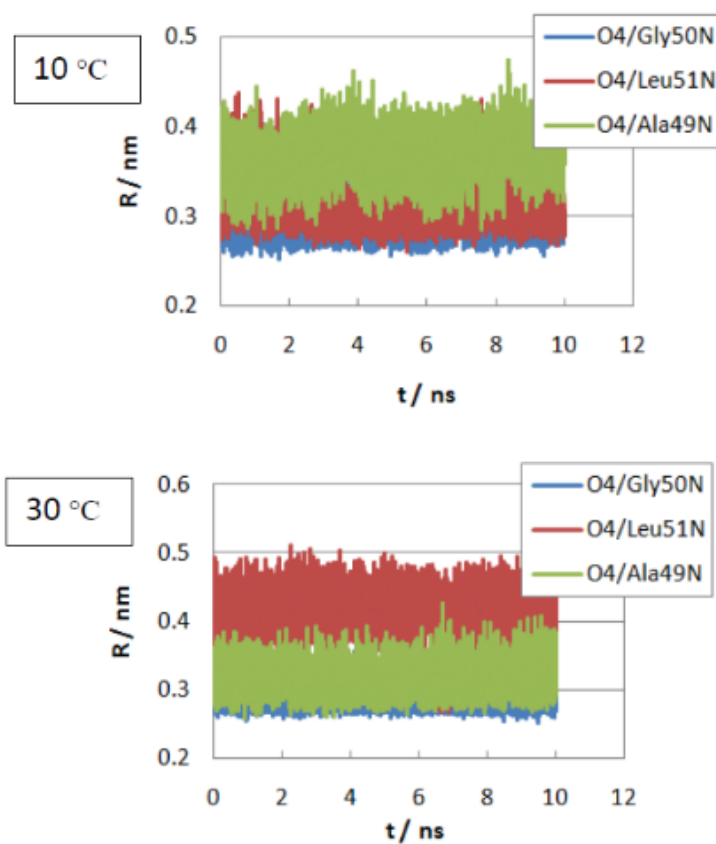
Figure S2.4 *H-bond dynamics between the Iso O4 atom and the indicated three nearby amino acids at (A) 10 ℃ and (B) 30 ℃.*
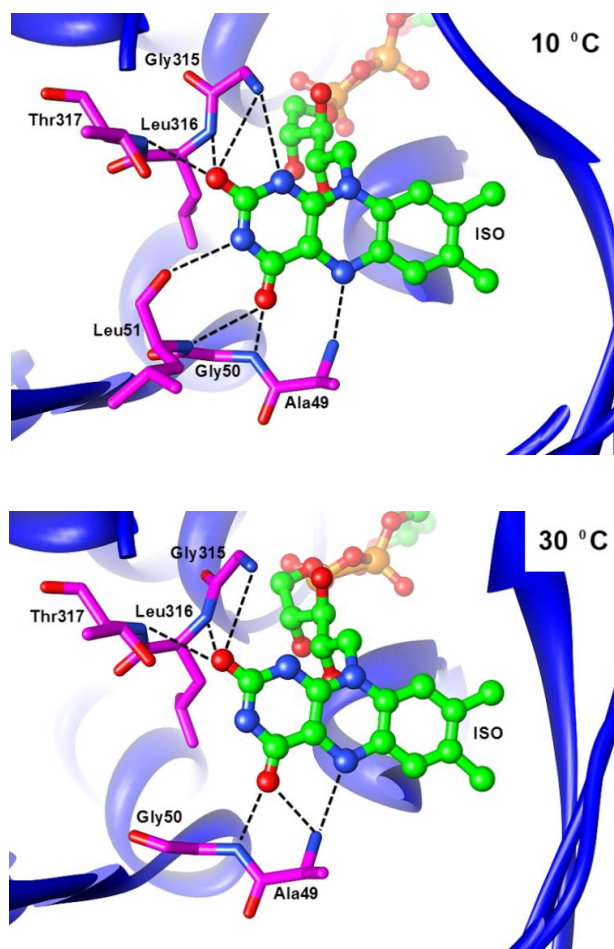
Figure S2.5 H-bond distances between the Iso atoms and the indicated nearby amino acids at (A) 10 °C and (B) 30 °C. Dashed lines represent the H-bonds.

SUPPLEMENTAL INFORMATION OF CHAPTER III

Non-Equivalent Conformations of D-Amino Acid Oxidase Dimer from Porcine Kidney between the Two Subunits. Molecular Dynamic Simulation and Photoinduced Electron Transfer
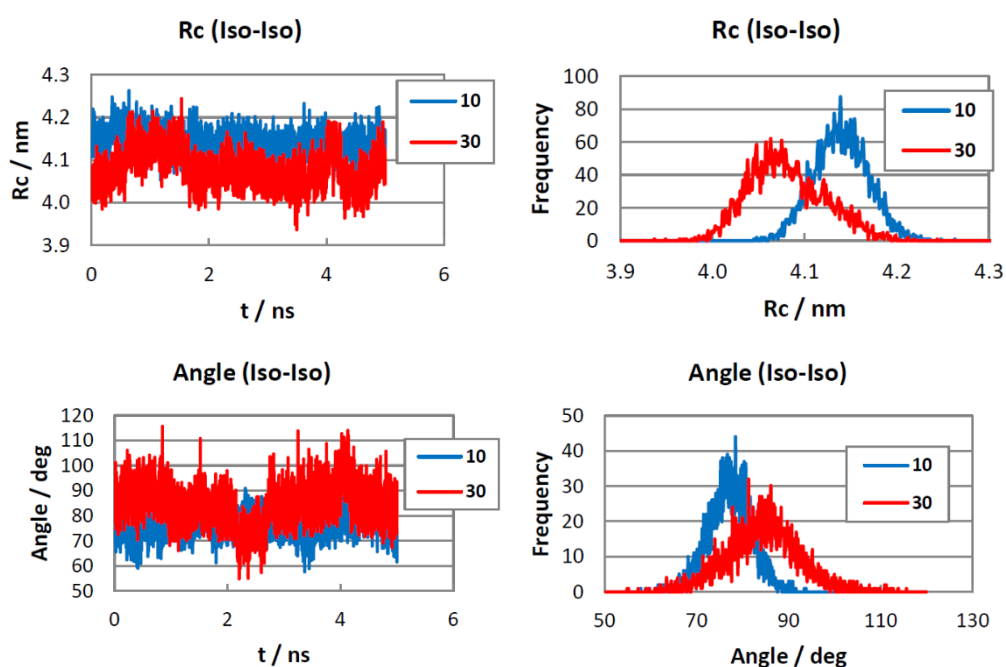
Figure S3.1 *Dynamics of inter-subunit structure. Left column shows dynamics of Rc between Iso in Sub A and Iso in Sub B (upper) and inter-Iso angle (lower). Right column shows distributions of these geometrical factors. 10 and 30 in the inserts denote 10 ℃ and 30 ℃.*
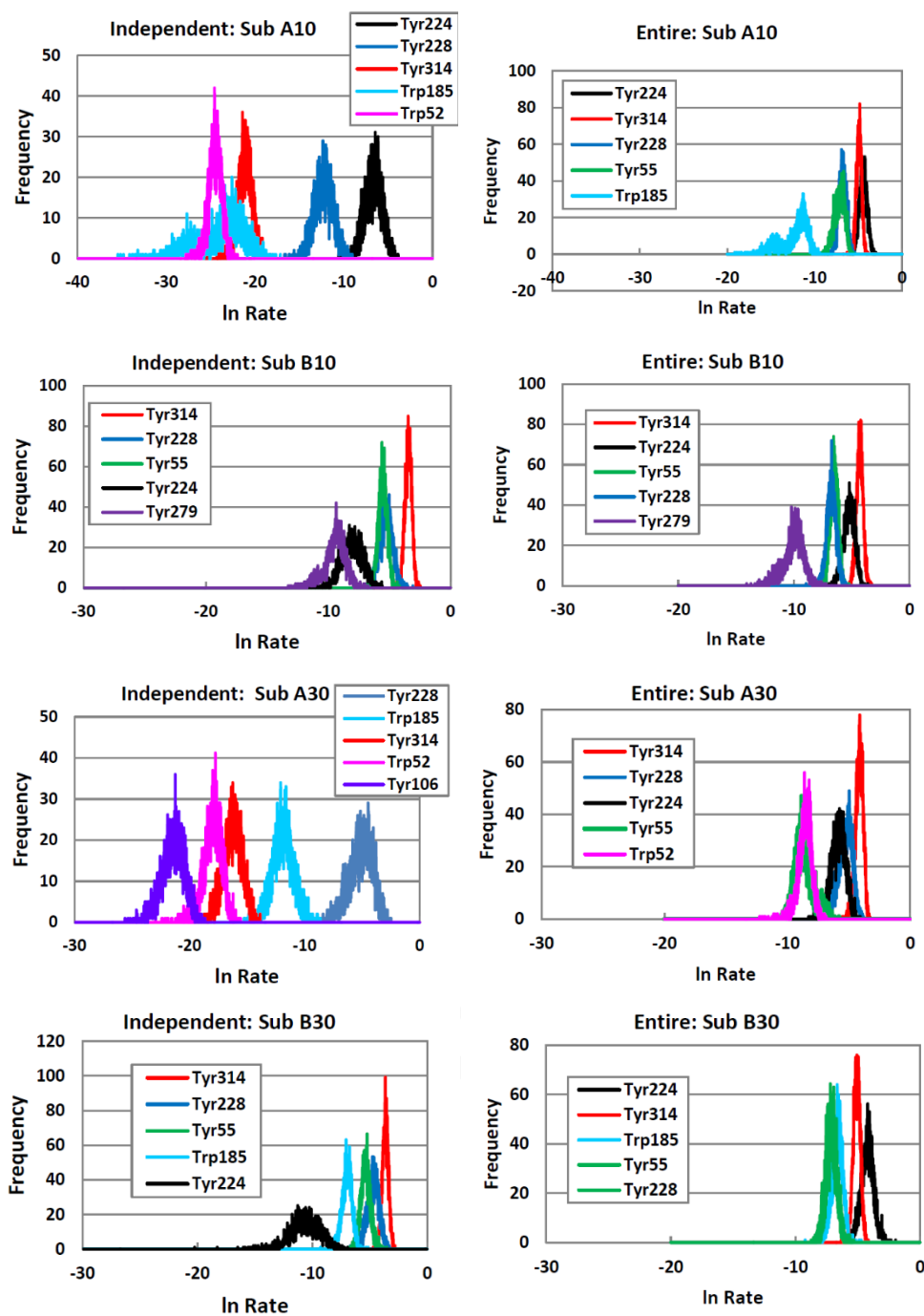
Figure S3.2 *Comparison of the logarithmic ET rate between Independent Model and Entire Model. In Independent model ET rates were obtained independently in Sub A and in Sub B. In Entire model the ET rates were obtained for the entire dimer. Sub A10 and Sub B10 denote Sub A and Sub at 10 ℃, and Sub A30 and Sub B30, Sub A and Sub B at 30 ℃, respectively. Inserts show amino acids with top fastest ET rates.*
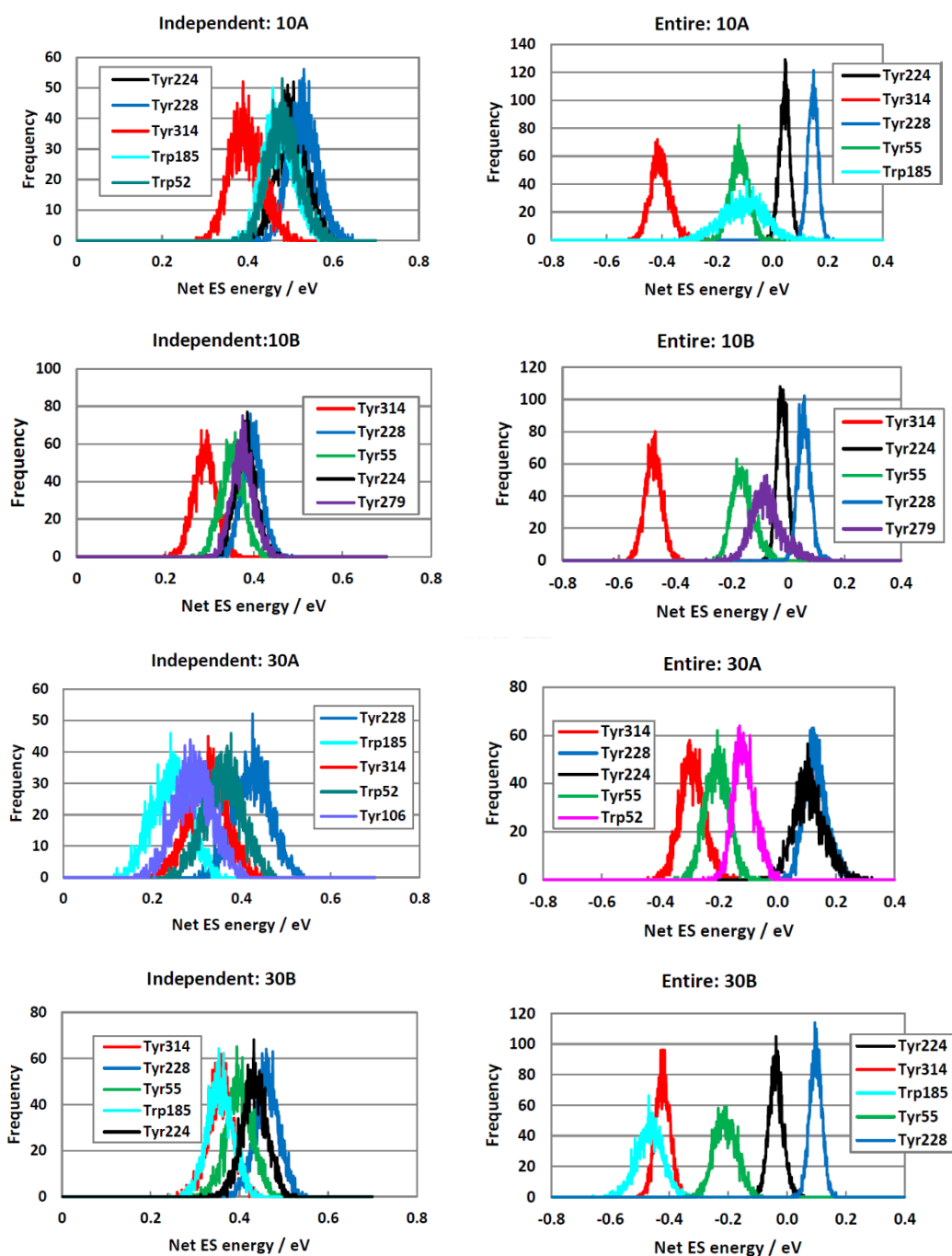
Figure S3.3 *Effect of subunit structure on the Net ES energy in DAAO dimer. In Independent model the Net ES energies were obtained independently in Sub A and in Sub B. In Entire model the Net ES energies were obtained for the entire dimer. Sub A10 and Sub B10 denote Sub A and Sub at 10 ℃, and Sub A30 and Sub B30, Sub A and Sub B at 30 ℃, respectively. Inserts show amino acids with top fastest ET rates.*
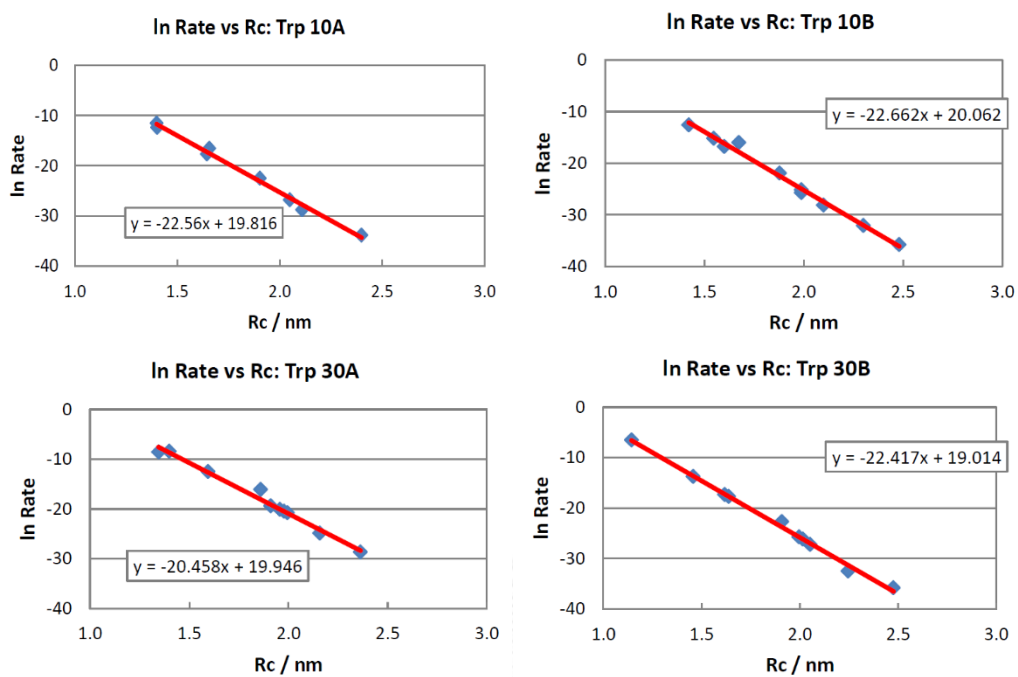
Figure S3.4 *Dutton law for Trp in DAAO. All Trps were taken into account. Inserts indicate approximate linear functions.*
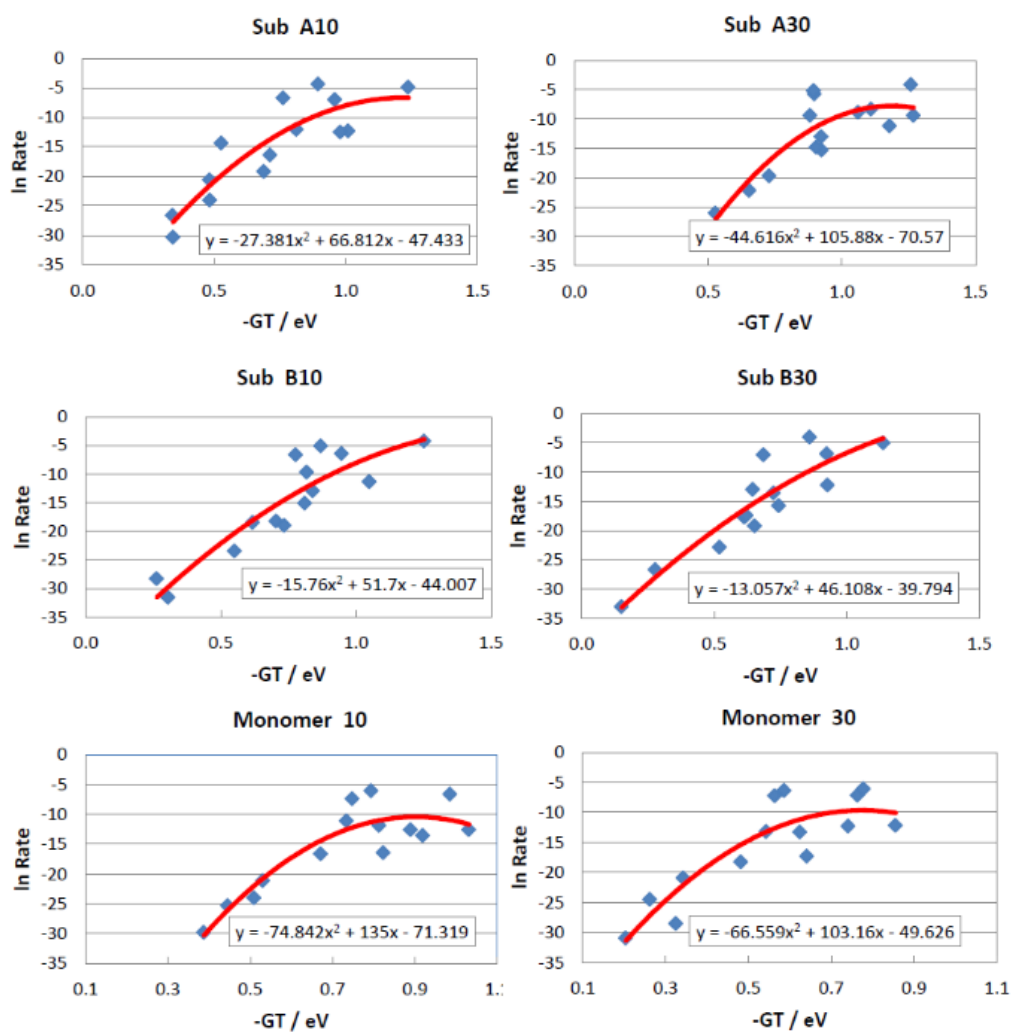
Figure S3.5 *Energy Gap law for Tyrs as ET donors. Inserts indicate approximate parabolic functions. Maximum rates in the dimer were expected at 1.2 eV of in Sub A10, at 1.6 eV in Sub B10, at 1.2 eV in Sub A30 and 1.8 eV in Sub B30. The maximum rates in monomer were expected at 0.90 eV at 10 °C and at 0.77 eV at 30 °C.*

SUPPLEMENTAL INFORMATION OF CHAPTER IV

Theoretical Analyses of the Fluorescence Lifetimes of

the D-Amino Acid Oxidase–Benzoate Complex Dimer from Porcine Kidney:

Molecular Dynamics Simulation and Photoinduced Electron Transfer

---
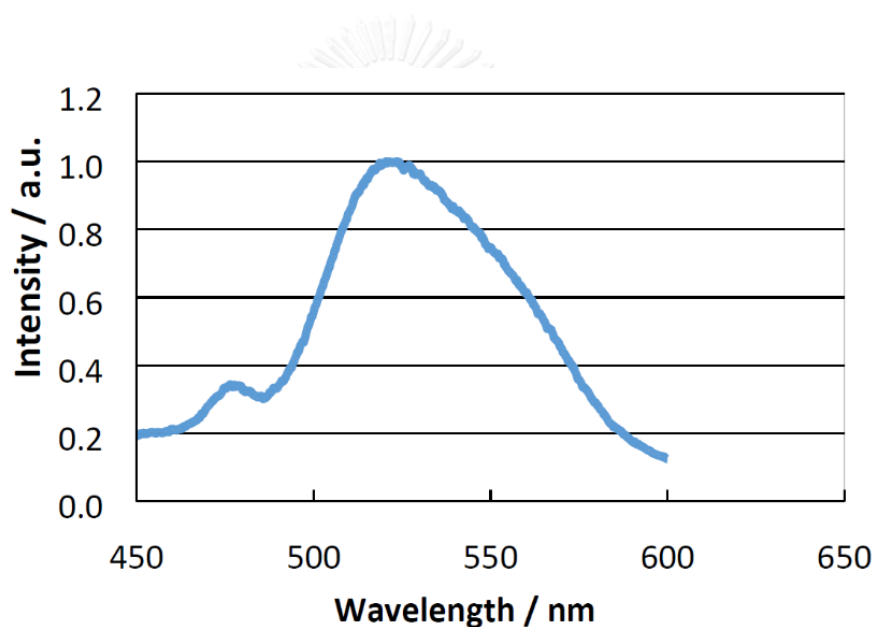
Figure S4.1 *Fluorescence spectrum of the DAOB dimer with an excitation wavelength of 410 nm. The protein was dissolved in 0.017 M pyrophosphate buffer (pH 8.3) at 10 μM.*
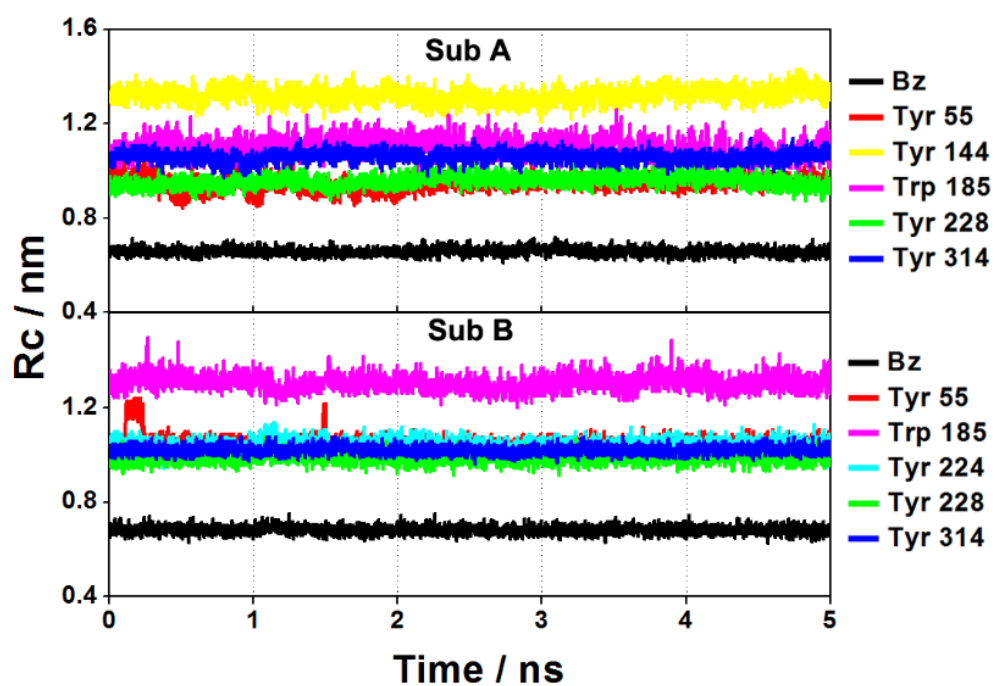
Figure S4.2 *Time-evolution of the Rc between Iso and the six nearest potential ET donors in the DAOB dimer. Rc denotes centre-to-centre distance.*
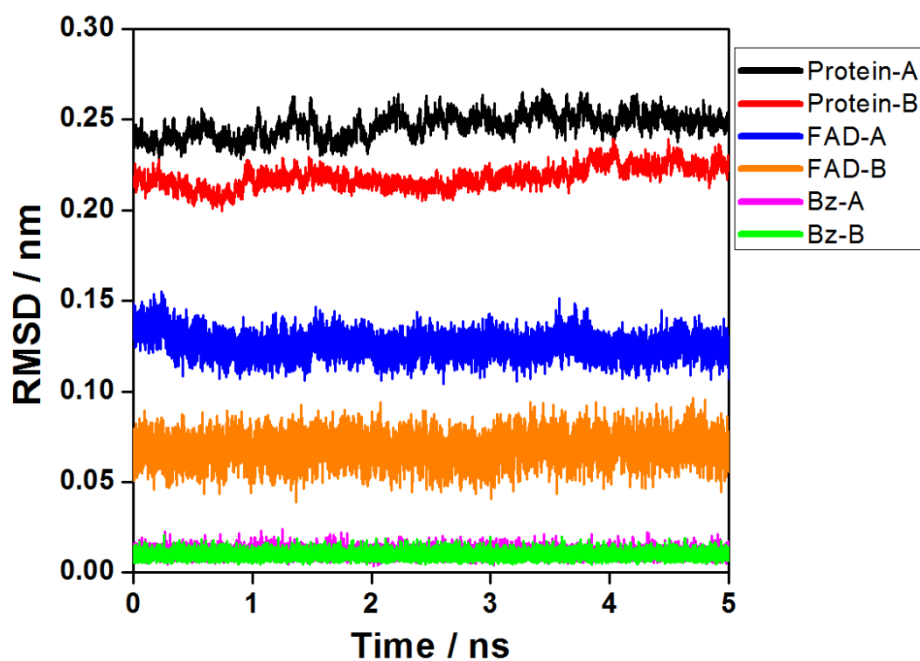
Figure S4.3 *Time-evolution of root of mean square deviation (RMSD). The RMSD were obtained by AMBER 10. MDS calculations from the last 5 ns of a 30 ns simulation. Protein-A and protein-B denote Sub A and Sub B in the DAOB dimer. FAD-A and FAD-B denote the FAD in Sub A and Sub B, and Bz-A and Bz-B denote Bz in Sub A and Sub B, respectively. RMSDs of FAD and Bz were steady over the MDS time range of 25–30 ns, whilst the subunits were almost at equilibrium.*
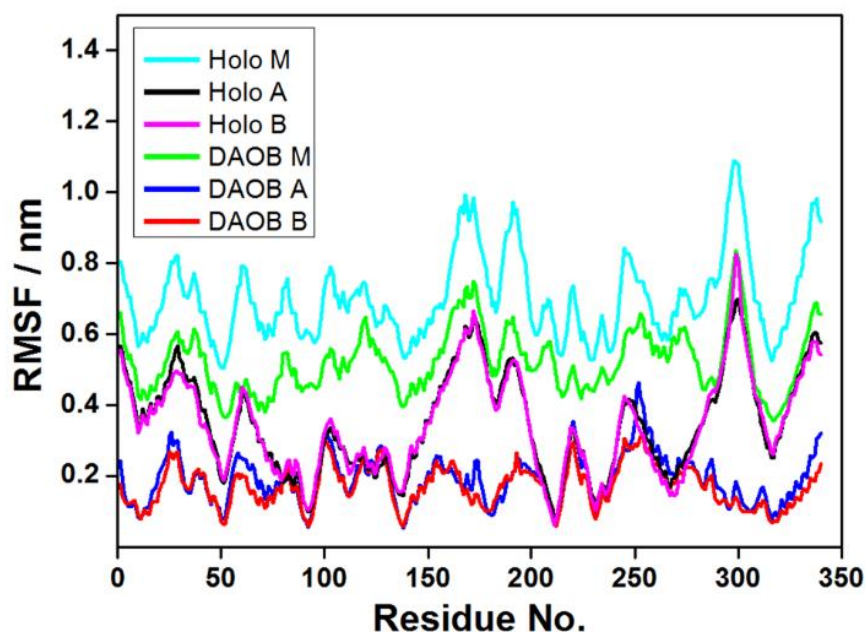
Figure S4.4 *Comparison of RMSF in DAOB dimer with other DAAO species. Root of mean square fluctuations (RMSF), as obtained by AMBER10. Holo M, Holo A and Holo B in insert denote the holoDAAO monomer, Sub A and Sub B of the holoDAAO dimer, respectively. DAOB M, DAOB A and DAOB B denote the monomer of DAOB, Sub A and Sub B of the DAOB dimer, respectively. RMSFs of the holoDAAO monomer were taken from Nueangaudom et al. (2012) [105], those for holoDAAO dimer from Nueangaudom et al. (2014) [109], and those of DAOB monomer from Nueangaudom et al. (2012) [106].*
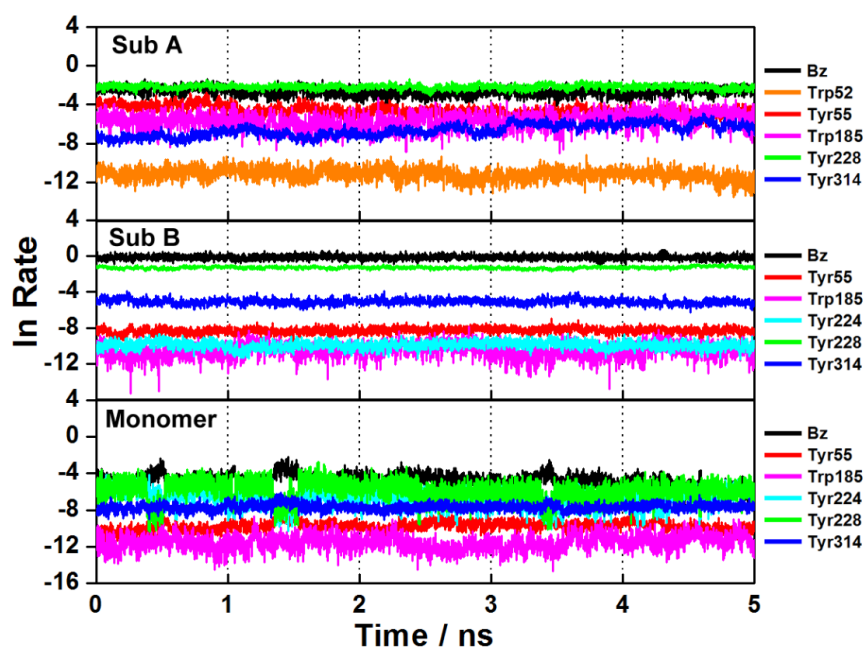
Figure S4.5 *Dynamics (time-evolution) of the logarithmic ET rate of the six fastest donors. Upper, middle and lower panels show the logarithmic ET rates of Sub A, Sub B and the monomer, respectively. The rates were obtained with Method 2.*
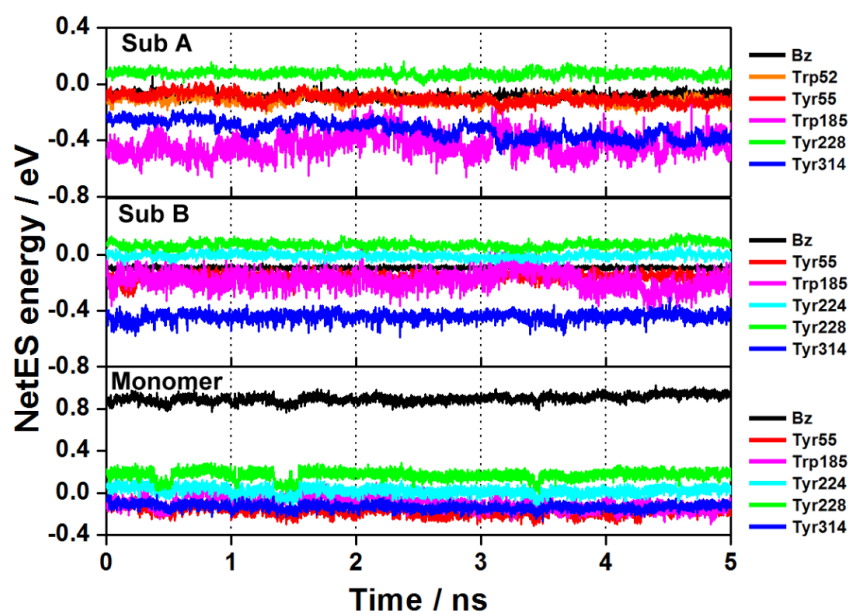
Figure S4.6 *Time-evolution of the NetES energy between the photoproducts as the Iso acceptor and the six fastest donators (ionic groups) in the DAOB dimer.*
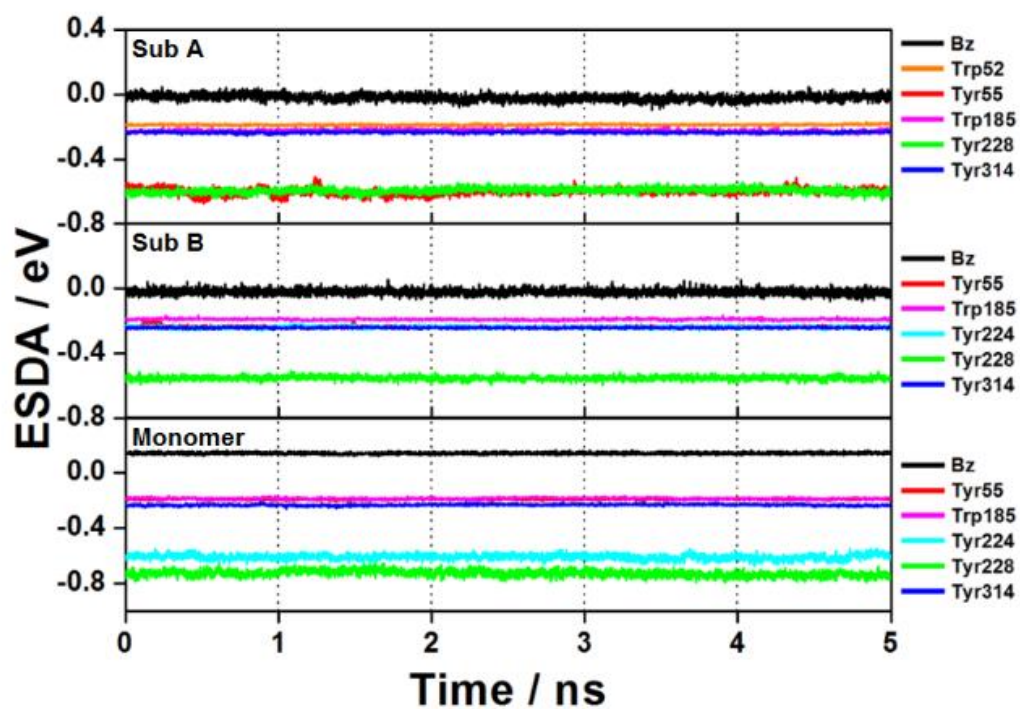
Figure S4.7 *Time-evolution of the ESDA between the Iso acceptor and the six fastest donators (Bz, Trp or Tyr cations) in the DAOB dimer. ESDA (electrostatic energy between the iso anion and the donor cation or neutral Bz) was derived as $-e^2 / \varepsilon_{DA} R_j$ from eqn (4.1) for Trp and Tyr, where the static dielectric constants ε_{DA}^A and ε_{DA}^B were used for Sub A and Sub B, respectively, or from eqn (4.11) for Bz.*
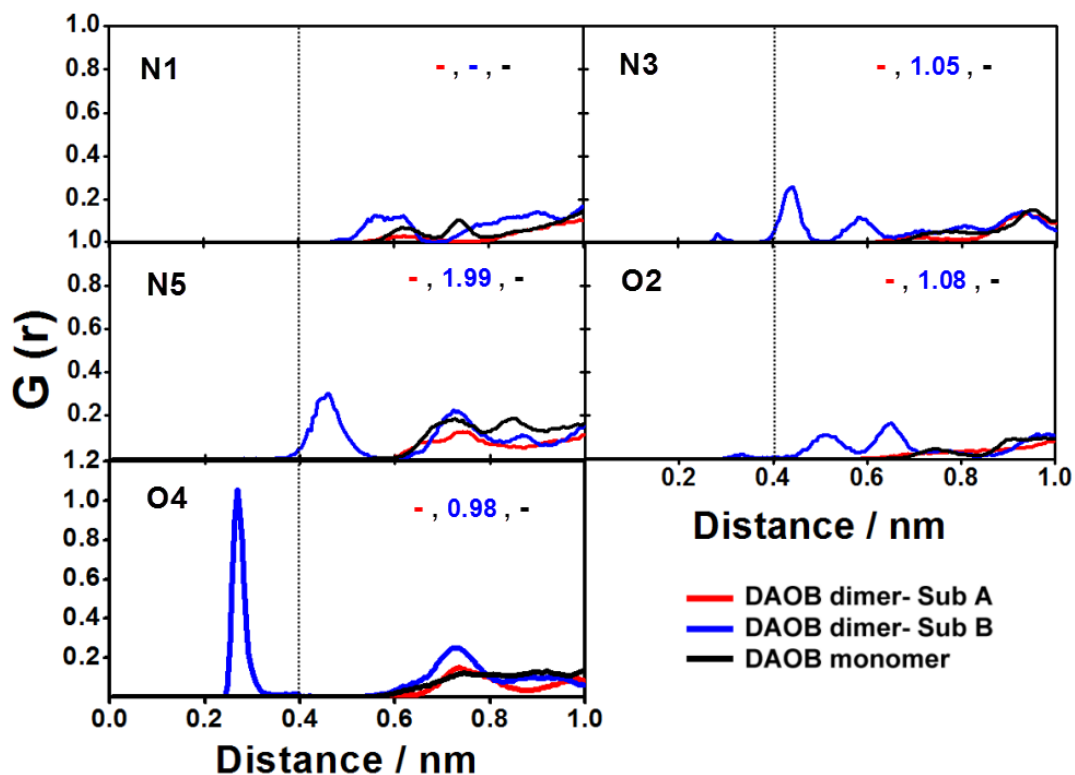
Figure S4.8 The radial distribution functions of water molecules near the heteroatoms of Iso. The radial distribution functions (RDF) were obtained by ptraj module of Amber10 program. Red, blue and black numbers are shown number of mean water molecules of DAOB dimer, Sub A and Sub B and DAOB monomer [106], respectively.
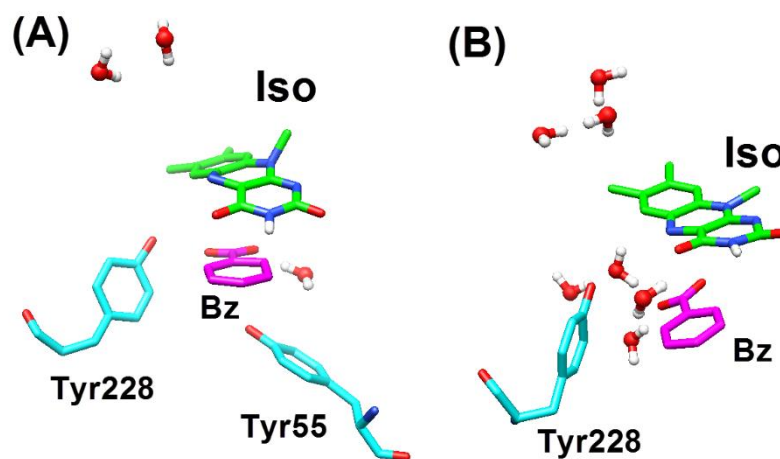
Figure S4.9 *Presence of water molecules near Iso and ET donors in a snapshot. Panel (A) shows Sub A and (B) Sub B. ET donors are shown with Rc shorter than 1 nm. Water molecules selected are shown with the distance from IsoN5 shorter than 0.7 nm.*
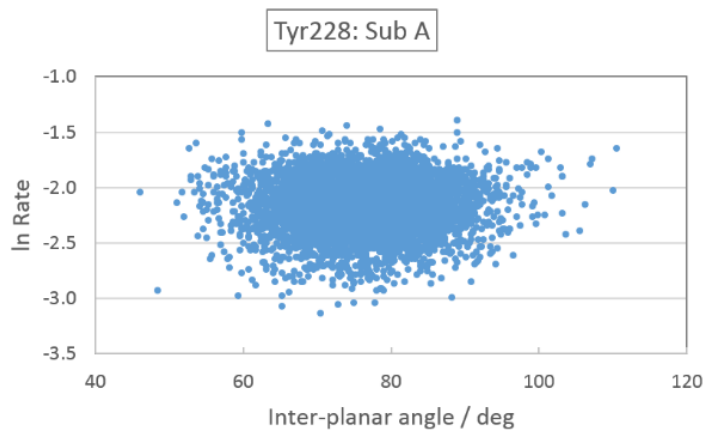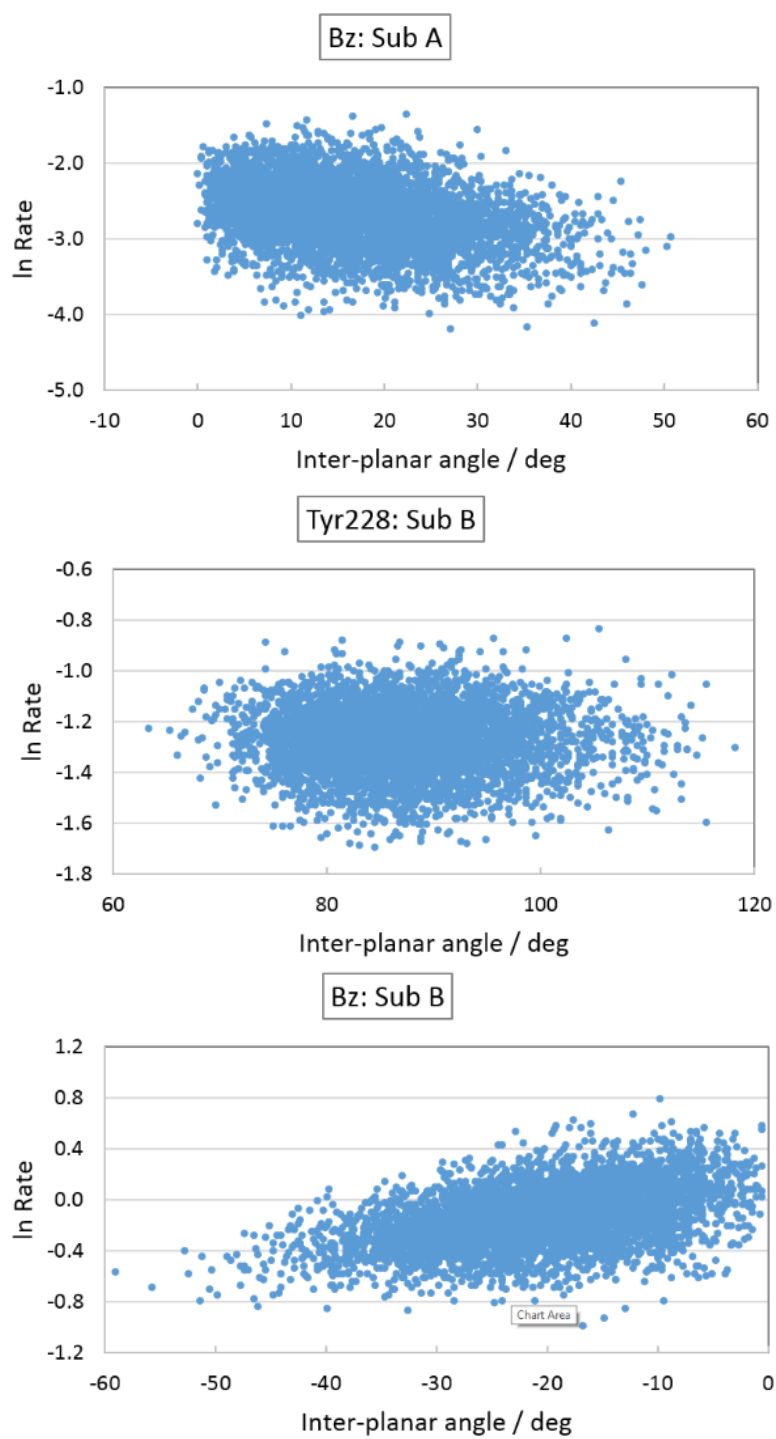
Figure S4.10 Relationship between logarithmic ET rates and inter-planar angles between Iso and main donors.
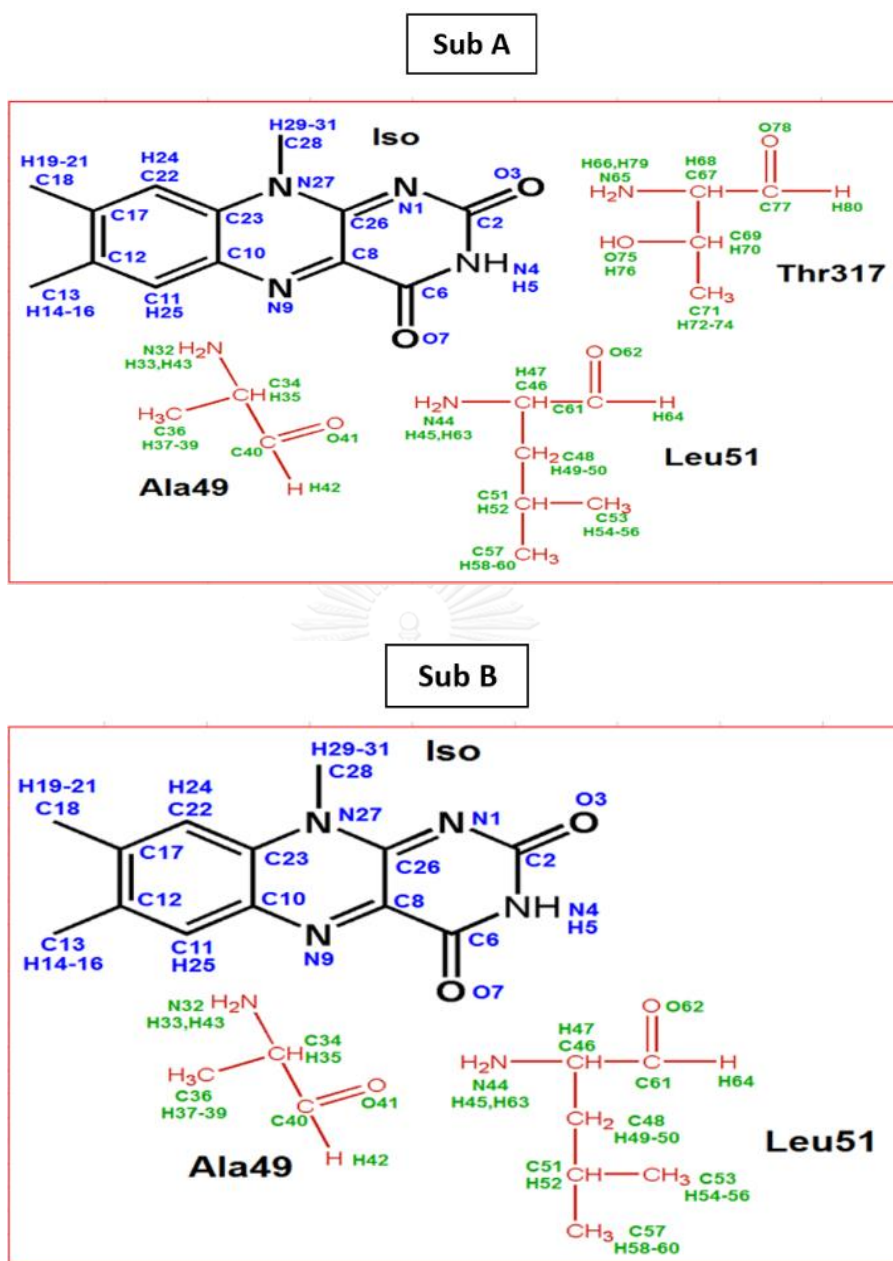
Figure S4.11 *Atom numbering of hydrogen bonded systems in DAOB dimer for MOPAC calculation. Iso forms hydrogen bondings (H-bond) with Ala49, Leu51 and Thr317 in Sub A, while it forms H-bonds with Ala49 and Leu51 in Sub B.*
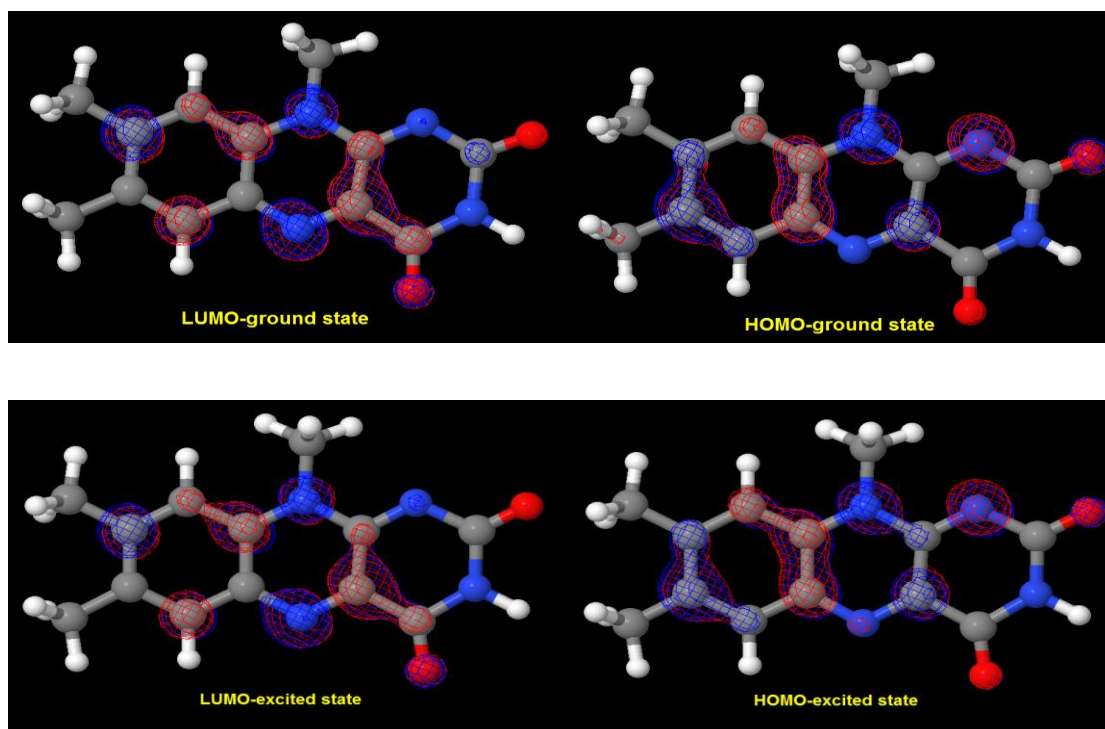
Figure S4.12 *HOMO-LUMO orbitals Iso alone. MOs were calculated with semi-empirical MOPAC method. PM6 basis set was used. Other key words were same with those in the previous work,[106] except for EPS (static dielectric constant) key words which were all 2.6 (ε_0^{DA} was nearly equal to ε_0^{DB}, 2.6, see Table 4.3) in the present work.*

Table S4.1 Decay parameters of the DAOB dimer. [a]

Wavelength (λ_i) (nm)	τ_1 (ps)	α_1	τ_2 (ps)	α_2
480	0.30	0.815	1.9	0.185
485	0.42	0.71	4.23	0.29
490	0.506	0.600	4.46	0.400
510	0.942	0.22	4.47	0.78
530	1.486	0.337	4.95	0.663
550	1.46	0.36	5.00	0.64
580	0.94	0.26	4.52	0.74
600	0.877	0.25	4.40	0.75
630	0.84	0.486	6.46	0.514
640	0.713	0.47	7.34	0.53

[a] Data are taken from Mataga et al. (2000).[15]

Table S4.2 ET parameters in the DAOB monomer obtained with a similar model as with the DAOB dimer. [a]

Protein	G_{Iso}^0 (eV)	R_0^{Bz} (nm)	ε_0	ε_0^{DA}	χ^2
DAOB monomer	8.53	0.384	5.78	2.45	4.38×10^{-21}

[a] ET parameters were recalculated with the model where the static dielectric constant in the region between Iso and the donors with Rc values of less than 1 nm (Bz, Tyr224 and Tyr228) [106] was ε_0^{DA} (eqn (4.2) and Nueungaudom et al. (2014) [109]). In the previous work [106] the dielectric constant in this region between Iso and these donors was assumed to be equal to ε_0.

Table S4.3 Charge density of Iso with and without H-bonds[a]

Molecule	Atom No.	Only Iso		Iso with H-bond			
				Ground		Excited	
		Ground	Excited	Sub A	Sub B	Sub A	Sub B
Iso	1	-0.613	-0.467	-0.616	-0.614	-0.440	-0.471
	2	0.747	0.713	0.750	0.750	0.716	0.717
	3	-0.519	-0.498	-0.514	-0.510	-0.480	-0.484
	4	-0.621	-0.616	-0.620	-0.624	-0.615	-0.616
	5	0.325	0.324	0.343	0.340	0.342	0.338
	6	0.659	0.651	0.662	0.661	0.653	0.653
	7	-0.501	-0.489	-0.535	-0.525	-0.511	-0.523
	8	-0.194	-0.122	-0.211	-0.212	-0.106	-0.131
	9	-0.101	-0.298	-0.093	-0.090	-0.277	-0.285
	10	-0.074	0.246	-0.075	-0.082	0.219	0.237
	11	-0.085	-0.319	-0.079	-0.075	-0.278	-0.302
	12	-0.028	0.247	-0.029	-0.035	0.230	0.244
	13	-0.477	-0.538	-0.477	-0.476	-0.537	-0.539
	14	0.174	0.197	0.173	0.172	0.197	0.196
	15	0.174	0.196	0.176	0.172	0.197	0.191
	16	0.172	0.190	0.172	0.175	0.190	0.200
	17	0.211	-0.060	0.216	0.217	-0.077	-0.065
	18	-0.526	-0.475	-0.527	-0.528	-0.476	-0.476
	19	0.189	0.174	0.189	0.179	0.175	0.171
	20	0.189	0.175	0.190	0.189	0.175	0.175
	21	0.179	0.171	0.179	0.190	0.171	0.175
	22	-0.348	-0.209	-0.352	-0.353	-0.209	-0.211
	23	0.193	-0.021	0.198	0.201	-0.026	-0.023
	24	0.194	0.181	0.195	0.194	0.183	0.182
	25	0.188	0.212	0.187	0.188	0.210	0.214
	26	0.384	0.323	0.387	0.387	0.317	0.329

	27	-0.137	-0.129	-0.138	-0.144	-0.179	-0.139
	28	-0.325	-0.335	-0.324	-0.324	-0.340	-0.343
	29	0.212	0.209	0.210	0.177	0.209	0.183
	30	0.179	0.188	0.178	0.212	0.183	0.217
	31	0.178	0.179	0.180	0.178	0.182	0.183
Ala49	32			-0.553	-0.553	-0.553	-0.557
	33			0.237	0.236	0.239	0.250
	34			-0.063	-0.062	-0.057	-0.058
	35			0.165	0.165	0.163	0.161
	36			-0.485	-0.480	-0.493	-0.489
	37			0.165	0.164	0.163	0.161
	38			0.172	0.169	0.171	0.170
	39			0.165	0.172	0.174	0.170
	40			0.349	0.353	0.344	0.347
	41			-0.503	-0.505	-0.505	-0.510
	42			0.128	0.120	0.131	0.133
	43			0.221	0.219	0.222	0.219
Leu51	44			-0.534	-0.535	-0.541	-0.536
	45			0.230	0.238	0.242	0.236
	46			-0.107	-0.095	-0.100	-0.102
	47			0.176	0.164	0.168	0.175
	48			-0.327	-0.325	-0.322	-0.330
	49			0.173	0.173	0.168	0.173
	50			0.149	0.154	0.154	0.151
	51			0.030	0.031	0.025	0.031
	52			0.108	0.107	0.110	0.106
	53			-0.508	-0.508	-0.508	-0.508
	54			0.155	0.160	0.156	0.160
	55			0.151	0.155	0.149	0.154
	56			0.161	0.151	0.160	0.153
	57			-0.509	-0.509	-0.507	-0.509

	58		0.153	0.154	0.154	0.154
	59		0.156	0.155	0.156	0.156
	60		0.159	0.158	0.157	0.158
	61		0.365	0.362	0.364	0.362
	62		-0.523	-0.520	-0.522	-0.526
	63		0.125	0.221	0.222	0.226
	64		0.225	0.118	0.121	0.121
Thr317	65		-0.525		-0.530	
	66		0.228		0.230	
	67		-0.227		-0.227	
	68		0.198		0.199	
	69		0.251		0.255	
	70		0.110		0.111	
	71		-0.538		-0.539	
	72		0.182		0.181	
	73		0.174		0.176	
	74		0.173		0.175	
	75		-0.590		-0.599	
	76		0.349		0.350	
	77		0.365		0.367	
	78		-0.492		-0.492	
	79		0.228		0.231	
	80		0.112		0.112	

[a] Charge densities were obtained with a semi-empirical MO of MOPAC (PM6). Other key words were same with those in the previous work,[106] except for EPS (static dielectric constant) key words which were all 2.6 (ε_0^{DA} was nearly equal to ε_0^{DB}, 2.6, see Table 4.3) in the present work. Ground and Excited denote the ground and excited states of Iso. Atom numbering of Iso and H-bond amino acids are indicated in Figure S4.11.

SUPPLEMENTAL INFORMATION OF CHAPTER V

Virtual Screening of Novel D-Amino Acid Oxidase Inhibitors

This article is in preparation for publication (2016).

Table S5.1 The results from docking, molecular properties, and activity score calculations of the 21 training set.

Comp.	IC_{50} (nM)	Docking score	FISA	PISA	Classify	Activity score
1	3.9	-9.737	132.784	234.505	Active	2.218
2	3.8	-9.257	159.349	207.306	Active	1.739
3	4.9	-8.14	159.384	196.55	Inactive	0.361
4	13	-9.244	158.5	193.066	Inactive	1.394
5	4.7	-8.444	148.548	28.055	Inactive	-3.264
6	2.7	-9.148	157.501	161.979	Active	0.593
7	120	-4.658	159.459	228.154	Inactive	-2.508
8	300	-7.947	161.387	14.739	Inactive	-3.770
9	670	-7.643	160.851	21.443	Inactive	-3.947
10	2.2	-8.361	150.389	217.21	Active	0.834
11	2	-9.308	162.308	181.368	Active	1.291
12	8.4	-9.597	158.298	163.414	Inactive	1.102
13	1.4	-9.737	159.703	169.436	Active	1.409
14	2.4	-9.821	156.801	135.226	Active	0.680
15	2.1	-9.62	162.402	142.091	Active	0.752
16	3.1	-9.344	162.61	167.658	Active	1.035
17	12	-8.8	154.253	140.989	Inactive	-0.297
18	2.9	-9.573	153.391	149.677	Active	0.664
19	1.5	-9.966	159.027	127.801	Active	0.717
20	63	-10.736	152.844	78.525	Inactive	0.284
21	13	-9.788	160.581	92.41	Inactive	-0.205

REFERENCES

[1]   Khoronenkova, S.V. and Tishkov, V.I. D-Amino acid oxidase: Physiological role and applications. Biochemistry (Moscow) 73(13) (2008): 1511-1518.

[2]   Tuominen, H.J., Tiihonen, J., and Wahlbeck, K. Glutamatergic drugs for schizophrenia: a systematic review and meta-analysis. Schizophrenia Research 72(2-3) (2005): 225-234.

[3]   Ferraris, D.V. and Tsukamoto, T. Recent advances in the discovery of D-amino acid oxidase inhibitors and their therapeutic utility in schizophrenia. Current Pharmaceutical Design 17(2) (2011): 103-11.

[4]   Weber, G. Fluorescence of riboflavin and flavin-adenine dinucleotide. Biochemical Journal 47(1) (1950): 114-121.

[5]   Karen, A., Ikeda, N., Mataga, N., and Tanaka, F. Picosecond laser photolysis studies of fluorescence quenching mechanisms of flavin: a direct observation of indole-flavin singlet charge transfer state formation in solutions and flavoenzymes. Photochemistry and Photobiology 37(5) (1983): 495-502.

[6]   Karen, A., Sawada, M.T., Tanaka, F., and Mataga, N. Dynamics of excited flavoproteins—picosecond laser photolysis studies. Photochemistry and Photobiology 45(1) (1987): 49-53.

[7]   Zhong, D. and Zewail, A.H. Femtosecond dynamics of flavoproteins: Charge separation and recombination in riboflavine (vitamin B2)-binding protein and in glucose oxidase enzyme. Proceedings of the National Academy of Sciences 98(21) (2001): 11867-11872.

[8]   van den Berg, P.A., van Hoek, A., Walentas, C.D., Perham, R.N., and Visser, A.J. Flavin fluorescence dynamics and photoinduced electron transfer in Escherichia coli glutathione reductase. Biophysical Journal 74(4) (1998): 2046-2058.

[9]   van den Berg, P.A.W., van Hoek, A., and Visser, A.J.W.G. Evidence for a novel mechanism of time-resolved flavin fluorescence depolarization in glutathione reductase. Biophysical Journal 87(4) (2004): 2577-2586.

[10]   van den Berg, P.A.W. and Visser, A.J.W.G. Tracking molecular dynamics of flavoproteins with time-resolved fluorescence spectroscopy. in New Trends in Fluorescence Spectroscopy, Valeur, B. and Brochon, J.-C. (ed.). Springer Berlin Heidelberg, 2001, pp. 457-485.

[11]   Chosrowjan, H., Taniguchi, S., Mataga, N., Nakanishi, T., Haruyama, Y., Sato, S., Kitamura, M., and Tanaka, F. Effects of the disappearance of one charge on ultrafast fluorescence dynamics of the fmn binding protein. The Journal of Physical Chemistry B 114(18) (2010): 6175-6182.

[12]   Chosrowjan, H., Taniguchi, S., Mataga, N., Tanaka, F., Todoroki, D., and Kitamura, M. Comparison between ultrafast fluorescence dynamics of fmn binding protein from desulfovibrio vulgaris, strain miyazaki, in solution vs crystal phases. The Journal of Physical Chemistry B 111(30) (2007): 8695-8697.

[13]   Chosrowjan, H., Taniguchi, S., Mataga, N., Tanaka, F., Todoroki, D., and Kitamura, M. Ultrafast fluorescence dynamics of FMN-binding protein from Desulfovibrio vulgaris (Miyazaki F) and its site-directed mutated proteins. Chemical Physics Letters 462(1–3) (2008): 121-124.

[14]   Mataga, N., Chosrowjan, H., Shibata, Y., and Tanaka, F. Ultrafast fluorescence quenching dynamics of flavin chromophores in protein nanospace. The Journal of Physical Chemistry B 102(37) (1998): 7081-7084.

[15]   Mataga, N., Chosrowjan, H., Shibata, Y., Tanaka, F., Nishina, Y., and Shiga, K. Dynamics and mechanisms of ultrafast fluorescence quenching reactions of flavin chromophores in protein nanospace. The Journal of Physical Chemistry B 104(45) (2000): 10667-10677.

[16]   Mataga, N., Chosrowjan, H., Taniguchi, S., Tanaka, F., Kido, N., and Kitamura, M. Femtosecond fluorescence dynamics of flavoproteins: Comparative studies on flavodoxin, its site-directed mutants, and riboflavin binding protein regarding ultrafast electron transfer in protein nanospaces. The Journal of Physical Chemistry B 106(35) (2002): 8917-8920.

[17]   Yagi, K., Tanaka, F., Nakashima, N., and Yoshihara, K. Picosecond laser fluorometry of FAD of D-amino acid oxidase-benzoate complex. Journal of Biological Chemistry 258(6) (1983): 3799-3802.

[18]   Tanaka, F., Tamai, N., Yamazaki, I., Nakashima, N., and Yoshihara, K. Temperature-induced changes in the coenzyme environment of D-amino acid oxidase revealed by the multiple decays of FAD fluorescence. Biophysical Journal 56(5) (1989): 901-909.

[19]   Mizutani, H., Miyahara, I., Hirotsu, K., Nishina, Y., Shiga, K., Setoyama, C., and Miura, R. Three-dimensional structure of porcine kidney D-amino acid oxidase at 3.0 Å resolution. Journal of Biochemistry 120(1) (1996): 14-17.

[20]   Kawazoe, T., Tsuge, H., Pilone, M.S., and Fukui, K. Crystal structure of human D-amino acid oxidase: context-dependent variability of the backbone conformation of the VAAGL hydrophobic stretch located at the si-face of the flavin ring. Protein Science 15(12) (2006): 2708-17.

[21]   Berry, J.F., Ferraris, D.V., Duvall, B., Hin, N., Rais, R., Alt, J., Thomas, A.G., Rojas, C., Hashimoto, K., Slusher, B.S., and Tsukamoto, T. Synthesis and sar of 1-hydroxy-1h-benzo[d]imidazol-2(3h)-ones as inhibitors of D-amino acid oxidase. ACS Medicinal Chemistry Letters 3(10) (2012): 839-843.

[22]   Krebs, H.A. Metabolism of amino-acids: Deamination of amino-acids. Biochemical Journal 29(7) (1935): 1620-1644.

[23]   Fonda, M.L. and Anderson, B.M. D-amino acid oxidase : III. Studies of flavin adenine dinucleotide binding. Journal of Biological Chemistry 243(21) (1968): 5635-5643.

[24]   Henn, S.W. and Ackers, G.K. Molecular sieve studies of interacting protein systems: IV. Molecular size of the D-amino acid oxidase apoenzyme subunit. Journal of Biological Chemistry 244(2) (1969): 465-470.

[25]   Henn, S.W. and Ackers, G.K. Molecular sieve studies of interacting protein systems. V. Association of subunits of D-amino acid oxidase apoenzyme. Biochemistry 8(9) (1969): 3829-3838.

[26]   Yagi, K. and Ohishi, N. Structure and function of D-amino acid oxidase: Iv. Electrophoretic and ultracentrifugal approach to the monomer equilibrium. Journal of Biochemistry 71(6) (1972): 993-998.

[27]   Antonini, E., Brunori, M., Bruzzesi, M.R., Chiancone, E., and Massey, V. Association-dissociation phenomena of D-amino acid oxidase. <u>Journal of Biological Chemistry</u> 241(10) (1966): 2358-2366.

[28]   Tojo, H., Horiike, K., Shiga, K., Nishina, Y., Watari, H., and Yamano, T. Self-association mode of a flavoenzyme D-amino acid oxidase from hog kidney. I. Analysis of apparent weight-average molecular weight data for the apoenzyme in terms of models. <u>Journal of Biological Chemistry</u> 260(23) (1985): 12607-12614.

[29]   Tojo, H., Horiike, K., Shiga, K., Nishina, Y., Watari, H., and Yamano, T. Self-association mode of a flavoenzyme D-amino acid oxidase from hog kidney. II. Stoichiometry of holoenzyme association and energetics of subunit association. <u>Journal of Biological Chemistry</u> 260(23) (1985): 12615-12621.

[30]   Shiga, K. and Shiga, T. The kinetic features of monomers and dimers in high- and low-temperature conformational states of D-amino acid oxidase. <u>Biochimica et Biophysica Acta (BBA) - Protein Structure</u> 263(2) (1972): 294-303.

[31]   Lugsanangarm, K., Pianwanit, S., Kokpol, S., Nunthaboot, N., Chosrowjan, H., Taniguchi, S., and Tanaka, F. Theoretical analyses of photoinduced electron transfer in medium chain acyl-CoA dehydrogenase: Electron transfer in the normal region. <u>Journal of Photochemistry and Photobiology A: Chemistry</u> 224(1) (2011): 80-90.

[32]   Lugsanangarm, K., Pianwanit, S., Kokpol, S., Tanaka, F., Chosrowjan, H., Taniguchi, S., and Mataga, N. Photoinduced electron transfer in wild type and mutated flavodoxin from Desulfovibrio vulgaris, strain Miyazaki F.: Energy gap law. <u>Journal of Photochemistry and Photobiology A: Chemistry</u> 219(1) (2011): 32-41.

[33]   Lugsanangarm, K., Pianwanit, S., Kokpol, S., Tanaka, F., Chosrowjan, H., Taniguchi, S., and Mataga, N. Analysis of photoinduced electron transfer in flavodoxin. <u>Journal of Photochemistry and Photobiology A: Chemistry</u> 217(2-3) (2011): 333-340.

[34]   Lugsanangarm, K., Pianwanit, S., Nueangaudom, A., Kokpol, S., Tanaka, F., Nunthaboot, N., Ogino, K., Takagi, R., Nakanishi, T., Kitamura, M., Taniguchi, S., and Chosrowjan, H. Mechanism of photoinduced electron transfer from tyrosine

to the excited flavin in the flavodoxin from Helicobacter pylori. A comparative study with the flavodoxin and flavin mononucleotide binding protein from Desulfovibrio vulgaris (Miyazaki F). Journal of Photochemistry and Photobiology A: Chemistry 268 (2013): 58-66.

[35]   Nunthaboot, N., Kido, N., Tanaka, F., Lugsanangarm, K., Nueangaudom, A., Pianwanit, S., and Kokpol, S. Relationship between rate of photoinduced electron transfer and hydrogen bonding chain of tyrosine-glutamine-flavin in flavin photoreceptors: Global analyses among four TePixDs and three AppAs. Journal of Photochemistry and Photobiology A: Chemistry 252 (2013): 14-24.

[36]   Nunthaboot, N., Lugsanangarm, K., Nueangaudom, A., Pianwanit, S., Kokpol, S., and Tanaka, F. Role of the electrostatic energy between the photo-products and ionic groups on the photoinduced electron transfer rates from aromatic amino acids to the excited flavin in five single-point substitution isoforms of the charged amino acid residue-13 in the FMN-binding protein. Molecular Simulation (2014): Ahead of Print.

[37]   Nunthaboot, N., Lugsanangarm, K., Nueangaudom, A., Pianwanit, S., Kokpol, S., and Tanaka, F. Photoinduced electron transfer modeling to simulate flavoprotein fluorescence decay. Methods in Molecular Biology 1076 (2014): 337-55.

[38]   Nunthaboot, N., Lugsanangarm, K., Pianwanit, S., Kokpol, S., Tanaka, F., Taniguchi, S., Chosrowjan, H., Nakanishi, T., and Kitamura, M. Bell-shaped dependence of the rate of ultrafast photoinduced electron transfer from aromatic amino acids to the excited flavin on the donor-acceptor distance in FMN binding proteins. Computational and Theoretical Chemistry 1030 (2014): 9-16.

[39]   Nunthaboot, N., Pianwanit, S., Kokpol, S., and Tanaka, F. Simultaneous analyses of photoinduced electron transfer in the wild type and four single substitution isomers of the FMN binding protein from Desulfovibrio vulgaris, Miyazaki F. Physical Chemistry Chemical Physics 13(13) (2011): 6085-6097.

[40]   Nunthaboot, N., Tanaka, F., and Kokpol, S. Analysis of photoinduced electron transfer in AppA. Journal of Photochemistry and Photobiology A: Chemistry 207(2-3) (2009): 274-281.

[41]   Nunthaboot, N., Tanaka, F., and Kokpol, S. Simultaneous analysis of photoinduced electron transfer in wild type and mutated AppAs. Journal of Photochemistry and Photobiology A: Chemistry 209(1) (2010): 79-87.

[42]   Nunthaboot, N., Tanaka, F., Kokpol, S., Chosrowjan, H., Taniguchi, S., and Mataga, N. Simultaneous analysis of ultrafast fluorescence decays of FMN binding protein and its mutated proteins by molecular dynamic simulation and electron transfer theory. The Journal of Physical Chemistry B 112(41) (2008): 13121-13127.

[43]   World Health Organization (WHO). Mental health. Available from: http://www.who.int/mental_health/management/schizophrenia/en/. Access Date: May, 2015.

[44]   Frisell, W.R., Hellerman, L., and Lowe, H.J. Flavoenzyme catalysis: substrate-competitive inhibition of D-amino acid oxidase. Journal of Biological Chemistry 223(1) (1956): 75-83.

[45]   Hondo, T., Warizaya, M., Niimi, T., Namatame, I., Yamaguchi, T., Nakanishi, K., Hamajima, T., Harada, K., Sakashita, H., Matsumoto, Y., Orita, M., and Takeuchi, M. 4-Hydroxypyridazin-3(2H)-one derivatives as novel D-amino acid oxidase inhibitors. Journal of Medicinal Chemistry 56(9) (2013): 3582-3592.

[46]   Smith, S.M., Uslaner, J.M., Yao, L., Mullins, C.M., Surles, N.O., Huszar, S.L., McNaughton, C.H., Pascarella, D.M., Kandebo, M., Hinchliffe, R.M., Sparey, T., Brandon, N.J., Jones, B., Venkatraman, S., Young, M.B., Sachs, N., Jacobson, M.A., and Hutson, P.H. The behavioral and neurochemical effects of a novel D-amino acid oxidase inhibitor compound 8 [4H-thieno [3,2-b]pyrrole-5-carboxylic acid] and D-serine. Journal of Pharmacology and Experimental Therapeutics 328(3) (2009): 921-930.

[47]   Adage, T., Trillat, A.C., Quattropani, A., Perrin, D., Cavarec, L., Shaw, J., Guerassimenko, O., Giachetti, C., Greco, B., Chumakov, I., Halazy, S., Roach, A., and Zaratin, P. In vitro and in vivo pharmacological profile of AS057278, a

selective D-amino acid oxidase inhibitor with potential anti-psychotic properties. European Neuropsychopharmacology 18(3) (2008): 200-14.

[48] Ferraris, D., Duvall, B., Ko, Y.S., Thomas, A.G., Rojas, C., Majer, P., Hashimoto, K., and Tsukamoto, T. Synthesis and biological evaluation of D-amino acid oxidase inhibitors. Journal of Medicinal Chemistry 51(12) (2008): 3357-9.

[49] Katane, M., Osaka, N., Matsuda, S., Maeda, K., Kawata, T., Saitoh, Y., Sekine, M., Furuchi, T., Doi, I., Hirono, S., and Homma, H. Identification of novel D-amino acid oxidase inhibitors by in silico screening and their functional characterization in vitro. Journal of Medicinal Chemistry 56(5) (2013): 1894-907.

[50] Xie, D., Wang, Y., Xie, J., Lu, J., Cui, J., Zhang, M., Fu, L., and Wang, Y. Quinoxaline-2,3-diones: potential D-amino acid oxidase (DAAO) inhibitors. Medicinal Chemistry Research 23(11) (2014): 4977-4989.

[51] Sparey, T., Abeywickrema, P., Almond, S., Brandon, N., Byrne, N., Campbell, A., Hutson, P.H., Jacobson, M., Jones, B., Munshi, S., Pascarella, D., Pike, A., Prasad, G.S., Sachs, N., Sakatis, M., Sardana, V., Venkatraman, S., and Young, M.B. The discovery of fused pyrrole carboxylic acids as novel, potent D-amino acid oxidase (DAO) inhibitors. Bioorganic & Medicinal Chemistry Letters 18(11) (2008): 3386-91.

[52] Raje, M., Hin, N., Duvall, B., Ferraris, D.V., Berry, J.F., Thomas, A.G., Alt, J., Rojas, C., Slusher, B.S., and Tsukamoto, T. Synthesis of kojic acid derivatives as secondary binding site probes of D-amino acid oxidase. Bioorganic & Medicinal Chemistry Letters 23(13) (2013): 3910-3.

[53] Ekins, S., Mestres, J., and Testa, B. In silico pharmacology for drug discovery: methods for virtual ligand screening and profiling. British Journal of Pharmacology 152(1) (2007): 9-20.

[54] Phatak, S.S., Stephan, C.C., and Cavasotto, C.N. High-throughput and in silico screenings in drug discovery. Expert Opinion on Drug Discovery 4(9) (2009): 947-959.

[55] Tanrikulu, Y., Kruger, B., and Proschak, E. The holistic integration of virtual screening in drug discovery. Drug Discovery Today 18(7-8) (2013): 358-64.

[56]   Callan, J.F., de Silva, A.P., and Magri, D.C. Luminescent sensors and switches in the early 21st century. <u>Tetrahedron</u> 61(36) (2005): 8551-8588.

[57]   Huang, L., Regan, J.M., and Quan, X. Electron transfer mechanisms, new applications, and performance of biocathode microbial fuel cells. <u>Bioresource Technology</u> 102(1) (2011): 316-323.

[58]   Sacchi, S., Pollegioni, L., Pilone, M., and Rossetti, C. Determination of D-amino acids using a D-amino acid oxidase biosensor with spectrophotometric and potentiometric detection. <u>Journal of Biomolecular Techniques</u> 12(2) (1998): 149-153.

[59]   Marcus, R.A. and Sutin, N. Electron transfers in chemistry and biology. <u>Biochimica et Biophysica Acta</u> 811 (1985): 265-322.

[60]   Hush, N.S. Adiabatic theory of outer sphere electron-transfer reactions in solution. <u>Transactions of the Faraday Society</u> 57(0) (1961): 557-580.

[61]   Kakitani, T. and Mataga, N. New energy gap laws for the charge separation process in the fluorescence quenching reaction and the charge recombination process of ion pairs produced in polar solvents. <u>Journal of Physical Chemistry</u> 89(1) (1985): 8-10.

[62]   Pollegioni, L., Piubelli, L., Sacchi, S., Pilone, M.S., and Molla, G. Physiological functions of D-amino acid oxidases: from yeast to humans. <u>Cellular and Molecular Life Sciences</u> 64(11) (2007): 1373-1394.

[63]   Madeira, C., Freitas, M.E., Vargas-Lopes, C., Wolosker, H., and Panizzutti, R. Increased brain D-amino acid oxidase (DAAO) activity in schizophrenia. <u>Schizophrenia Research</u> 101(1–3) (2008): 76-83.

[64]   Boks, M.P.M., Rietkerk, T., van de Beek, M.H., Sommer, I.E., de Koning, T.J., and Kahn, R.S. Reviewing the role of the genes G72 and DAAO in glutamate neurotransmission in schizophrenia. <u>European Neuropsychopharmacology</u> 17(9) (2007): 567-572.

[65]   Yagi, K., Naoi, M., Harada, M., Okamurda, K., Hidaka, H., Ozawa, T., and Kotaki, A. Structure and function of D-amino acid oxidase: I. further purification of hog kidney D-amino acid oxidase and its hydrodynamic and optical rotatory properties. <u>Journal of Biochemistry</u> 61(5) (1967): 580-597.

[66] Massey, V., Curti, B., and Ganther, H. A temperature-dependent conformational change in D-amino acid oxidase and its effect on catalysis. Journal of Biological Chemistry 241(10) (1966): 2347-2357.

[67] Koster, J.F. and Veeger, C. The relation between temperature-inducible allosteric effects and the activation energies of amino-acid oxidases. Biochim Biophys Acta 167(1) (1968): 48-63.

[68] Sturtevant, J.M. and Mateo, P.L. Proposed temperature-dependent conformational transition in D-amino acid oxidase: a differential scanning microcalorimetric study. Proceedings of the National Academy of Sciences of the United States of America 75(6) (1978): 2584-2587.

[69] Mattevi, A., Vanoni, M.A., Todone, F., Rizzi, M., Teplyakov, A., Coda, A., Bolognesi, M., and Curti, B. Crystal structure of D-amino acid oxidase: A case of active site mirror-image convergent evolution with flavocytochrome b2. Proceedings of the National Academy of Sciences of the United States of America 93(15) (1996): 7496-7501.

[70] Todone, F., Vanoni, M.A., Mozzarelli, A., Bolognesi, M., Coda, A., Curti, B., and Mattevi, A. Active site plasticity in D-amino acid oxidase: A crystallographic analysis. Biochemistry 36(19) (1997): 5853-5860.

[71] Miura, R., Setoyama, C., Nishina, Y., Shiga, K., Mizutani, H., Miyahara, I., and Hirotsu, K. Structural and mechanistic studies on D-amino acid oxidase · Substrate complex: Implications of the crystal structure of enzyme · Substrate analog complex. Journal of Biochemistry 122(4) (1997): 825-833.

[72] Mizutani, H., Miyahara, I., Hirotsu, K., Nishina, Y., Shiga, K., Setoyama, C., and Miura, R. Three-dimensional structure of the purple intermediate of porcine kidney D-amino acid oxidase. Optimization of the oxidative half-reaction through alignment of the product with reduced flavin. Journal of Biochemistry 128(1) (2000): 73-81.

[73] Kawazoe, T., Tsuge, H., Pilone, M.S., and Fukui, K. Crystal structure of human D-amino acid oxidase: Context-dependent variability of the backbone conformation of the VAAGL hydrophobic stretch located at the si-face of the flavin ring. Protein Science 15(12) (2006): 2708-2717.

[74]   Tilocca, A., Gamba, A., Vanoni, M.A., and Fois, E. First-principles molecular dynamics investigation of the D-amino acid oxidative half-reaction catalyzed by the flavoenzyme D-amino acid oxidase. Biochemistry 41(48) (2002): 14111-14121.

[75]   Saam, J., Rosini, E., Molla, G., Schulten, K., Pollegioni, L., and Ghisla, S. O$_2$ reactivity of flavoproteins: Dynamic access of dioxygen to the active site and role of a H$^+$ relay system in D-amino acid oxidase. Journal of Biological Chemistry 285(32) (2010): 24439-24446.

[76]   Nakashima, N., Yoshihara, K., Tanaka, F., and Yagi, K. Picosecond fluorescence lifetime of the coenzyme of D-amino acid oxidase. Journal of Biological Chemistry 255(11) (1980): 5261-5263.

[77]   Tanaka, F., Tamai, N., and Yamazaki, I. Picosecond-resolved fluorescence spectra of D-amino-acid oxidase. A new fluorescent species of the coenzyme. Biochemistry 28(10) (1989): 4259-62.

[78]   Marcus, R.A. On the theory of oxidation‐reduction reactions involving electron transfer. I. The Journal of Chemical Physics 24(5) (1956): 966-978.

[79]   Marcus, R.A. Chemical and electrochemical electron-transfer theory. Annual Review of Physical Chemistry 15(1) (1964): 155-196.

[80]   Moser, C.C., Keske, J.M., Warncke, K., Farid, R.S., and Dutton, P.L. Nature of biological electron transfer. Nature 355(6363) (1992): 796-802.

[81]   Bixon, M. and Jortner, J. Non-Arrhenius temperature dependence of electron-transfer rates. The Journal of Physical Chemistry 95(5) (1991): 1941-1944.

[82]   Bixon, M. and Jortner, J. Charge separation and recombination in isolated supermolecules. The Journal of Physical Chemistry 97(50) (1993): 13061-13066.

[83]   Bixon, M., Jortner, J., Cortes, J., Heitele, H., and Michel-Beyerle, M.E. Energy gap law for nonradiative and radiative charge transfer in isolated and in solvated supermolecules. The Journal of Physical Chemistry 98(30) (1994): 7289-7299.

[84]   Toshiaki, K., Akira, Y., and Noboru, M. Theoretical Analysis of Energy-Gap Laws of Electron-Transfer Reactions. in Electron Transfer in Inorganic, Organic, and Biological Systems: American Chemical Society, 1991, pp. 45-69.

[85]   Kakitani, T., Yoshimori, A., and Mataga, N. Effects of the donor-acceptor distance distribution on the energy gap laws of charge separation and charge recombination reactions in polar solutions. The Journal of Physical Chemistry 96(13) (1992): 5385-5392.

[86]   Kakitani, T., Matsuda, N., Yoshimori, A., and Mataga, N. Present and future perspectives of theoretical aspects of photoinduced charge separation and charge recombination reactions in solution. Progress in Reaction Kinetics 20(4) (1995): 347-381.

[87]   Nunthaboot, N., Tanaka, F., Kokpol, S., Chosrowjan, H., Taniguchi, S., and Mataga, N. Simulation of ultrafast non-exponential fluorescence decay induced by electron transfer in FMN binding protein. Journal of Photochemistry and Photobiology A: Chemistry 201(2–3) (2009): 191-196.

[88]   Case, D.A., Darden, T.A., Cheatham III, T.E., Simmerling, C.L., Wang, J., Duke, R.E., Luo, R., Crowley, M., Walker, R.C., Zhang, W., Merz, K.M., Wang, B., Hayik, S., Roitberg, A., Seabra, G., Kolossváry, I., Wong, K.F., Paesani, F., Vanicek, J., Wu, X., Brozell, S.R., Steinbrecher, T., Gohlke, H., Yang, L., Tan, C., Mongan, J., Hornak, V., Cui, G., Mathews, D.H., Seetin, M.G., Sagui, C., Babin, V., and P.A., K. AMBER 10, University of California, San Francisco, 2008.

[89]   Wang, J., Cieplak, P., and Kollman, P.A. How well does a restrained electrostatic potential (RESP) model perform in calculating conformational energies of organic and biological molecules? Journal of Computational Chemistry 21(12) (2000): 1049-1074.

[90]   Wang, J., Wolf, R.M., Caldwell, J.W., Kollman, P.A., and Case, D.A. Development and testing of a general Amber force field. Journal of Computational Chemistry 25(9) (2004): 1157-1174.

[91]   Bayly, C.I., Cieplak, P., Cornell, W.D., and Kollman, P.A. A well-behaved electrostatic potential based method using charge restraints for deriving atomic charges: The RESP model. Journal of Physical Chemistry 97(40) (1993): 10269-10280.

[92]   Essmann, U., Perera, L., Berkowitz, M.L., Darden, T., Lee, H., and Pedersen, L.G. A smooth particle mesh Ewald method. The Journal of Chemical Physics 103(19) (1995): 8577-8593.

[93]   Ryckaert, J.P., Ciccotti, G., and Berendsen, H.J.C. Numerical integration of the cartesian equations of motion of a system with constraints: molecular dynamics of n-alkanes. Journal of Computational Physics 23(3) (1977): 327-341.

[94]   Tanaka, F., Chosrowjan, H., Taniguchi, S., Mataga, N., Sato, K., Nishina, Y., and Shiga, K. Donor–acceptor distance-dependence of photoinduced electron-transfer rate in flavoproteins. The Journal of Physical Chemistry B 111(20) (2007): 5694-5699.

[95]   Tanaka, F., Rujkorakarn, R., Chosrowjan, H., Taniguchi, S., and Mataga, N. Analyses of donor–acceptor distance-dependent rates of photo-induced electron transfer in flavoproteins with three kinds of electron transfer theories. Chemical Physics 348(1–3) (2008): 237-241.

[96]   Vorsa, V., Kono, T., Willey, K.F., and Winograd, N. Femtosecond photoionization of ion beam desorbed aliphatic and aromatic amino acids: Fragmentation via α-cleavage reactions. Journal of Physical Chemistry B 103(37) (1999): 7889-7895.

[97]   Tro, N.J. Chemistry: A Molecular Approach. 2nd ed. New Jersey: Pearson Prentice Hall, 2008: pp. 348-349.

[98]   Beratan, D., Betts, J., and Onuchic, J. Protein electron transfer rates set by the bridging secondary and tertiary structure. Science 252(5010) (1991): 1285-1288.

[99]   Skourtis, S.S., Lin, J., and Beratan, D.N. The effects of bridge motion on electron transfer reactions mediated by tunneling. in Modern methods for theoretical physical chemistry of biopolymers, Starikov, E.B., Lewis, J.P., and Tanaka, S. (ed.). Elsevier Science, 2006, pp. 357 - 382.

[100]   Beratan, D.N. and Balabin, I.A. Heme–copper oxidases use tunneling pathways. Proceedings of the National Academy of Sciences 105(2) (2008): 403-404.

[101]   Miura, R., Setoyama, C., Nishina, Y., Shiga, K., Miyahara, I., Mizutani, H., and Hirotsu, K. Porcine kidney D-amino acid oxidase: the three-dimensional

structure and its catalytic mechanism based on the enzyme–substrate complex model. Journal of Molecular Catalysis B: Enzymatic 12(1–6) (2001): 43-52.

[102] Tishkov, V.I. and Khoronenkova, S.V. D-amino acid oxidase: structure, catalytic mechanism, and practical application. Biochemistry (Moscow) 70(1) (2005): 40-54.

[103] Kawazoe, T., Park, H.K., Iwana, S., Tsuge, H., and Fukui, K. Human D-amino acid oxidase: an update and review. The Chemical Record 7(5) (2007): 305-315.

[104] Sacchi, S., Caldinelli, L., Cappelletti, P., Pollegioni, L., and Molla, G. Structure–function relationships in human D-amino acid oxidase. Amino Acids 43(5) (2012): 1833-1850.

[105] Nueangaudom, A., Lugsanangarm, K., Pianwanit, S., Kokpol, S., Nunthaboot, N., and Tanaka, F. Structural basis for the temperature-induced transition of D-amino acid oxidase from pig kidney revealed by molecular dynamic simulation and photo-induced electron transfer. Physical Chemistry Chemical Physics 14(8) (2012): 2567-2578.

[106] Nueangaudom, A., Lugsanangarm, K., Pianwanit, S., Kokpol, S., Nunthaboot, N., and Tanaka, F. The mechanism of photoinduced electron transfer in the D-amino acid oxidase–benzoate complex from pig kidney: Electron transfer in the inverted region. Journal of Photochemistry and Photobiology A: Chemistry 250 (2012): 6-17.

[107] Yoshimori, A., Kakitani, T., Enomoto, Y., and Mataga, N. Shapes of the electron-transfer rate vs energy gap relations in polar solutions. The Journal of Physical Chemistry 93(26) (1989): 8316-8323.

[108] Matsuda, N., Kakitani, T., Denda, T., and Mataga, N. Examination of the viability of the Collins-Kimball model and numerical calculation of the time-dependent energy gap law of photoinduced charge separation in polar solution. Chemical Physics 190(1) (1995): 83-95.

[109] Nueangaudom, A., Lugsanangarm, K., Pianwanit, S., Kokpol, S., Nunthaboot, N., and Tanaka, F. Non-equivalent conformations of D-amino acid oxidase dimer from porcine kidney between the two subunits. Molecular dynamics simulation

and photoinduced electron transfer. <u>Physical Chemistry Chemical Physics</u> 16(5) (2014): 1930-1944.

[110] Gray, H.B. and Winkler, J.R. Photoinduced electron transfer in ruthenium-modified cytochrome c. <u>Pure and Applied Chemistry</u> 64(9) (1992): 1257-1262.

[111] Nishimoto, K., Watanabe, Y., and Yagi, K. Hydrogen bonding of flavoprotein. I. Effect of hydrogen bonding on electronic spectra of flavoprotein. <u>Biochim Biophys Acta</u> 526(1) (1978): 34-41.

[112] Bendall, D.S. <u>Protein Electron Transfer</u>. Oxford, UK: BIOS Scientific Publishers Ltd., 1996.

[113] Gray, H.B. and Winkler, J.R. Electron Transfer in Proteins. <u>Annual Review of Biochemistry</u> 65(1) (1996): 537-561.

[114] <u>Biophysics of Electron Transfer and Molecular Bioelectronics</u>. Electronics and Biotechnology Advanced (Elba) Forum Series, ed. Nicolini, C.: Springer, 1999.

[115] Bixon, M. and Jortner, J. Electron Transfer—from Isolated Molecules to Biomolecules, Part1. in <u>Advances in Chemical Physics</u>: John Wiley & Sons, Inc., 1999, pp. 35-202.

[116] Warshel, A. and Parson, W.W. Dynamics of biochemical and biophysical reactions: insight from computer simulations. <u>Quarterly Reviews of Biophysics</u> 34(4) (2001): 563-679.

[117] Dixon, M. and Kleppe, K. D-amino acid oxidase I. Dissociation and recombination of the holoenzyme. <u>Biochimica et Biophysica Acta (BBA) - Nucleic Acids and Protein Synthesis</u> 96(3) (1965): 357-367.

[118] Dixon, M. and Kleppe, K. D-amino acid oxidase II. Specificity, competitive inhibition and reaction sequence. <u>Biochimica et Biophysica Acta (BBA) - Nucleic Acids and Protein Synthesis</u> 96(3) (1965): 368-382.

[119] Krebs, H.A. Metabolism of amino-acids: Deamination of amino-acids. <u>Biochemical Journal</u> 29(7) (1935): 1620-44.

[120] WHO. <u>Mental health</u>. Available from: http://www.who.int/mental_health/management/schizophrenia/en/. Access Date: May, 2013.

[121] Duplantier, A.J., Becker, S.L., Bohanon, M.J., Borzilleri, K.A., Chrunyk, B.A., Downs, J.T., Hu, L.Y., El-Kattan, A., James, L.C., Liu, S., Lu, J., Maklad, N., Mansour, M.N., Mente, S., Piotrowski, M.A., Sakya, S.M., Sheehan, S., Steyn, S.J., Strick, C.A., Williams, V.A., and Zhang, L. Discovery, SAR, and pharmacokinetics of a novel 3-hydroxyquinolin-2(1H)-one series of potent D-amino acid oxidase (DAAO) inhibitors. Journal of Medicinal Chemistry 52(11) (2009): 3576-85.

[122] Hopkins, S.C., Heffernan, M.L., Saraswat, L.D., Bowen, C.A., Melnick, L., Hardy, L.W., Orsini, M.A., Allen, M.S., Koch, P., Spear, K.L., Foglesong, R.J., Soukri, M., Chytil, M., Fang, Q.K., Jones, S.W., Varney, M.A., Panatier, A., Oliet, S.H., Pollegioni, L., Piubelli, L., Molla, G., Nardini, M., and Large, T.H. Structural, kinetic, and pharmacodynamic mechanisms of D-amino acid oxidase inhibition by small molecules. Journal of Medicinal Chemistry 56(9) (2013): 3710-24.

[123] Schrödinger Release 2013-1: Schrödinger Suite 2013 Protein Preparation Wizard; Epik version 2.4, S., New York, NY, 2013; Impact version 5.9, Schrödinger, New York, NY, 2013; Prime version 3.2, Schrödinger, New York, NY, 2013. (2013).

[124] Jorgensen, W.L., Maxwell, D.S., and Tirado-Rives, J. Development and testing of the OPLS all-atom force field on conformational energetics and properties of organic liquids. Journal of the American Chemical Society 118(45) (1996): 11225-11236.

[125] Lipinski, C.A., Lombardo, F., Dominy, B.W., and Feeney, P.J. Experimental and computational approaches to estimate solubility and permeability in drug discovery and development settings. Advanced Drug Delivery Reviews 46(1-3) (2001): 3-26.

[126] Thai, K.-M. and Ecker, G.F. A binary QSAR model for classification of hERG potassium channel blockers. Bioorganic & Medicinal Chemistry 16(7) (2008): 4107-4119.

[127] Fells, J.I., Tsukahara, R., Liu, J., Tigyi, G., and Parrill, A.L. 2D binary QSAR modeling of LPA3 receptor antagonism. Journal of Molecular Graphics and Modelling 28(8) (2010): 828-833.

[128]   Jurik, A., Reicherstorfer, R., Zdrazil, B., and Ecker, G.F. Classification of high-activity Tiagabine analogs by binary QSAR modeling. Molecular Informatics 32(5-6) (2013): 415-419.

[129]   Manvar, A., Khedkar, V., Patel, J., Vora, V., Dodia, N., Patel, G., Coutinho, E., and Shah, A. Synthesis and binary QSAR study of antitubercular quinolylhydrazides. Bioorganic & Medicinal Chemistry Letters 23(17) (2013): 4896-4902.

[130]   Moorthy, N.S.H.N., Cerqueira, N.M.F.S.A., Ramos, M.J., and Fernandes, P.A. Ligand based analysis on HMG-CoA reductase inhibitors. Chemometrics and Intelligent Laboratory Systems 140 (2015): 102-116.

APPENDIX

VITA

Personal Data

Name	Arthit Neangaudom
Nationality	Thai
Date of Birth	5 October 1986
Email Address	arthit_n.udom@hotmail.com,
	nueangaudom.a@gmail.com

Education

2005 – 2009 B.Sc. in Chemistry (2nd honor)

Department of Chemistry, Faculty of Science,

Mahasarakham University, Mahasarakham, Thailand

2009 – 2015 Ph.D. in Chemistry

Department of Chemistry, Faculty of Science,

Chulalongkorn University, Bangkok, Thailand